BioMed Research International

Advances in Diagnostic Imaging Technologies to Evaluate the Retina and the Optic Disc

Guest Editors: Antonio Ferreras, Michele Figus, Paolo Frezzotti, and Michele Iester

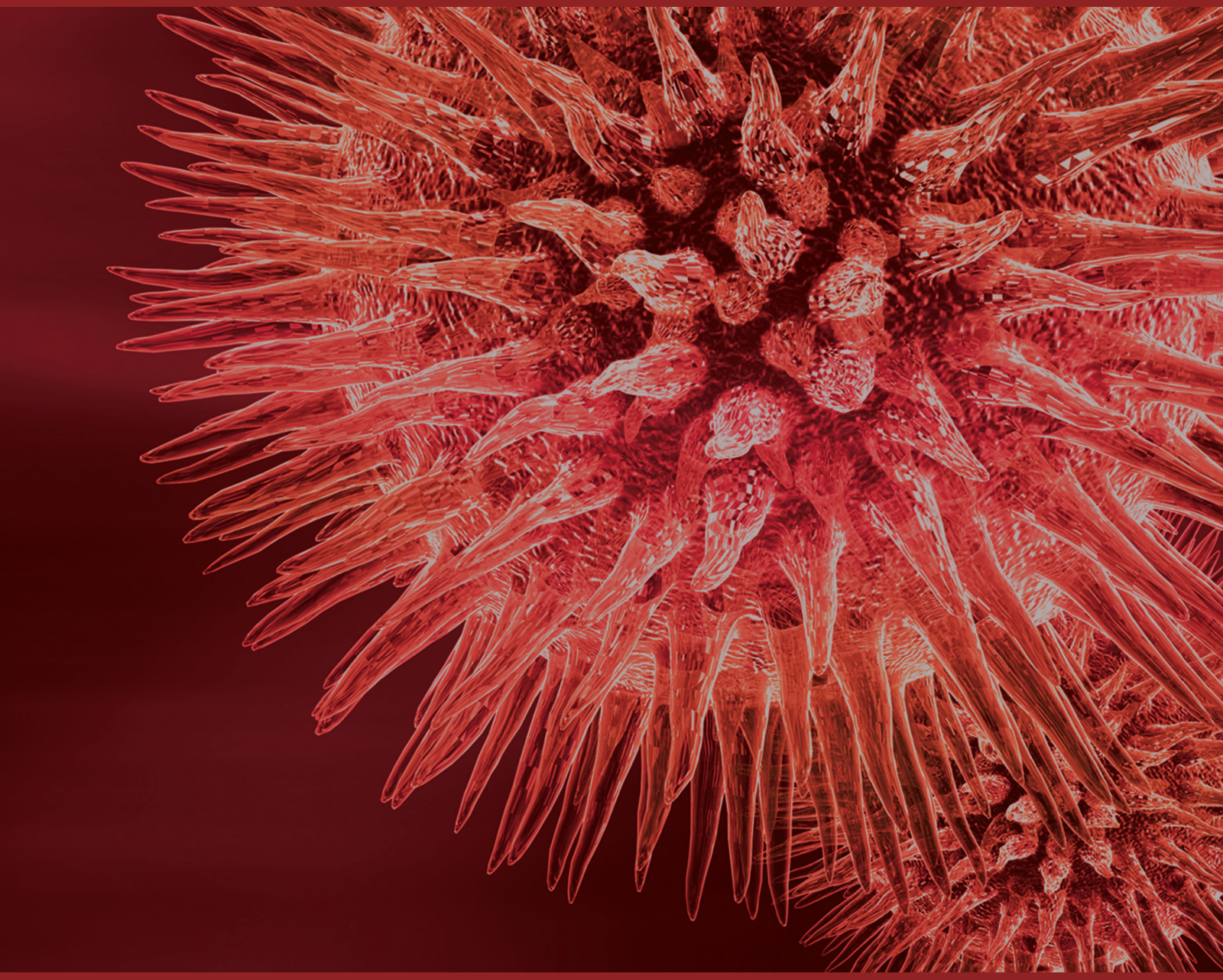

Advances in Diagnostic Imaging Technologies to Evaluate the Retina and the Optic Disc

BioMed Research International

Advances in Diagnostic Imaging Technologies to Evaluate the Retina and the Optic Disc

Guest Editors: Antonio Ferreras, Michele Figus, Paolo Frezzotti, and Michele Iester

Contents

Hindawi Publishing Corporation
BioMed Research International
Volume 2015, Article ID 371312, 2 pages
http://dx.doi.org/10.1155/2015/371312

Editorial

Advances in Diagnostic Imaging Technologies to Evaluate the Retina and the Optic Disc

Antonio Ferreras,[1,2] Michele Figus,[3] Paolo Frezzotti,[4] and Michele Iester[5]

[1] *Department of Ophthalmology, Miguel Servet University Hospital, 50009 Zaragoza, Spain*
[2] *University of Zaragoza, 50009 Zaragoza, Spain*
[3] *Department of Neurosciences, University of Pisa, 56100 Pisa, Italy*
[4] *Department of Ophthalmology, University of Siena, 53100 Siena, Italy*
[5] *Clinica Oculistica, DINOGMI, University of Genoa, 16132 Genoa, Italy*

Correspondence should be addressed to Antonio Ferreras; aferreras@msn.com

Received 30 April 2015; Accepted 30 April 2015

Current diagnostic and therapeutic decisions based on the outcomes of imaging technologies have become a common practice in every ophthalmic subspecialty. New devices and tools for evaluating the retina and optic nerve head, such as scanning laser polarimetry and spectral-domain optical coherence tomography (OCT), are widely used in clinical practice. These technologies provide objective quantitative measurements and in vivo real-time images of ocular structures. The performance of imaging devices is continuously being improved, and thus knowledge of their applications, advantages, and limitations must also be continuously updated to optimize their management by clinicians.

While imaging technologies require relatively transparent media, the variability of the measurements acquired by these devices is low, making these instruments useful for monitoring changes over time. In this issue, M. Ara et al. report excellent reproducibility of scanning laser polarimetry in healthy and glaucoma patients. In their review article, J. J. Garcia-Medina et al. evaluated the effects of posterior capsule opacification and found that image quality improves after capsulotomy, but a new baseline for future comparisons should be established. Additionally, R. L. Brautaset et al. report that OCT allows for the acquisition of reliable macular measurements in individuals with moderate to severe keratoconus.

M. Cavallari et al. developed a semiautomated, computer-based method to detect and quantify retinal vessel abnormalities by analyzing digital fundus photographs. This tool was successfully used to evaluate patients with hypertensive retinopathy and cerebral autosomal dominant arteriopathy with subcortical infarcts and leukoencephalopathy.

G. S. K. Yau et al. compared central macular thickness measured by OCT in Chinese children and found that it was thicker in myopic eyes compared to emmetropic and hyperopic eyes.

Three papers regarding the role of the ganglion cell complex in different disorders, multiple sclerosis, age-related macular degeneration, and glaucoma, demonstrated that the same tool could be used with different approaches depending on the disease: "Comparative Diagnostic Accuracy of Ganglion Cell-Inner Plexiform and Retinal Nerve Fiber Layer Thickness Measures by Cirrus and Spectralis Optical Coherence Tomography in Relapsing-Remitting Multiple Sclerosis" by J. J. Gonzalez-Lopez et al.; "Can Variability of Pattern ERG Signal Help to Detect Retinal Ganglion Cells Dysfunction in Glaucomatous Eyes?" by A. Mavilio et al.; and "Ganglion Cell Complex Evaluation in Exudative Age-Related Macular Degeneration after Repeated Intravitreal Injections of Ranibizumab" by A. Perdicchi et al. J. J. Gonzalez-Lopez et al. observed a better sensitivity-specificity balance for the macular ganglion cell complex measured with OCT in relapsing-remitting multiple sclerosis than peripapillary retinal nerve fiber layer thickness, while A. Mavilio et al. found that reduction of the ganglion cell complex was related to reduced amplitude and increased variability of the phase of the

steady-state pattern electroretinogram in glaucoma. On the other hand, A. Perdicchi et al. demonstrated that the loading phase for ranibizumab in aged-related macular degeneration had no toxic effects on the ganglion cell complex.

R. Mastropasqua et al. and M. Di Nicola et al. provide reviews regarding advanced morphologic and functional magnetic resonance techniques in glaucoma and functional and structural abnormalities in deferoxamine retinopathy, respectively. Information concerning magnetic resonance imaging in glaucoma is limited and mostly based on mouse models and patients with advanced glaucoma. Nevertheless, some results support the potential for these techniques to detect early glaucomatous changes. M. Di Nicola et al. revealed that imaging technologies (color fundus photographs, autofluorescence, and OCT) may facilitate the management of deferoxamine retinopathy and their report highlights the need for guidelines to enhance the diagnosis and follow-up of these patients.

A wide variety of image modalities and optic enhancements, including fundus autofluorescence, microperimetry, adaptive optics, or faster OCTs, recently emerged. Using different image modalities, clinicians can emphasize the features of a particular anatomic structure of a tissue. M. Bertolotto et al. evaluated various paracentral hyperautofluorescence retinal patterns and their relationship with changes in the retinal layers. Hyperautofluorescence was mainly related to a "window effect" rather than an accumulation of lipofuscin. Adaptive optics combined with OCT or fundus photography allow for high-resolution images due to the improvement in lateral resolution by correcting for aberrations in the eye. This technology reaches resolutions close to 2 to 4 μm, which is high enough to identify even cone photoreceptors. D. Supriya et al. report strong correlations between retinal sensitivity, evaluated by microperimetry, and the mean cone packing density at different macular eccentricities measured with an adaptive optics retinal camera. Further studies are required, however, to determine normative variations in cone structure-function correlation.

OCT has changed many protocols and ways of managing different ocular diseases. Moreover, OCT has modified how clinicians look at the retina. The assessment of retinal abnormalities based on evaluation of every layer rather than the global thickness has advanced ophthalmology. Because images evaluated through OCT provide information of the actual retina anatomy, but not exactly the same information as obtained with histology; last year an international panel of experts in vitreoretinal diseases and imaging suggested a consensus nomenclature for the classification of retinal and choroidal layers and bands observed in OCT scans (IN•OCT consensus). P. Tortorella et al. evaluated the changes in two of these retinal layers, the photoreceptor inner segment ellipsoid band and the interdigitation zone, in eyes with uveitic macular edema. Interruption of these lines was related to poor visual acuity. R. L. M. Wong et al. report that the outer retinal layer thickness (distance between the external limiting membrane and retinal pigment epithelium) correlated better than total thickness with visual acuity in patients with diabetic macular edema.

In summary, this issue includes different points of view presented by diverse authors covering several topics related to advances in imaging techniques for ophthalmic diseases. This publication will provide valuable information that should be helpful in clinical practice.

Antonio Ferreras
Michele Figus
Paolo Frezzotti
Michele Iester

Hindawi Publishing Corporation
BioMed Research International
Volume 2015, Article ID 729392, 6 pages
http://dx.doi.org/10.1155/2015/729392

Clinical Study

Repeatability and Reproducibility of Retinal Nerve Fiber Layer Parameters Measured by Scanning Laser Polarimetry with Enhanced Corneal Compensation in Normal and Glaucomatous Eyes

Mirian Ara,[1] Antonio Ferreras,[1,2] Ana B. Pajarin,[3] Pilar Calvo,[1] Michele Figus,[4] and Paolo Frezzotti[5]

[1]*Department of Ophthalmology, Miguel Servet University Hospital, Aragon Health Sciences Institute, 50009 Zaragoza, Spain*
[2]*Department of Surgery, Gynecology and Obstetrics, University of Zaragoza, 50009 Zaragoza, Spain*
[3]*Department of Family Medicine, Seminario Primary Health Care Center, 50009 Zaragoza, Spain*
[4]*Department of Neurosciences, University of Pisa, 56100 Pisa, Italy*
[5]*Department of Ophthalmology, University of Siena, 53100 Siena, Italy*

Correspondence should be addressed to Antonio Ferreras; aferreras@msn.com

Received 7 September 2014; Accepted 4 March 2015

Academic Editor: Alfredo García-Layana

Objective. To assess the intrasession repeatability and intersession reproducibility of peripapillary retinal nerve fiber layer (RNFL) thickness parameters measured by scanning laser polarimetry (SLP) with enhanced corneal compensation (ECC) in healthy and glaucomatous eyes. *Methods*. One randomly selected eye of 82 healthy individuals and 60 glaucoma subjects was evaluated. Three scans were acquired during the first visit to evaluate intravisit repeatability. A different operator obtained two additional scans within 2 months after the first session to determine intervisit reproducibility. The intraclass correlation coefficient (ICC), coefficient of variation (COV), and test-retest variability (TRT) were calculated for all SLP parameters in both groups. *Results*. ICCs ranged from 0.920 to 0.982 for intravisit measurements and from 0.910 to 0.978 for intervisit measurements. The temporal-superior-nasal-inferior-temporal (TSNIT) average was the highest (0.967 and 0.946) in normal eyes, while nerve fiber indicator (NFI; 0.982) and inferior average (0.978) yielded the best ICC in glaucomatous eyes for intravisit and intervisit measurements, respectively. All COVs were under 10% in both groups, except NFI. TSNIT average had the lowest COV (2.43%) in either type of measurement. Intervisit TRT ranged from 6.48 to 12.84. *Conclusions*. The reproducibility of peripapillary RNFL measurements obtained with SLP-ECC was excellent, indicating that SLP-ECC is sufficiently accurate for monitoring glaucoma progression.

1. Introduction

Progressive death of retinal ganglion cells and their axons in the retina leads to characteristic changes in the optic nerve head, which are the typical signs of glaucomatous optic neuropathy. These structural changes also result in functional visual field loss as measured by standard automated perimetry (SAP). Therefore, evaluating the retinal nerve fiber layer (RNFL) and monitoring its changes are key components in glaucoma management. Objective and quantitative assessment of the RNFL largely relies on digital imaging technologies, including scanning laser polarimetry (SLP).

SLP is an imaging technology used to measure the birefringence of the RNFL. Polarized light passing through a birefringent structure, such as the RNFL, experiences a phase shift (retardation) that is linearly related to the RNFL thickness [1]. The cornea and the lens also exhibit birefringent properties, which are neutralized in the SLP with variable corneal compensation (VCC) [2]. Although SLP-VCC usually compensates correctly the birefringence of the anterior pole,

atypical birefringence pattern images may be observed in some cases [3]. Thus, the latest generation of SLP, SLP with enhanced corneal compensation (ECC), includes an enhancement module to improve the performance of SLP-VCC for detecting RNFL damage [4–7] and progressive RNFL changes [8].

SLP has a theoretical advantage in detecting changes because reduction of RNFL retardance resulting from disruption of the microtubules could be evident before the actual loss of nerve fibers due to injury of the optic nerve. The present study assessed the intravisit and intervisit reproducibility of peripapillary SLP-ECC parameters in healthy and glaucomatous eyes.

2. Methods

2.1. Subjects. The Institutional Review Board (Clinical Research Ethics Committee of Aragon, CEICA) approved the study design and all methods adhered to the principles of the Declaration of Helsinki. Informed consent was obtained from all participants. Healthy eyes were consecutively recruited from patients referred for refraction that underwent routine examination without abnormal ocular findings, hospital staff, and relatives of patients. The glaucoma group was recruited consecutively from an ongoing longitudinal follow-up study at the Miguel Servet University Hospital. This group included patients with primary open-angle glaucoma, pseudoexfoliative glaucoma, and pigmentary glaucoma. One hundred and forty-two white individuals were evaluated (82 healthy control subjects and 60 patients with glaucoma). When both eyes fulfilled the inclusion criteria, only one eye per subject was randomly included in the study.

Inclusion criteria were age between 18 and 80 years, refractive error not exceeding a 5-diopter sphere and a 3-diopter cylinder, best-corrected visual acuity of at least 20/25 (Snellen scale), and transparent ocular media. Participants with any history of cardiovascular, severe hematologic, or neuroophthalmologic disease, optic nerve abnormalities (e.g., tilted disc, drusen), or angle anomalies; any retinal disease (e.g., macular degeneration, diabetic retinopathy, and retinal detachment); or ocular surgery within 1 month of enrollment were excluded.

All subjects underwent a comprehensive ophthalmic examination, comprising a review of their medical and ophthalmologic history, determination of best-corrected visual acuity, slit lamp biomicroscopy, Goldmann applanation tonometry, central corneal ultrasonic pachymetry (OcuScan RxP; Alcon Laboratories Inc., Irvine, CA), fundus examination, and at least two reliable SAPs (24-2 Swedish Interactive Threshold Algorithm Standard examinations; Humphrey Field Analyzer, model 750i; Carl Zeiss Meditec, Dublin, CA). If fixation losses were higher than 20% or false-positive or false-negative rates were higher than 15%, the tests were repeated at least 3 days apart to avoid a fatigue effect. Abnormal SAP results were defined as typical glaucomatous defects with a pattern standard deviation significantly increased beyond the 5% level and/or a Glaucoma Hemifield Test result outside normal limits.

2.2. Classification into Groups. Healthy eyes were defined by an intraocular pressure of 21 mmHg or less and normal SAP. Glaucomatous eyes were defined as those with intraocular pressure readings of at least 21 mmHg and consistent abnormal visual field defects on SAP.

2.3. Scanning Laser Polarimetry with Enhanced Corneal Compensation Imaging. The same operator acquired the first three scans (15-minute intertest intervals) at the initial visit using the same SLP-ECC (GDx PRO, Carl Zeiss Meditec, software version 1.0) following a standard protocol to assess intrasession variability. A different operator obtained the fourth and fifth scans at two additional visits at least 4 weeks apart (±1 week) to assess intersession variability. All scans were acquired through undilated pupils with low ambient light. The participants kept their head still during each scan acquisition and looked at the internal fixation point to obtain the best alignment. A primary scan was captured before each calculation to compensate for the corneal birefringence.

The ECC mode introduced a predetermined large birefringence bias to shift the total retardation to a higher value to remove noise and minimize the effect of atypical patterns [9]. Following image acquisition, the birefringent bias was removed mathematically, point by point, from the final RNFL image. Calculations were performed on a ring of fixed-sized tissue centered on the optic disc automatically determined by the SLP-ECC software.

In this study, we excluded images that were obtained during eye movement. Only good quality images from SLP were accepted: centered and well-focused scans with a quality scan score higher than 6. SLP parameters included in the statistical analysis were nerve fiber indicator (NFI), temporal-superior-nasal-inferior-temporal (TSNIT) average, superior average, inferior average, and TSNIT standard deviation. Although some studies indicate that the NFI is the most sensitive parameter of SLP for glaucoma diagnosis [10, 11], its calculation method is based on various parameters and the result does not directly indicate RNFL thickness.

2.4. Statistical Analysis. All statistical analyses were calculated using IBM SPSS (version 20; IBM Corporation, Somers, NY) and MedCalc (version 12; MedCalc, Mariakerke, Belgium) statistical software. After checking for a normal distribution of variables, two-tailed Student's t-tests were used to calculate differences between normal subjects and patients with glaucoma.

The SLP measurement variability was assessed by the intraclass correlation coefficient (ICC), coefficient of variation (COV), and the test-retest variability (TRT). The ICC is a statistic that condenses the reproducibility of a parameter for a given group of subjects. A large ICC suggests small fluctuations among repeated measurements in the same individual. The ICC value can range from 0 to a maximum of 1 [12]. The COVs were calculated as the relevant standard deviation divided by the mean of the measurement values expressed as a percentage. TRT was defined as two times the standard deviation.

Table 1: Demographic and clinical characteristics of the sample.

	Control ($n = 82$)				Glaucoma ($n = 60$)				p^*
	Minimum	Maximum	Mean	SD	Minimum	Maximum	Mean	SD	
Age (y)	38	70	55.73	6.92	43	76	58.27	8.95	0.091
BCVA (Snellen)	20/25	1	0.92	0.09	20/25	1	0.90	0.10	0.263
IOP (mmHg)	13	20	17.95	2.06	23	45	27.69	5.87	<0.001
CCT (μm)	476	619	563.53	36.58	470	600	533.49	28.68	<0.001
MD SAP (dB)	−1.48	1.75	−0.31	1.16	−29.74	−1.28	−7.04	7.04	<0.001
PSD SAP	0.94	1.86	1.42	0.21	2.05	14.33	5.63	3.60	<0.001
VFI	98	100	99.51	0.64	14	97	85.72	18.80	<0.001

*Student's t-test between the control and glaucoma groups.
SD: standard deviation; BCVA: best-corrected visual acuity; IOP: intraocular pressure; CCT: central corneal thickness, MD: mean deviation; SAP: standard automated perimetry; PSD: pattern standard deviation; VFI: Visual Field Index.

Repeatability was considered to be the variation in measurements acquired by the same operator under the same conditions at the same visit. Reproducibility was considered the ability of SLP to consistently obtain the same measurement performed by different operators at different visits. Thus, the intravisit analysis only included the three measurements obtained at the first visit, while the intervisit reproducibility included all five scans acquired during the study.

3. Results

3.1. Demographic Parameters. The present study comprised 142 subjects ranging in age from 38 to 76 years (mean 57.6): 60 eyes with stable open-angle glaucoma and 82 healthy eyes (control group). Other demographic and clinical characteristics of the sample are shown in Table 1.

3.2. Reproducibility of SLP-ECC Parameters. Table 2 shows the comparison of SLP parameters between the normal and glaucoma groups. Intravisit and intervisit ICCs were excellent for all RNFL parameters (Tables 3 and 4). TSNIT average had the highest values (0.967 for intravisit and 0.946 for intervisit measurements) in normal eyes, while NFI (0.982 for intravisit analysis) and inferior average (0.978 for intervisit analysis) had the best values in glaucomatous eyes. TSNIT standard deviation (0.928) and NFI (0.910) exhibited the lowest ICC values for the intra- and intervisit measurements, respectively, in the normal group. Superior average (0.920 for the intravisit and 0.917 for the intervisit analysis) produced the lowest ICCs in the glaucoma group. All COVs were under 10% for both the intravisit and intervisit measurements in both groups, except the NFI. TSNIT average had the lowest intravisit (2.43% in the normal group and 4.40% in the glaucoma group) and intervisit COVs (2.68% in the normal group and 4.71% in the glaucoma group). The TRT for NFI ranged from 6.48 to 6.55 in the normal group and from 10.61 to 12.84 in the glaucoma group. The intervisit TRT was 2.73 for the TSNIT average in the normal group and 3.93 in the glaucoma group. The TSNIT standard deviation had the lowest intervisit TRT (2.83) in the glaucoma group.

4. Discussion

The reproducibility of measurements obtained with any diagnostic test is key for diagnostic accuracy and for monitoring changes over time. Glaucomatous progression is typically slow, and, for that reason, it may be difficult to identify small changes during follow-up. The validity of a test for detecting this change depends on its ability to differentiate actual progression from the inherent variability among measurements. Quantifying measurement variability is, therefore, critical. Visual field assessment results are subject to long-term fluctuations, which limit the ability to detect glaucoma progression between two consecutive tests [13, 14]. On the other hand, while a series of fundus photographs can be used to evaluate changes in the optic disc, the subjective nature of this method and the requirement for experienced evaluators limit its accuracy for detecting progression as well as its general applicability [15, 16].

SLP assesses RNFL thickness around the optic nerve head. Because the technology is based on reflectivity, measurement is hampered by polarization of the ocular media, which can lead to measurement errors induced by non-RNFL birefringence. Improvements in this technology, including ECC, have led to more reproducible results and more accurate discrimination between healthy and glaucomatous eyes [17].

Although other investigators have evaluated the repeatability of RNFL measurements using SLP-ECC, the present study is unique in the fact that it demonstrates not only repeatability but also reproducibility of SLP-ECC parameters over time. Thus, our study design (measurements at 3 different visits) and 2 study groups (normal and glaucomatous eyes) provide new information regarding the reproducibility of SLP reported to date. We found that RNFL measurements acquired with SLP-ECC had low variability (high ICCs and low COVs) for healthy and glaucomatous eyes. These findings are consistent with those of Sehi et al. [7] who evaluated the repeatability of SLP-VCC and SLP-ECC. Mai et al. [18] evaluated the repeatability of RNFL measurements acquired with SLP-ECC in 16 normal subjects, 32 subjects with ocular hypertension, and 35 glaucoma patients and reported similar results but found that the measurement reproducibility in glaucomatous eyes was slightly worse than that in healthy eyes.

Table 2: SLP parameters for the five tests performed in the normal and glaucoma groups.

	Control ($n = 82$)				Glaucoma ($n = 60$)				p^*
	Min.	Max.	Mean	SD	Min.	Max.	Mean	SD	
Intravisit measurements									
First measurement									
NFI	2	48	19.26	8.52	2	98	48.25	30.97	<0.001
TSNIT average	37.4	65.4	51.18	4.76	25.8	58.3	41.91	8.54	<0.001
Superior average	46.6	77.8	62.29	6.50	3.1	70.2	46.85	13.56	<0.001
Inferior average	45.9	87.4	63.83	7.31	26.2	76.2	52.46	11.96	<0.001
TSNIT SD	15	34.1	24.48	3.76	8.9	29.3	19.30	5.79	<0.001
Second measurement									
NFI	3	58	19.04	9.48	2	98	49.35	31.17	<0.001
TSNIT average	40	69	51.04	4.88	17	58	41.85	8.95	<0.001
Superior average	46	84	62.26	7.20	15	72	47.78	12.70	<0.001
Inferior average	49	79	63.58	6.94	13	76	51.27	13.61	<0.001
TSNIT SD	15	33	24.49	3.69	6	31	19.28	6.32	<0.001
Third measurement									
NFI	3	44	18.87	8.48	5	98	46.90	30.03	<0.001
TSNIT average	43	61	51.18	4.26	24	58	42.57	8.58	<0.001
Superior average	50	79	62.19	6.14	23	74	49.25	12.38	<0.001
Inferior average	52	79	63.99	6.68	26	76	52.88	12.06	<0.001
TSNIT SD	17	32	24.68	3.46	8	32	19.65	5.74	<0.001
Intervisit measurements									
Fourth measurement									
NFI	2	42	15.94	9.47	6	98	47.59	32.09	<0.001
TSNIT average	43	63	52.58	5.01	25	56	41.95	8.82	<0.001
Superior average	50	80	64.73	8.07	23	69	48.66	13.13	<0.001
Inferior average	53	82	65.92	7.23	28	73	51.93	12.37	<0.001
TSNIT SD	17	36	25.65	4.11	9	29	19.55	6.21	<0.001
Fifth measurement									
NFI	2	64	18.19	11.84	3	98	49.98	31.23	<0.001
TSNIT average	41	61	51.54	5.01	23	59	40.89	8.90	<0.001
Superior average	49	80	62.47	7.38	20	75	47.36	13.83	<0.001
Inferior average	48	83	64.90	7.80	27	72	50.91	12.28	<0.001
TSNIT SD	13	36	24.77	4.42	7	30	18.86	6.28	<0.001

*Student's t-test between the control and glaucoma groups.
Min.: minimum; Max.: maximum; NFI: nerve fiber indicator; TSNIT: temporal-superior-nasal-inferior-temporal; SD: standard deviation.

Table 3: Intravisit repeatability and intervisit reproducibility of SLP-ECC parameters in the normal group ($n = 82$).

GDx parameters	Intravisit						Intervisit					
	ICC	ICC 95% CI		p	COV (%)	TRT SD	ICC	ICC 95% CI		p	COV (%)	TRT SD
		Upper limit	Lower limit					Upper limit	Lower limit			
NFI	0. 935	0.906	0.956	<0.001	21.82	6.55	0.910	0.855	0.947	<0.001	19.91	6.48
TSNIT average	0.967	0.949	0.979	<0.001	2.43	2.51	0.946	0.912	0.968	<0.001	2.68	2.73
Superior average	0.940	0.913	0.959	<0.001	3.86	4.84	0.938	0.900	0.963	<0.001	3.88	4.90
Inferior average	0.944	0.919	0.962	<0.001	3.69	4.76	0.934	0.894	0.961	<0.001	3.82	4.84
TSNIT SD	0.928	0.896	0.951	<0.001	6.20	3.03	0.912	0.857	0.948	<0.001	8.54	3.56

ICC: intraclass correlation coefficient; CI: confidence interval; COV: coefficient of variation; TRT SD: test-retest variability; NFI: nerve fiber indicator; TSNIT: temporal-superior-nasal-inferior-temporal; SD: standard deviation.

Table 4: Intravisit repeatability and intervisit reproducibility of SLP-ECC parameters in the glaucoma group ($n = 60$).

GDx parameters	Intravisit						Intervisit					
	ICC	ICC 95% CI		p	COV (%)	TRT SD	ICC	ICC 95% CI		p	COV (%)	TRT SD
		Upper limit	Lower limit					Upper limit	Lower limit			
NFI	0.982	0.972	0.989	<0.001	19.38	10.61	0.975	0.958	0.985	<0.001	15.82	12.84
TSNIT average	0.977	0.961	0.986	<0.001	4.40	3.53	0.977	0.961	0.986	<0.001	4.71	3.93
Superior average	0.920	0.878	0.950	<0.001	7.42	6.65	0.917	0.863	0.952	<0.001	7.88	6.86
Inferior average	0.960	0.939	0.975	<0.001	5.68	5.48	0.978	0.964	0.987	<0.001	5.36	5.13
TSNIT SD	0.951	0.924	0.969	<0.001	9.11	3.23	0.970	0.951	0.983	<0.001	8.30	2.83

ICC: intraclass correlation coefficient; CI: confidence interval; COV: coefficient of variation; TRT SD: test-retest variability; NFI: nerve fiber indicator; TSNIT: temporal-superior-nasal-inferior-temporal; SD: standard deviation.

Although we also evaluated the reproducibility of the NFI, it does not seem to be the best parameter for detecting glaucoma progression. NFI is a machine-learning classifier based on a linear support vector machine, not a parameter to measure disease severity. We found that NFI showed the best ICC (0.982) in the intravisit session and extremely good intervisit session reproducibility (ICC = 0.975) in the glaucoma group, but in all cases with a worse COV. In fact, the Guided Progression Analysis software provided by the manufacturer does not rely on the NFI to compare measurements over time, but on the TSNIT average, superior average, and inferior average, as well as different maps and graphs.

Sánchez-García et al. [19] recently evaluated the repeatability of RNFL parameters measured with SLP-VCC in 75 normal eyes and reported good results. They compared the variability between SLP-VCC, Cirrus optical coherence tomography, and confocal scanning laser tomography. They observed less fluctuation between examinations with SLP-VCC, particularly in the superior RNFL. It should be noted, however, that their intravisit measurements were based on only two scans. Similar findings for intravisit variability were reported by Rao et al. [20], who assessed the repeatability of SLP-ECC in 140 eyes of 73 healthy subjects. Their COVs ranged between 1.7% (average TSNIT) and 11.4% (NFI).

Garas et al. [21] used the COV to assess the intravisit repeatability of RNFL thicknesses measured with RTVue-100 spectral-domain optical coherence tomography, SLP-VCC, and SLP-ECC in 37 eyes, including 14 normal or ocular hypertensive eyes and 23 eyes with moderate to severe glaucoma. COVs for the average thickness and the RNFL thickness in the four quadrants were less than 10% in eyes with moderate to severe glaucoma.

The present study has some limitations. First, only good quality images with a signal strength of at least 7 were included in the statistical analysis, which might have influenced the upper and lower limits of the variability of SLP-ECC parameters. Thus, our results can be applied to patients with moderate and good quality scans, while worse reproducibility results may be expected when diagnosing glaucoma progression based on a series that includes poor quality images. Further studies are needed to clarify the effect of low quality scans, such as those obtained in subjects with media opacities, which is common in daily clinical practice. Second, some glaucoma patients had previous experience with SLP testing, which might have contributed to the low variability observed in this group. This seems unlikely, because there is no evidence that SLP requires a training period due to a learning effect. Third, despite the fact that our sample comprised a wide range of glaucoma severities, our results may not extrapolate to all clinical situations [22].

In conclusion, intravisit and intervisit measurements of peripapillary RNFL obtained with SLP-ECC had excellent reproducibility. Clinicians must take into account the reproducibility of every SLP-ECC parameter to differentiate variability and true progression when monitoring patients with glaucoma.

Conflict of Interests

The authors declare that there is no conflict of interests regarding the publication of this paper.

Acknowledgment

The paper is supported in part by the Instituto de Salud Carlos III Grant PI1101239 with FEDER funds.

References

[1] R. N. Weinreb, S. Shakiba, and L. Zangwill, "Scanning laser polarimetry to measure the nerve fiber layer of normal and glaucomatous eyes," *American Journal of Ophthalmology*, vol. 119, no. 5, pp. 627–636, 1995.

[2] Q. Zhou and R. N. Weinreb, "Individualized compensation of anterior segment birefringence during scanning laser polarimetry," *Investigative Ophthalmology and Visual Science*, vol. 43, no. 7, pp. 2221–2228, 2002.

[3] H. Bagga, D. S. Greenfield, and W. J. Feuer, "Quantitative assessment of atypical birefringence images using scanning laser polarimetry with variable corneal compensation," *American Journal of Ophthalmology*, vol. 139, no. 3, pp. 437–446, 2005.

[4] M. Sehi, D. C. Guaqueta, and D. S. Greenfield, "An enhancement module to improve the atypical birefringence pattern using scanning laser polarimetry with variable corneal compensation," *The British Journal of Ophthalmology*, vol. 90, no. 6, pp. 749–753, 2006.

[5] T. A. Mai, N. J. Reus, and H. G. Lemij, "Diagnostic accuracy of scanning laser polarimetry with enhanced versus variable corneal compensation," *Ophthalmology*, vol. 114, no. 11, pp. 1988–1993, 2007.

[6] C. Bowd, I. M. Tavares, F. A. Medeiros, L. M. Zangwill, P. A. Sample, and R. N. Weinreb, "Retinal nerve fiber layer thickness and visual sensitivity using scanning laser polarimetry with variable and enhanced corneal compensation," *Ophthalmology*, vol. 114, no. 7, pp. 1259–1265, 2007.

[7] M. Sehi, D. C. Guaqueta, W. J. Feuer, and D. S. Greenfield, "Scanning laser polarimetry with variable and enhanced corneal compensation in normal and glaucomatous eyes," *American Journal of Ophthalmology*, vol. 143, no. 2, pp. 272–279, 2007.

[8] F. A. Medeiros, L. M. Zangwill, L. M. Alencar, P. A. Sample, and R. N. Weinreb, "Rates of progressive retinal nerve fiber layer loss in glaucoma measured by scanning laser polarimetry," *The American Journal of Ophthalmology*, vol. 149, no. 6, pp. 908–915, 2010.

[9] M. Tóth and G. Holló, "Enhanced corneal compensation for scanning laser polarimetry on eyes with atypical polarisation pattern," *The British Journal of Ophthalmology*, vol. 89, no. 9, pp. 1139–1142, 2005.

[10] F. A. Medeiros, L. M. Zangwill, C. Bowd, and R. N. Weinreb, "Comparison of the GDx VCC scanning laser polarimeter, HRT II confocal scanning laser ophthalmoscope, and stratus OCT optical coherence tomograph for the detection of glaucoma," *Archives of Ophthalmology*, vol. 122, no. 6, pp. 827–837, 2004.

[11] A. Ferreras, L. E. Pablo, A. B. Pajarín, J. García-Feijoo, and F. M. Honrubia, "Scanning laser polarimetry: logistic regression analysis for perimetric glaucoma diagnosis," *Eye*, vol. 23, no. 3, pp. 593–600, 2009.

[12] P. E. Shrout and J. L. Fleiss, "Intraclass correlations: uses in assessing rater reliability," *Psychological Bulletin*, vol. 86, no. 2, pp. 420–428, 1979.

[13] H. D. Jampel, S. Vitale, Y. Ding et al., "Test-retest variability in structural and functional parameters of glaucoma damage in the glaucoma imaging longitudinal study," *Journal of Glaucoma*, vol. 15, no. 2, pp. 152–157, 2006.

[14] P. Fogagnolo, C. Sangermani, F. Oddone et al., "Long-term perimetric fluctuation in patients with different stages of glaucoma," *The British Journal of Ophthalmology*, vol. 95, no. 2, pp. 189–193, 2011.

[15] A. Azuara-Blanco, L. J. Katz, G. L. Spaeth, S. A. Vernon, F. Spencer, and I. M. Lanzl, "Clinical agreement among glaucoma experts in the detection of glaucomatous changes of the optic disk using simultaneous stereoscopic photographs," *The American Journal of Ophthalmology*, vol. 136, no. 5, pp. 949–950, 2003.

[16] L. E. Pablo, A. Ferreras, P. Fogagnolo, M. Figus, and A. B. Pajarín, "Optic nerve head changes in early glaucoma: a comparison between stereophotography and Heidelberg retina tomography," *Eye*, vol. 24, no. 1, pp. 123–130, 2010.

[17] K. A. Townsend, G. Wollstein, and J. S. Schuman, "Imaging of the retinal nerve fibre layer for glaucoma," *The British Journal of Ophthalmology*, vol. 93, no. 2, pp. 139–143, 2009.

[18] T. A. Mai, N. J. Reus, and H. G. Lemij, "Retinal nerve fiber layer measurement repeatability in scanning laser polarimetry with enhanced corneal compensation," *Journal of Glaucoma*, vol. 17, no. 4, pp. 269–274, 2008.

[19] M. Sánchez-García, R. Rodríguez De La Vega, M. González-Hernández, and M. González De La Rosa, "Variability and reproducibility of 3 methods for measuring the thickness of the nerve fiber layer," *Archivos de la Sociedad Española de Oftalmología*, vol. 88, no. 10, pp. 393–397, 2013.

[20] H. L. Rao, C. R. Venkatesh, K. Vidyasagar et al., "Retinal nerve fiber layer measurements by scanning laser polarimetry with enhanced corneal compensation in healthy subjects," *Journal of Glaucoma*, vol. 23, no. 9, pp. 589–593, 2014.

[21] A. Garas, M. Tóth, P. Vargha, and G. Holló, "Comparison of repeatability of retinal nerve fiber layer thickness measurement made using the RTVue fourier-domain optical coherence tomograph and the GDx scanning laser polarimeter with variable or enhanced corneal compensation," *Journal of Glaucoma*, vol. 19, no. 6, pp. 412–417, 2010.

[22] M. Gonzalez-Hernandez, L. E. Pablo, K. Armas-Dominguez, R. R. de la Vega, A. Ferreras, and M. G. de la Rosa, "Structure-function relationship depends on glaucoma severity," *The British Journal of Ophthalmology*, vol. 93, no. 9, pp. 1195–1199, 2009.

Hindawi Publishing Corporation
BioMed Research International
Volume 2015, Article ID 847694, 4 pages
http://dx.doi.org/10.1155/2015/847694

Clinical Study

Central Macular Thickness in Children with Myopia, Emmetropia, and Hyperopia: An Optical Coherence Tomography Study

Gordon S. K. Yau,[1] Jacky W. Y. Lee,[1,2] Tiffany T. Y. Woo,[1] Raymond L. M. Wong,[3] and Ian Y. H. Wong[2]

[1]*Department of Ophthalmology, Caritas Medical Centre, 111 Wing Hong Street, Kowloon, Hong Kong*
[2]*Department of Ophthalmology, University of Hong Kong, Room 301, Level 3 Block B, Cyberport 4, 100 Cyberport Road, Hong Kong*
[3]*Department of Ophthalmology and Visual Sciences, Hong Kong Eye Hospital, 147K Argyle Street, Kowloon, Hong Kong*

Correspondence should be addressed to Jacky W. Y. Lee; jackywylee@gmail.com

Received 4 August 2014; Accepted 17 August 2014

Academic Editor: Michele Iester

Purpose. To investigate the central macular thickness (CMT) in myopic, emmetropic, and hyperopic Chinese children using Optical Coherence Tomography. *Methods.* 168 right eyes of Chinese subjects aged 4–18 were divided into 3 groups based on their postcycloplegic spherical equivalent: myopes (< −1.0 D); emmetropes (≥ −1.0 to ≤+1.0 D); and hyperopes (>+1.0 D) and the CMT was compared before/after age adjustment. The CMT was correlated with age, axial length, and peripapillary retinal nerve fibre layer (RNFL). *Results.* The mean CMT was 274.9 ± 50.3 μm and the mean population age was 7.6 ± 3.3 years. The CMT was thickest in the myopes (283.3 ± 57.3 μm, $n = 56$), followed by the hyperopes (266.2 ± 55.31 μm, $n = 60$) and then emmetropes (259.8 ± 28.7 μm, $n = 52$) (all $P < 0.0001$). When adjusted for age, myopes had a thicker CMT than the other 2 groups (all $P < 0.0001$) but there was no CMT difference between the emmetropes and hyperopes ($P > 0.05$). There was no significant correlation between CMT with age, axial length, or peripapillary RNFL (all $P \geq 0.2$). *Conclusion.* Chinese children with myopia had a thicker CMT than those with emmetropia or hyperopia. There was no correlation of the CMT with age, axial length, or peripapillary RNFL thickness.

1. Introduction

Macular diseases such as macula edema and macula degenerations (hereditary or acquired) can severely affect central vision. Assessment of macular thickness is essential for the diagnosis and monitoring of these diseases. Optical coherence tomography (OCT) is a noninvasive imaging modality for the objective evaluation of the central retinal morphology as well as the measurement of retinal thicknesses [1, 2]. OCT has been demonstrated to be a well-tolerated investigational tool for glaucoma in children as young as the age of 4 [3]. Previous studies have found that female gender, greater birth weight, and infants with an older gestational age have been associated with a thinner central macular (foveal) thickness (CMT) [4, 5]. The CMT also varies with age and ethnicity [6, 7].

The correlation of refractive errors correlate with CMT is still an area of controversy. Huynh et al. [8] found that the CMT was thicker in hyperopic children while Wakitani et al. [9] reported a thicker CMT in myopic children and Lim et al. [10] found no significant correlation between refractive errors and CMT.

The prevalence of myopia ranges from 22.7% to 38.7% based on large population studies, with a higher prevalence in East Asian regions [11–13]. With age, the refractive status often changes from hyperopia to myopia; hence, it is important to understand the dynamic changes of CMT and refractive errors for the paediatric population. The purpose

of this study was to investigate the influence of refractive errors on CMT by comparing its differences in children with myopia, emmetropia, and hyperopia.

2. Patients and Methods

The study was conducted in accordance with the Declaration of Helsinki and no patient personal data was disclosed in the study. Study approval was obtained from the Institutional Review Board of the Hospital Authority of Hong Kong. Informed consent was obtained from the parents or legal guardian of the subjects.

This cross-sectional study recruited consecutive cases of paediatric subjects aged 4 to 18, attending the Ophthalmology specialist outpatient clinic of Caritas Medical Centre in Hong Kong Special Administrative Region, from 2013 to 2014. Subjects with only eye, ocular tumors, congenital glaucoma, congenital cataract, congenital nystagmus, microphthalmos, optic nerve or retinal disease, active ocular infections, corneal scars, and severe visual impairment of any cause (Snellen best corrected visual acuity ≤ 0.1) and amblyopia were excluded.

All subjects underwent a complete ophthalmological examination including ocular alignment and motility assessments as well as anterior and posterior segment examinations after pupil dilatation with a Tropicamide 1% and Phenylephrine hydrochloride 2.5% ophthalmic solution (Mydrin-P; Santen Pharmaceutical, Osaka, Japan).

2.1. Spherical Equivalent and Axial Length. All subjects received cycloplegic refraction with 3 drops of Cyclopentolate hydrochloride 1% (Bausch & Lomb, 1400 N. Goodman St., Rochester, NY, United States of America) administered 5 minutes apart to relieve all accommodative components. After at least 30 minutes, postcycloplegic autorefraction with a kerato-refractometer (Topcon KR-8900 by Topcon Europe Medical B.V., Essebaan 11, Capelle a/d Ijssel, Netherlands) was performed by an optometrist with at least 5 years of experience with paediatric assessment. The spherical equivalent was calculated in diopters (D). Axial length measurements in millimeters (mm) were obtained with the noncontact optical biometry (IOL Master; Carl Zeiss Meditec AG, Max-Dohrn-Straße 8-10, Berlin, Germany). Axial length measurements were performed 3 times by a single technician who was masked to subjects' clinical information, and the average of the 3 values was recorded. Poor signal values as well as values that differed by more than 0.1 mm were rejected and the measurement was repeated.

2.2. Optical Coherence Tomography Imaging. The Spectralis Spectral Domain OCT (Heidelberg Engineering, 1808 Aston Ave., Suite 103, Carlsbad, CA, USA) was performed after cycloplegia, by a single imaging technician who was masked to subjects' clinical information.

2.3. Peripapillary RNFL Thickness. Scans were centred on the optic disc with a scanning diameter of 3.5 mm and 768 A-scans were obtained using the high speed (HS) mode. To improve image quality, automatic real time (ART) function was used to obtain multiple frames during scanning and to optimize images by noise reduction. Scans were repeated 3 times and assessed for signal strength and centration. Scans with signal strength quality ≤ 16 or poor centration were excluded. RNFL thickness was analysed with the RNFL Single Exam Report OU with fovea-to-disc technology. The RNFL thickness of each of the 4 quadrants and the global RNFL thickness were recorded in micrometers (μm).

2.4. Central Macula Thickness Measurement. The Spectralis OCT has an axial image resolution of 7 μm, a lateral resolution of 14 μm, and a scanning velocity up to 40,000 A scans per second. CMT measurements were acquired using a dense (25-line) horizontal Raster Scan protocol, centred on the fovea with a distance of 240 μm between the horizontal scans. The TruTrack active eye tracking system was used to increase scan quality.

2.5. Statistics. Subjects were divided into 3 groups based on their postcycloplegic spherical equivalent: myopic (<−1.0 D); emmetropic (≥−1.0 to ≤+1.0 D); and hyperopic (>+1.0 D). Only the right eye of each subject was used for statistical analysis. Statistical significance was considered when $P < 0.05$. Means were expressed with standard deviations.

One-way ANOVA with Tukey's Multiple Comparison Test was used to compare the CMT among the 3 spherical equivalent groups before and after age adjustment. The *t*-test was used to compare the CMT between female and male subjects.

Pearson correlation was used to analyze the association between the following:

(i) CMT versus RNFL (global and quadrant) thicknesses,

(ii) CMT versus age,

(iii) CMT versus axial length.

3. Results

Of the 168 subjects eligible for the study, the mean age was 7.6 ± 3.3 years. The mean CMT was 274.9 ± 50.3 μm. There were 85 female and 83 male subjects; all were of Chinese ethnicity. There was no difference in the CMT between the female (268.9 ± 52.6 μm) and male (272 ± 45.0 μm) subjects ($P = 0.7$). There were 56 (33.3%) myopic eyes, 52 (31.0%) emmetropic eyes, and 60 (36.7%) hyperopic eyes. The age of the 3 groups was significantly different: 10.1 ± 4.1 years (myopic group), 6.9 ± 2.7 years (emmetropic group), and 6.5 ± 2.1 years (hyperopic group) (all $P < 0.0001$).

There was no statistically significant correlation of the CMT with RNFL, age, or axial length. The parameter means and correlations are summarized in Table 1.

The mean spherical equivalent was −3.9 ± 2.2 D in the myopic group, +0.1 ± 0.5 D in the emmetropic group, and +2.9 ± 1.5 D in the hyperopic group (all $P < 0.001$). The mean CMT in the myopic, emmetropic, and hyperopic groups was 283.3 ± 57.3 μm, 259.8 ± 28.7 μm, and 266.2 ± 55.31 μm, respectively. The CMT in the myopic group was significantly thicker than the emmetropic group ($P < 0.0001$) but there

Table 1: Correlation of CMT with RNFL, age, and axial length.

	Mean	Pearson r	P value
	RNFL		
Inferior	130.9 ± 25.3 μm	0.04	0.64
Superior	126.4 ± 23.1 μm	0.07	0.38
Nasal	65.01 ± 20.2 μm	0.11	0.16
Temporal	88.3 ± 20.5 μm	0.04	0.62
Average	102.7 ± 14.4 μm	0.10	0.20
	Age		
7.8 ± 3.5 years	−0.09	0.26	
	Axial length		
	22.9 ± 1.5 mm	0.004	0.96

RNFL: retinal nerve fibre layer.

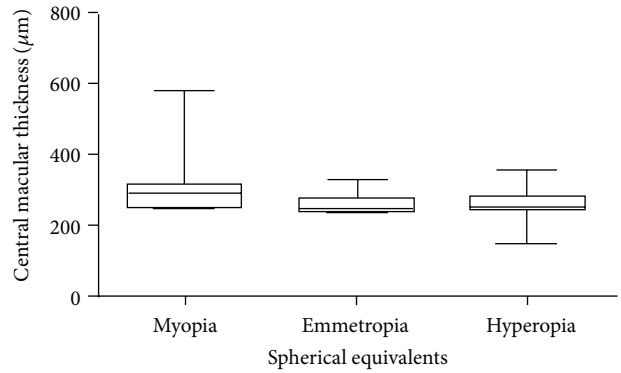

Figure 1: Differences in age-adjusted central macular thickness (mean ± standard deviation) in the myopic, emmetropic, and hyperopic children.

was no significant difference between the mean CMT of the other groups (all $P > 0.05$). Even though age was not found to be associated with CMT, in view of the statistically different age distribution of the 3 spherical equivalent groups, the mean CMT was reanalysed after age matching among the 3 spherical equivalent groups to eliminate the potential influence of age differences. When adjusted for age, the myopic group (298.2 ± 69.6 μm) had a significantly thicker CMT than both the emmetropic (261.3 ± 21.5 μm) and hyperopic group (265.3 ± 40.4) (both $P < 0.0001$). There was no significant difference in CMT between the emmetropic and hyperopic group ($P > 0.05$) (Figure 1).

4. Discussion

In our study, 33.3% of the study children had myopia and their mean age (10.1 ± 4.1 years) was significantly older than their emmetropic and hyperopic counterparts (all $P < 0.0001$).

Our findings were in agreement with Fan et al., who likewise reported that, in a population of Chinese children, 36.71 ± 2.87% were myopic and that the prevalence of myopia was positively correlated with age [14]. The higher prevalence of myopia in East Asian Children when compared with European Caucasians was found to be attributed to parental myopia and more myopigenic activities like long hours of near work and few outdoor time [15, 16].

In our study, we found that the mean CMT in the myopic group was 298.2 ± 69.6 μm which was significantly thicker than both the emmetropic (261.3 ± 21.5 μm) and hyperopic group (265.3 ± 40.4 μm) (both $P < 0.0001$). This finding was in agreement with Wakitani et al. [9] and Zhang et al. [6] but in contrast to Huynh et al. [8] who reported that CMT was positively correlated with hyperopia in an Australian paediatric population. These discrepancies can be largely explained by racial and age differences. Huynh et al. [8] only recruited 6-year-olds in their study while our study population consisted of children between the ages of 4–18. Thus, the proportion of hyperopia is much higher in Huynh's population given the younger age and predominant Caucasian race in their study. We are in agreement with the postulation by Wakitani et al. [9] that myopic eyes, the thicker CMT, serves as a compensatory mechanism at the expense of a thinner peripheral retina in order to preserve the fovea, which is more essential to vision.

Previous studies have demonstrated the gender difference of CMT with males who have thicker CMTs [4, 6, 8]. However, we did not defect any difference in CMT between males and females in our study ($P = 0.7$). There was no significant correlation between age and CMT in our study ($r = -0.09$; $P = 0.26$) which was in agreement with Zhang et al., Eriksson et al., and Göbel et al. [6, 17, 18]. Previous studies involving a Hong Kong Chinese population have demonstrated a positive correlation between axial length and CMT as reported by Lam et al. [19] ($r = 0.374$; $P < 0.001$) and Wong et al. [20] ($r = 5.37$; $P = 0.001$). However, we did not find any significant correlation between axial length and CMT in our study ($r = 0.004$; $P = 0.96$). These differences in associations can be attributed to the differences in sample size among different studies as well as differences in scanning protocol used among different OCT machines [21, 22].

Furthermore, there was no significant correlation between the peripapillary RNFL thickness and CMT. To the best of our knowledge, this is first study to investigate this correlation. This serves as a milestone for future research into this area for the paediatric population since, in adults, the peripapillary RNFL thickness has been associated with the CMT [23, 24], which can be used as a proxy measure of the RNFL in glaucoma patients with preexisting anatomical defects of the optic nerve hindering traditional RNFL monitoring by OCT. A longitudinal follow-up of our study population would also be useful to investigate the serial changes in CMT that comes with age and axial length elongation. Nevertheless, this is one of the few studies using the Spectralis OCT machine to quantify the CMT in a Chinese paediatric population and found that children with myopia had a thicker CMT than those with emmetropia or hyperopia. There was no correlation of the CMT with age, axial length, or peripapillary RNFL thickness. As this study was based on a Chinese pediatric population, the results may not be generalizable for other age groups and ethnicities.

Conflict of Interests

The authors declare that there is no conflict of interests regarding the publication of this paper.

References

[1] M. R. Hee, C. A. Puliafito, C. Wong et al., "Quantitative assessment of macular edema with optical coherence tomography," *Archives of Ophthalmology*, vol. 113, no. 8, pp. 1019–1029, 1995.

[2] W. Soliman, B. Sander, and T. M. Jørgensen, "Enhanced optical coherence patterns of diabetic macular oedema and their correlation with the pathophysiology," *Acta Ophthalmologica Scandinavica*, vol. 85, no. 6, pp. 613–617, 2007.

[3] M. A. El-Dairi, S. Holgado, S. G. Asrani, L. B. Enyedi, and S. F. Freedman, "Correlation between optical coherence tomography and glaucomatous optic nerve head damage in children," *British Journal of Ophthalmology*, vol. 93, no. 10, pp. 1325–1330, 2009.

[4] W. K. Song, S. C. Lee, E. S. Lee, C. Y. Kim, and S. S. Kim, "Macular thickness variations with sex, age, and axial length in healthy subjects: a spectral domain-optical coherence tomography study," *Investigative Ophthalmology and Visual Science*, vol. 51, no. 8, pp. 3913–3918, 2010.

[5] M. T. Yasser, A. Pai, H. Li et al., "Association of birth parameters with OCT measured macular and retinal nerve fibre layer thickness," *Investigative Ophthalmology & Visual Science*, vol. 52, no. 3, pp. 1709–1715, 2011.

[6] Z. Zhang, X. He, J. Zhu, K. Jiang, W. Zheng, and B. Ke, "Macular measurements using optical coherence tomography in healthy Chinese school age children," *Investigative Ophthalmology & Visual Science*, vol. 52, no. 9, pp. 6377–6383, 2011.

[7] C. Al-Hadda, A. Barikian, M. Jaroudi et al., "Spectral domain optical coherence tomography in children: normative data and biometric correlations," *BMC Ophthalmology*, vol. 14, no. 1, p. 53, 2014.

[8] S. C. Huynh, Y. W. Xiu, E. Rochtchina, and P. Mitchell, "Distribution of macular thickness by optical coherence tomography: findings from a population-based study of 6-year-old children," *Investigative Ophthalmology and Visual Science*, vol. 47, no. 6, pp. 2351–2357, 2006.

[9] Y. Wakitani, M. Sasoh, M. Sugimoto, Y. Ito, M. Ido, and Y. Uji, "Macular thickness measurements in healthy subjects with different axial lengths using optical coherence tomography," *Retina*, vol. 23, no. 2, pp. 177–182, 2003.

[10] M. C. Lim, S. T. Hoh, P. J. Foster et al., "Use of optical coherence tomography to assess variations in macular retinal thickness in myopia," *Investigative Ophthalmology & Visual Science*, vol. 46, no. 3, pp. 974–978, 2005.

[11] J. Katz, J. M. Tielsch, and A. Sommer, "Prevalence and risk factors for refractive errors in an adult inner city population," *Investigative Ophthalmology and Visual Science*, vol. 38, no. 2, pp. 334–340, 1997.

[12] T. Y. Wong, P. J. Foster, J. Hee, and et al, "Prevalence and risk factors for refractive errors in adult Chinese in Singapore," *Investigative Ophthalmology and Visual Science*, vol. 41, no. 9, pp. 2486–2494, 2000.

[13] Q. Wang, B. E. K. Klein, R. Klein, and S. E. Moss, "Refractive status in the Beaver Dam eye study," *Investigative Ophthalmology and Visual Science*, vol. 35, no. 13, pp. 4344–4347, 1994.

[14] D. S. Fan, D. S. Lam, R. F. Lam et al., "Prevalence, incidence, and progression of myopia of school children in Hong Kong," *Investigative Ophthalmology & Visual Science*, vol. 45, no. 4, pp. 1071–1175, 2004.

[15] A. N. French, I. G. Morgan, P. Mitchell, and K. A. Rose, "Patterns of myopigenic activities with age, gender and ethnicity in Sydney schoolchildren," *Ophthalmic and Physiological Optics*, vol. 33, no. 3, pp. 318–328, 2013.

[16] A. N. French, I. G. Morgan, P. Mitchell, and K. A. Rose, "Risk factors for incident myopia in Australian schoolchildren," *Ophthalmology*, vol. 120, no. 10, pp. 2100–2108, 2013.

[17] U. Eriksson, G. Holmström, A. Alm, and E. Larsson, "A population-based study of macular thickness in full-term children assessed with Stratus OCT: normative data and repeatability," *Acta Ophthalmologica*, vol. 87, no. 7, pp. 741–745, 2009.

[18] W. Göbel, F. Hartmann, and W. Haigis, "The correlation between retina thickness and axial length as well as age, measured by optical coherence tomography," *Ophthalmologe*, vol. 98, no. 2, pp. 157–162, 2001.

[19] D. S. Lam, K. S. Leung, S. Mohamed et al., "Regional variations in the relationship between macular thickness measurements and myopia," *Investigative Ophthalmology & Visual Science*, vol. 48, no. 1, pp. 376–382, 2007.

[20] A. C. M. Wong, C. W. N. Chan, and S. P. Hui, "Relationship of gender, body mass index, and axial length with central retinal thickness using optical coherence tomography," *Eye*, vol. 19, no. 3, pp. 292–297, 2005.

[21] S. Grover, R. K. Murthy, V. S. Brar, and K. V. Chalam, "Comparison of retinal thickness in normal eyes using stratus and spectralis optical coherence tomography," *Investigative Ophthalmology and Visual Science*, vol. 51, no. 5, pp. 2644–2647, 2010.

[22] U. E. K. Wolf-Schnurrbusch, L. Ceklic, C. K. Brinkmann et al., "Macular thickness measurements in healthy eyes using six different optical coherence tomography instruments," *Investigative Ophthalmology and Visual Science*, vol. 50, no. 7, pp. 3432–3437, 2009.

[23] F. A. Medeiros, L. M. Zangwill, C. Bowd, R. M. Vessani, R. Susanna Jr., and R. N. Weinreb, "Evaluation of retinal nerve fiber layer, optic nerve head, and macular thickness measurements for glaucoma detection using optical coherence tomography," *The American Journal of Ophthalmology*, vol. 139, no. 1, pp. 44–55, 2005.

[24] D. Manasia, L. Voinea, I. D. Vasinca et al., "Correlation between macular changes and the peripapillary nerve fiber layer in primary open angle glaucoma," *Journal of Medicine and Life*, vol. 7, no. 1, pp. 55–59, 2014.

Hindawi Publishing Corporation
BioMed Research International
Volume 2015, Article ID 853728, 5 pages
http://dx.doi.org/10.1155/2015/853728

Clinical Study

Correlation between Visual Acuity, Inner Segment/Outer Segment Junction, and Cone Outer Segment Tips Line Integrity in Uveitic Macular Edema

Paolo Tortorella, Enzo D'Ambrosio, Ludovico Iannetti, Federica De Marco, and Maurizio La Cava

Chorioretinal Diagnostic Service UOC Ophthalmology C, Department of Ophthalmology, "Sapienza" University of Rome, Viale del Policlinico, 15500161 Rome, Italy

Correspondence should be addressed to Ludovico Iannetti; l.iannetti@policlinicoumberto1.it

Received 24 July 2014; Revised 27 October 2014; Accepted 5 November 2014

Academic Editor: Michele Iester

Purpose. To investigate the correlation between best-corrected visual acuity (BCVA), the foveal inner segment/outer segment (IS/OS) junction or ellipsoid portion of inner segment (EPIS/ellipsoid zone), and the cone outer segment tips (COST) line or interdigitation zone integrity in eyes with uveitic macular edema (ME). *Method*. A retrospective observational study involving all patients from January 2012 to December 2013 with uveitic ME was performed. All patients underwent BCVA using Snellen charts spectral-domain optical coherence tomography (SD-OCT) examination using Spectralis OCT (Heidelberg Engineering, Heidelberg, Germany). *Results*. Fifty-two eyes from 45 patients were included in this study. Multivariate analysis showed a negative correlation between BCVA and the central retinal subfield thickness (CST), the cystoid pattern of edema, and the interdigitation zone interruption. Univariate logistic analysis showed a strong correlation between the ellipsoid zone and the interdigitation zone integrity. *Conclusions*. The ellipsoid zone defect, the interdigitation zone interruption, and the CST are correlated with poor vision. Visual acuity is also strongly affected by the cystoid pattern. The interdigitation zone integrity appears to be the most important factor in the visual prognosis of uveitic ME.

1. Introduction

Macular edema (ME) is a typical, but nonspecific, complication of uveitis and occurs most frequently in those with vitreous involvement. ME is among the leading causes of decreased vision in patients with uveitis [1, 2].

In the literature, ME is described in intermediate uveitis (25–70%), anterior uveitis (20–26%), panuveitis (35%), and posterior uveitis (20%) and it can dramatically affect vision [3].

Acute retinal necrosis, birdshot chorioretinopathy, Adamantiades-Behçet's disease, juvenile idiopathic arthritis, and sarcoidosis are the most common uveitis entities associated with ME [4].

Optical coherence tomography (OCT) is a noncontact and noninvasive diagnostic technique, which is increasingly used for diagnosing macular pathology and evaluating the response to therapy [4–7]. OCT provides a fundamental contribution to the diagnosis, guidance, and treatment of retinal pathologies such as macular edema, macular holes, epiretinal membranes, central serous chorioretinopathy, and age-related macular degeneration [5, 6].

In previous studies [2, 4, 8, 9] OCT findings were used to describe the three different morphologic patterns of ME: diffuse macular edema (DME), cystoid macular edema (CME), and serous retinal detachment (SRD). CME consists of low-reflective intraretinal spaces, clearly defined and separated by thin, high-reflective retinal tissue [2]. CME is one of the most frequent complications of uveitis and causes both blindness and visual impairment (29% and 41%, resp.) in uveitic patients [10]. DME consists of increased macular thickness, small low-reflective areas with spongy appearance of the retinal layers and SRD consists of a neuroretinal layer separation from the retinal pigment epithelium (RPE) [2].

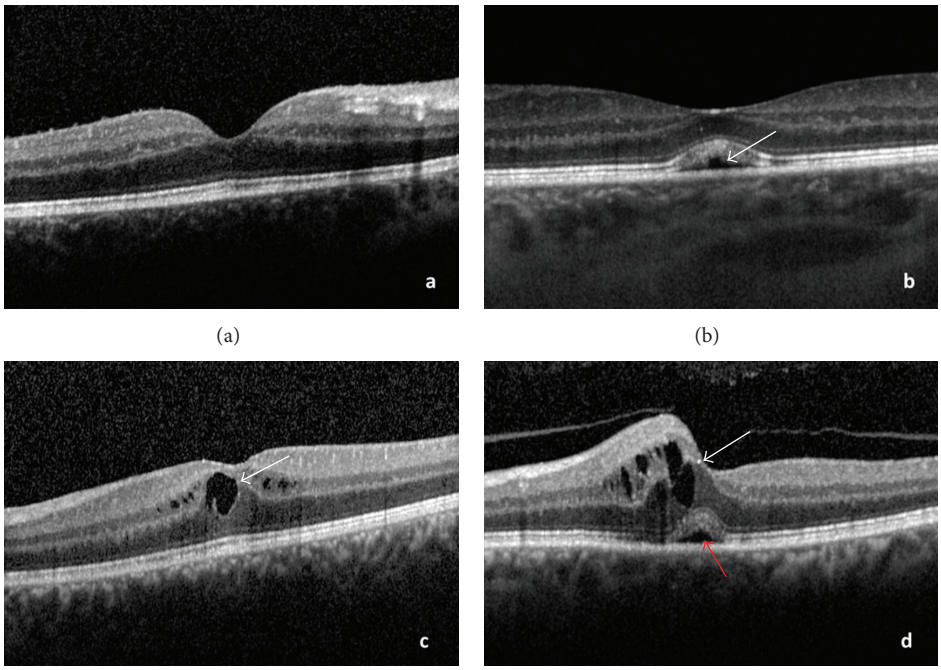

Figure 1: (a) Diffuse macular edema (DME). (b) DME associated with serous detachment of the neuroepithelium (SRD) (white arrow). (c) Cystoid macular edema (CME) (white arrow). (d) CME (white arrow) associated with SRD (red arrow).

Spectral-domain OCT (SD-OCT), the new OCT generation, was introduced recently. It provides a higher resolution and image formation up to 100-fold faster than the conventional time-domain OCT [11]. SD-OCT is equipped with an automatic and time system that performs the average of multiple B scan frames of the same site, providing an improved image quality [8]. The ability of SD-OCT to create images of tissue morphology in situ and in real time has been termed "optical biopsy." High-resolution cross-sectional OCT scans can assist detailed analysis and evaluation of retinal lesions [7].

The integrity of the outer retinal layers—and particularly the photoreceptor layer—has gained much interest because of its close correlation with visual function [12]. A number of studies have highlighted this important correlation, encouraging a detailed analysis of the external retinal layers [13–17].

On SD-OCT, the outer retina has four distinct hyperreflective lines, which represent the external limiting membrane (ELM), inner and outer segments of the photoreceptors (IS/OS) junction otherwise named ellipsoid portion of inner segment (EPIS/ellipsoid zone), the cone outer segment tips (COST) otherwise named interdigitation zone, referred to as the intermediate line or Verhoeff's membrane, and the RPE. The innermost ELM is formed by the back reflection of the zonulae adherentes that joins the inner segment to the Müller cells. The EPIS is thought to represent the boundary between the inner and outer segments of the photoreceptors and is localized between the ELM and the RPE histologically. The interdigitation zone represents the outer tip of the cones. The outermost RPE line separates the photoreceptors from Bruch's membrane and choriocapillaris [12].

The purpose of the present study was to investigate the correlation between the best-corrected visual acuity (BCVA), the foveal EPIS, and interdigitation zone integrity in eyes with uveitic ME.

2. Materials and Methods

A retrospective observational study was performed on all patients with uveitic ME from January 2012 to December 2013. Inclusion criteria were ME diagnosed ophthalmoscopically associated with any anatomical type of uveitis (anterior, intermediate, posterior, and diffuse).

Exclusion criteria were other coexisting ocular diseases limiting visual acuity (VA): amblyopia, cataract, optic atrophy, macular epiretinal membrane (ERM), macular hole, or central scars.

Informed consent was obtained from all patients involved in this research. The study was conducted in accordance with local and regional regulations, good clinical practice, and the tenets of the Declaration of Helsinki.

The BCVA using Snellen charts was performed. ME was diagnosed by clinical examination.

All patients underwent SD-OCT examination with Spectralis OCT (Heidelberg Engineering, Heidelberg, Germany). Raster scans (20×15 degrees) consisting of 37 high-resolution horizontal B-scans were performed. SD-OCT evaluation was performed by three ophthalmologists.

Four patterns of ME, DME (Figure 1(a)), CME (Figure 1(c)), and SRD in combination with DME (Figure 1(b)) or with CME (Figure 1(d)), corresponding

to a concentric zone of 1 mm in diameter around the fovea, were defined as reported previously [2].

An evaluation of the central subfield retinal thickness (CST), the integrity or disruption of the interdigitation zone (Figure 2(a)), the integrity or disruption of the EPIS (Figure 2(b)), and the integrity or disruption of the interdigitation zone and the EPIS together (Figure 2(c)) was performed.

The CST measurement was considered a continuous variable and the mean ± SD was calculated. The decimal BCVA was measured on the Snellen decimal chart and considered ordinal data. As seen in the population distribution analysis of BCVA, the underlying population distribution did not exhibit a normal continuous distribution, even considering the BCVA above unity. Moreover, for retrospective studies, the truncation to 10/10 introduces a ceiling effect, making the normality assumption unsuitable (even asymptomatically) nor fixable using logMAR conversion. Thus, the median (1st–3rd quartile) values were reported. For the multivariate analysis, ordinal probit regression analysis (with CLM in the "ordinal" package) was used in the "*R* for statistical computing" environment, version 2.16 [18–20]. The correlations between the BCVA and CST, ME pattern, the integrity of the foveal EPIS, and the interdigitation zone were evaluated by multivariate correlation analysis. The full model was then evaluated by applying a stepwise procedure in both directions, automatically and manually, exploring interaction terms. The coefficients for the CLM model indicate the direction and strength of the effect of the covariate and were reported graphically, rather than numerically; + (−) was used to represent coefficients between 0 and 1 (−1) and ++ (− −) for coefficients >1 (< −1). *P* values were calculated using the Wald test. The CST in the multivariate analysis was intended to measure a 100 μm increase in thickness. Univariate logistic regression analysis between the interdigitation zone interruption and the EPIS interruption was performed in *R* using GLM.

3. Results

Fifty-two eyes from 45 patients affected by uveitis, complicated by ME, with a median age of 32 years (Q_1–Q_3 9–77) were included in this study. The patients comprised 22 males and 23 females. Demographic and clinical characteristics of the study population are summarized in Table 1.

According to the site of inflammation, following the criteria of the Standardization of Uveitis Nomenclature [21], uveitis was classified as anterior in 12 eyes (23.07%), intermediate in 20 (38.46%), posterior in 7 (13.46%), and diffuse in 13 (25%) eyes.

The median duration of uveitis at examination was 48 months (Q_1–Q_3 2–204). The median BCVA was 0.6 (Q_1–Q_3 0.03–1.0). The mean (SD) CST was 411 μm (±203).

SDOCT revealed DME in 39 eyes (75%), CME in 13 eyes (25%), and foveal SRD in 11 eyes (21.15%). SRD was found in combination with other forms of ME. In particular, three eyes (5.76%) presented SRD in combination with DME and eight eyes (15.38%) presented SRD in combination with CME.

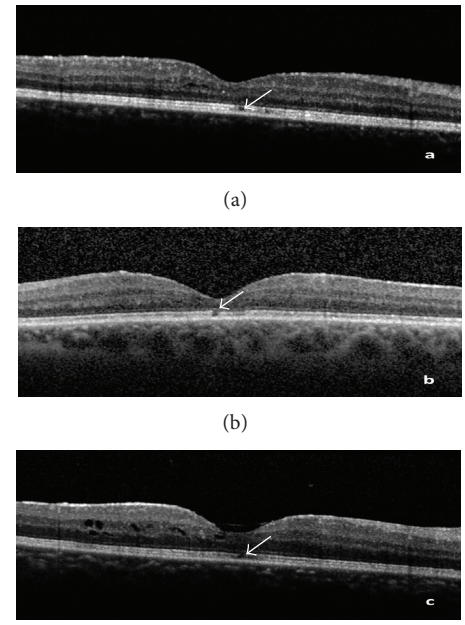

(a)

(b)

(c)

Figure 2: (a) Disruption of interdigitation zone. (b) Disruption of the EPIS. (c) Disruption of interdigitation zone and EPIS together (white arrows).

Table 1: Demographic and clinical characteristics of the study population.

Median age (Q_1–Q_3)	32 (9–77)
Gender	
Male/female	22/23
Median FU mos (Q_1–Q_3)	25.5 (1–260)
Median duration (Q_1–Q_3)	48 (2–204)
Laterality	
Unilateral	38 (84.4%)
Bilateral	7 (15.6%)
Anatomic location of uveitis (eyes)	
Anterior	12 (23.1%)
Intermediate	20 (38.5%)
Posterior	7 (13.5%)
Panuveitis	13 (25%)
Classification of uveitis (patients)	
Idiopathic	36 (80%)
TBC	2 (4.4%)
Behçet	2 (4.4%)
VKH	2 (4.4%)
JIA	5 (11.1%)
Birdshot	1 (2.2%)
B27 + AAU	2 (4.4%)

The median BCVA in eyes with DME was 0.7 (Q_1–Q_3 0.03–1.0), that in eyes with CME was 0.6 (Q_1–Q_3 0.06–1.0), and that in eyes with foveal SRD was 0.4 (Q_1–Q_3 0.03–1.0).

Table 2: Number of eyes, mean foveal thickness, and median BCVA according to the different morphological features observed.

	N of eyes (% on 52 eyes)	Mean CST ± SD	Median BCVA (Q_1–Q_3)
DME	39 (75%)	354 ± 124	0.7 (0.03–1.0)
CME	13 (25%)	430 ± 222	0.6 (0.06–1.0)
SRD	11 (21.2%)	432 ± 154	0.4 (0.03–1.0)
No SRD	41 (78.8%)	406 ± 216	0.7 (0.06–1.0)
DME + SRD	3 (5.8%)	372 ± 176	0.7 (0.1–1.0)
CME + SRD	8 (15.4%)	467 ± 257	0.6 (0.1–1.0)
COST line disruption	13 (25%)	602 ± 303	0.2 (0.06–0.8)
COST line integrity	39 (75%)	348 ± 99	0.8 (0.03–1.0)
IS/OS junction disruption	26 (50%)	480 ± 253	0.35 (0.06–1.0)
IS/OS junction integrity	26 (50%)	342 ± 102	0.9 (0.03–1.0)

Interruption of the EPIS was observed in 26 eyes (50%), and interruption of the interdigitation zone in 13 eyes (25%). The median BCVA in eyes with EPIS interruption was 0.35 (Q_1–Q_3 0.06–1.0) and it was 0.2 (Q_1–Q_3 0.06–0.8) in eyes with interdigitation zone interruption. The morphological features on SD-OCT with the corresponding CST and BCVA are reported in Table 2.

The multivariate regression showed a negative correlation between BCVA and CST ($P = 0.0009$), CME ($P = 0.012$), interdigitation zone interruption ($P = 0.0005$), and age ($P = 0.003$). The univariate logistic analysis showed a strong correlation between the EPIS segment and the interdigitation zone integrity ($P = 0.04$). In the multivariate analysis the EPIS or interdigitation zone interruption had the same effect and led to generation of comparable models (ANOVA LR $P = 0.29$).

4. Discussion

This study showed the correlations between VA and the cystoid pattern of ME, CST, EPIS, and interdigitation zone integrity in uveitic ME.

VA was strongly affected by the cystoid pattern ($P = 0.012$). High values of CST, which represent the increase in thickness and volume of the foveal area, negatively affect visual function ($P = 0.0009$). These results are in agreement with previous studies of ME secondary to uveitis [2, 8, 9].

In our study, the interdigitation zone interruption was the factor most significantly associated with poor vision ($P = 0.0005$). No previous study has investigated the correlation between VA and the interdigitation zone integrity in patients with uveitic ME. However, the importance of interdigitation zone integrity has been reported in other studies of various ocular diseases [13, 14, 22–24].

Ito et al. showed a strong correlation between VA and the status of the external limiting membrane (ELM), the status of the EPIS, and the status of the interdigitation zone in diabetic ME [13].

Shimozono et al. considered the status of the interdigitation zone, in conjunction with the EPIS, to be a useful prognostic factor after ERM surgery. The photoreceptor status at 1 month, especially the interdigitation zone, was the parameter most strongly correlated with the BCVA at 6 months after ERM surgery [14].

Itoh et al. reported a strong correlation between the interdigitation zone defect and the BCVA after pars plana vitrectomy for ERM removal. The interdigitation zone defect was significantly correlated with postoperative BCVA at 3, 6, 9, and 12 months, but not 1 month, postoperatively, suggesting continuous postoperative recovery from 1 to 12 months [22].

Itoh et al. investigated the correlation between the recovery of foveal cone microstructure and the BCVA after macular hole surgery. Eyes with an intact ELM and EPIS at 12 months and a distinct or irregular interdigitation zone had significantly better BCVA than those with a disrupted interdigitation zone [23]. Itoh et al. also showed that the length of the interdigitation zone defect was significantly correlated with VA at each postoperative timepoint. The integrity of the interdigitation zone, rather than the EPIS and ELM lines, may be a better clinical indicator of postoperative visual recovery in patients with surgically closed macular holes. They concluded that measurement of the preoperative length of the interdigitation zone may be an objective predictive factor of postoperative visual recovery [24].

It has been reported that disruption of the EPIS is associated with poor vision in uveitic ME [2].

Maheshwary et al. reported a significant negative correlation between VA and disruption of the EPIS in patients with diabetic ME. The rate of EPIS disruption evaluated by SD-OCT was revealed to be a significant predictor of VA [25].

In our previous study, EPIS disruption was strongly associated with CSF in uveitic ME but appears to be independent of the site of inflammation [2]. In this study, the differences among the groups were not statistically significant due to the small sample size.

Our statistical analysis showed a strong correlation between the EPIS and the interdigitation zone integrity ($P = 0.04$) which has not been reported previously in uveitic ME. EPIS disruption and the interdigitation zone defect, when considered together, showed a negative correlation with BCVA.

In conclusion, decreased vision has not been reported to be associated with the interdigitation zone defect in ME secondary to uveitis. Interdigitation zone integrity appears to be the most important factor in the visual prognosis of uveitic

ME. An EPIS defect and interdigitation zone interruption and retinal thickness are correlated with poor vision. Also, the cystoid pattern affects VA. Further studies should investigate the prognostic role of the interdigitation zone in uveitic ME.

Disclosure

No funding was received for this work by National Institutes of Health, Wellcome Trust, Howard Hughes Medical Institute, or other institutes. The English language in this document has been checked by at least two professional editors, both of whom are native speakers of English. For a certificate, please see http://www.textcheck.com/certificate/of7ahl.

Conflict of Interests

The authors declare that there is no conflict of interests regarding the publication of this paper. They have no financial interest in any of the products mentioned in the paper.

References

[1] M. H. Levin, M. Pistilli, E. Daniel et al., "Incidence of visual improvement in uveitis cases with visual impairment caused by macular edema," *Ophthalmology*, vol. 121, no. 2, pp. 588.e1–595.e1, 2014.

[2] L. Iannetti, G. Spinucci, A. Abbouda, D. De Geronimo, P. Tortorella, and M. Accorinti, "Spectral-domain optical coherence tomography in uveitic macular edema: morphological features and prognostic factors," *Ophthalmologica*, vol. 228, no. 1, pp. 13–18, 2012.

[3] P. Pivetti-Pezzi, M. Accorinti, M. La Cava, R. A. M. C. Gisoldi, and M. A. Abdulaziz, "Endogenous uveitis: an analysis of 1,417 cases," *Ophthalmologica*, vol. 210, no. 4, pp. 234–238, 1996.

[4] N. N. Markomichelakis, I. Halkiadakis, E. Pantelia et al., "Course of macular edema in uveitis under medical treatment," *Ocular Immunology and Inflammation*, vol. 15, no. 2, pp. 71–79, 2007.

[5] C. A. Puliafito, M. R. Hee, C. P. Lin et al., "Imaging of macular diseases with optical coherence tomography," *Ophthalmology*, vol. 102, no. 2, pp. 217–229, 1995.

[6] A. Domalpally, M. M. Altaweel, J. H. Kempen et al., "Optical coherence tomography evaluation in the multicenter uveitis steroid treatment (MUST) trial," *Ocular Immunology and Inflammation*, vol. 20, no. 6, pp. 443–447, 2012.

[7] S. Onal, I. Tugal-Tutkun, P. Neri, and C. P Herbort, "Optical coherence tomography imaging in uveitis," *International Ophthalmology*, vol. 34, no. 2, pp. 401–435, 2014.

[8] L. Iannetti, M. Accorinti, M. Liverani, C. Caggiano, R. Abdulaziz, and P. Pivetti-Pezzi, "Optical coherence tomography for classification and clinical evaluation of macular edema in patients with uveitis," *Ocular Immunology and Inflammation*, vol. 16, no. 4, pp. 155–160, 2008.

[9] N. N. Markomichelakis, I. Halkiadakis, E. Pantelia et al., "Patterns of macular edema in patients with uveitis: qualitative and quantitative assessment using optical coherence tomography," *Ophthalmology*, vol. 111, no. 5, pp. 946–953, 2004.

[10] A. Rothova, M. S. A. Suttorp-van Schulten, W. Frits Treffers, and A. Kijlstra, "Causes and frequency of blindness in patients with intraocular inflammatory disease," *British Journal of Ophthalmology*, vol. 80, no. 4, pp. 332–336, 1996.

[11] S. Wolf and U. Wolf-Schnurrbusch, "Spectral-domain optical coherence tomography use in macular diseases: a review," *Ophthalmologica*, vol. 224, no. 6, pp. 333–340, 2010.

[12] I. Y. Wong, L. P. Iu, H. Koizumi, and W. W. Lai, "The inner segment/outer segment junction: what have we learnt so far?" *Current Opinion in Ophthalmology*, vol. 23, no. 3, pp. 210–218, 2012.

[13] S.-I. Ito, N. Miyamoto, K. Ishida, and Y. Kurimoto, "Association between external limiting membrane status and visual acuity in diabetic macular oedema," *British Journal of Ophthalmology*, vol. 97, no. 2, pp. 228–232, 2013.

[14] M. Shimozono, A. Oishi, M. Hata et al., "The significance of cone outer segment tips as a prognostic factor in epiretinal membrane surgery," *American Journal of Ophthalmology*, vol. 153, no. 4, pp. 698.e1–704.e1, 2012.

[15] Y. Mitamura, S. Mitamura-Aizawa, T. Katome et al., "Photoreceptor impairment and restoration on optical coherence tomographic image," *Journal of Ophthalmology*, vol. 2013, Article ID 518170, 7 pages, 2013.

[16] M. Pircher, J. S. Kroisamer, F. Felberer, H. Sattmann, E. Götzinger, and C. K. Hitzenberger, "Temporal changes of human cone photoreceptors observed in vivo with SLO/OCT," *Biomedical Optics Express*, vol. 2, no. 1, pp. 100–112, 2011.

[17] V. J. Srinivasan, B. K. Monson, M. Wojtkowski et al., "Characterization of outer retinal morphology with high-speed, ultrahigh-resolution optical coherence tomography," *Investigative Ophthalmology and Visual Science*, vol. 49, no. 4, pp. 1571–1579, 2008.

[18] R Core Team, *R: A Language and Environment for Statistical Computing*, R Foundation for Statistical Computing, Vienna, Austria, 2012.

[19] R. H. B. Christensen, "Ordinal-regression models for ordinal data," R Package Version 22, 2010.

[20] R. H. B. Christensen, "Analysis of ordinal data with cumulative link models-estimation with the R-package ordinal," 2011.

[21] D. A. Jabs, R. B. Nussenblatt, J. T. Rosenbaum, and Standardization of Uveitis Nomenclature (SUN) Working Group, "Standardization of uveitis nomenclature for reporting clinical data. Results of the first international workshop," *The American Journal of Ophthalmology*, vol. 140, no. 3, pp. 509–516, 2005.

[22] Y. Itoh, M. Inoue, T. Rii, K. Hirota, and A. Hirakata, "Correlation between foveal cone outer segment tips line and visual recovery after epiretinal membrane surgery," *Investigative Ophthalmology and Visual Science*, vol. 54, no. 12, pp. 7302–7308, 2013.

[23] Y. Itoh, M. Inoue, T. Rii, T. Hiraoka, and A. Hirakata, "Significant correlation between visual acuity and recovery of foveal cone microstructures after macular hole surgery," *American Journal of Ophthalmology*, vol. 153, no. 1, pp. 111.e1–119.e1, 2012.

[24] Y. Itoh, M. Inoue, T. Rii, T. Hiraoka, and A. Hirakata, "Correlation between length of foveal cone outer segment tips line defect and visual acuity after macular hole closure," *Ophthalmology*, vol. 119, no. 7, pp. 1438–1446, 2012.

[25] A. S. Maheshwary, S. F. Oster, R. M. S. Yuson, L. Cheng, F. Mojana, and W. R. Freeman, "The association between percent disruption of the photoreceptor inner segment- outer segment junction and visual acuity in diabetic macular edema," *American Journal of Ophthalmology*, vol. 150, no. 1, pp. 63.e1–67.e1, 2010.

Hindawi Publishing Corporation
BioMed Research International
Volume 2015, Article ID 268796, 6 pages
http://dx.doi.org/10.1155/2015/268796

Clinical Study

Ganglion Cell Complex Evaluation in Exudative Age-Related Macular Degeneration after Repeated Intravitreal Injections of Ranibizumab

Andrea Perdicchi,[1] Giacomo Peluso,[1] Daniela Iacovello,[1] Marco Balestrieri,[1] Martina Delle Fave,[1] Solmaz Abdolrahimzadeh,[2] Gian Luca Scuderi,[1] Vito Fenicia,[1] and Santi Maria Recupero[1]

[1]*Ophthalmology Unit, NESMOS Department, Sant'Andrea Hospital, Faculty of Medicine and Psychology, "Sapienza" University of Rome, Via di Grottarossa 1035-1039, 00189 Rome, Italy*
[2]*Ophthalmology Unit, Azienda Policlinico Umberto I, "Sapienza" University of Rome, Viale del Policlinico 155, 00186 Rome, Italy*

Correspondence should be addressed to Giacomo Peluso; peluso.doc@gmail.com

Received 21 August 2014; Revised 17 October 2014; Accepted 26 October 2014

Academic Editor: Antonio Ferreras

Purpose. To detect the effects of intravitreal ranibizumab injections on GCC in patients with wet AMD. *Methods*. 32 wet AMD eyes were selected and submitted at three ranibizumab injections. RTVue-OCT GCC and MM5 protocol were performed before treatment and twenty days after each injection. *Results*. At baseline mean GCC thickness was 93.9 ± 18.5 μm. Twenty days after each intravitreal injection it was, respectively, 85.8 ± 10.1, 86.5 ± 9.3, and 91.1 ± 11.5 μm, without statistical significance. A significant improvement in visual acuity ($P = 0.031$) and a reduction of mean foveal ($P = 0.001$) and macular thickness ($P = 0.001$) were observed. *Conclusion*. The clinical results confirm therapeutic efficacy of intravitreal injections of ranibizumab in wet AMD. A contemporary not statistically significant reduction of GCC thickness suggests that the loading phase of ranibizumab does not have any toxic effects on ganglion cell complex.

1. Introduction

Age-related macular degeneration (AMD) is the most common cause of severe vision deficiency in elderly people in industrialized countries [1]. Wet or neovascular AMD is characterized by growth of new blood vessels caused by an abnormal release of the vascular endothelial growth factor-A (VEGF-A). This process leads to intra- and subretinal hemorrhagic and/or exudative alterations, with a consequent hemorrhagic detachment of the macular area and subsequent degeneration scar with central vision loss in varying amounts depending on the case [2]. The use of antiangiogenic drugs (anti-VEGF-A antibodies), administered by intravitreal injection, is one of the most effective treatments of neovascular AMD [3]. Recently many antiangiogenic and steroid drugs have been proposed in the treatment of exudative AMD and other rare retinal diseases and among these, ranibizumab in particular, administered by intravitreal injections, was mainly used in the treatment of exudative AMD [4–10]. Usually a sequence of three intravitreal injections of ranibizumab, at one-month intervals, represents the first dose or so-called "loading phase" of therapy in exudative AMD [11]. Additional intravitreal injections may be administered as needed according to the clinical progress of maculopathy and data provided by optical coherence tomography (OCT) and fluorescein angiography (FAG).

It should be considered that VEGF-A is also an important neurotrophic factor involved in the central nervous system, for the development of many cell types, including glial and neural cells [12]. Therefore, if on one hand the administration of anti-VEGF-A drugs inhibits chorioretinal neoangiogenesis that is present in wet AMD, on the other it may also inhibit the neuroprotective function of VEGF-A, with toxic effects on the retinal nerve structures. The macula region contains

over 50% of all retinal ganglion cells and is probably the ideal region to detect early cell loss and changes over time because of the high density of cells. The function and structure of the retinal ganglion cells complex (GCC) encompass three layers in the inner retina: (1) the retinal nerve fiber layer (RNFL) which is made up of the ganglion cell axons, (2) the ganglion cell layer (GCL) which is made up of the ganglion cell bodies, and (3) the inner-plexiform layer (IPL) which is made up of the ganglion cell dendrites. It is also essential to realize that GCC analysis is not limited to the differential diagnosis and management of glaucoma but also is appliable in numerous neurological and retinal conditions.

The aim of our study was to detect the potential alteration and toxicity induced by the loading phase of therapy with ranibizumab (three intravitreal injections in three months) on ganglion cell complex (GCC) thickness measured by OCT in patients with wet AMD.

2. Methods

32 eyes of 32 patients, 16 men and 16 women, aged between 75 and 95 years (mean age ± SD, 79.4 ± 7.1 years) diagnosed with wet AMD, were selected. Inclusion criteria were best visual acuity better than 0.7 logMAR units at Snellen optotype in the eye affected by neovascular AMD, intraocular pressure (IOP) less than 20 mmHg, without current or past topic hypotensive therapy, and ultrasonic pachymetry between 520 and 580 μm. None of the patients had been previously treated with intravitreal injections. Exclusion criteria included retinal diseases responsible for maculopathy such as diabetic and/or hypertensive retinopathy or thrombosis of the retinal central vein. Other exclusion criteria were advanced cataract, anterior and/or posterior uveitis, optic neuritis, or dioptric means opacity that would make an OCT examination unreliable. According to the declaration of Helsinki, at the time of recruitment, informed consent to participate in the study was read and signed by all patients.

A complete ocular examination was performed on all patients within the week before the first intravitreal injection of ranibizumab, with the measurement of best corrected visual acuity by the ETDRS system and calculated in logMAR units, biomicroscopy of the anterior and posterior segments by slit lamp, examination of the ocular fundus with binocular indirect ophthalmoscopy, and evaluation of the retinal vascularization by fluorescein angiography (FAG). Intraocular pressure (IOP) was measured by Goldmann applanation tonometer and ICare tonometer [13].

Selected eyes were subsequently subjected to a cycle of three intravitreal injections of 0.5 mg of ranibizumab in a volume of 0.05 mL monthly. An OCT examination was performed the week before and twenty days after each injection. Ganglion cell complex (GCC) thickness was evaluated by GCC protocol of RTVue-OCT instrument (OPTOVUE), to assess the average value expressed in millimicrons (μm) of three layers constituting GCC (nerve fiber layer, ganglion cell layer, and inner plexiform layer) [14, 15], (Figure 1).

A macular map of 5 mm (MM5) protocol of RTVue-OCT was used to assess foveal and macular thickness (Figure 2).

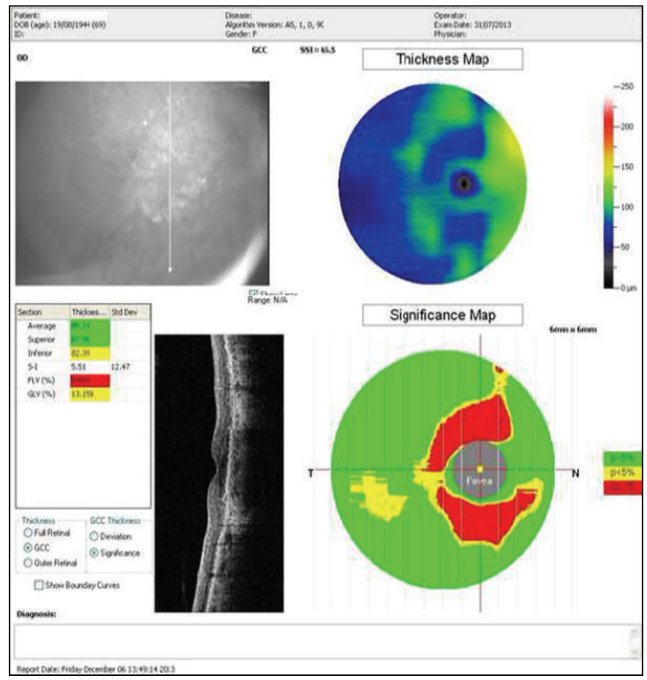

Section	Thickness (μm)	
	OD	OS
Average	93.12	93.75
Superior	90.99	92.75
Inferior	95.26	94.87

Figure 1: Thickness map, significance map, and average value of GCC.

Table 1: Baseline parameters.

Baseline	Eyes (n = 32)
Age (years)	79.4 ± 7.1
Sex M/F	16/16
Visual acuity (logMAR units)	0.34 ± 0.22
IOP (mmHg)	15 ± 1.9
Foveal thickness (μm)	354.3 ± 61.9
Macular thickness (μm)	326.8 ± 30.6
GCC thickness (μm)	93.9 ± 18.5

A numerical value, expressed in millimicrons (μm), placed at the center of the scanning macular map is the foveal thickness. Macular thickness was calculated by summing the values of thickness of each of the 9 map areas provided by OCT (central, inner/outer superior, inner/outer inferior, inner/outer nasal, and inner/outer temporal) and divided by the same number of areas.

Macular, foveal, and GCC thickness were evaluated at every control performed within 20 days after each injection of ranibizumab. All RTVue-OCT parameters were compared with the baseline parameters of each patient (Table 1). Intraocular pressure (IOP) was measured after each injection of ranibizumab at 3 times: an hour after treatment and the

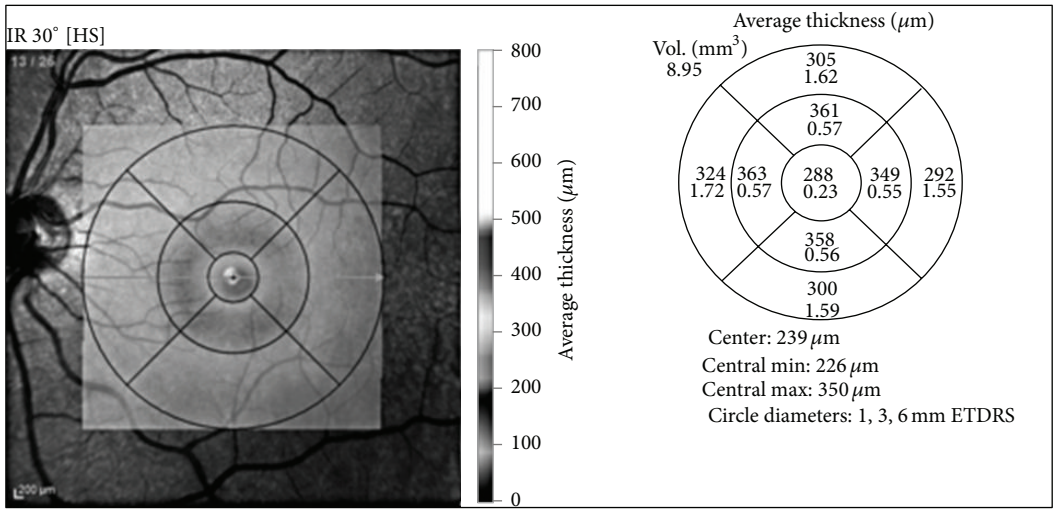

Figure 2: Example of macular map, divided into 9 areas.

day after and a third one at the control performed twenty days after the intravitreal injection.

3. Statistical Analysis

Student's t-test for independent data and for paired data was used to compare parameters assessed before and after each intravitreal injection. All quantitative values were expressed as mean and standard deviations (SDs). P value lower than 0.05 was considered statistically significant. Confidence interval was calculated at 95%. All tests were performed by SPSS software (Statistical Package for Social Science, 9th version) for Windows.

4. Results

In affected eyes mean visual acuity before treatment (baseline) was 0.34 ± 0.22 logMAR units. An average increase of −0.05 ± 0.06 logMAR units ($P = 0.019$) was observed 20 days after the first intravitreal (IVT) injection of ranibizumab, An average increase of −0.04 ± 0.17 logMAR units ($P = 0.004$) was observed 20 days after the second injection, and a steady mean visual acuity of 0.22 ± 0.27 logMAR units ($P = 0.031$) was observed 20 days after the third injection (Table 2).

Assessed mean ganglion cell complex (GCC) thickness was 93.9 ± 18.5 μm before the first injection (baseline). At a distance of 20 days after each intravitreal (IVT) injection, it was, respectively, 85.8 ± 10.1, 86.5 ± 9.3, and 91.1 ± 11.5 μm with an average reduction of 8.1 ± 20.2 μm ($P = 0.123$) after the 1st injection, 7.3 ± 22.3 μm ($P = 0.193$) after the 2nd, and 2.7 ± 19.6 μm ($P = 0.577$) after the 3rd (Table 3).

Assessed mean foveal thickness was 354.3 ± 61.9 μm before the first intravitreal injection (baseline). Foveal thickness was significantly reduced after each intravitreal (IVT) injection: 295.8 ± 56.6 μm after the first injection (mean reduction from baseline 58.5 ± 74.6 μm, $P = 0.005$), 290.2 ± 60.9 μm after the second injection (mean reduction from baseline 64.1 ± 82.6 μm, $P = 0.006$), and 290.8 ± 43.9 μm (mean reduction from baseline 63.4 ± 66.6 μm, $P = 0.001$) after the third (Table 4).

Table 2: Mean visual acuity (logMAR units).

	Cases ($n = 32$)	Difference from baseline	P value
Baseline	0.34 ± 0.22		
1° IVT	0.26 ± 0.23	−0.05 ± 0.06	(P) = 0.019
2° IVT	0.20 ± 0.23	−0.04 ± 0.17	(P) = 0.004
3° IVT	0.22 ± 0.27	−0.26 ± 0.23	(P) = 0.031

Table 3: Mean GCC thickness (μm).

	Cases ($n = 32$)	P value	95% CI
Baseline	93.9 ± 18.5		
1° IVT	85.8 ± 10.1	(P) = 0.123	−2.41; 18.46
2° IVT	86.5 ± 9.3	(P) = 0.193	−4.13; 18.88
3° IVT	91.1 ± 11.5	(P) = 0.577	−7.39; 12.83

Assessed mean macular thickness was 326.8 ± 30.6 μm before the first injection (baseline). Also macular thickness was significantly reduced after each intravitreal (IVT) injection: 289.7 ± 28.6 μm after the first injection (mean reduction from baseline 37.1 ± 32.3 μm, $P < 0.05$), 282.8 ± 28.5 μm after the second injection (mean reduction from baseline 39.2 ± 30.2 μm, $P < 0.05$), and 291.3 ± 27.1 μm (mean reduction from baseline 32.8 ± 22.9 μm, $P < 0.05$) after the third (Table 5).

Assessed mean macular outer layer thickness was 201.9 ± 30.8 μm before the first injection (baseline). Also macular outer layer thickness was significantly reduced after each intravitreal (IVT) injection: 184.3 ± 24.6 μm after the first injection (mean reduction from baseline 17.6 ± 7.3 μm, $P < 0.05$), 176.6 ± 26.4 μm after the second injection (mean reduction from baseline 25.3 ± 7.2 μm, $P < 0.05$), and 183.1 ± 22.5 μm (mean reduction from baseline 18.8 ± 8.9 μm, $P < 0.05$) after the third (Table 6).

Table 4: Mean foveal thickness (μm).

	Cases ($n = 32$)	P value	95% CI
Baseline	354.3 ± 61.9		
1° IVT	295.8 ± 56.6	(P) = 0.005	20.14; 96.91
2° IVT	290.2 ± 60.9	(P) = 0.006	21.63; 106.59
3° IVT	290.8 ± 43.9	(P) = 0.001	29.18; 97.75

Table 5: Mean macular thickness (μm).

	Cases ($n = 32$)	P value	95% CI
Baseline	326.8 ± 30.6		
1° IVT	289.7 ± 28.6	(P) = 0.001	20.42; 53.74
2° IVT	282.8 ± 28.5	(P) = 0.001	23.08; 55.31
3° IVT	291.3 ± 27.1	(P) = 0.001	20.11; 45.49

Table 6: Mean macular outer layer thickness (μm).

	Cases ($n = 32$)	P value	95% CI
Baseline	201.9 ± 30.8		
1° IVT	184.3 ± 24.6	(P) = 0.001	13.28; 41.90
2° IVT	176.6 ± 26.4	(P) = 0.001	15.92; 46.66
3° IVT	183.1 ± 22.5	(P) = 0.001	5.58; 31.97

Table 7: Mean intraocular pressure (mmHg).

	Cases ($n = 32$)	P value	95% CI
Baseline	15 ± 1.9		
1° IVT	15 ± 1.7	(P) = 0.450	−0.70; 1.50
2° IVT	14 ± 1.3	(P) = 0.127	−0.32; 2.32
3° IVT	15 ± 2.1	(P) = 0.181	−0.38; 1.85

Mean intraocular pressure (IOP) of wet AMD-affected eyes, measured with the two different instruments, at baseline was 15 ± 1.9 mmHg. A statistically significant IOP increase was not recorded after each intravitreal (IVT) injection of ranibizumab in any patient: mean IOP variation was 0.4 ± 1.9 mmHg ($P = 0.450$) after the first injection, 1.0 ± 2.3 mmHg ($P = 0.127$) after the second, and 0.7 ± 2.01 mmHg ($P = 0.181$) after the third (Table 7).

5. Discussion

VEGF-A is known as being directly responsible for wet-form AMD chorioretinal neoangiogenesis, but it also plays a neuroprotective function in retinal nervous structures such as ganglion cell layer (GCC) and nerve fiber layer (RNFL), interacting especially with VEGFR2-receptor that is largely expressed over neuroretina [16–18]. It is observed that retinal nerve structures change in rats treated with six intravitreal injections of ranibizumab at weekly intervals. Progressive retinal ganglion cells degeneration, following injections, was recorded by assessing photopic full-field and focal-macular electroretinogram (ERG) reduced response [19]. In humans, retinal nerve fiber layer (RNFL) thickness reduction, evaluated by optical coherence tomography (OCT), was recorded after several intravitreal injections of ranibizumab. Nevertheless they do not change human macular and peripheral ganglion cells function, with no alterations of full-field and focal-macular ERG intensity response observed [20, 21]. According to this scientific evidence and having today a specific software of RTVue-OCT for ganglion cell complex (GCC) thickness and near retinal layers examination, the purpose of this study was to evaluate GCC modifications assessed by OCT, after 3 intravitreal injections of ranibizumab administered monthly (loading therapy in exudative AMD), irrespective of any anatomical and functional improvement detected. GCC modifications might strictly depend on ranibizumab toxic action due to inhibition of the neuroprotective function of VEGF-A or on a temporary IOP increase caused by intravitreal injection. In fact it is known that IOP increase resulting from intraocular volume increase, and following GCC ischemic events, is a possible complication of an intravitreal injection of ranibizumab [22–24]. Nevertheless, it is observed that it occurs only a few minutes following the injection, with intraocular pressure normalization within 30 minutes, without therapy [25, 26]. This study, in which IOP values appear stable one hour after the injection of ranibizumab and 24 hours after and 20 days following the treatment without a statistically significant mean IOP change (0.4 ± 1.9, $P = 0.450$ after the first injection; 1.0 ± 2.3, $P = 0.127$ after the second; and 0.7 ± 2.01, $P = 0.181$ after the third), confirms these results. In this study the OCT examination shows that GCC thickness slightly decreases from baseline values 20 days after ranibizumab intravitreal administration, especially after the first of the three intravitreal injections, although this variation does not appear statistically meaningful. The results of our study that for the first time provide a quantification of GCC thickness changes after the loading phase of ranibizumab confirm a slight GCC anatomical reduction that is nevertheless not statistically significant, resulting from the direct action of ranibizumab and not from an intraocular pressure increase following the injection. According to other authors, GCC reduction observed after intravitreal ranibizumab may result from a progressive arteriolar vasoconstriction, a consequent retinal ischemia associated with glutamate release that may damage ganglion cells, particularly sensitive to this substance [27–29]. The lack of significant anatomical GCC decrease after the first 3 intravitreal injections of ranibizumab suggests the acceptable safety of this therapy (GCC average reduction: 8.1 ± 20.2, $P = 0.123$ after the first injection; 7.3 ± 22.3, $P = 0.193$ after the second; and 2.7 ± 19.6, $P = 0.577$ after the third). In addition ranibizumab efficacy in reducing macular edema, induced by typical wet-form AMD choroidal neovascularization, is also confirmed by foveal and macular thickness decrease from baseline values, assessed by OCT MM5 protocol (resp., $P = 0.005$ and $P = 0.001$ after the first injection, $P = 0.006$ and $P = 0.001$ after the second, and $P = 0.001$ and $P = 0.001$ after the third). In addition the significant reduction of the outer retinal layer thickness after the loading phase of ranibizumab ($P = 0.001$ after each injection versus baseline) confirms that the pathological retinal changes in typical wet-form AMD are mainly localized

in this layer while the GCC is on the contrary localized in the inner retinal layer.

6. Conclusion

Statistically significant reduction of macular edema and improvement in mean visual acuity, associated with stable intraocular pressure, are fairly certain evidence of the clinical efficacy of the treatment with ranibizumab.

Today GCC thickness changes in patients who require intravitreal injections of ranibizumab following loading-phase therapy are unknown. It is not yet known whether additional intravitreal injections of anti-VEGF-A can progressively affect the ganglion cell thickness and function, and this will be the subject of future study [30, 31].

Conflict of Interests

The authors declare that there is no conflict of interests regarding the publication of this paper.

References

[1] C. C. W. Klaver, J. J. M. Assink, R. Van Leeuwen et al., "Incidence and progression rates of age-related maculopathy: the rotterdam study," *Investigative Ophthalmology and Visual Science*, vol. 42, no. 10, pp. 2237–2241, 2001.

[2] H. Oh, H. Takagi, C. Takagi et al., "The potential angiogenic role of macrophages in the formation of choroidal neovascular membranes," *Investigative Ophthalmology and Visual Science*, vol. 40, no. 9, pp. 1891–1898, 1999.

[3] R. Steinbrook, "The price of sight—ranibizumab, bevacizumab, and the treatment of macular degeneration," *The New England Journal of Medicine*, vol. 355, no. 14, pp. 1409–1412, 2006.

[4] V. Fenicia, S. Abdolrahimzadeh, G. Mannino, S. Verrilli, M. Balestrieri, and S. M. Recupero, "Intravitrealbevacizumab in the successful management of choroidal metastases secondary to lung and breast cancer unresponsive to systemictherapy: a case series," *Eye*, 2014.

[5] V. Fenicia, M. Balestrieri, A. Perdicchi, G. Maraone, and S. M. Recupero, "Intravitreal injection of dexamethasone implant in serous macular detachment associated with Waldenström's disease," *Case Reports in Ophthalmology*, vol. 4, no. 2, pp. 64–69, 2013.

[6] A. Ciarnella, S. Verrilli, V. Fenicia et al., "Intravitreal ranibizumab and laser photocoagulation in the management of idiopathic juxtafoveolar retinal telangiectasia type 1: a case report," *Case Reports in Ophthalmology*, vol. 3, no. 3, pp. 298–303, 2012.

[7] P. J. Rosenfeld, D. M. Brown, J. S. Heier et al., "Ranibizumab for neovascular age-related macular degeneration," *The New England Journal of Medicine*, vol. 355, no. 14, pp. 1419–1431, 2006.

[8] A. Lambiase, S. Abdolrahimzadeh, and S. M. Recupero, "An update on intravitreal implants in use for eye disorders," *Drugs of Today*, vol. 50, no. 3, pp. 239–249, 2014.

[9] R. L. Avery, D. J. Pieramici, M. D. Rabena, A. A. Castellarin, M. A. Nasir, and M. J. Giust, "Intravitreal bevacizumab (Avastin) for neovascular age-related macular degeneration," *Ophthalmology*, vol. 113, no. 3, pp. 363–372, 2006.

[10] D. Vavvas and D. J. D'Amico, "Pegaptanib (Macugen): treating neovascular age-related macular degeneration and current role in clinical practice," *Ophthalmology Clinics of North America*, vol. 19, no. 3, pp. 353–360, 2006.

[11] P. Mitchell, J.-F. Korobelnik, P. Lanzetta et al., "Ranibizumab (Lucentis) in neovascular age-related macular degeneration: evidence from clinical trials," *British Journal of Ophthalmology*, vol. 94, no. 1, pp. 2–13, 2010.

[12] E. Storkebaum, D. Lambrechts, and P. Carmeliet, "VEGF: once regarded as a specific angiogenic factor, now implicated in neuroprotection," *BioEssays*, vol. 26, no. 9, pp. 943–954, 2004.

[13] G. L. Scuderi, N. C. Cascone, F. Regine, A. Perdicchi, A. Cerulli, and S. M. Recupero, "Validity and limits of the rebound tonometer (ICare): clinical study," *European Journal of Ophthalmology*, vol. 21, no. 3, pp. 251–257, 2011.

[14] B. Lumbroso and R. Brancato, *Guida pratica all'interpretazione dell'OCT*, Editore I.N.C., Roma, Italy, 2004.

[15] http://www.oct-optovue.com/GCC-RTVue-version4.pdf.

[16] K. Yang and C. L. Cepko, "Flk-1, a receptor for vascular endothelial growth factor (VEGF), is expressed by retinal progenitor cells," *The Journal of Neuroscience*, vol. 16, no. 19, pp. 6089–6099, 1996.

[17] I. Kim, A. M. Ryan, R. Rohan et al., "Constitutive expression of VEGF, VEGFR-1, and VEGFR-2 in normal eyes," *Investigative Ophthalmology and Visual Science*, vol. 40, no. 9, pp. 2115–2121, 1999.

[18] R. E. Gilbert, D. Vranes, J. L. Berka et al., "Vascular endothelial growth factor and its receptors in control and diabetic rat eyes," *Laboratory Investigation*, vol. 78, no. 8, pp. 1017–1027, 1998.

[19] K. Nishijima, Y.-S. Ng, L. Zhong et al., "Vascular endothelial growth factor-A is a survival factor for retinal neurons and a critical neuroprotectant during the adaptive response to ischemic injury," *The American Journal of Pathology*, vol. 171, no. 1, pp. 53–67, 2007.

[20] J. M. Martinez-de-la-Casa, A. Ruiz-Calvo, F. Saenz-Frances et al., "Retinal nerve fiber layer thickness changes in patients with age-related macular degeneration treated with intravitreal ranibizumab," *Investigative Ophthalmology and Visual Science*, vol. 53, no. 10, pp. 6214–6218, 2012.

[21] T. Nishimura, S. Machida, T. Harada, and D. Kurosaka, "Retinal ganglion cell function after repeated intravitreal injections of ranibizumab in patients with age-related macular degeneration," *Clinical Ophthalmology*, vol. 6, no. 1, pp. 1073–1082, 2012.

[22] L. Wu, M. A. Martínez-Castellanos, H. Quiroz-Mercado et al., "Twelve-month safety of intravitreal injections of bevacizumab (Avastin): results of the pan-american collaborative retina study group (PACORES)," *Graefe's Archive for Clinical and Experimental Ophthalmology*, vol. 246, no. 1, pp. 81–87, 2008.

[23] J. E. Kim, A. V. Mantravadi, E. Y. Hur, and D. J. Covert, "Short-term intraocular pressure changes immediately after intravitreal injections of antivascular endothelial growth factor agents," *The American Journal of Ophthalmology*, vol. 146, no. 6, pp. 930.e1–934.e1, 2008.

[24] R. E. P. Frenkel, L. Mani, A. R. Toler, and M. P. C. Frenkel, "Intraocular pressure effects of pegaptanib (Macugen) injections in patients with and without glaucoma," *American Journal of Ophthalmology*, vol. 143, no. 6, pp. 1034–1035, 2007.

[25] J. Flammer, "The concept of visual field defects," *Graefe's Archive for Clinical and Experimental Ophthalmology*, vol. 224, pp. 389–392, 1986.

[26] L. Maffei and A. Fiorentini, "Electroretinographic responses to alternating gratings before and after section of the optic nerve," *Science*, vol. 211, no. 4485, pp. 953–955, 1981.

[27] K. S. Kim, H. R. Chang, and S. Song, "Ischaemic change after intravitreal bevacizumab (Avastin) injection for macular oedema secondary to non-ischaemic central retinal vein occlusion," *Acta Ophthalmologica*, vol. 86, no. 8, pp. 925–927, 2008.

[28] K. Yokoyama, T. Choshi, K. Kimoto, K. Shinoda, and K. Nakatsuka, "Retinal circulatory disturbances following intracameral injection of bevacizumab for neovascular glaucoma," *Acta Ophthalmologica*, vol. 86, no. 8, pp. 927–928, 2008.

[29] R. Siliprandi, R. Canella, G. Carmignoto et al., "N-methyl-D-aspartate-induced neurotoxicity in the adult rat retina," *Visual Neuroscience*, vol. 8, no. 6, pp. 567–573, 1992.

[30] V. E. S. Jeganathan and N. Verma, "Safety and efficacy of intravitreal anti-VEGF injections for age-related macular degeneration," *Current Opinion in Ophthalmology*, vol. 20, no. 3, pp. 223–225, 2009.

[31] D. F. Martin, M. G. Maguire, G.-S. Ying, J. E. Grunwald, S. L. Fine, and G. J. Jaffe, "Ranibizumab and bevacizumab for neovascular age-related macular degeneration," *The New England Journal of Medicine*, vol. 364, no. 20, pp. 1897–1908, 2011.

Hindawi Publishing Corporation
BioMed Research International
Volume 2015, Article ID 249617, 12 pages
http://dx.doi.org/10.1155/2015/249617

Review Article

Functional and Structural Abnormalities in Deferoxamine Retinopathy: A Review of the Literature

Maura Di Nicola,[1] Giulio Barteselli,[1,2] Laura Dell'Arti,[1] Roberto Ratiglia,[1] and Francesco Viola[1]

[1] *Ophthalmological Unit, Department of Clinical Sciences and Community Health, Ca' Granda Foundation-Ospedale Maggiore Policlinico, University of Milan, Via Francesco Sforza 35, 20122 Milan, Italy*
[2] *Genentech, Inc., 1 DNA Way, South San Francisco, CA 94080, USA*

Correspondence should be addressed to Francesco Viola; francesco.viola@unimi.it

Received 12 September 2014; Accepted 20 November 2014

Academic Editor: Michele Figus

Deferoxamine mesylate (DFO) is the most commonly used iron-chelating agent to treat transfusion-related hemosiderosis. Despite the clear advantages for the use of DFO, numerous DFO-related systemic toxicities have been reported in the literature, as well as sight-threatening ocular toxicity involving the retinal pigment epithelium (RPE). The damage to the RPE can lead to visual field defects, color-vision defects, abnormal electrophysiological tests, and permanent visual deterioration. The purpose of this review is to provide an updated summary of the ocular findings, including both functional and structural abnormalities, in DFO-treated patients. In particular, we pay particular attention to analyzing results of multimodal technologies for retinal imaging, which help ophthalmologists in the early diagnosis and correct management of DFO retinopathy. Fundus autofluorescence, for example, is not only useful for screening patients at high-risk of DFO retinopathy, but is also a prerequisite for identify specific high-risk patterns of RPE changes that are relevant for the prognosis of the disease. In addition, optical coherence tomography may have a clinical usefulness in detecting extent and location of different retinal changes in DFO retinopathy. Finally, this review wants to underline the need for universally approved guidelines for screening and followup of this particular disease.

1. Introduction

Deferoxamine mesylate (DFO) is the most used iron-chelating drug to treat hemosiderosis secondary to transfusions. Deferoxamine mesylate is most commonly administered as a slow subcutaneous infusion but can also be given intramuscularly or, less commonly, intravenously [1]. Long-term treatment with blood transfusions effectively prevents various complications of sickle cell anemia and can sustain patients with chronic congenital and acquired refractory anemia, including beta-thalassemia syndromes, myelodysplastic syndromes, myelofibrosis, aplastic anemia, and other disorders [1]. The use of iron-chelating agents is crucial for the management of such diseases. Since the human body has no physiologic mechanisms to discard excess iron [2], the frequent blood transfusions required in these conditions inevitably produce iron overload. If not treated, chronic iron overload can result in multiple organ toxicities including potentially fatal cardiac toxicity, hepatic fibrosis or cirrhosis, impaired growth, failure of sexual maturation, and diabetes [3]. In patients with thalassemia who undergo transfusion from infancy, iron-induced liver disease and endocrine disorders develop during childhood and are almost inexorably followed by death from iron-induced cardiomyopathy in adolescence [1]. Deferoxamine mesylate has also been used for the treatment of acute iron intoxication and as a screening test for increased aluminum body stores in chronic renal failure [4, 5]. Deferoxamine mesylate has high affinity for ferric iron, thus removing iron from hemosiderin, ferritin, and transferrin [6].

2. Complications of Deferoxamine Mesylate Therapy

2.1. Side Effects. Despite the clear advantages for the use of DFO, numerous significant drug-related toxicities have

been reported in the literature. Systemic toxicities included cardiovascular, respiratory, gastrointestinal, cutaneous, and nervous systems [1], in addition to the propensity for bone dysplasia [7] and high-frequency sensorineuronal hearing loss [8–10]. Furthermore, DFO therapy may induce ocular toxicity consisting of retinal pigment epithelium (RPE) changes, visual loss, and impaired night vision [6, 11]. As a result, the damage to the RPE can lead to visual field defects, decreased visual acuity, color-vision defects, and decreased responses during electroretinogram (ERG) and electrooculogram (EOG) [11–13]. Since the 1980s, several case reports and small case series have been reported confirming these findings, which may develop not only after high-dose intravenous but also after subcutaneous administration (Table 1) [6, 9–30]. Varying conclusions have been reported regarding reversibility of DFO toxicity [26]; while usually visual deficits recover after cessation of the medication [15, 31], some authors reported permanent visual deterioration [13] or even progression of the retinopathy even after DFO discontinuation [29, 32].

2.2. Mechanism of Toxicity. The mechanism of DFO toxicity has been extensively studied; however, it is still not well understood. Rahi et al. were the first to perform a histologic and ultrastructure examination of an eye diagnosed with DFO retinopathy [16]. They reported abnormalities that resembled apoptotic changes of the RPE. These changes included patchy depigmentation in the equatorial as well as the posterior fundus, swelling and calcification of mitochondria, disorganization of the plasma membrane, loss of microvilli from the apical surface, and vacuolation of the cytoplasm. RPE cells appeared enlarged and projected into the subretinal space, which sometimes showed detached and rounded RPE cells containing typical melanin accumulation. Thickening of Bruch membrane overlying the RPE was noted as well.

It is also known that administration of DFO results in high fecal iron, copper, and zinc excretion due to the drug's chelation properties [33]. De Virgiliis et al. hypothesized that DFO retinopathy may be related to either serum or intracellular zinc and copper deficiencies [33]. Indeed, zinc or zinc compounds are known to enhance the antioxidative capability of RPE cells [34, 35]. Pall et al. hypothesized that DFO retinopathy may occur in situations where the dose of DFO is too high compared to the stores of iron present [36]. In these situations, the excess DFO could bind copper and result in copper-induced autooxidative damage.

More recently, Klettner et al. examined the direct toxic effect of DFO on cultured primary RPE cells [37]. These investigators were the first to clarify in vitro that the toxic effect of DFO to the RPE is direct and not secondary to trace element depletion. In addition, they showed that the cell death was mediated by the activation of p38 mitogen-activated protein kinases. These protein kinases were previously shown to be important for the execution of programmed cell death after toxic stimuli [26]. Finally, the investigators indicated a general involvement of p38 in stress-induced cell death in RPE cells, since p38 is also involved in oxidative stress.

2.3. Incidence. There are different estimates of the incidence of retinal toxicity due to DFO. Olivieri et al. reported that 5.6% of patients receiving DFO therapy had RPE changes [9]. In a series of 52 regularly transfused patients who received DFO by subcutaneous or intravenous infusion, Cohen et al. found that only two patients had abnormal visual screening tests; one of them was symptomatic and one was not [10]. Chen et al. reported on a series of 30 transfusion-dependent patients receiving DFO in a dose of 40 to 50 mg/kg subcutaneously overnight for 8 to 10 hours by pump, 4 to 7 days per week, and detected no visual abnormality [8]. In another series of 84 children with transfusional hemochromatosis, drug-related ocular toxicity was found only in one patient (1.2%) [26]. Finally, our group has recently reported on a large series of 197 consecutive adult patients with beta-thalassemia syndromes receiving chronic treatment with DFO and found abnormal fundus autofluorescence (FAF) which is not related to other diseases in 9% of the patients [29].

2.4. Risk Factors. A clear relationship between drug dosage and development of DFO retinopathy could not be identified in most case series [6, 14]. Previously cited risk factors for visual loss in DFO retinopathy included blood-retinal barrier breakdown associated with diabetes [14] and rheumatoid arthritis [15], renal failure [13], and metabolic encephalopathy [15]. It is believed that blood-retinal breakdown, which can be due to iron overload-induced diabetes or to the drug itself, may increase DFO levels in the RPE and retina, thus intensifying the local toxic effects of the drug [6]. It has also been suggested that older age and longer duration of DFO treatment may be associated with more advanced forms of retinopathy in patients with beta-thalassemia syndromes [32, 38].

3. Clinical Presentation

Previously reported ocular findings of DFO toxicity include cataract, optic neuropathy, optic atrophy, and macular or equatorial pigmentary degeneration [6, 9, 10, 12, 15, 33]. On fundus examination, the acute stage of DFO retinopathy is characterized by retinal opacification or loss of transparency, as well as EOG and ERG attenuation [6]. This stage is followed by macular and/or equatorial RPE pigmentary mottling, which persists even after functional recovery. Multiple case reports have described characteristic fundus lesions of DFO retinopathy seen by ophthalmoscopy and fundus photography; these lesions included pigmentary retinopathy, bull's eye maculopathy, and vitelliform maculopathy [15, 19, 21, 25, 27]. However, the use of high-resolution imaging technologies has demonstrated that DFO retinopathy may present ophthalmoscopically with a variety of RPE degenerative patterns resembling pattern dystrophies or may present with only minimal changes in the macula that can be easily missed by indirect ophthalmoscopy [29]. Multimodal imaging using confocal laser scanning ophthalmoscopy (cSLO) was shown to be extremely useful in detecting early RPE changes related to DFO retinopathy, as well as in analyzing longitudinal modifications of the disease.

Table 1: Summary of cases with DFO retinopathy in the literature.

Author, year	Patients with DFO retinopathy	DFO administration	DFO duration	Retinal findings (patients)	Elettrophysiology findings (patients)	Visual field findings (patients)
Davies et al., 1983 [11]	2	IV	—	—	ERG: abnormal	—
Arden et al., 1984 [14]	18	SC	4 to 5 years	RPE hyperpigmentation	EOG: subnormal (12); ERG: reduced cone function (7); PERG: reduced responses (18)	Visual field constriction
Lakhanpal et al., 1984 [12]	7	IV	—	Macular and peripheral RPE mottling	—	—
Blake et al., 1985 [15]	3	IV	5 to 12 days	Pigmentary retinopathy and macular RPE mottling	EOG: abnormal; ERG: subnormal	—
Rahi et al., 1986 [16]	1	IM and then SC and then IV	24 years	—	ERG: subnormal; EOG: abnormal	Visual field constriction and central scotoma
Olivieri et al., 1986 [9]	5	SC	—	Macular RPE mottling	—	—
Bene et al., 1989 [13]	1	—	—	—	—	—
Ravelli et al., 1990 [17]	5	IV	5 months	Macular RPE mottling (4)	EOG: abnormal	Central scotoma (1)
Cohen et al., 1990 [10]	2	—	—	Macular RPE mottling (1)	—	—
Mehta et al., 1994 [18]	1	SC	—	—	—	—
Haimovici et al., 2002 [6]	16	SC (5) and IV then SC (2), IV (1), IP (1), and NK (7)	1 month to 10 years	RPE opacification (5) and RPE mottling (14)	ERG: reduced cone and rod function; EOG: abnormal	—
Bansal et al., 2003 [19]	1	—	26 years	Bull's eye maculopathy	—	—
Kertes et al., 2004 [23]	1	SC	18 months	Macular RPE mottling	Multifocal ERG: reduced responses	—
Arora et al., 2004 [20]	1	IV	3 years	Macular RPE mottling	ERG: normal rods responses, reduced cone responses	—
Hidajat et al., 2004 [22]	1	SC	2 years	Macular RPE mottling	EOG: flat or subnormal	—
Gonzales et al., 2004 [21]	2	SC (1) and IV (1)	11 months (SC); 3 years (IV)	RPE mottling (1) and vitelliform lesion (1)	ERG: reduced cone responses; EOG normal (1)	—
Lai et al., 2006 [24]	1	SC and then IV	14 years (SC); 4 months (IV)	Macular and peripheral RPE mottling	ERG: reduced cone and rod responses; EOG: abnormal	—
Lu et al., 2007 [25]	1	SC	36 years	Pigmentary retinopathy	ERG: reduced rod responses	Central, paracentral scotoma
Baath et al., 2008 [26]	1	SC	1 to 17 years	Macular RPE mottling	ERG: reduced rod responses	—
Genead et al., 2010 [27]	1	IM and then SC	20 years	Vitelliform lesion and RPE mottling	ERG: normal cone and rode function	Central scotoma
Simon et al., 2012 [28]	1	SC and then IV	23 years (SC); 10 weeks (IV)	Macular RPE mottling	ERG: reduced cone and rod responses; EOG: abnormal	Visual field constriction
Viola et al., 2012 [29]	18	SC	10 to 55 years	Pattern dystrophy-like changes (8) and minimal RPE mottling (10)	—	—
Wu et al., 2014 [30]	1	SC and then IV	20 years (SC); 42 days (IV)	Macular and peripheral RPE mottling	—	—

DFO: deferoxamine; RPE: retinal pigment epithelium; IV: intravenous; SC: subcutaneous; IP: intraperitoneal; IM: intramuscular; NK: unknown; ERG: electroretinogram; EOG: electrooculogram.

4. Tests for Functional Abnormalities

4.1. Electrophysiology. Electrophysiological tests have been widely used to establish the diagnosis of DFO retinopathy. They are essential for gathering information on the location and extent of retinal dysfunction in patients with this pathology. The degree of functional loss in DFO retinopathy can be assessed by using ERG or also EOG. Electrophysiology is a valuable tool that is usually confirmatory for the diagnosis, and sometimes may also indicate more widespread dysfunction than may be implied by funduscopy alone. Electrophysiology performed in rats given intravenous DFO showed early dose-related suppression of b-wave amplitude [39, 40] that in some cases were reversible [41]. Arden et al. studied 43 patients with thalassemia major and intermedia requiring regular blood transfusions without any ocular symptoms. They found that while EOG and ERG results where only slightly and insignificantly lower than average, pattern ERG abnormalities were much more pronounced [14]. Multifocal ERG was found to be helpful as well in demonstrating areas of decreasing function over time in DFO maculopathy [23]. A longitudinal ERG study in 11 beta-thalassemia major patients receiving DFO suggested scotopic dysfunction, most likely related to iron toxicity [42]. Lakhanpal et al. used electrophysiological tests to study eight patients who developed ocular toxicity while undergoing DFO therapy for transfusional haemosiderosis and suggested toxicity at the level of the RPE and photoreceptors [12]. Haimovici et al. performed electrophysiological tests on 16 patients with visual loss and macular pigmentary changes related to DFO retinopathy. They found reduced ERG amplitudes and reduced EOG light-peak to dark-trough ratios indicating retinal and RPE injury [6]. Electrophysiological results may also normalize after splenectomy and cessation of DFO therapy [22].

4.2. Visual Field. Several case reports and case series reported on visual field alterations in patients undergoing long-term DFO treatment. The most common alterations were a generalized constriction of the visual field [14, 28] or central-paracentral scotomata [17, 25, 27]. Rahi et al. reported a case that presented with both central scotoma and constriction of the peripheral field in each eye [16]. These abnormalities resolved after withdrawal of high-dose therapy.

4.3. Microperimetry. To date, microperimetric results in DFO retinopathy have not been reported in the literature. However, microperimetry can be a useful tool to study the impact of macular RPE changes on visual function in this disease. The latest models of microperimeters incorporate a color fundus camera for image registration and an autotracking system to facilitate the accurate measurement of retinal sensitivity within the central visual field, even in patients with unstable or extrafoveal fixation. This allows detection of absolute scotomata, relative scotomata, or abnormally reduced retinal sensitivity in patients with macular pathologies. Examples of microperimetric results in eyes with DFO retinopathy are shown in Figure 1.

5. Tests for Structural Abnormalities

5.1. Fluorescein Angiography. In the past, fluorescein angiography (FA) has been widely used to diagnose DFO retinopathy [6, 17, 20, 21, 23, 27, 28]. In the earliest stages, when ophthalmoscopy shows loss of retinal transparency only, FA shows patchy blocked fundus fluorescence followed by late staining (Figure 2). When pigment mottling develops, FA shows mottled fluorescence in the early-phase angiogram with late hyperfluorescence [6]. However, these FA findings are not pathognomonic of DFO retinopathy. With the advent of noninvasive high-resolution imaging technologies such as the cSLO, FA is now only rarely required for the diagnosis of patients with DFO retinopathy.

5.2. Fundus Autofluorescence on Confocal Scanning Laser Ophthalmoscopy. To date, FAF imaging using cSLO seems to be the most effective clinical adjunct for the diagnosis and evaluation of patients with DFO retinopathy [29]. The FAF signal generally provides indirect information on the level of metabolic activity of the RPE, since it represents an index of lipofuscin accumulation [43]. Fundus autofluorescence appearance of a normal fundus is characterized by a homogeneous background autofluorescence arising from the RPE, with a gradual decrease in macular FAF intensity towards the foveola that results from the masking effect of yellow macular pigment. This suggests that, in vivo, FAF imaging may represent a suitable noninvasive diagnostic tool to detect early RPE abnormalities in various retinal disorders, including drug-related retinal toxicity [44]. Indeed, it has been shown that FAF imaging is superior to ophthalmoscopy in detection of early characteristic RPE abnormalities in patients at risk of DFO retinopathy, as well as in monitoring the disease progression over time [29].

In 2012, our group described a variety of phenotypic patterns of abnormal FAF in thalassemic patients who needed long-term DFO treatment with the use of a cSLO device [29]. The topographic FAF alterations were classified into four different patterns using a slightly modified classification for age-related macular degeneration published by the FAM Study group [45]. The characteristics of each pattern are described below.

(1) Minimal Change Pattern (Figure 3). Eyes with only minimal variations from the normal FAF appearance, with irregularly increased or decreased background FAF, are included in this group. Increased FAF signal, which may result from mottling of the RPE, is characterized by relatively small spots of less than 100 microns in diameter within the macula. The spots have well-defined borders and in some cases correspond to visible alterations on color fundus photographs, such as focal hyperpigmentation.

(2) Focal Pattern (Figure 4). This pattern is defined by the presence of at least one medium-sized spot, more than 100 microns but less than 200 microns in diameter, of markedly increased FAF that is much brighter than the surrounding background FAF. The borders appear well-defined, with no gradual decrease of FAF observed between the background

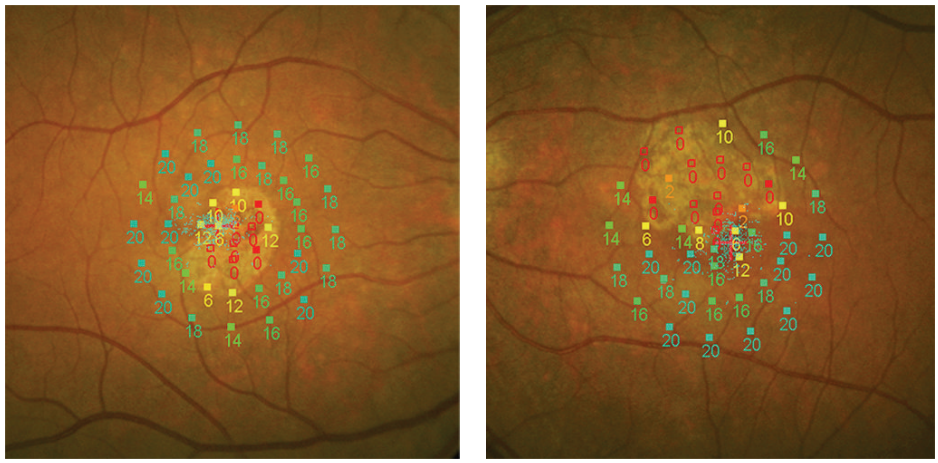

(a) (b)

Figure 1: Microperimetric results in two eyes with DFO retinopathy. Absolute scotomata are present in macular areas of RPE atrophy as seen on fundus photography. Relative scotomata or reduced retinal sensitivity are present in the adjacent areas where RPE changes may or may not be visible.

(a) (b)

Figure 2: Early (a) and late phase (b) fluorescein angiography in an eye with DFO retinopathy. The angiogram showed patchy blocked fundus fluorescence in early phase in the macula, followed by late staining.

and the area with focally increased FAF. On color fundus photographs these spots may correspond to visible alterations, such as focal hyperpigmented areas.

(3) Patchy Pattern (Figure 5). This pattern is characterized by the presence of at least one large area, more than 200 microns in diameter, of markedly increased FAF. These areas are brighter than the surrounding background FAF, usually with well-defined borders. Nevertheless, coalescence of these areas usually occurs, resembling a pattern dystrophy. The corresponding abnormalities are visible on color fundus photographs and include both hyperpigmentation and hypopigmentation. To note, the affected area can often appear larger in FAF imaging than that expected from the color fundus photographs and sometimes it includes different intensities of hyperautofluorescence.

(4) Speckled Pattern (Figure 6). The speckled pattern is defined by the simultaneous presence of a variety of FAF changes that extend beyond the macula. Typically, these abnormalities include multiple small areas of irregularly increased and decreased FAF. On color fundus photographs, these abnormalities sometimes correspond to visible alterations such as focal hyperpigmentation and hypopigmentation. The pathologic areas seem to be fewer and smaller than the corresponding color fundus photographs.

As reported by our group, the detected FAF alterations in DFO retinopathy were always bilateral but asymmetrical [29]. The most frequent pattern was the minimal change pattern (56%), followed by the focal pattern (17%), the patchy pattern (16%), and the speckled pattern (11%). No association was found between pattern type and duration of DFO treatment. Areas of increased FAF signal indicated diffuse accumulation

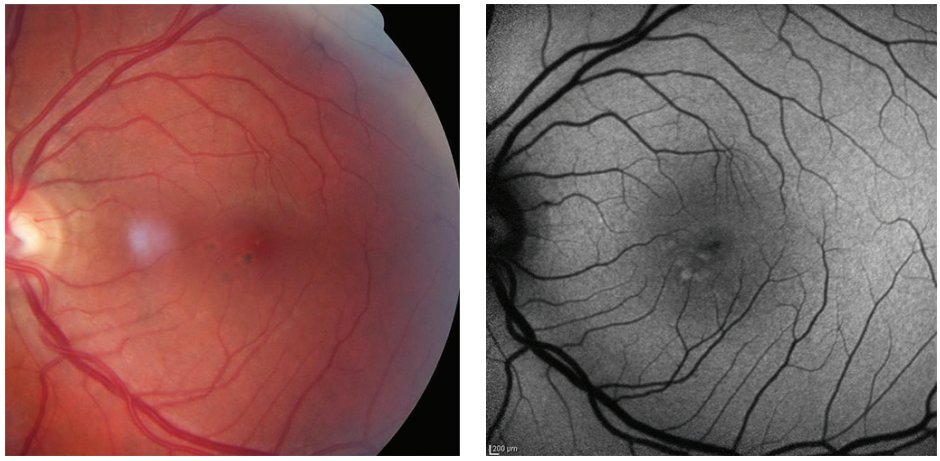

(a) (b)

Figure 3: Color photo (a) and FAF image (b) of a minimal change pattern of DFO retinopathy.

(a) (b)

Figure 4: Color photo (a) and FAF image (b) of a focal pattern of DFO retinopathy.

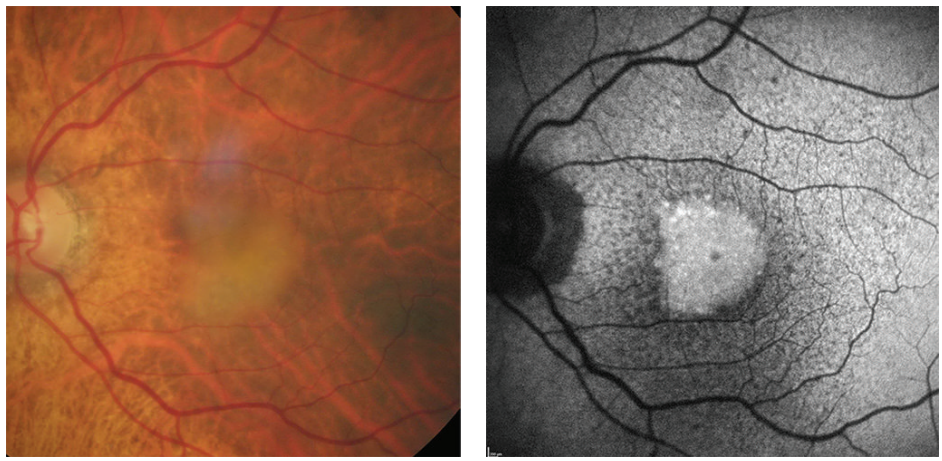

(a) (b)

Figure 5: Color photo (a) and FAF image (b) of a patchy pattern of DFO retinopathy.

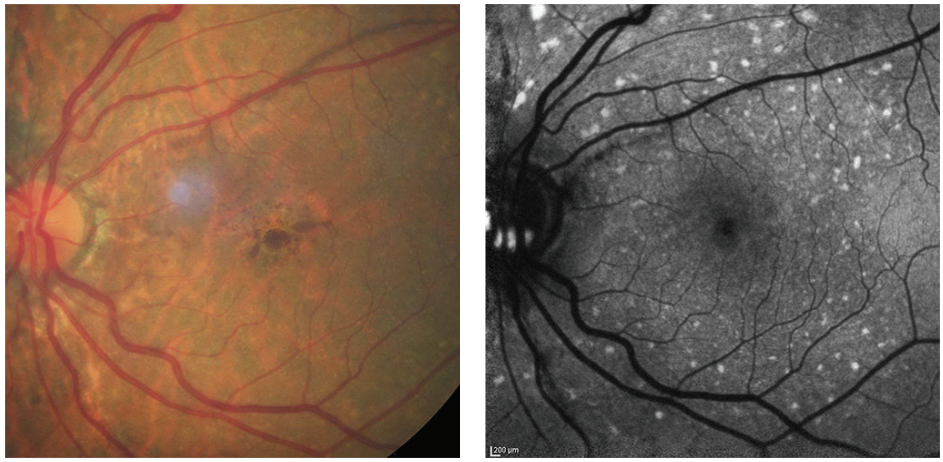

(a) (b)

Figure 6: Color photo (a) and FAF image (b) of a speckled pattern of DFO retinopathy.

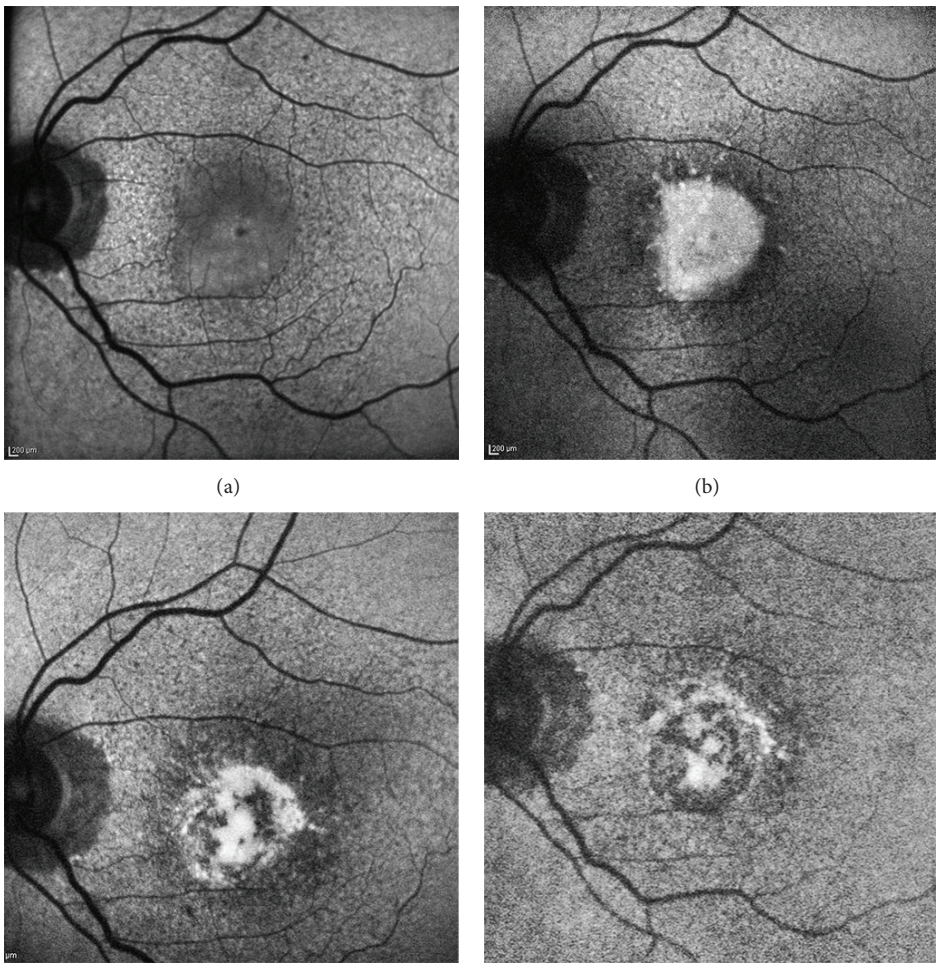

(a) (b)

(c) (d)

Figure 7: Serial fundus autofluorescence (FAF) images of a patient with patchy pattern during a 5-year follow-up. (a) Presence of a patchy area with mildly increased FAF in the inferior macula at baseline examination, involving the fovea. (b) At year 2, the patchy area showed a much greater and uniform increased FAF signal compared to the previous visit. (c) At year 4, part of the patchy area of increased FAF signal started disappearing, and areas of retinal pigment epithelium atrophy started developing. (d) At year 5, most parts of the patchy area of increased FAF signal shrunk and disappeared, leading to frank retinal pigment epithelium atrophy in the macula.

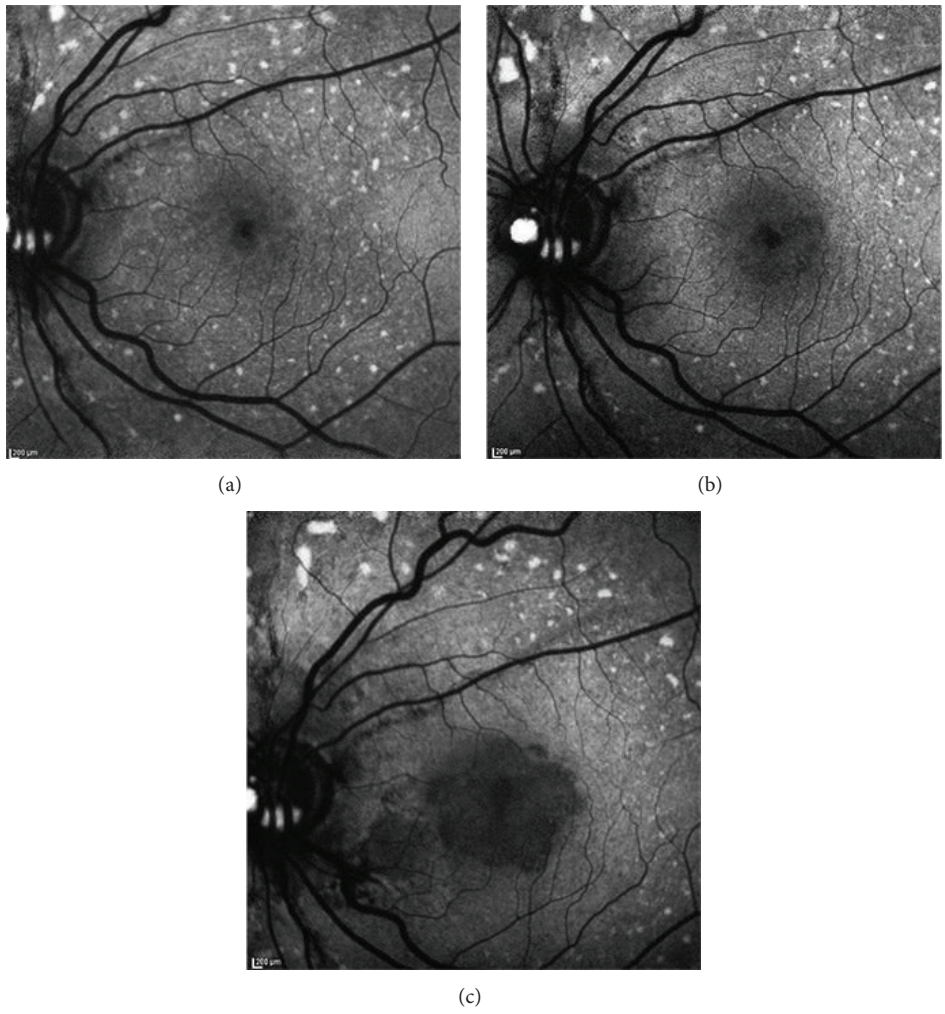

(a) (b)

(c)

Figure 8: Serial fundus autofluorescence (FAF) images of a patient with speckled pattern during a 3-year follow-up. (a) At baseline examination, multiple granular spots of increased FAF were clearly detected in the macula and also beyond the vascular arcades. In the perifoveal area the spots were partially confluent. (b) After 1 year, the perifoveal spots began to progressively disappear and initial RPE atrophy occurred. (c) At year 3, further enlargement of the RPE atrophy in the macula as well as further reduction of the perimacular spots of increased FAF signal were clearly detected.

of autofluorescent fluorophores within a thickened RPE-Bruch membrane complex or also focal accumulation of autofluorescent outer segment-derived retinoid products in the subretinal space. The different intensities of hyperautofluorescence could be related to the presence of various materials within different retinal locations.

Besides being extremely helpful for detecting early RPE changes, FAF has been shown to be very useful in evaluating the clinical course of DFO retinopathy as well. To date, the longest average follow-up of cases of DFO retinopathy using multimodal imaging including FAF is 20 months (range: 10 to 45 months) [32]. In cases of minimal changes in the macula, a slight enlargement of the affected areas developed over the course of the years if DFO was not discontinued. Limited FAF changes were detected in eyes with focal pattern, independently from the ongoing or discontinued DFO treatment. In cases of patchy pattern (Figure 7) or speckled pattern (Figure 8), follow-up examinations revealed progressive development of RPE atrophy in the previously affected hyperautofluorescent areas. In addition, RPE atrophy progressively enlarged during the ensuing visits, leading to irreversible vision loss. Notably, none of the patients with patchy pattern could discontinue DFO treatment due to their precarious systemic conditions [29, 32].

Patients with minimal changes in the macula were found to be younger than patients with the other patterns [32]. It was therefore hypothesized that minimal changes related to DFO retinopathy may progress into other patterns with increasing age of the patients. However, a longitudinal study with longer follow-up duration is necessary to detect a significant disease progression from one pattern to another.

5.3. Spectral Domain Optical Coherence Tomography. Spectral domain optical coherence tomography (SD-OCT) may have a clinical usefulness in detecting extent and location of the different retinal degenerations in DFO retinopathy

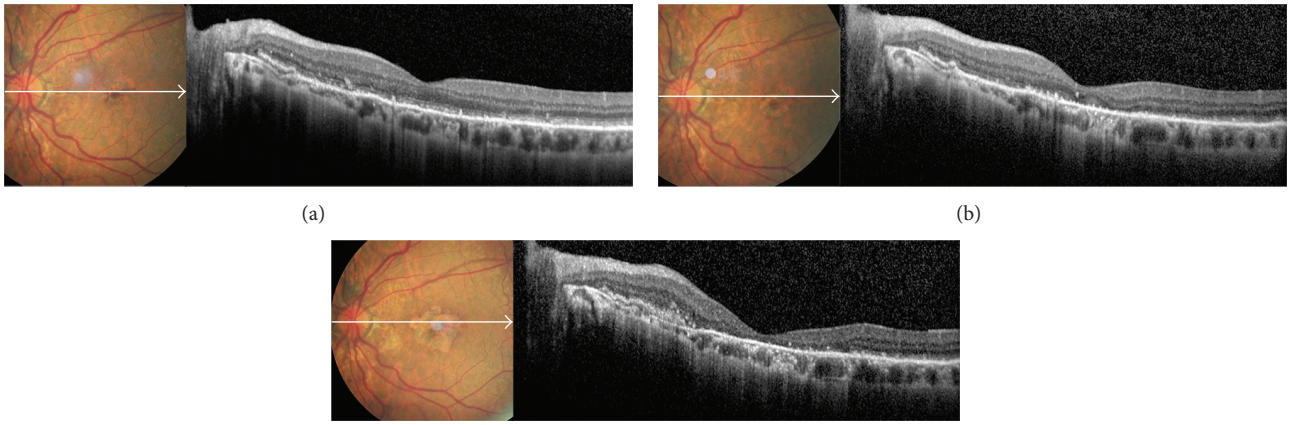

(a) (b) (c)

Figure 9: Serial color photos and OCT scans of a patient with speckled pattern during a 3-year follow-up. (a) At baseline examination, pigmented material was visible in the fovea, with small yellow flecks extending beyond the vascular arcades. On OCT scan, granular hyperreflective deposits were detected in the subretinal space, extending into the outer plexiform layer and interrupting the overlying external limiting membrane. (b) After 1 year, initial RPE atrophy was visible around the fovea, with disruption of the outer retinal layers on OCT scan. (c) At year 3, frank RPE atrophy developed in the macula; OCT scan showed atrophy of the outer retinal layers and RPE, as well as thinning of the inner retina.

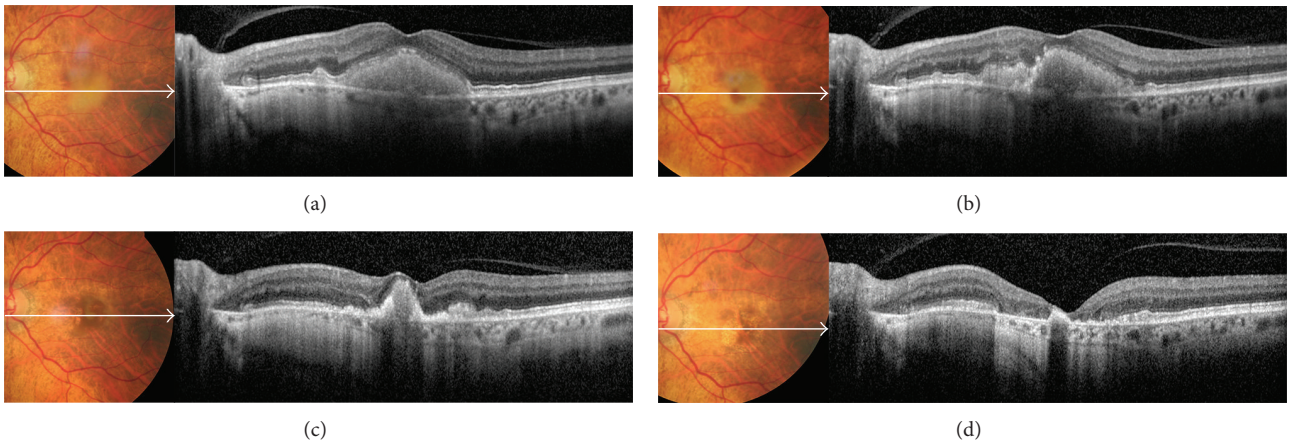

(a) (b) (c) (d)

Figure 10: Serial color photos and OCT scans of a patient with patchy pattern during a 5-year follow-up. (a) At baseline examination, yellowish vitelliform-like material was visible on fundus photo; OCT scan showed that the material was homogeneous, mildly hyperreflective, and localized in the subretinal space above the RPE. It was associated with a diffusely thickened inner segment/outer segment junction and intact external limiting membrane. (b) After 1 year, the vitelliform material started resorbing inferonasally to the fovea; on OCT scan, the subretinal material was no more homogeneous. (c) At year 3, the vitelliform material shrunk, and initial RPE and photoreceptors atrophy were appreciated perifoveally. (d) At year 5, the vitelliform material was completely resorbed; OCT scan showed absence of external limiting membrane, marked thinning of the outer nuclear layer, and frank RPE and photoreceptors atrophy in the macula.

[30, 32]. Some SD-OCT devices can also couple OCT scan and bidimensional cSLO image to simultaneously colocalize posterior structures with high accuracy [46]. In early stage of the disease, SD-OCT usually shows only focal thickenings or bumps of the RPE, resembling basal laminar drusen. As the disease progresses, the coalescence of these bumps of pigmented material appears on SD-OCT as thick and hyperreflective dome-shaped lesions that disrupts the architecture of the overlying outer retinal layers. As the pigmented material reabsorbs, RPE becomes progressively thinner (Figure 9). Sometimes vitelliform-like material could develop in the subretinal space above the RPE (Figure 10), associated with a diffusely thickened inner segment/outer segment junction. In advanced stages of DFO retinopathy, frank RPE and photoreceptors atrophy may develop in the macula, as well as migration of hyperreflective subretinal deposits towards the outer plexiform layer interrupting the overlying external limiting membrane [32].

6. Management

Currently, there are no approved guidelines for the screening and follow-up of DFO retinopathy in patients requiring regular blood transfusions. Also, there is no treatment available for patients with DFO retinopathy other than drug discontinuation or dose reduction. To minimize risks of

DFO retinopathy, it has been suggested to not exceed doses of 50 mg/kg of body weight in patients with iron overload and to decrease the dose as the hepatic iron concentration approaches normal levels [1]. Although treatment with DFO may reduce endocrine complications of iron overload, such as a delay of puberty, the chelator itself can interfere with growth [47], apparently as a result of skeletal dysplasia [48]. To minimize this effect, the dose of DFO in children should not exceed 25 to 30 mg/kg [49]. Since ocular changes related to DFO toxicity are potentially sight-threatening, we believe that regular ocular checkups are essential for patients undergoing treatment. The presence of minimal changes in the macula can be followed every 6 months, but patients with certain toxicity such as bilateral pattern dystrophy-like changes should stop the drug immediately unless the risks of their underlying disease outweigh the risks of permanent and possibly progressive visual loss. Even after cessation of the drug, we recommend patients to return for reexamination every 3 months.

New iron-chelating therapies (deferasirox and deferiprone) are now available in the market, but their long-term ocular safety has not been comprehensively investigated. Moreover, the data considering side effects of deferiprone and deferasirox are controversial [50, 51], yet there are studies in which deferiprone seems to display fewer side effects than DFO [52]. In particular, deferasirox could cause potentially fatal renal and hepatic impairment or failure as well as gastrointestinal hemorrhage [1]. These adverse effects were reported to occur more frequently in older patients and in patients with high-risk myelodysplastic syndromes, thrombocytopenia, or underlying renal or hepatic impairment. Deferiprone could cause diarrhea and gastrointestinal effects, arthropathy, increased levels of serum liver enzymes, and progression of hepatic fibrosis associated with an increase in iron overload or hepatitis C. The most serious adverse effects are agranulocytosis and neutropenia; weekly monitoring of the neutrophil count is recommended [1].

7. Conclusion

Deferoxamine mesylate is the most important drug for the treatment of hemosiderosis secondary to long-term treatment with blood transfusions. Many different ocular toxicities have been reported in the literature, with the most serious being sight-threatening retinopathy. Currently, no "gold standard" exists for identification of the ocular toxicity prior to its development. This has led to the importance of repeated ophthalmologic examinations for screening patients. With the development of high-resolution noninvasive imaging technologies, we believe that FAF can be used as a rapid and reliable way to evaluate DFO retinopathy. Fundus autofluorescence imaging on a cSLO device not only is useful for screening patients at high-risk of the disease, but it also allows longitudinal evaluation of eyes with DFO retinopathy. These changes are more widespread on FAF imaging than expected from fundoscopy, and DFO retinopathy may also present with different FAF patterns that are relevant for the prognosis of the disease. Fundus autofluorescence imaging is a prerequisite for identifying specific high-risk characteristics (such as patchy or speckled patterns) that may be helpful in the decision to discontinue or switch iron-chelating therapy to prevent disease progression and irreversible visual loss due to RPE atrophy. In addition to FAF imaging, SD-OCT may have a clinical usefulness in detecting extent and location of different retinal changes in DFO retinopathy. Further, longitudinal, multicenter studies with longer follow-up and larger population may clarify any relationship with the onset of a particular FAF pattern, any progression from one pattern to another, and whether or not retinal alterations have functional (e.g., localized scotomas) and/or prognostic (e.g., on the development of choroidal neovascularization) consequences.

Conflict of Interests

Giulio Barteselli is a full-time employee at Genentech, Inc. (a member of the Roche Group). The other authors have no financial interests to disclose.

Authors' Contribution

Dr. Maura Di Nicola and Dr. Giulio Barteselli contributed equally as first authors.

References

[1] G. M. Brittenham, "Iron-chelating therapy for transfusional iron overload," *The New England Journal of Medicine*, vol. 364, no. 2, pp. 146–156, 2011.

[2] J. B. Porter, "A risk-benefit assessment of iron-chelation therapy," *Drug Safety*, vol. 17, no. 6, pp. 407–421, 1997.

[3] A. Jacobs, "Iron overload: clinical and pathologic aspects," *Seminars in Hematology*, vol. 14, no. 1, pp. 89–113, 1977.

[4] P. Ackrill, A. J. Ralston, J. P. Day, and K. C. Hodge, "Successful removal of aluminium from patient with dialysis encephalopathy," *The Lancet*, vol. 2, no. 8196, pp. 692–693, 1980.

[5] H. K. Stummvoll, H. Graf, and V. Meisinger, "Effect of desferrioxamine on aluminum kinetics during hemodialysis," *Mineral and Electrolyte Metabolism*, vol. 10, no. 4, pp. 263–266, 1984.

[6] R. Haimovici, D. J. D'Amico, E. S. Gragoudas, S. Sokol, and Deferoxamine Retinopathy Study Group, "The expanded clinical spectrum of deferoxamine retinopathy," *Ophthalmology*, vol. 109, no. 1, pp. 164–171, 2002.

[7] Y.-L. Chan, C.-W. W. Chu, K.-W. Chik, L.-M. Pang, M.-K. Shing, and C.-K. Li, "Deferoxamine-induced dysplasia of the knee: sonographic features and diagnostic performance compared with magnetic resonance imaging," *Journal of Ultrasound in Medicine*, vol. 20, no. 7, pp. 723–728, 2001.

[8] S.-H. Chen, D.-C. Liang, H.-C. Lin, S.-Y. Cheng, L.-J. Chen, and H.-C. Liu, "Auditory and visual toxicity during deferoxamine therapy in transfusion-dependent patients," *Journal of Pediatric Hematology/Oncology*, vol. 27, no. 12, pp. 651–653, 2005.

[9] N. F. Olivieri, J. R. Buncic, E. Chew et al., "Visual and auditory neurotoxicity in patients receiving subcutaneous deferoxamine infusions," *The New England Journal of Medicine*, vol. 314, no. 14, pp. 869–873, 1986.

[10] A. Cohen, M. Martin, J. Mizanin, D. F. Konkle, and E. Schwartz, "Vision and hearing during deferoxamine therapy," *The Journal of Pediatrics*, vol. 117, no. 2, pp. 326–330, 1990.

[11] S. C. Davies, J. L. Hungerford, G. B. Arden, R. E. Marcus, M. H. Miller, and E. R. Huehns, "Ocular toxicity of high-dose intravenous desferrioxamine," *The Lancet*, vol. 2, no. 8343, pp. 181–184, 1983.

[12] V. Lakhanpal, S. S. Schocket, and R. Jiji, "Deferoxamine (Desferal)-induced toxic retinal pigmentary degeneration and presumed optic neuropathy," *Ophthalmology*, vol. 91, no. 5, pp. 443–451, 1984.

[13] C. Bene, A. Manzler, D. Bene, and G. Kranias, "Irreversible ocular toxicity from single "challenge" dose of deferoxamine," *Clinical Nephrology*, vol. 31, no. 1, pp. 45–48, 1989.

[14] G. B. Arden, B. Wonke, C. Kennedy, and E. R. Huehns, "Ocular changes in patients undergoing long-term desferrioxamine treatment," *British Journal of Ophthalmology*, vol. 68, no. 12, pp. 873–877, 1984.

[15] D. R. Blake, P. Winyard, J. Lunec et al., "Cerebral and ocular toxicity induced by desferrioxamine," *The Quarterly Journal of Medicine*, vol. 56, no. 219, pp. 345–355, 1985.

[16] A. H. S. Rahi, J. L. Hungerford, and I. Ahmed, "Ocular toxicity of desferrioxamine: light microscopic histochemical and ultrastructural findings," *The British Journal of Ophthalmology*, vol. 70, no. 5, pp. 373–381, 1986.

[17] M. Ravelli, P. Scaroni, S. Mombelloni et al., "Acute visual disorders in patients on regular dialysis given desferrioxamine as a test," *Nephrology Dialysis Transplantation*, vol. 5, no. 11, pp. 945–949, 1990.

[18] A. M. Mehta, R. E. Engstrom Jr., and A. E. Kreiger, "Deferoxamine-associated retinopathy after subcutaneous injection," *American Journal of Ophthalmology*, vol. 118, no. 2, pp. 260–262, 1994.

[19] V. Bansal, I. Elgarbly, F. D. Ghanchi, and P. L. Atkinson, "Bull's eye maculopathy with deferoxamine," *European Journal of Haematology*, vol. 70, no. 6, pp. 420–421, 2003.

[20] A. Arora, S. Wren, and K. G. Evans, "Desferrioxamine related maculopathy: a case report," *The American Journal of Hematology*, vol. 76, no. 4, pp. 386–388, 2004.

[21] C. R. Gonzales, A. P. Lin, R. E. Engstrom, and A. E. Kreiger, "Bilateral vitelliform maculopathy and deferoxamine toxicity," *Retina*, vol. 24, no. 3, pp. 464–467, 2004.

[22] R. R. Hidajat, J. L. McLay, D. H. Goode, and R. L. Spearing, "EOG as a monitor of desferrioxamine retinal toxicity," *Documenta Ophthalmologica*, vol. 109, no. 3, pp. 273–278, 2004.

[23] P. J. Kertes, T. K. M. Lee, and S. G. Coupland, "The utility of multifocal electroretinography in monitoring drug toxicity: deferoxamine retinopathy," *Canadian Journal of Ophthalmology*, vol. 39, no. 6, pp. 656–661, 2004.

[24] T. Y. Lai, G. K. Lee, W. M. Chan, and D. S. Lam, "Rapid development of severe toxic retinopathy associated with continuous intravenous deferoxamine infusion," *The British Journal of Ophthalmology*, vol. 90, no. 2, pp. 243–244, 2006.

[25] M. Lu, R. M. Hansen, M. J. Cunningham, S. E. Eklund, and A. B. Fulton, "Effects of desferoxamine on retinal and visual function," *Archives of Ophthalmology*, vol. 125, no. 11, pp. 1581–1582, 2007.

[26] J. S. Baath, W.-C. Lam, M. Kirby, and A. Chun, "Deferoxamine-related ocular toxicity: Incidence and outcome in a pediatric population," *Retina*, vol. 28, no. 6, pp. 894–899, 2008.

[27] M. A. Genead, G. A. Fishman, A. Anastasakis, and M. Lindeman, "Macular vitelliform lesion in desferrioxamine-related retinopathy," *Documenta Ophthalmologica*, vol. 121, no. 2, pp. 161–166, 2010.

[28] S. Simon, P. A. Athanasiov, R. Jain, G. Raymond, and J. S. Gilhotra, "Desferrioxamine-related ocular toxicity: a case report," *Indian Journal of Ophthalmology*, vol. 60, no. 4, pp. 315–317, 2012.

[29] F. Viola, G. Barteselli, L. Dell'Arti et al., "Abnormal fundus autofluorescence results of patients in long-term treatment with deferoxamine," *Ophthalmology*, vol. 119, no. 8, pp. 1693–1700, 2012.

[30] C. H. Wu, C. P. Yang, C. C. Lai, W. C. Wu, and Y. H. Chen, "Deferoxamine retinopathy: spectral domain-optical coherence tomography findings," *BMC Ophthalmology*, vol. 14, article 88, 2014.

[31] M. G. Marciani, P. Cianciulli, N. Stefani et al., "Toxic effects of high-dose deferoxamine treatment in patients with iron overload: an electrophysiological study of cerebral and visual function," *Haematologica*, vol. 76, no. 2, pp. 131–134, 1991.

[32] F. Viola, G. Barteselli, L. Dell'Arti et al., "Multimodal imaging in deferoxamine retinopathy," *Retina*, vol. 34, pp. 1428–1438, 2014.

[33] S. de Virgiliis, M. Congia, M. P. Turco et al., "Depletion of trace elements and acute ocular toxicity induced by desferrioxamine in patients with thalassaemia," *Archives of Disease in Childhood*, vol. 63, no. 3, pp. 250–255, 1988.

[34] A. E. Leure-duPree and C. J. McClain, "The effect of severe zinc deficiency on the morphology of the rat retinal pigment epithelium," *Investigative Ophthalmology and Visual Science*, vol. 23, no. 4, pp. 425–434, 1982.

[35] D. Tate and D. Newsome, "A novel zinc compound (zinc monocysteine) enhances the antioxidant capacity of human retinal pigment epithelial cells," *Current Eye Research*, vol. 31, no. 7-8, pp. 675–683, 2006.

[36] H. Pall, D. R. Blake, P. Winyard et al., "Ocular toxicity of desferrioxamine—an example of copper promoted auto-oxidative damage?" *The British Journal of Ophthalmology*, vol. 73, no. 1, pp. 42–47, 1989.

[37] A. Klettner, S. Koinzer, V. Waetzig, T. Herdegen, and J. Roider, "Deferoxamine mesylate is toxic for retinal pigment epithelium cells *in vitro*, and its toxicity is mediated by p38," *Cutaneous and Ocular Toxicology*, vol. 29, no. 2, pp. 122–129, 2010.

[38] G. Barteselli, L. Dell'Arti, R. P. Finger et al., "The spectrum of ocular alterations in patients with β-thalassemia syndromes suggests a pathology similar to pseudoxanthoma elasticum," *Ophthalmology*, vol. 121, no. 3, pp. 709–718, 2014.

[39] P. L. Gehlbach, R. L. Purple, P. E. Hallaway, and B. E. Hedlund, "Polymer conjugation reduces deferoxamine induced retinopathy in an albino rat model," *Investigative Ophthalmology & Visual Science*, vol. 34, no. 10, pp. 2871–2877, 1993.

[40] P. A. Good, A. Claxson, C. J. Morris, and D. R. Blake, "A model for desferrioxamine-induced retinopathy using the albino rat," *Ophthalmologica*, vol. 201, no. 1, pp. 32–36, 1990.

[41] G. B. Arden, "Desferrioxamine administered intravenously by infusion causes a reduction in the electroretinogram in rabbits anaesthetized with urethane," *Human Toxicology*, vol. 5, no. 4, pp. 229–236, 1986.

[42] C. Jiang, R. M. Hansen, B. E. Gee, S. S. Kurth, and A. B. Fulton, "Rod and rod mediated function in patients with β-thalassemia major," *Advances in Ophthalmology*, vol. 96, no. 4, pp. 333–345, 1998.

[43] F. C. Delori, C. K. Dorey, G. Staurenghi, O. Arend, D. G. Goger, and J. J. Weiter, "*In vivo* fluorescence of the ocular fundus exhibits retinal pigment epithelium lipofuscin characteristics," *Investigative Ophthalmology & Visual Science*, vol. 36, no. 3, pp. 718–729, 1995.

[44] U. Kellner, A. B. Renner, and H. Tillack, "Fundus autofluorescence and mfERG for early detection of retinal alterations in patients using chloroquine/hydroxychloroquine," *Investigative Ophthalmology & Visual Science*, vol. 47, no. 8, pp. 3531–3538, 2006.

[45] A. Bindewald, A. C. Bird, S. S. Dandekar et al., "Classification of fundus autofluorescence patterns in early age-related macular disease," *Investigative Ophthalmology and Visual Science*, vol. 46, no. 9, pp. 3309–3314, 2005.

[46] G. Barteselli, D.-U. Bartsch, F. Viola et al., "Accuracy of the heidelberg spectralis in the alignment between near-infrared image and tomographic scan in a model eye: a multicenter study," *The American Journal of Ophthalmology*, vol. 156, no. 3, pp. 588–592, 2013.

[47] V. de Sanctis, M. Roos, T. Gasser et al., "Impact of long-term iron chelation therapy on growth and endocrine functions in thalassaemia," *Journal of Pediatric Endocrinology and Metabolism*, vol. 19, no. 4, pp. 471–480, 2006.

[48] Y.-L. Chan, L.-M. Pang, K.-W. Chik, J. C. Y. Cheng, and C.-K. Li, "Patterns of bone diseases in transfusion-dependent homozygous thalassaemia major: predominance of osteoporosis and desferrioxamine-induced bone dysplasia," *Pediatric Radiology*, vol. 32, no. 7, pp. 492–497, 2002.

[49] N. F. Olivieri and G. M. Brittenham, "Iron-chelating therapy and the treatment of thalassemia," *Blood*, vol. 89, no. 3, pp. 739–761, 1997.

[50] G. J. Kontoghiorghes, "Deferasirox: uncertain future following renal failure fatalities, agranulocytosis and other toxicities," *Expert Opinion on Drug Safety*, vol. 6, no. 3, pp. 235–239, 2007.

[51] D. J. Roberts, S. J. Brunskill, C. Doree, S. Williams, J. Howard, and C. J. Hyde, "Oral deferiprone for iron chelation in people with thalassaemia," *The Cochrane Database of Systematic Reviews*, no. 3, Article ID CD004839, 2007.

[52] G. J. Kontoghiorghes, K. Pattichi, M. Hadjigavriel, and A. Kolnagou, "Transfusional iron overload and chelation therapy with deferoxamine and deferiprone (L1)," *Transfusion and Apheresis Science*, vol. 23, no. 3, pp. 211–223, 2000.

Hindawi Publishing Corporation
BioMed Research International
Volume 2015, Article ID 813242, 8 pages
http://dx.doi.org/10.1155/2015/813242

Review Article

Does Posterior Capsule Opacification Affect the Results of Diagnostic Technologies to Evaluate the Retina and the Optic Disc?

Jose Javier Garcia-Medina,[1,2,3,4] Monica del Rio-Vellosillo,[5] Vicente Zanon-Moreno,[3,4,6] Enrique Santos-Bueso,[7] Roberto Gallego-Pinazo,[3,4,8] Antonio Ferreras,[4,9] and Maria Dolores Pinazo-Duran[3,4,10]

[1] *Department of Ophthalmology, General University Hospital Reina Sofia, Avenida Intendente Jorge Palacios 1, 30003 Murcia, Spain*
[2] *Department of Ophthalmology and Optometry, School of Medicine, University of Murcia, Avenida Intendente Jorge Palacios 1, 30003 Murcia, Spain*
[3] *Ophthalmology Research Unit "Santiago Grisolia", Avenida Gaspar Aguilar, 90, 46017 Valencia, Spain*
[4] *Oftared-Retics, Instituto de Salud Carlos III, 28029 Madrid, Spain*
[5] *Department of Anesthesia, University Hospital Virgen de la Arrixaca, Ctra. Madrid-Cartagena, s/n, El Palmar, 30120 Murcia, Spain*
[6] *Department of Preventive Medicine & Public Health and CIBER Physiopathology of Obesity and Nutrition, School of Medicine, University of Valencia, Avenida Blasco Ibañez 15-17, 46010 Valencia, Spain*
[7] *Department of Ophthalmology, San Carlos University Hospital, Calle Profesor Martín Lagos, S/N, 28040 Madrid, Spain*
[8] *Department of Ophthalmology, University Hospital La Fe, Bulevar del Sur, 46026 Valencia, Spain*
[9] *Miguel Servet University Hospital, Aragon Health Sciences Institute, Paseo Isabel la Catolica, 1-3, 50009 Zaragoza, Spain*
[10] *Department of Ophthalmology, University School of Medicine, University of Valencia, Avenida Blasco Ibañez 15-17, 46010 Valencia, Spain*

Correspondence should be addressed to Jose Javier Garcia-Medina; josegarciam@yahoo.com

Received 14 July 2014; Accepted 1 February 2015

Academic Editor: Paolo Frezzotti

The visual outcome obtained after cataract removal may progressively decline because of posterior capsular opacification (PCO). This condition can be treated by creating an opening in the posterior lens capsule by Nd:YAG laser capsulotomy. PCO optical imperfections cause several light reflection, refraction, and diffraction phenomena, which may interfere with the functional and structural tests performed in different ocular locations for the diagnosis and follow-up of ocular disease, like macular and optic nerve diseases. Some parameters measured by visual field examinations, scanning laser polarimetry, and optical coherence tomography (OCT) have changed after PCO removal. Imaging quality also changes following capsulotomy. Consequently, the results of ancillary tests in pseudophakic eyes for studying ocular diseases like glaucoma or maculopathies should be correlated with other clinical examinations, for example, slit-lamp biomicroscopy or funduscopy. If PCO is clinically significant, a new baseline should be set for future comparisons following capsulotomy when using automated perimetry and scanning laser polarimetry. To perform OCT in the presence of PCO, reliable examinations (considering signal strength) apparently guarantee that measurements are not influenced by PCO.

1. Introduction

Phacoemulsification with implantation of intraocular lens in the capsular bag is the most frequent surgical procedure performed in ophthalmology. However, the visual gain obtained after cataract removal may progressively decline due to posterior capsular opacification (PCO) [1].

Despite variations in surgical techniques, intraocular lens material or design, implantation of additional devices,

and pharmacological interventions, PCO remains the most frequent long term complication after cataract surgery [1]. Published PCO rates are variable. However, a meta-analysis concluded that approximately 25% of patients operated from extracapsular cataract surgery suffered visually significant PCO within 5 years of the operation [2].

PCO is due to the proliferation of lens residual epithelial cells from the lens equator following cataract extraction, which induces visual alteration by direct interaction with light passing through the visual axis [3]. According to the distribution of proliferation, the resulting opacities may adopt a morphologic pattern or two or even a combination of both: (a) fibrous-type PCO (fibrous epithelial layers) and (b) pearl-type PCO (groups of swollen, optically active, opacified grape-like epithelial growth) [4]. In clinical terms, these changes can diminish visual acuity significantly, alter contrast sensitivity, and cause glare and monocular diplopia [5–7].

Metaplasia of epithelial cells may also induce capsular folds because of mechanical forces. In general terms, these epithelial cells may transform into myofibroblasts, which have contractile properties and allow the posterior capsule to wrinkle [4]. These phenomena may create visual distortions, including a Maddox rod effect, metamorphopsia-like phenomena, or glare [8].

All of these effects together, these being irregular formations of fibrous proliferation, pearls, and puckers of the posterior capsule generate special properties that affect light reflection, refraction, and diffraction, which may interfere not only with patient vision (Figure 1), but also with functional and structural ocular diagnostic tests [2].

PCO-induced visual affection can be solved by laser Nd:YAG capsulotomy by producing an opening in the posterior capsule and avoiding distortion of light in its passage [1, 4].

An observation made before and after capsulotomy of the outcome of different diagnostic examinations to estimate ocular diseases provides a better understanding of the effects of PCO on such technologies. Recent research suggests that PCO may affect the appropriate ocular disease assessments made by automated perimetry, scanning laser polarimetry, or optical coherence tomography, as seen in Table 1.

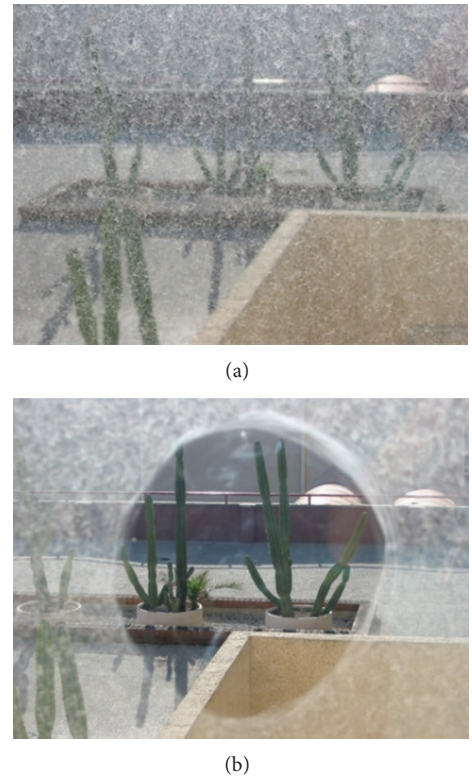

(a)

(b)

Figure 1: Simulation of vision in a PCO-affected eye before (a) and after Nd:YAG capsulotomy (b).

2. Effect of PCO on Automated Perimetry

A visual field test through white-on-white automated perimetry is a widely used technique and is a useful tool for the diagnosis and follow-up of several ocular disorders, such as glaucoma and neuroophthalmological diseases [9, 10]. Translucent irregularities in the anterior ocular pole, for example, cataracts or PCO, can be a confusing factor that may lead to an inappropriate interpretation of automated perimetry, even when it is not uncommon to encounter patients who are affected or are suspected of being affected, by concurrent entities, for example, PCO and glaucoma or PCO and macular oedema. The ophthalmologist must assess how much visual impairment is due to PCO and how much is related to the other concomitant disorder.

The effect that cataract has on automated perimetry has been well investigated [11–13]. Our research group completed a study in eyes of patients with PCO who underwent a white-on-white automated perimetry test (Humphrey SITA standard programme 24-2) immediately before Nd:YAG capsulotomy and between postsurgery weeks 1 and 8 [14]. The compared pre- and postlaser perimetric indices were mean defect (MD) and pattern standard deviation (PSD).

MD is the average measure of how depressed the patient's visual field is (compared with a control of the same age). Several researchers have reported that MD improved after cataract surgery [11–13]. Similarly according to our results, amelioration of MD occurred after capsulotomy [14].

PSD is a measure of how the different adjacent points on a visual field are. If an area is focally depressed, PSD will rise given the major difference between the points in scotoma and their normal adjacent points. PSD remains unchanged after cataract removal [11–13]. Compared to PCO, however, the PSD in our study improved significantly after capsulotomy. This change could be explained by optical PCO features. PCO translucent opacities apparently induce erratic light-scatter within the eye, which results in a combination of underilluminated retinal areas and in an increased PSD. Yet when these irregularities have been eliminated through capsulotomy, retinal illumination can be more uniform, so PSD lowers [14].

As the clinical slit-lamp examination aspect can be somewhat guesswork-related and as the automated perimetry analysis corroborates, cataracts depress an automated visual

Table 1: Studies considering the influence of PCO on test results.

Author (year) [reference number]	Test	n	Precapsulotomy BCVA (mean ± SD)	Postcapsulotomy BCVA (mean ± SD)	Results after capsulotomy
García-Medina et al. (2006) [14].	AP	26	0.35 ± 0.11 (decimal scale)	0.84 ± 0.14 (decimal scale)	MD and PSD improved.
García-Medina et al. (2006) [23]	SLP	28	0.41 ± 0.12 (decimal scale)	0.85 ± 0.13 (decimal scale)	NFI and TSS increased. Significant decreases of all absolute parameters.
Vetrugno et al. (2007) [24]	SLP	158	0.3 ± 0.6 (LogMar)	0.05 ± 0.2 (LogMar)	Inferior ratio and TSNIT SD decreased. Superior/nasal increased.
Brittain et al. (2007) [25]	SLP	20	0.32 ± un (LogMar)	0.14 ± un (LogMar)	TSS and TSNIT SD increased. TSNIT score decreased.
Arraes et al. (2008) [26]	SLP	37	0.2 ± un (decimal scale)	0.8 ± un (decimal scale)	No significant difference between parameters.
Hougaard et al. (2001) [35]	TD-OCT	13	0.29 ± un (decimal scale)	0.39 ± un (decimal scale)	Signal-to-noise ratio increased but no changes in macular thickness.
Garcia-Medina et al. (2007) [32]	TD-OCT	32	0.25 ± 0.17 (decimal scale)	0.77 ± 0.22 (decimal scale)	SS increased but no changes in pRNFL thicknesses (in reliable exams).
González-Ocampo-Dorta et al. (2008) [40]	TD-OCT	32	0.25 ± 0.17 (decimal scale)	0.77 ± 0.22 (decimal scale)	SS increased but no changes in macular thicknesses (in reliable exams).
Altiparmak et al. (2010) [36]	TD-OCT	54	0.47 ± 0.3 (decimal scale)	0.91 ± 0.14 (decimal scale)	No change of the foveal thickness.
Giocanti-Aurégan et al. (2011) [37]	TD-OCT	30	0.6 ± 0.3 (LogMar)	0.1 ± 0.3 (LogMar)	No change of the foveal thickness.
Wróblewska-Czajka et al. (2012) [38]	TD-OCT	55	NA	NA	No change of the central macular thickness.
Kara et al. (2012) [31]	TD-OCT	98	0.49 ± 0.28 (LogMar)	0.09 ± 0.11 (LogMar)	SS and pRNFL thicknesses increased.
Garcia-Medina et al. (2013) [34]	SD-OCT	37	0.27 ± 0.19 (decimal scale)	0.83 ± 0.18 (decimal scale)	All pRNFL thickness parameters increased. No changes when considering reliable examinations.
Garcia-Medina et al. (2013) [41]	SD-OCT	35	0.23 ± 0.28 (decimal scale)	0.81 ± 0.16 (decimal scale)	All macular thickness parameters increased. No changes when considering reliable examinations.
Ruiz-Casas et al. (2013) [39]	SD-OCT	31	0.4 ± NA	0.8 ± NA	No change of the foveal thickness.

BCVA: best-corrected visual acuity, SD: standard deviation, AP: automated perimetry, MD: mean deviation, PSD: pattern standard deviation, SLP: scanning laser polarimetry, NFI: nerve fiber indicator, TSS: typical scan score, TSNIT: temporal-superior-nasal-inferior-temporal, NA: not available, TD-OCT: time domain optical coherence tomography, SD-OCT: spectral domain optical coherence tomography, SS: signal strength, and pRNFL = peripapillary retinal nerve fiber layer.

field quite uniformly. So they constitute homogeneous opacities. However, PCOs depress the visual field heterogeneously. Therefore, they have been demonstrated as being polymorphous opacities that may even mimic pathological patterns [14], such as glaucoma arcuate scotoma, which are susceptible to elimination after capsulotomy (Figure 2).

In conclusion, PCO has proven to be a heterogeneous mean opacity. This polymorphism may alter visual field results. For practical purposes, a perimetric defect produced by a PCO can be confused in some cases with a pathologic perimetric defect (false-positive). Consequently, presence of PCO should be taken into account while evaluating any automated perimetry in eyes operated from cataracts.

3. Influence of Posterior Capsular Opacification on Scanning Laser Polarimetry

Scanning laser polarimetry (SLP) is a technology for estimating retinal nerve fibre layer (RNFL) thickness *in vivo* at a specific location [15]. It is based on the principle that a polarised laser beam changes its polarisation status when passing through a birefringent tissue. The RNFL is made up of highly ordered parallel axon bundles that contain microtubules, which is the source of its birefringence [15]. As polarised light passes through the RNFL and is reflected back, it undergoes a phase shift. This change in polarisation

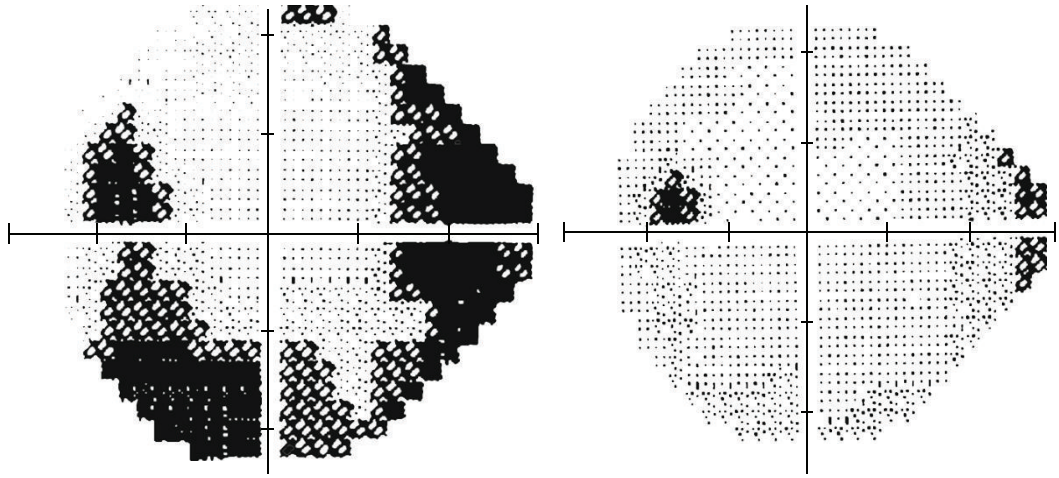

(a) (b)

Figure 2: Perimetric defect that mimics inferior arcuate scotoma in a PCO-affected eye (a). The defect partially disappeared after capsulotomy (b).

(retardation), as measured by SLP, correlates with RNFL thickness [16, 17]. Therefore, SLP allows a quantitative assessment of the degree of thinning of the peripapillary RNFL. Such information has been demonstrated as being clinically useful in screening and following up both glaucoma [18–20] and nonglaucomatous optic neuropathies, such as anterior ischaemic optic neuropathy, optic nerve head drusen, and demyelinating optic neuritis [21].

Nevertheless, the RNFL is not the only birefringent structure in the eye. The anterior segment also has birefringent properties, mainly the cornea. Therefore, total retardation of a subject's eye is the sum of both the anterior segment and RNFL birefringence. Accuracy of SLP measurements depends on the ability to isolate RNFL retardation from total ocular retardation [21].

To reduce the effect of anterior segment polarisation, the newest GDx generation incorporates a variable corneal compensator (VCC) that enables compensation of the anterior segment birefringence (ASB) in each individual eye [21].

Several research works into the effect that PCO and subsequent Nd:YAG capsulotomy have on the SLP results of RNFL retardation measurements have been conducted [22–26]. With this purpose in mind, our research group performed a study into PCO-affected eyes and SLP, selected using GDx VCC, on each patient before and after capsulotomy. We compensated ASB before doing any SLP examination. We compared the SLP parameters before and after PCO removal. We concluded that PCO removal is associated with remarkably significant changes in all the SLP measurements. Briefly, our results suggest that thickness parameters are higher before than after capsulotomy. In other words, SLP examination with GDx VCC may overestimate RNFL retardation measurements in PCO-affected eyes. Therefore, the glaucoma diagnosis in PCO can be underestimated on the basis of the SLP results (false-negatives) (Figure 3) [22, 23]. Furthermore, some SLP measurements (nasal average and nerve fibre indicator) have been significantly associated with best-corrected visual acuity (BCVA) before capsulotomy, which suggests that this technology may be useful for quantifying the degree of PCO [23]. However other authors have not found as many changes in the GDx parameters before and after

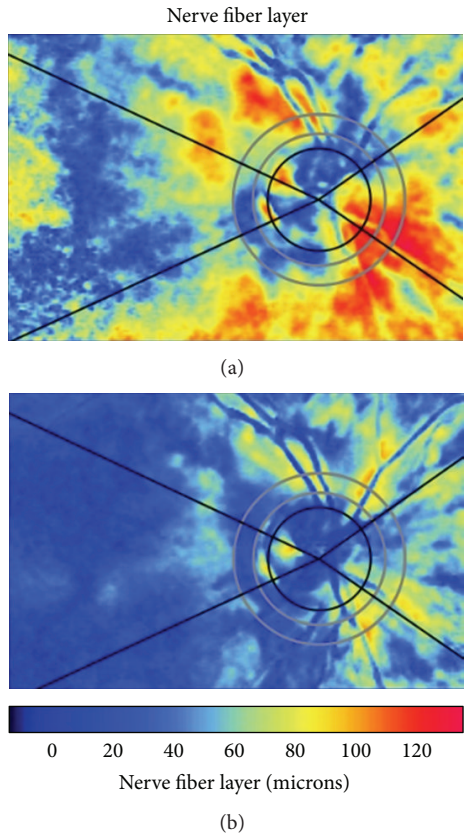

Figure 3: Scanning laser polarimetry examination before (a) and after Nd:YAG capsulotomy (b). Note that the thickness measurements reduce after PCO removal.

PCO removal. Vetrugno et al. [24] reported modifications in symmetry, inferior ratio, superior, nasal, and temporal-superior-nasal-inferior-temporal SD whereas Brittain et al. [25] showed significant changes in the typical scan score and temporal-superior-nasal-inferior-temporal average. In addition, Arraes et al. did not show any significant difference between the thickness parameters before and after posterior capsulotomy in patients with moderate degrees of PCO [26]. The variability of the results can be related to the fact that anterior segment birefringence is only assessed before and after laser capsulotomy [23] or only before capsulotomy [25]. The characteristics of the population included in these studies can also be related to this variability noted in the results [23–25].

We also performed a study on a new series of PCO affected eyes that supports our previous conclusions of GDx VCC measurements. In this study we also observed that corneal polarisation axis and corneal polarisation magnitude (the two parameters that determine ASB) changed significantly after PCO removal [27, 28].

Although the results of different studies in the literature are not fully coincident, it is advisable to not only repeat the SLP examination after capsulotomy to serve as a new baseline for the future but also recompensate ASB after Nd:YAG laser application to obtain reliable measurements using GDx VCC.

4. Effect of PCO on Optical Coherence Tomography

Optical coherence tomography (OCT) generates high resolution, 2-dimensional cross-sectional images of the internal microstructure of ocular structures. Transverse images of the device are produced using low coherence tomography, an optical measuring technique that is analogous to a B-scan ultrasound, but instead of sound waves, OCT uses a laser-generated beam of light. Two kinds of OCT are available to date: time domain OCT and, more recently, spectral domain OCT. Although both types of OCT use the same basic working principles, the scan rate and axial resolution have improved in spectral domain OCT [29].

OCT explored structures like the peripapillary RNFL and the central retina (including total macular thickness). RNFL thickness, measured by OCT, has been used to study glaucomatous neuropathy, anterior ischaemic optic neuropathy, optic nerve head drusen, demyelinating optic neuritis, traumatic optic tract lesion, Leber hereditary optic neuropathy, and toxic optic neuropathy [21]. Macular assessment by OCT has proved to be a very useful tool for studying the vitreoretinal interface, intraretinal oedema, neuroepithelial detachment, impairments in normal retina architectonics, and its pigment epithelium or choroidal disorders, no matter what its aetiology is [30].

In theory, PCO optical translucent imperfections can alter this beam of light and can, consequently, induce artifactual results in OCT thickness and quality parameters. Several studies have been performed to answer this question.

In relation to peripapillary RNFL measurements, Kara et al. [31] recently investigated the effect that PCO has on the results of RNFL thickness measured by time domain OCT (Stratus, Zeiss). These authors divided eyes into groups according to each signal strength (SS) value obtained, including unreliable (SS < 5) and reliable examinations (SS > 5). They also compared the thickness in each group independently and observed that the lower the SS value, the greater the precapsulotomy RNFL average underestimation and the more significant the results. They concluded that RNFL thickness is affected by PCO. Our group previously carried out a similar study with time domain OCT (Stratus, Zeiss) [32, 33]. We also obtained a significant increase in SS but found no changes in RNFL thicknesses after capsulotomy in reliable scans. When considering all the scans (reliable: SS ≥ 6 and unreliable examinations: SS < 6), we concluded that PCO induces an underestimation of RNFL thickness parameters (Figure 4) as measured by spectral domain OCT (Cirrus, Zeiss). However when analyzing only reliable examinations, no changes between pre- and postlaser measurements were observed [34]. This finding suggests that the prelaser SS value may orientate the degree of reliability of the results, as previously described by Kara et al. [31].

As far as the central retina is concerned, macular thickness parameters have also been compared before and after Nd:YAG capsulotomy in several studies in order to directly assess OCT performance or to indirectly check the safety of the procedures for evaluating macular cystoid oedema as a complication of PCO removal. Most research has shown in both the short and long term that macular thickness parameters, as measured by OCT, have not been seen to change after Nd:YAG laser capsulotomy [35–39]. In one study by our group performed with time domain OCT (Stratus, Zeiss), we concluded that OCT image quality is influenced by PCO. Nd:YAG capsulotomy results in a measurable improvement in quality and improves the number of valuable examinations. However, valuable OCT scans in patients with PCO did not show changes in macular thickness measurements, not even in the presence of severe PCO [40]. In a more recent study using spectral domain OCT (Cirrus, Zeiss), we concluded that all the parameters in the comparisons thickness were higher after capsulotomy than they were before (Figure 5). Yet when we considered only patients with a signal strength of ≥6 (reliable scans), no significant differences were observed in the measurements taken before and after PCO removal [41].

5. Additional Comments

Some other concerns should be taken into account when considering the influence of PCO on the above-mentioned tests. Firstly, PCO may have different patterns, that is, central, paracentral, and diffuse ones, which may differently affect the quality and the results of functional and structural tests. The example of the visual field may reflect a paracentral PCO (Figure 2). However to the best of our knowledge, this fact has not been considered in studies to date. Secondly, some data indicate the relation between degree of PCO and test abnormality. Degree of PCO could have also been estimated directly by BCVA. In one study on automated perimetry, the correlation results revealed that BCVA, MD, and PSD were

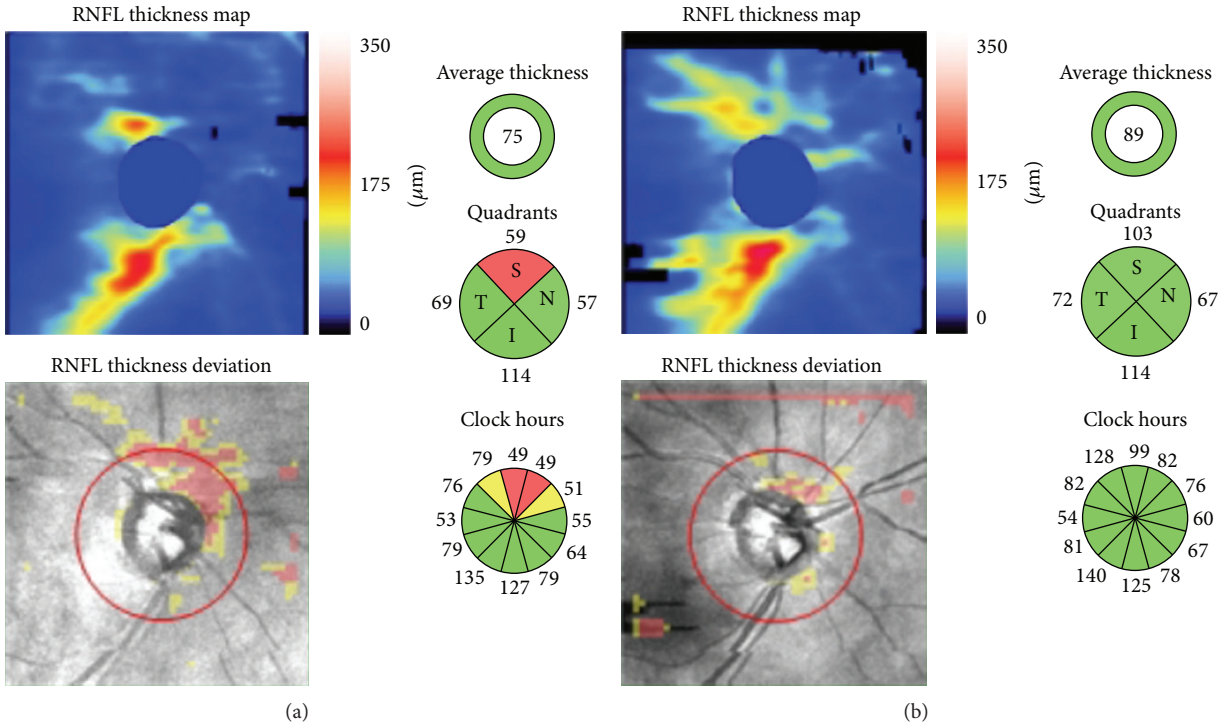

Figure 4: OCT maps of RNFL thickness before (a) and after (b) capsulotomy. Note that thickness measurements increase in the top half of the map after PCO removal.

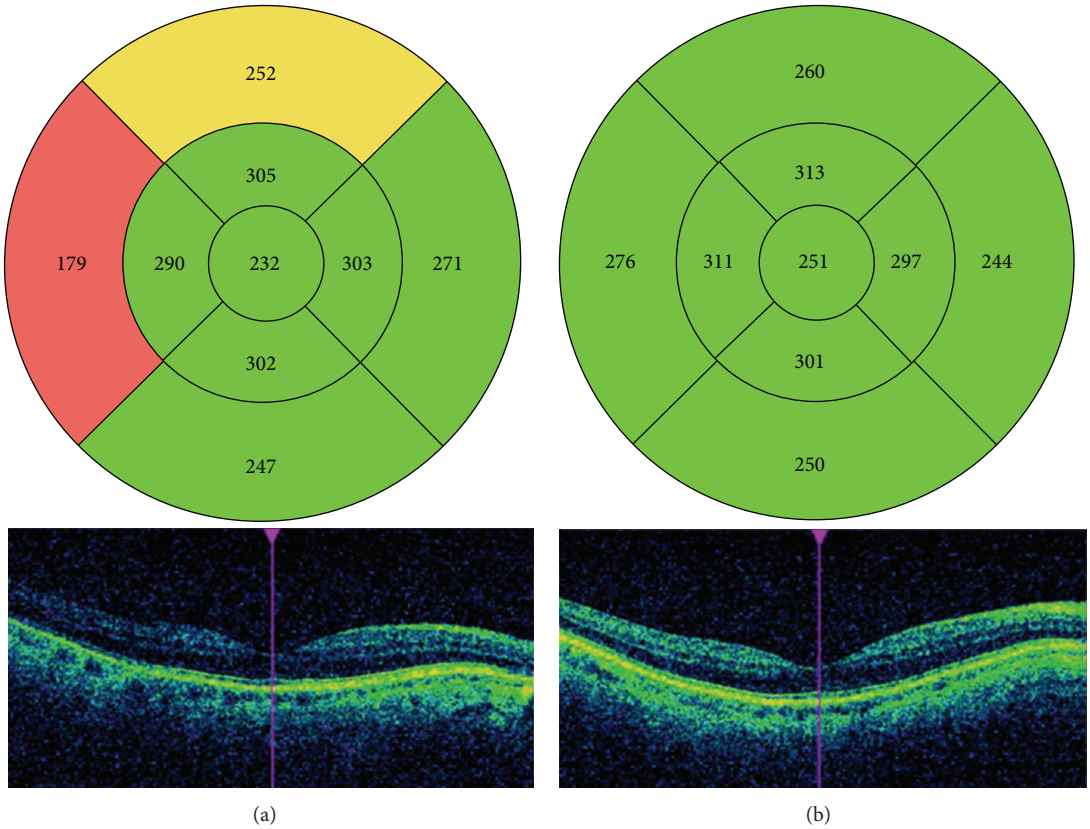

Figure 5: OCT maps of total macular thickness before (a) and after (b) the capsulotomy. Note that most of the thickness measurements increase and image quality improves after PCO removal.

significantly associated both before and after capsulotomy [14]. Another study showed some SLP measurements associated significantly with BCVA before capsulotomy, which indicates that this technology may be useful for quantifying degree of PCO [23]. In relation to OCT, the correlation found between BCVA and SS before capsulotomy suggests that SS could be considered an objective indicator of degree of PCO [40]. Kara et al. [31] also found a significant correlation between, on the one hand, preoperative BCVA and SS and, on the other hand, between preoperative BCVA and degree of PCO. Finally, differences between instruments may be due to, at least in part, differences in inclusion criteria between studies and characteristics of included eyes.

6. Conclusion

Optical translucent imperfections of PCO induce special properties relating to reflection, refraction, and diffraction that may alter the ancillary tests used in the diagnosis and follow-up of different optic nerve diseases.

In fact the results of automated perimetry and SLP have been shown to change after capsulotomy. In addition, OCT quality imaging of RNFL thickness is influenced by PCO. However, no change has been observed after PCO removal in the retinal nerve fibre layer parameters of pseudophakic eyes by reliable examinations before capsulotomy, as measured by OCT.

Thus, features of ancillary tests in pseudophakic eyes for studying optic nerve diseases should be well-interpreted and should correlate with other clinical examinations, such as slit-lamp biomicroscopy. If a clinically significant PCO is detected, new measurements should be considered after PCO removal to serve as a baseline for future comparisons, especially when using automated perimetry and SLP. As for OCT in the presence of PCO, reliable examinations (considering signal strength) apparently guarantee that the measurements taken before and after capsulotomy are similar.

Conflict of Interests

The authors declare that there is no conflict of interests regarding the publication of this paper.

References

[1] O. Findl, W. Buehl, P. Bauer, and T. Sycha, "Interventions for preventing posterior capsule opacification," *Cochrane Database of Systematic Reviews*, no. 3, Article ID CD003738, 2007.

[2] D. A. Schaumberg, M. R. Dana, W. G. Christen, and R. J. Glynn, "A systematic overview of the incidence of posterior capsule opacification," *Ophthalmology*, vol. 105, no. 7, pp. 1213–1221, 1998.

[3] D. J. Apple, K. D. Solomon, M. R. Tetz et al., "Posterior capsule opacification," *Survey of Ophthalmology*, vol. 37, no. 2, pp. 73–116, 1992.

[4] I. M. Wormstone, L. Wang, and C. S. C. Liu, "Posterior capsule opacification," *Experimental Eye Research*, vol. 88, no. 2, pp. 257–269, 2009.

[5] M. Claesson, L. Klaren, C. Beckman, and J. Sjostrand, "Glare and contrast sensitivity before and after Nd:YAG laser capsulotomy," *Acta Ophthalmologica*, vol. 72, no. 1, pp. 27–32, 1994.

[6] P. Sunderraj, J. R. Villada, P. W. Joyce, and A. Watson, "Glare testing in pseudophakes with posterior capsule opacification," *Eye*, vol. 6, no. 4, pp. 411–413, 1992.

[7] J. J. García Medina, M. García Medina, M. D. Pinazo Durán, and M. Morales Suarez-Varela, "Monocular diplopia after neodymium: YAG laser capsulotomy," *Graefe's Archive for Clinical and Experimental Ophthalmology*, vol. 243, no. 12, pp. 1288–1290, 2005.

[8] J. T. Holladay, J. E. Bishop, and J. W. Lewis, "Diagnosis and treatment of mysterious light streaks seen by patients following extacapsular cataract extraction," *The American Intra-Ocular Implant Society Journal*, vol. 11, no. 1, pp. 21–23, 1985.

[9] S. P. Donahue, "Perimetry techniques in neuro-ophthalmology," *Current Opinion in Ophthalmology*, vol. 10, no. 6, pp. 420–428, 1999.

[10] M. Wall, S. G. Punke, T. L. Stickney, C. F. Brito, K. R. Withrow, and R. H. Kardon, "SITA standard in optic neuropathies and hemianopias: a comparison with full threshold testing," *Investigative Ophthalmology and Visual Science*, vol. 42, no. 2, pp. 528–537, 2001.

[11] B. L. Lam, W. L. M. Alward, and H. E. Kolder, "Effect of cataract on automated perimetry," *Ophthalmology*, vol. 98, no. 7, pp. 1066–1070, 1991.

[12] S. D. Smith, J. Katz, and H. A. Quigley, "Effect of cataract extraction on the results of automated perimetry in glaucoma," *Archives of Ophthalmology*, vol. 115, no. 12, pp. 1515–1519, 1997.

[13] Y. Y. Kim, J. S. Kim, D. H. Shin, B. C. Kim, and H. R. Jung, "Effect of cataract extraction on blue-on-yellow visual field," *The American Journal of Ophthalmology*, vol. 132, no. 2, pp. 217–220, 2001.

[14] J. J. García-Medina, M. García-Medina, M. T. Arbona-Nadal, and M. D. Pinazo-Duran, "Effect of posterior capsular opacification removal on automated perimetry," *Eye*, vol. 20, no. 5, pp. 537–545, 2006.

[15] Q. Zhou and R. W. Knighton, "Light scattering and form birefringence of parallel cylindrical arrays that represent cellular organelles of the retinal nerve fiber layer," *Applied Optics*, vol. 36, no. 10, pp. 2273–2285, 1997.

[16] R. N. Weinreb, A. W. Dreher, A. Coleman, H. Quigley, B. Shaw, and K. Reiter, "Histopathologic validation of Fourier-ellipsometry measurements of retinal nerve fiber layer thickness," *Archives of Ophthalmology*, vol. 108, no. 4, pp. 557–560, 1990.

[17] A. W. Dreher, K. Reiter, and R. N. Weinreb, "Spatially resolved birefringence of the retinal nerve fiber layer assessed with a retinal laser ellipsometer," *Applied Optics*, vol. 3, no. 19, pp. 3730–3735, 1992.

[18] N. T. Choplin and D. C. Lundy, "The sensitivity and specificity of scanning laser polarimetry in the detection of glaucoma in a clinical setting," *Ophthalmology*, vol. 108, no. 5, pp. 899–904, 2001.

[19] R. N. Weinreb, C. Bowd, and L. M. Zangwill, "Glaucoma detection using scanning laser polarimetry with variable corneal polarization compensation," *Archives of Ophthalmology*, vol. 121, no. 2, pp. 218–224, 2003.

[20] N. J. Reus and H. G. Lemij, "Diagnostic accuracy of the GDx VCC for glaucoma," *Ophthalmology*, vol. 111, no. 10, pp. 1860–1865, 2004.

[21] G. L. Trick, F. Y. Calotti, and B. Skarf, "Advances in imaging of the optic disc and retinal nerve fiber layer," *Journal of Neuro-Ophthalmology*, vol. 26, no. 4, pp. 284–295, 2006.

[22] J. J. García Medina, M. García Medina, M. Shahin, and M. D. Pinazo Durán, "Posterior capsular opacification affects scanning laser polarimetry examination," *Graefe's Archive for Clinical and Experimental Ophthalmology*, vol. 244, no. 4, pp. 520–523, 2006.

[23] J. J. García-Medina, M. García-Medina, S. G.-O. Dorta, M. D. Pinazo-Durán, R. Gallego-Pinazo, and V. C. Zanón-Moreno, "Effect of posterior capsular opacification removal on scanning laser polarimetry measurements," *Graefe's Archive for Clinical and Experimental Ophthalmology*, vol. 244, no. 11, pp. 1398–1405, 2006.

[24] M. Vetrugno, F. Masselli, G. Greco et al., "The influence of posterior capsule opacification on scanning laser polarimetry," *Eye*, vol. 21, no. 6, pp. 760–763, 2007.

[25] C. J. Brittain, K. C. S. Fong, C. C. Hull, and I. H. Gillespie, "Changes in scanning laser polarimetry before and after laser capsulotomy for posterior capsular opacification," *Journal of Glaucoma*, vol. 16, no. 1, pp. 112–116, 2007.

[26] T. A. Arraes, H. D. Cavalcanti, J. Arraes, A. C. de Souza Leão, and M. F. Sena, "Analysis of the nerve fiber layer using GDx in pseudophakic patients with posterior capsular opacification," *Arquivos Brasileiros de Oftalmologia*, vol. 71, no. 1, pp. 75–78, 2008.

[27] J. J. Garcia-Medina, M. Garcia-Medina, V. C. Zanon-Moreno et al., "The influence of posterior capsular opacification removal on anterior segment birefringence parameters as measured by scanning laser polarimetry," *Clinical and Experimental Ophthalmology*, vol. 35, no. 5, pp. 414–420, 2007.

[28] J. J. Garcia-Medina, S. Gonzalez-Ocampo, and M. Garcia-Medina, "Scanning laser polarimetry: what could we measure?" *Clinical and Experimental Ophthalmology*, vol. 36, no. 1, pp. 100–101, 2008.

[29] D. S. Grewal and A. P. Tanna, "Diagnosis of glaucoma and detection of glaucoma progression using spectral domain optical coherence tomography," *Current Opinion in Ophthalmology*, vol. 24, no. 2, pp. 150–161, 2013.

[30] J. J. Wong, T. C. Chen, L. Q. Shen, and L. R. Pasquale, "Macular imaging for glaucoma using spectral-domain optical coherence tomography: a review," *Seminars in ophthalmology*, vol. 27, no. 5-6, pp. 160–166, 2012.

[31] N. Kara, H. Altinkaynak, K. Yuksel, T. Kurt, and A. Demirok, "Effects of posterior capsular opacification on the evaluation of retinal nerve fiber layer as measured by stratus optical coherence tomography," *Canadian Journal of Ophthalmology*, vol. 47, no. 2, pp. 176–180, 2012.

[32] J. J. Garcia-Medina, S. Gonzalez-Ocampo-Dorta, A. Feliciano-Sanchez et al., "Changes in optical coherence tomography after posterior capsular opacification removal. poster communication number 95," in *Proceedings of the Congress of the American Academy of Ophthalmology*, New Orleans, La, USA, 2007, http://aao.scientificposters.com/epsSearchAAO.cfm.

[33] J. J. García-Medina, M. García-Medina, and S. González-Ocampo-Dorta, "Posterior capsular opacification: one factor to be considered for the study of the optic nerve," *Archivos de la Sociedad Espanola de Oftalmologia*, vol. 84, no. 1, pp. 1–4, 2009.

[34] J. J. Garcia Medina, J. J. Gómez Fernández, S. Valentino et al., "Influence of the posterior capsular opacification in the measurement of thickness of macular ganglion cell complex and retinal nerve fiber layer by means of spectral domain OCT," in *Proceedings of the 8th Congress of the Spanish Society of Glaucoma*, Córdoba, Spain, March 2013, http://www.sociedadglaucoma.com/nova/NNws_ShwNewDup?codigo=3567&cod_primaria=1453&cod_secundaria=100765.

[35] J. L. Hougaard, M. Wang, B. Sander, and M. Larsen, "Effects of pseudophakic lens capsule opacification on optical coherence tomography of the macula," *Current Eye Research*, vol. 23, no. 6, pp. 415–421, 2001.

[36] U. E. Altiparmak, I. Ersoz, D. Hazirolan, B. Koklu, R. Kasim, and S. Duman, "The impact of Nd:YAG capsulotomy on foveal thickness measurement by optical coherence tomography," *Ophthalmic Surgery Lasers and Imaging*, vol. 41, no. 1, pp. 67–71, 2010.

[37] A. Giocanti-Aurégan, J. Tilleul, C. Rohart et al., "OCT measurement of the impact of Nd:YAG laser capsulotomy on foveal thickness," *Journal Francais d'Ophtalmologie*, vol. 34, no. 9, pp. 641–646, 2011.

[38] E. Wróblewska-Czajka, E. Wylegała, D. Tarnawska, A. Nowińska, and D. Dobrowolski, "Assessment of retinal thickness obtain by optical coherence tomography after Nd: YAG capsulotomy," *Klinika Oczna*, vol. 114, no. 3, pp. 194–197, 2012.

[39] D. Ruiz-Casas, C. Barrancos, J. L. Alio II, M. Ruiz-Guerrero, and F. J. Muñoz-Negrete, "Effect of posterior neodymium:YAG capsulotomy. Safety evaluation of macular foveal thickness, intraocular pressure and endothelial cell loss in pseudophakic patients with posterior capsule opacification," *Archivos de la Sociedad Espanola de Oftalmologia*, vol. 88, no. 11, pp. 415–422, 2013.

[40] S. González-Ocampo-Dorta, J. J. García-Medina, A. Feliciano-Sánchez, and G. Scalerandi, "Effect of posterior capsular opacification removal on macular optical coherence tomography," *European Journal of Ophthalmology*, vol. 18, no. 3, pp. 435–441, 2008.

[41] J. J. Garcia-Medina, J. J. Gómez-Fernández, S. Valentino, M. Morcillo-Guardiola, J. C. Villada-Sánchez, and A. Pastor Grau, "Effects of posterior capsule opacification on macular thickness measurements by spectral domain OCT. International SIRCOVA-OFTARED Congress Abstract," *Ophthalmic Research*, vol. 50, pp. 27–53, 2013, http://www.karger.com/Article/Pdf/351623.

Hindawi Publishing Corporation
BioMed Research International
Volume 2015, Article ID 981471, 5 pages
http://dx.doi.org/10.1155/2015/981471

Research Article

Relationship between Outer Retinal Layers Thickness and Visual Acuity in Diabetic Macular Edema

Raymond L. M. Wong,[1,2] Jacky W. Y. Lee,[1,3] Gordon S. K. Yau,[3] and Ian Y. H. Wong[1]

[1]*Department of Ophthalmology, The University of Hong Kong, Room 301, Level 3, Block B, Cyberport 4, Pokfulam, Hong Kong*
[2]*Department of Ophthalmology and Visual Science, The Chinese University of Hong Kong, Kowloon, Hong Kong*
[3]*Department of Ophthalmology, Caritas Medical Centre, Kowloon, Hong Kong*

Correspondence should be addressed to Ian Y. H. Wong; wongyhi@hku.hk

Received 10 September 2014; Accepted 23 March 2015

Academic Editor: Paolo Frezzotti

Purpose. To investigate the correlation of outer retinal layers (ORL) thickness and visual acuity (VA) in patients with diabetic macular edema (DME). *Methods*. Consecutive DME patients seen at the Retina Clinic of The University of Hong Kong were recruited for OCT assessment. The ORL thickness was defined as the distance between external limiting membrane (ELM) and retinal pigment epithelium (RPE) at the foveal center. The correlation between total retinal thickness, ORL thickness, and vision was calculated. *Results*. 78 patients with DME were recruited. The mean age was 58.1 years (±11.5 years) and their mean visual acuity measured with Snellen chart was 0.51 (±0.18). The correlation coefficient between total retinal thickness and visual acuity was 0.34 ($P < 0.001$) whereas the correlation coefficient was 0.65 between ORL thickness and visual acuity ($P < 0.001$). *Conclusion*. ORL thickness correlates better with vision than the total retinal thickness. It is a novel OCT parameter in the assessment of DME. Moreover, it could be a potential long term visual prognostic factor for patients with DME.

1. Introduction

Diabetes mellitus is one of the commonest chronic diseases affecting all populations especially developed countries. Diabetic macular edema (DME), being a complication of diabetes, is an important cause of visual loss in developed countries [1, 2]. Treatment of diabetic macular edema is readily available and management guidelines of diabetic macular edema have largely evolved around the use of new laser machines, newer pharmacological agents such as antivascular endothelial growth factors (anti-VEGF), and different steroid preparations [3–7]. In the past decade, the evaluation of treatment efficacy was mainly based on visual acuity measurements and the detection of structural improvement on optical coherence tomography (OCT) scans. Undoubtedly, the fast, objective, and noninvasive OCT has emerged into a valuable tool, not only in DME, but also in other macular diseases such as age-related macular degeneration (AMD) and central serous chorioretinopathy. However, the correlation between OCT measured variables and visual acuity has not been well established. Although reports have shown good correlation of OCT measured macular changes with vision, there were also reports that produced contradicting results [8]. A comprehensive understanding of the various OCT measured parameters in DME and its clinical implications is yet to be determined.

The advancement in optical coherence tomography (OCT) technologies including the increase in speed of scanning and higher axial resolution (up to ~3 microns for certain OCT machines) has made visualization of the retinal microstructures possible [9–11]. Reports have looked into the morphological changes happening in the outer retinal hyperreflective bands in subjects with various retinal diseases. The integrity of the inner segment/outer segment (IS/OS) junction has been found to correlate well with visual acuity in subjects with retinal conditions such as retinitis pigmentosa and postmacular hole operation [12, 13]. The length of the photoreceptor outer segment (PROS) has also been reported to be able to predict visual acuity in DME more accurately than the more commonly used

macular thickness [14]. Another important retinal segmentation noticeable on spectral- (Fourier-) domain OCT, the external limiting membrane (ELM), and its correlation with visual acuity in diabetic macular edema has not been well studied. Being situated between the cell nucleus and inner segments of photoreceptors, ELM may also be a possible OCT based parameter to be used indirectly in the assessment of photoreceptor functions. The aim of this study was to find out the correlation between visual acuity and the distance between the ELM and the retinal pigment epithelium (RPE), as a novel parameter in the assessment of DME.

2. Methods

2.1. Study Subjects. Consecutive patients with DME seen at the Eye Clinic of The University of Hong Kong over a 3-month period were recruited for this study after informed consent. Inclusion criteria were diabetic patients aged 18 or above and capable of giving consent and having DME as evidenced clinically with a slit lamp biomicroscopy or on OCT scans. Major exclusion criteria included poor media clarity that would affect vision and hinder satisfactory OCT image acquisition and presence of conditions other than DME that would affect macular thickness which were also excluded, such as age-related macular degeneration, vitreomacular traction, epiretinal membrane, full thickness or lamellar macular holes, and other causes of macular edema such as retinal venous occlusion. Eyes with subretinal fluid at fovea were excluded as well because their presence would result in falsely high measurement of outer retinal layers thickness (ORL thickness), since the distance is defined in this study as the distance between ELM and RPE. Baseline demographics of patients were collected. Best-corrected visual acuity (BCVA) was measured with Snellen's visual acuity charts. A comprehensive ocular examination including dilated fundal slit lamp biomicroscopy and macular OCT scan were performed. If both of patient's eyes were eligible for recruitment, only the right eye was used in the data analysis. This study has been approved by the Institutional Review Board of The University of Hong Kong and was performed in accordance with the Declaration of Helsinki.

2.2. Optical Coherence Tomography. Scanning with the Spectralis HRA + OCT system (version 3.2.1.0, Heidelberg Engineering, Inc., Heidelberg, Germany) was performed using the built-in 7-line raster scan protocol. Images were averaged from 100 frames for the purpose of noise reduction. The OCT scans were excluded if the image quality was less than 30 decibels. All study eyes were dilated with mydriatic eye drops before image acquisition. Patients were instructed to fixate on the intrinsic fixation target during the whole process of OCT scanning. If the patient was not fixating well and the center of image was not on center of the fovea, manual adjustment was performed. The OCT scans were performed by a single experienced optometrist.

2.3. Determination of Outer Retinal Layer (ORL) Thickness. The Spectralis sd-OCT data were analyzed on the Heidelberg Explorer by a single retina specialist. The horizontal line scans crossing foveal centers of patients were chosen for analysis. The internal limiting membrane (ILM), ELM, and RPE segmentation of retina were manually set. When the hyperreflective layers were identified, the point of maximal brightness of each band was chosen to be the locations of the corresponding ELM and RPE bands. The central foveal point thickness was defined as the distance between the ILM and RPE at the foveal center whereas the ORL thickness was the distance between ELM and RPE at the foveal center. Patients with disruption of ELM or RPE segmentation on OCT scans were excluded.

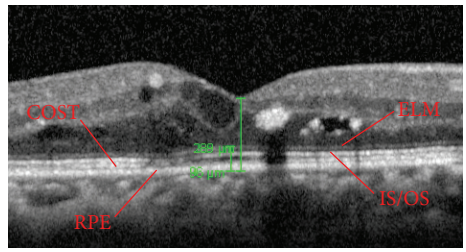

Figure 1: Representative ELM and RPE segmentation on optical coherence tomography (OCT) scan for measurement of central foveal point thickness and outer retinal layers (ORL) thickness. ELM, external limiting membrane. IS/OS, inner segment/outer segment. COST, cone outer segment tips. RPE, retinal pigment epithelium.

2.4. Statistical Analysis. Linear regression and Pearson correlation analysis were performed to find out the correlation between visual acuity, central foveal point thickness, and ORT thickness. All the calculations and statistical analyses were performed using GraphPad Prism (version 6.0c).

3. Results

A total of 78 eligible patients were recruited. The mean age was 58.1 years (±11.5 years). 37 of the 78 patients were male (47.4%), therefore making almost 1 : 1 male : female ratio. Their mean spherical equivalent was −1.30 dioptres (±2.46 dioptres) and their mean Snellen visual acuity was 0.51 (±0.18). The mean central foveal point thickness of these 78 patients was 398.0 μm (±74.3 μm) whereas the mean outer retinal thickness was 115.7 μm (±35.6 μm). Representative example of ILM, ELM, and RPE segmentation and measurement is shown in Figure 1.

The correlation coefficient (r) and the square of correlation coefficient (r^2) between the central foveal point thickness and Snellen visual acuity were 0.34 and 0.12 in our study patients, respectively ($P < 0.001$). On the other hand, the correlation coefficient (r) and square of correlation coefficient (r^2) between ORL thickness and Snellen visual acuity were −0.65 and 0.42, respectively ($P < 0.001$).

4. Discussion

Diabetic macular edema is traditionally diagnosed clinically with biomicroscopic fundal examination. With the

Table 1: Comparison of the results of the current study with other similar studies.

	Number of subjects	Parameters	r^2	P value
Present study	**78**	**ELM-RPE**	**0.42**	**<0.001**
Forooghian et al. [14], 2010	30	IS/OS-RPE	0.37–0.66*	<0.001
DRCR.net [8], 2007	251	CRT	0.27	<0.001
Ozdemir et al. [15], 2005	20	CRT	0.54	<0.001
Catier et al. [16], 2005	27	CRT	0.30	0.003
Bandello et al. [17], 2005	28	CRT	0.33	0.001
Laursen et al. [18], 2004	23	CRT	0.08	0.20
Massin et al. [19], 2003	15	CRT	0.13	0.19
Martidis et al. [20], 2002	16	CRT	0.15	0.14
Otani and Kishi [21], 2001	11	CRT	0.34	0.06

r^2, square of correlation coefficient. ELM, external limiting membrane. RPE, retinal pigment epithelium. IS/OS, inner segment/outer segment junction. CRT, central retinal thickness.
*Range of r^2 for macular grid, central subfield, and central point measurement.

advancement of technology, OCT becomes an objective and highly reliable method in the assessment of such conditions. Besides measuring the actual macular thickening of the macula edema, newer generation OCT systems are capable of visualizing microretinal structures. Studies carried out worldwide have reported contradicting results regarding the correlation between central retinal thickness and visual acuity in DME [15–21]. Instead of using the total retinal thickness, Forooghian et al. measured the distance between photoreceptor inner segment/outer segment junction and RPE layer to approximate the length of photoreceptor outer segment (PROS) in patients with DME [14]. Forooghian's study showed that PROS length correlated better with patients' vision than macular thickness measurement. However, the intrasession repeatability of the PROS measurement with the self-developed OCT segmentation prototype software algorithm of Forooghian and his fellow colleagues was lower than the measurement of total macular retinal thickness with the Carl Zeiss OCT built-in software.

External limiting membrane is situated between cell nuclei of photoreceptors and their inner segments. The ORL thickness, as defined in this study as the distance between ELM and RPE, is therefore the sum of the length of photoreceptors inner segments and outer segments. It is known that photoreceptor outer segment contains disks filled with opsin, which is responsible for absorbing photons for later signal transduction. Therefore it is reasonable to deduce that if certain disease process damages photoreceptor and decreases the length of photoreceptor outer segment, vision would be compromised. This has already been proven to be true in DME by Forooghian and colleagues. On the other hand, the inner segment of photoreceptor is as important as the outer segment for cell functions because it is the reservoir of mitochondria; therefore it is responsible for the storage of ATP and thus for energy generation. Since both inner and outer segments of photoreceptors play an important role in the visual pathway, the change in ORL thickness should have important implications in visual potential. We believe this parameter can shed light on the overall health status of photoreceptors. Moreover, macular edema may be resolved but damage to photoreceptors does not; therefore a decrease in ORL thickness would be a more important visual prognostic factor than the total retinal thickness which may change over time.

In this study, we used Spectralis sd-OCT to quantify the foveal ORL thickness of our patients. We reported a relatively high correlation of the ORL thickness with visual acuity ($r = 0.65$, $P < 0.001$). In other words, we observed that the larger the ORL thickness is, the better the visual acuity would be. The correlation between total retinal thickness at the foveal center and visual acuity in our DME patients was not as good as the ORL thickness, with correlation coefficient of merely 0.34 ($P < 0.001$). This demonstrates good agreement between the findings of our study and Forooghian's study.

When compared with findings from other studies, we demonstrated that the ORL thickness and vision are more correlated than central retinal thickness and vision, although not as good as the correlation between PROS length and vision (Table 1). It is worth noting that ORL thickness is by definition longer than PROS length; therefore the same amount of systematic or random error in measurement would produce lower effect on the final result. For example, the mean PROS length on OCT is 32 μm at fovea for DME patients [14] and the mean ORL thickness we obtained in this study is 115.7 μm; if a random error of 5 μm is generated by the OCT measurement, it would be 15.6% of the true PROS length but only 4.3% of the true ORL thickness. Moreover, there is only one study in the literature investigating the relationship of PROS length and vision in 30 DME patients. Provided that the repeatability of PROS length measurement is not excellent and the higher percentage error for any absolute error generated due to the shorter PROS length when compared to ORL thickness, it would be beneficial to conduct a larger scale study to compare the correlation between PROS length, ORL thickness and vision in order to further understand the strengths and shortcomings of the two different OCT parameters in the assessment of DME.

There are a number of limitations in our study and the assessment of ORL thickness. Patients with minimal DME without OCT scans done might have been missed

during clinical assessment and therefore might not have been recruited in our study. Moreover, the exclusion of patients with subretinal fluid or disruption of ELM or RPE may also lead to selection bias.

It is time consuming to identify the ELM and RPE bands since all the segmentation was identified manually. It is also important to note that the measurement performed in this study was at the central foveal point rather than the measurement of central subfield thickness in most other studies; therefore our results of foveal thickness should not be directly compared to those from other studies.

ORL thickness of the foveal center may reflect a patient's visual potential at the point of fixation; however, activities of daily living such as reading rely highly on paracentral vision as well since it is necessary to locate the following word before one can move the point of fixation to the next word or next line with eye movement. ORL thickness measurement at foveal center does not adequately reflect this aspect of visual function. In order to address this problem, a new software algorithm could be developed to automatically locate the ELM segmentation after OCT scan is performed so as to calculate the ORL thickness in the central subfield instead of the foveal center.

Despite the promising results, ORL thickness cannot explain all the variations in vision since other factors such as macular ischaemia might play a role as well.

To conclude, we reported the use of ORL thickness as a novel OCT parameter in the assessment of DME patients and demonstrated that it is better correlated with vision than the total foveal point thickness. Further studies should be conducted to investigate the potential of using ORL thickness as a long term visual prognostic factor in DME patients.

Conflict of Interests

The authors have no financial interests to disclose.

Acknowledgment

Work related to this project was funded by departmental funding of the corresponding author's institution.

References

[1] J. H. Kempen, B. J. O'Colmain, M. C. Leske et al., "The prevalence of diabetic retinopathy among adults in the United States," *Archives of Ophthalmology*, vol. 122, no. 4, pp. 552–563, 2004.

[2] Early Treatment Diabetic Retinopathy Study Research Group, "Photocoagulation for diabetic macular edema. Early Treatment Diabetic Retinopathy Study report number 1," *Archives of Ophthalmology*, vol. 103, no. 12, pp. 1796–1806, 1985.

[3] J. K. Luttrull and G. Dorin, "Subthreshold diode micropulse laser photocoagulation (SDM) as invisible retinal phototherapy for diabetic macular edema: a review," *Current Diabetes Reviews*, vol. 8, no. 4, pp. 274–284, 2012.

[4] Q. D. Nguyen, D. M. Brown, D. M. Marcus et al., "Ranibizumab for diabetic macular edema: results from 2 phase iii randomized trials: RISE and RIDE," *Ophthalmology*, vol. 119, no. 4, pp. 789–801, 2012.

[5] M. J. Elman, N. M. Bressler, H. Qin et al., "Expanded 2-year follow-up of ranibizumab plus prompt or deferred laser or triamcinolone plus prompt laser for diabetic macular edema," *Ophthalmology*, vol. 118, no. 4, pp. 609–614, 2011.

[6] G. E. Lang, A. Berta, B. M. Eldem et al., "Two-year safety and efficacy of ranibizumab 0.5 mg in diabetic macular edema: interim analysis of the restore extension study," *Ophthalmology*, vol. 120, no. 10, pp. 2004–2012, 2013.

[7] Q. D. Nguyen, S. M. Shah, A. A. Khwaja et al., "Two-year outcomes of the ranibizumab for edema of the mAcula in diabetes (READ-2) study," *Ophthalmology*, vol. 117, no. 11, pp. 2146–2151, 2010.

[8] Diabetic Retinopathy Clinical Research Network, D. J. Browning, A. R. Glassman et al., "Relationship between optical coherence tomography-measured central retinal thickness and visual acuity in diabetic macular edema," *Ophthalmology*, vol. 114, no. 3, pp. 525–536, 2007.

[9] V. J. Srinivasan, B. K. Monson, M. Wojtkowski et al., "Characterization of outer retinal morphology with high-speed, ultrahigh-resolution optical coherence tomography," *Investigative Ophthalmology and Visual Science*, vol. 49, no. 4, pp. 1571–1579, 2008.

[10] A. Chan, J. S. Duker, H. Ishikawa, T. H. Ko, J. S. Schuman, and J. G. Fujimoto, "Quantification of photoreceptor layer thickness in normal eyes using optical coherence tomography," *Retina*, vol. 26, no. 6, pp. 655–660, 2006.

[11] M. Shahidi, Z. Wang, and R. Zelkha, "Quantitative thickness measurement of retinal layers imaged by optical coherence tomography," *American Journal of Ophthalmology*, vol. 139, no. 6, pp. 1056–1061, 2005.

[12] S. Aizawa, Y. Mitamura, T. Baba, A. Hagiwara, K. Ogata, and S. Yamamoto, "Correlation between visual function and photoreceptor inner/outer segment junction in patients with retinitis pigmentosa," *Eye*, vol. 23, no. 2, pp. 304–308, 2009.

[13] T. Baba, S. Yamamoto, M. Arai et al., "Correlation of visual recovery and presence of photoreceptor inner/outer segment junction in optical coherence images after successful macular hole repair," *Retina*, vol. 28, no. 3, pp. 453–458, 2008.

[14] F. Forooghian, P. F. Stetson, S. A. Meyer et al., "Relationship between photoreceptor outer segment length and visual acuity in diabetic macular edema," *Retina*, vol. 30, no. 1, pp. 63–70, 2010.

[15] H. Ozdemir, M. Karacorlu, and S. A. Karacorlu, "Regression of serous macular detachment after intravitreal triamcinolone acetonide in patients with diabetic macular edema," *The American Journal of Ophthalmology*, vol. 140, no. 2, pp. 251.e1–251.e6, 2005.

[16] A. Catier, R. Tadayoni, M. Paques et al., "Characterization of macular edema from various etiologies by optical coherence tomography," *American Journal of Ophthalmology*, vol. 140, no. 2, pp. 200.e1–200.e9, 2005.

[17] F. Bandello, A. Polito, M. del Borrello, N. Zemella, and M. Isola, "'Light' versus 'classic' laser treatment for clinically significant diabetic macular oedema," *British Journal of Ophthalmology*, vol. 89, no. 7, pp. 864–870, 2005.

[18] M. L. Laursen, F. Moeller, B. Sander, and A. K. Sjoelie, "Subthreshold micropulse diode laser treatment in diabetic macular oedema," *British Journal of Ophthalmology*, vol. 88, no. 9, pp. 1173–1179, 2004.

[19] P. Massin, G. Duguid, A. Erginay, B. Haouchine, and A. Gaudric, "Optical coherence tomography for evaluating diabetic macular edema before and after vitrectomy," *American Journal of Ophthalmology*, vol. 135, no. 2, pp. 169–177, 2003.

[20] A. Martidis, J. S. Duker, P. B. Greenberg et al., "Intravitreal triamcinolone for refractory diabetic macular edema," *Ophthalmology*, vol. 109, no. 5, pp. 920–927, 2002.

[21] T. Otani and S. Kishi, "Tomographic findings of foveal hard exudates in diabetic macular edema," *American Journal of Ophthalmology*, vol. 131, no. 1, pp. 50–54, 2001.

Hindawi Publishing Corporation
BioMed Research International
Volume 2015, Article ID 160454, 7 pages
http://dx.doi.org/10.1155/2015/160454

Review Article

Advanced Morphological and Functional Magnetic Resonance Techniques in Glaucoma

Rodolfo Mastropasqua,[1] Luca Agnifili,[2] Peter A. Mattei,[2] Massimo Caulo,[3] Vincenzo Fasanella,[2] Riccardo Navarra,[3] Leonardo Mastropasqua,[2] and Giorgio Marchini[1]

[1]*Ophthalmology Unit, Department of Neurological, Neuropsychological, Morphological and Movement Sciences, University of Verona, 37121 Verona, Italy*
[2]*Ophthalmology Clinic, Department of Medicine and Aging Science, G. d'Annunzio University of Chieti-Pescara, 65100 Chieti, Italy*
[3]*Department of Neuroscience and Imaging, G. d'Annunzio University of Chieti-Pescara, 65100 Chieti, Italy*

Correspondence should be addressed to Luca Agnifili; l.agnifili@unich.it

Received 13 September 2014; Revised 13 December 2014; Accepted 24 December 2014

Academic Editor: Antonio Ferreras

Glaucoma is a multifactorial disease that is the leading cause of irreversible blindness. Recent data documented that glaucoma is not limited to the retinal ganglion cells but that it also extends to the posterior visual pathway. The diagnosis is based on the presence of signs of glaucomatous optic neuropathy and consistent functional visual field alterations. Unfortunately these functional alterations often become evident when a significant amount of the nerve fibers that compose the optic nerve has been irreversibly lost. Advanced morphological and functional magnetic resonance (MR) techniques (morphometry, diffusion tensor imaging, arterial spin labeling, and functional connectivity) may provide a means for observing modifications induced by this fiber loss, within the optic nerve and the visual cortex, in an earlier stage. The aim of this systematic review was to determine if the use of these advanced MR techniques could offer the possibility of diagnosing glaucoma at an earlier stage than that currently possible.

1. Introduction

Glaucoma is the leading cause of irreversible blindness worldwide. The definition of glaucoma was mainly based on the presence of a typical optic neuropathy along with elevated intraocular pressure (IOP). The IOP still remains the most important risk factor for the onset and progression of the disease. This pathology is characterized by a multifactorial etiology, grouping numerous diseases that share common pathological features of the optic disc [1]. Unfortunately, early diagnosis of glaucoma still remains the main challenge. The literature supports the hypothesis that the first signs of visual field (VF) impairment (that is still the gold standard for diagnosis) appear when a significant amount (between 40 and 50%) of retinal ganglion cells (RGC) has been irreversibly lost [2]. Therefore, diagnostic approaches based on morphology, such as the optical coherence tomography (OCT), have been proposed to anticipate the perimetric diagnosis of glaucoma [3–5]. In the human retina, glaucoma mainly causes the selective death of RGC, whose dendrites comprise the optic nerve, which in turn provides the majority of the input of the primary visual cortex. Previous studies indicated that neuronal plasticity results in a cascade of modifications in structures following modification of neural input [6–8]. Thus a reduction of the number of viable RGC should result in a reduction in the number of dendrites found in the optic nerve, resulting in a decrease in the sensory input of the primary motor cortex, which should decrease the number of functional connections with secondary visual cortex areas. Given that these anatomical structures increase in size with increasing complexity of function, it can be hypothesized that smaller modifications may be more evident in the posterior visual pathway.

Magnetic resonance imaging (MRI) techniques are for the most part nonquantitative; that is, they are not directly comparable over time. Techniques that do provide quantitative results include morphological measurements such as

cortical thickness measured on anatomical scans, diffusion tensor imaging (DTI) that provides information concerning the microstructural integrity of white fiber tracts, arterial spin labeling (ASL) that provides a quantitative estimate of blood perfusion in mL of blood per mg of tissue, and functional connectivity (FC) that estimates the synchronization of anatomically distinct regions of the cortex from blood-oxygen-level-dependent contrast imaging (BOLD) acquisitions. The aim of this systematic review was to determine if these advanced MR techniques could possibly diagnose glaucoma at an earlier stage than that which is currently possible with the VF.

2. Methods Used for Literature Searches

PubMed searches were performed on July 31, 2014, using the phrases "glaucoma" and "primary visual cortex" and either "freesurfer" or "voxel-based," "optic nerve" and "diffusion tensor," "primary visual cortex" and "arterial spin labeling," and "primary visual cortex" and "functional connectivity" for publications from 1980 to April 2014. Articles in English were fully reviewed. Articles in other languages were reviewed only when an abstract in English was available.

3. Results

3.1. Morphometry. Techniques to quantitatively evaluate morphological aspects of the brain can be divided into two principle groups: voxel-based and surface-based. The first uses a statistical approach to assign a probability that a voxel is occupied by grey matter. The latter determines vertices that define the surface of the grey matter-cerebral-spinal fluid and the grey-white matter interfaces and uses these vertices to estimate the cortical thickness with a submillimeter precision.

Bogorodzki et al., in a study on the voxel-based technique [9], reported that a group of 14 patients with unilateral vision loss due to end-stage open-angle glaucoma showed a statistically significant thinning of the visual cortex compared to a group of 12 normal age-matched subjects.

In another study with advanced glaucoma patients that used a 3-dimensional magnetization-prepared rapid gradient-echo sequence of MRI and optimized voxel-based morphometry a significant decrease in the bilateral grey matter volume in the lingual, calcarine, postcentral, superior frontal, and inferior frontal gyrus and rolandic operculum as well as in the right cuneus, right inferior occipital gyrus, left paracentral lobule, and right supramarginal gyrus was found [10].

Hernowo et al. [11] found a significant reduction in volume of the visual pathway structures between the eyes and the visual cortex, including the optic nerves, the optic chiasm, the optic tracts, the LGN, and the optic radiations, in eight patients with VF loss due to primary open-angle glaucoma (POAG). Based on these findings, the authors proposed that MRI, in combination with automated morphometry, could be used to aid the detection and assessment of glaucomatous damage posterior visual pathways.

Li et al. [12] reported that atrophy and degeneration of the visual-related cortex existed in the dorsal and ventral visual pathways in the advanced stage of POAG but were absent in the early stage.

Interestingly, Williams et al. reported that brain changes varied according to the glaucoma stage. The right and left inferior occipital gyri, right middle occipital gyrus, right inferior temporal gyrus, and right occipital lobe white matter were larger in glaucomatous patients than in healthy subjects. In multivariate regression analysis, 38% of all brain structures had independent associations between decreasing volume and more advanced glaucoma. These findings suggested that in patients with glaucoma the extent of cortical brain changes correlates with disease severity [13].

Given that the cortical thickness of the visual cortex showed a strong correlation with aging, when corrected for sex [14], one may speculate that a possible diagnostic test could be the comparison of a patient suspected of having glaucoma in an early stage to a group of healthy controls with the same age. Or the patient with manifest glaucoma could undergo repeated MRI scans in order to identify modifications in cortical thickness induced by disease progression.

Figures 1 to 3 represent a patient with early stage glaucoma. While VF is still normal (Figure 1), morphological defects of the retinal nerve fiber layer (RNFL) (Figure 2(a)) and ganglion cell layer/inner plexiform layer (GCL/IPL) complex (Figure 2(b)) (as seen with spectral domain optical coherence tomography) are already evident. MRI morphological technique for evaluating cortical thickness shows a thinned cortex in the primary visual area (Figure 3).

3.2. Diffusion Tensor Imaging. DTI noninvasively evaluates the microstructural integrity of tissue by sensitizing the MRI signal to the random motion of water molecules via diffusion encoding gradients. Tissue that is organized as fibers, such as nerves and white matter tracks, gives a highly anisotropic signal. A modification towards a more isotropic signal indicates a loss of structural integrity. Figure 4 shows two DTI scans using classical acquisition protocol on the right and a priori information concerning the orientation of the optic nerve on the left in the same patient shown in the previous figures (Figure 4). The latter shows an improvement in signal-to-noise ratio, a more homogenous measurement, and an increase in length of the traceable fiber lengths.

Xu et al. [15] evaluated the use of this imaging modality to investigate the optic nerve in mice and humans. They reported that the optic nerve degeneration following retinal ischemia exhibited a distinct pathological progression. The axonal injury preceded demyelination without significant destruction of overall axonal cytoskeletons in their mouse model. These modifications could be detected with parallel and perpendicular diffusivity, respectively. The same results were not observed in humans probably due to technical difficulties.

Fiedorowicz et al. [16] reported that changes observable with DTI in the optic nerve correlated with the progression of glaucoma. Specifically, they observed a statistically significant correlation between the increase in mean diffusivity (MD) and a decrease in fractional anisotropy (FA) with increasing severity of glaucoma.

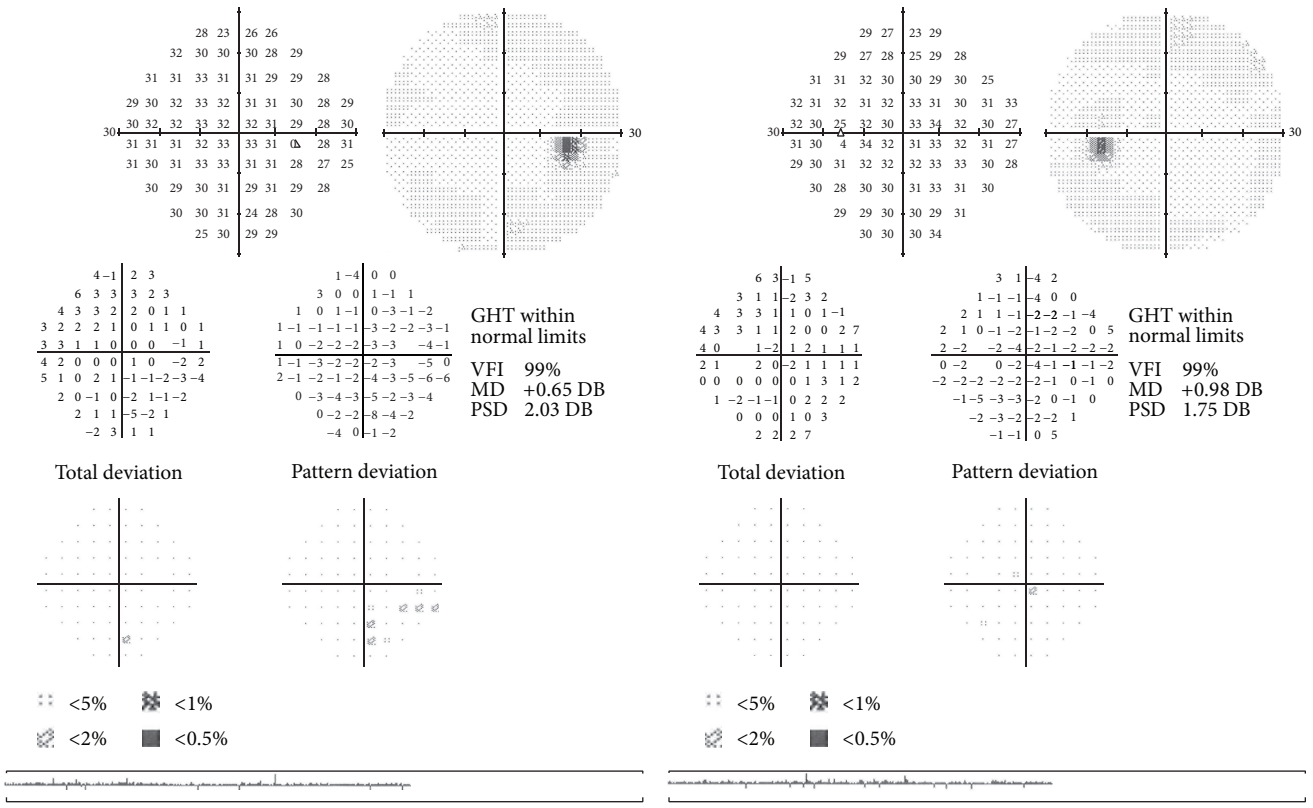

Figure 1: Normal visual field examination (Humphrey field analyzer II 750 (Carl Zeiss Meditec, Inc., Dublin, CA; 30-2 test, full-threshold)) of a patient in an early stage of glaucoma.

Michelson et al. [17] reported that the morphology of the papilla correlated, after elimination of the effect of covariates, with the axonal integrity and demyelination of the optic radiation in controls and glaucoma.

Garaci et al. [18] evaluated both the optic nerve and the optic radiation and reported that these structures had significantly higher MD and significantly lower FA in patients with glaucoma compared to controls. Notably, MD and FA in the optic nerves correlated with glaucoma severity, suggesting that these parameters could serve as complementary indicators of disease severity.

Nucci et al. [19] reported that MD and FA were correlated with morphological features of the optic nerve head and retinal nerve fiber layer (RNFL) documented with scanning laser polarimetry (GDx-VCC), confocal scanning laser ophthalmoscopy (Heidelberg Retina Tomograph, HRT-III), and optical coherence tomography (Stratus OCT). Specifically, MD displayed the strongest correlation with linear cup/disc ratio (LCDR) from HTR-III, RNFL thickness from OCT, and nerve fiber index (NFI) from GDx, while FA strongly correlated with LCDR. These findings suggested that DTI could be a valuable complementary diagnostic method to assess structural modifications of retinal ganglion cells and optic nerve in glaucoma.

In another study by the same group [20], the authors found that at early glaucoma stage MD values were higher at the proximal site of the optic nerve head with respect to the distal site. On the contrary, a decrease in FA was observed only relative to patient stage, independent of optic nerve site. Moreover, during the early stage of glaucoma, an increase in overall diffusivities was evident at the proximal site, whereas at the distal site a decrease of the largest diffusivity and an increase in both the intermediate and the smallest diffusivities were observed. The authors concluded that the high sensitivity of FA along with the high specificity of MD at the proximal site could provide reliable indexes for the identification of structural damage at early stages.

The main limitation is the diameter of the human optic nerve, which is on the order of 3-4 mm and is located in an area that shows magnetic field susceptibility artifacts [21]. This limit can be overcome with the use of modified diffusion tensor techniques and with the improvement of the signal-to-noise ratio obtainable with newer and higher magnetic field MR scanners.

3.3. Arterial Spin Labeling. ASL measures tissue perfusion by labeling the water present in blood (i.e., modifying the orientation of the spins) in one volume and then measuring the amount of these spins after the blood has passed into another volume. The measurements of perfusion are comparable with those obtained with positron emission tomography [22].

Lavery et al. [23] reported that a reduced ocular blood flow in DBA/2J mice compared with C57BL/6 control mice. This result supported the hypothesis that ischemia or hypoxia was a possible contributing factor in the optic neuropathy in the DBA/2J mouse model of glaucoma.

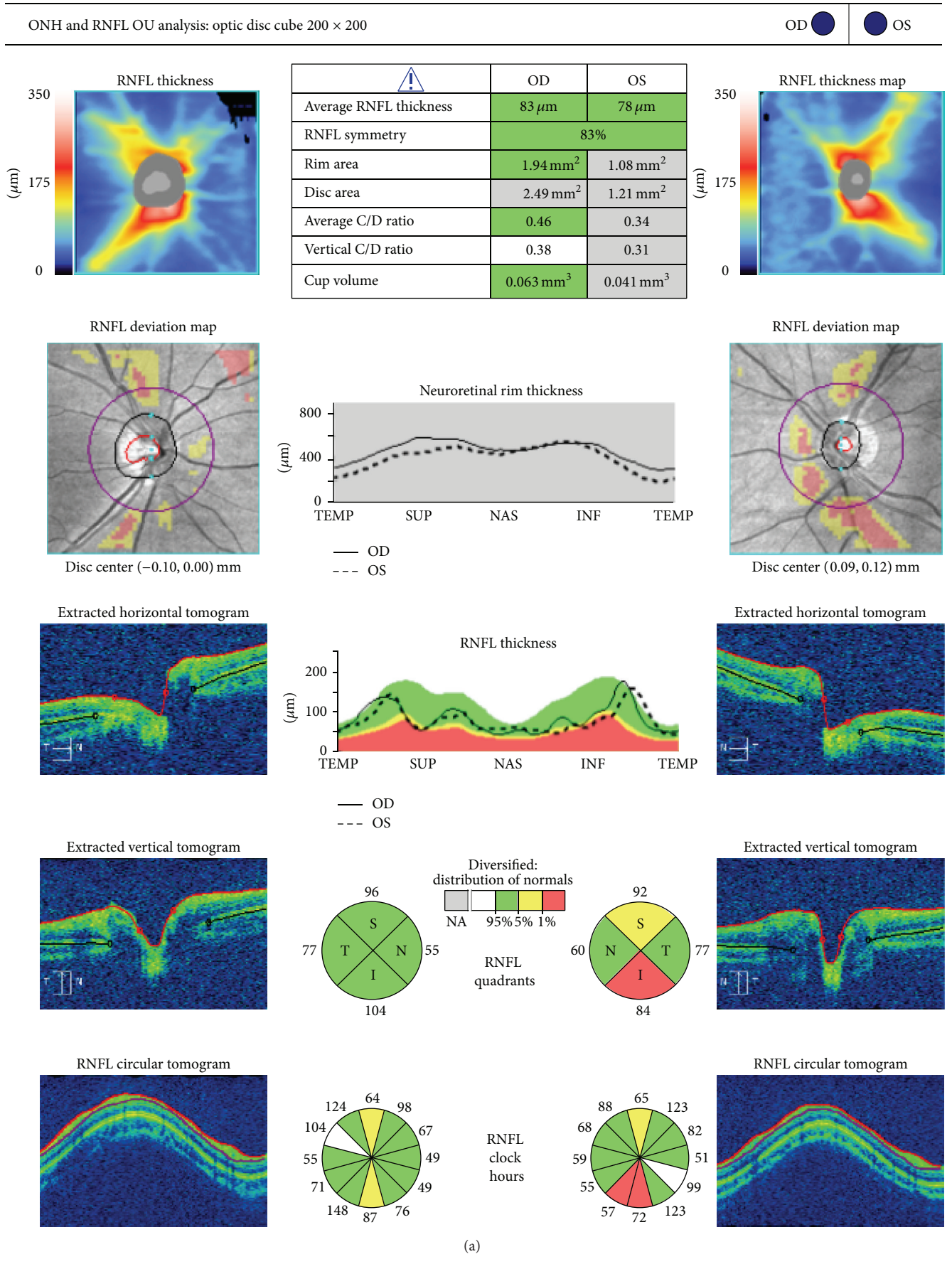

(a)

Figure 2: Continued.

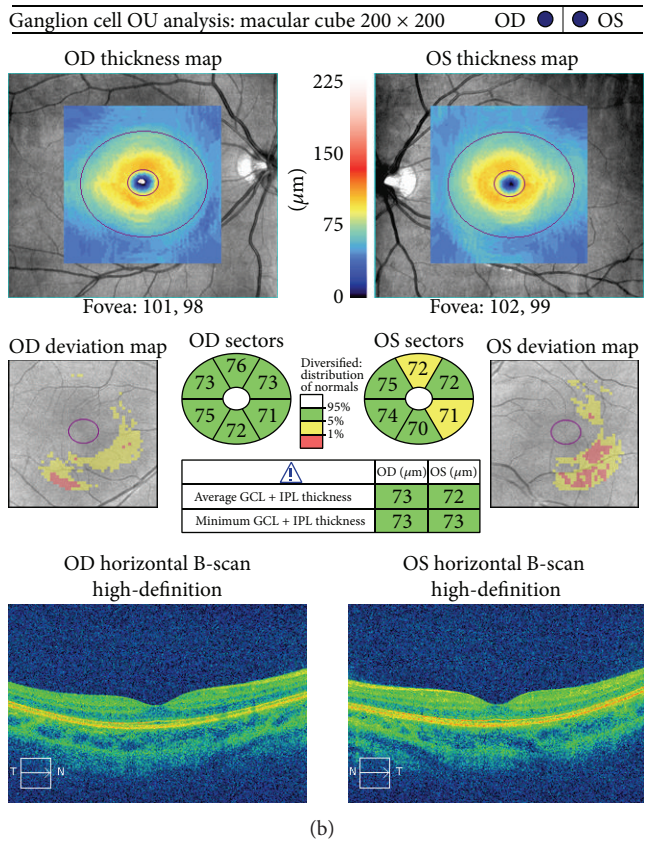

(b)

Figure 2: Spectral domain optical coherence tomography (Cirrus, Carl Zeiss Meditec, Inc., Dublin, CA, version 6.5 software) of the same patient, showing the peripapillary RNFL (a) and macular GCL/IPL (ganglion cell layer/inner plexiform layer) (b) glaucomatous defects.

Duncan et al. [24] reported that resting blood perfusion in human primary visual cortex in 10 patients with POAG correlated with the loss of visual function. They concluded that altered cerebral perfusion was an indication of postretinal glaucomatous neurodegeneration caused by damage to the retinal ganglion cells.

Presently, the main limitations of ASL are the lack of its widespread diffusion and the low signal-to-noise ratio that increase the acquisition time. These limits will probably be overcome with the increased diffusion of high field scanners and improved acquisition protocols and postprocessing techniques.

3.4. Functional Connectivity. Resting-state FC is the connectivity between brain regions that share functional properties. After the acquisition of a BOLD sequence of a patient at rest with their eyes open, postprocessing determines which regions present a temporal correlation in BOLD-signal fluctuations. In order to evaluate the visual system or any other functional system, a predetermined set of regions of interest are used (seed based). To date, only two studies have been published using this method to evaluate the visual system.

Dai et al. [25] reported that the FC of the visual cortex with associative visual areas in 22 patients with POAG was modified compared to 22 age-matched healthy controls. There was also a disrupted connectivity between the primary and higher visual areas. That is, the communication between the primary visual area and higher visual cortices was decreased, as was the positive FC between both of these areas and more remote regions of the brain. The authors speculated that areas of increased positive FC with visual cortices may represent compensatory recruitment or diminished inhibitory input.

Frezzotti et al. [26] reported abnormalities in structure and FC within and outside visual system in 13 patients with advanced POAG compared to 12 age-matched healthy controls. These modifications correlated with VF parameters in poorer performing eyes. These findings suggest that structural and functional changes in glaucoma go beyond the visual system, suggesting that POAG can be considered a neurodegenerative vision disease falling within the group of neurodegenerative disorders and, as such, results in widespread modifications of the brain.

The main limitations of FC analysis include difficulties and time required for postprocessing of the BOLD acquisitions and interpretation of the results.

4. Summary and Conclusions

Glaucoma is a multifactorial disease that involves retinal ganglion cells and also structures of the central visual pathway [8]. The application of progressively more advanced imaging technologies in the field of glaucoma is rapidly growing, allowing a more accurate knowledge of the pathophysiology

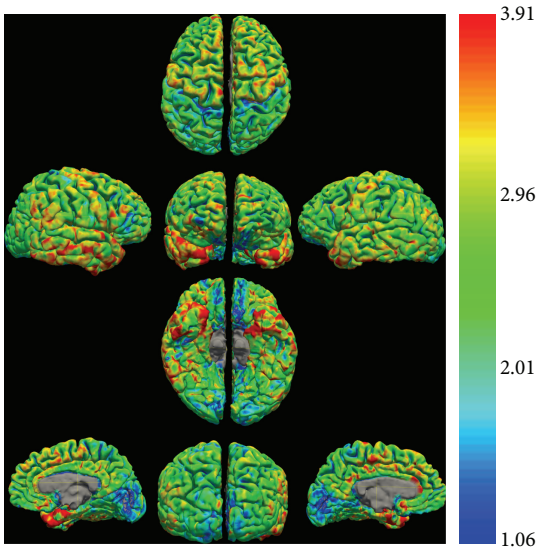

Figure 3: Cortical thickness estimates of the same patient as Figures 1 and 2. Note that the major concentration of the thinnest cortex (blue on the color scale) is located in the primary visual cortex and presents a greater extension on the left hemisphere.

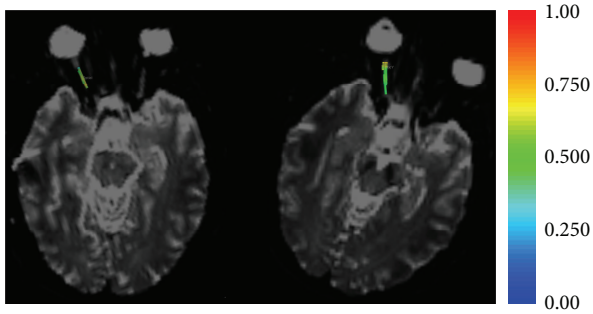

Figure 4: DTI of the same patient as Figures 1 and 2. The fibers traced on the right optic nerve are colored with the fractional anisotropy measured at each point along the nerve (see legend). Note that the variation in color on the right (classic isometric sequence) is greater than that on the left (a priori sequence with the majority of the directions lying in the direction of the optic nerve). The greater variation indicates a greater variability in measurement: in other words the standard deviation of the sequence on the right is greater. The higher precision of the new sequence would be useful for the smaller modifications that should be present in the early stages of glaucoma.

of the disease, earlier diagnosis, and a better evaluation of responses to therapies [5, 27, 28].

The introduction of advanced neuroimaging techniques may facilitate the study of the entire visual pathway, opening new frontiers in the early detection of the disease and in the evaluation of the therapeutic efficacy of novel neuroprotective strategies.

In summary, voxel-based morphometry can detect modifications of visual pathways structures mainly in advanced stages of glaucoma. Even though morphometry shows an evident correlation between cortical brain modifications and the stage of disease, the application of this method for the early diagnosis of the disease still has limits. DTI generally found an increase in MD and a decrease in FA in patients with glaucoma, modifications that significantly correlated with increasing severity of disease. Interestingly, these modifications also occurred at early stage of glaucoma, being more evident at the proximal site of the optic nerve head with respect to distal sites. This suggests that each portion of the optic pathway should be precisely pondered when attempting to identify the initial signs of disease. Studies that used ASL to detect cerebral perfusion abnormalities in patients with glaucoma are very limited. Presently, the application of this method has focused on identifying contributing factors involved in optic neuropathy onset and progression. FC documented important alterations between primary and associative visual areas and also between nonvisual areas, suggesting that glaucoma should be considered as a neurodegenerative disorder with widespread ramifications in the brain.

In conclusion, the number of studies that evaluated modifications observable with advanced MRI techniques is progressively growing even though especially limited in patients with glaucoma in advanced stage. But the results support the potential for these techniques for detecting the modifications induced in an early stage of glaucoma.

Conflict of Interests

None of the authors have a proprietary interest in the development or marketing of any of the products mentioned in this paper. The authors declare that there is no conflict of interests regarding the publication of this paper.

Authors' Contribution

Rodolfo Mastropasqua and Luca Agnifili equally contributed to this work and share primary authorship.

References

[1] R. J. Casson, G. Chidlow, J. P. M. Wood, J. G. Crowston, and I. Goldberg, "Definition of glaucoma: clinical and experimental concepts," *Clinical and Experimental Ophthalmology*, vol. 40, no. 4, pp. 341–349, 2012.

[2] R. S. Harwerth, M. L. J. Crawford, L. J. Frishman, S. Viswanathan, E. L. Smith III, and L. Carter-Dawson, "Visual field defects and neural losses from experimental glaucoma," *Progress in Retinal and Eye Research*, vol. 21, no. 1, pp. 91–125, 2002.

[3] H. L. Rao, U. K. Addepalli, S. Chaudhary et al., "Ability of different scanning protocols of spectral domain optical coherence tomography to diagnose preperimetric glaucoma," *Investigative Ophthalmology and Visual Science*, vol. 54, no. 12, pp. 7252–7257, 2013.

[4] P. Carpineto, M. Ciancaglini, A. Aharrh-Gnama, L. Agnifili, and L. Mastropasqua, "Optical coherence tomography and retinal thickness analyzer features of spontaneous resolution of vitreomacular traction syndrome: a case report," *European Journal of Ophthalmology*, vol. 14, no. 1, pp. 67–70, 2004.

[5] P. Carpineto, M. Nubile, L. Agnifili et al., "Reproducibility and repeatability of Cirrus HD-OCT peripapillary retinal nerve fibre layer thickness measurements in young normal subjects," *Ophthalmologica*, vol. 227, no. 3, pp. 139–145, 2012.

[6] A. Pascual-Leone, A. Amedi, F. Fregni, and L. B. Merabet, "The plastic human brain cortex," *Annual Review of Neuroscience*, vol. 28, pp. 377–401, 2005.

[7] C. Briganti, C. Sestieri, P. A. Mattei et al., "Reorganization of functional connectivity of the language network in patients with brain gliomas," *The American Journal of Neuroradiology*, vol. 33, no. 10, pp. 1983–1990, 2012.

[8] C. Nucci, A. Martucci, M. Cesareo et al., "Brain involvement in glaucoma: advanced neuroimaging for understanding and monitoring a new target for therapy," *Current Opinion in Pharmacology*, vol. 13, no. 1, pp. 128–133, 2013.

[9] P. Bogorodzki, E. Piątkowska-Janko, J. Szaflik, J. P. Szaflik, M. Gacek, and P. Grieb, "Mapping cortical thickness of the patients with unilateral end-stage open angle glaucoma on planar cerebral cortex maps," *PLoS ONE*, vol. 9, no. 4, Article ID e93682, 2014.

[10] W. W. Chen, N. Wang, S. Cai et al., "Structural brain abnormalities in patients with primary open-angle glaucoma: a study with 3T MR imaging," *Investigative Ophthalmology & Visual Science*, vol. 54, no. 1, pp. 545–554, 2013.

[11] A. T. Hernowo, C. C. Boucard, N. M. Jansonius, J. M. M. Hooymans, and F. W. Cornelissen, "Automated morphometry of the visual pathway in primary open-angle glaucoma," *Investigative Ophthalmology and Visual Science*, vol. 52, no. 5, pp. 2758–2766, 2011.

[12] C. Li, P. Cai, L. Shi et al., "Voxel-based morphometry of the visual-related cortex in primary open angle glaucoma," *Current Eye Research*, vol. 37, no. 9, pp. 794–802, 2012.

[13] A. L. Williams, J. Lackey, S. S. Wizov et al., "Evidence for widespread structural brain changes in glaucoma: a preliminary voxel-based MRI study," *Investigative Ophthalmology and Visual Science*, vol. 54, no. 8, pp. 5880–5887, 2013.

[14] A. M. Fjell, L. T. Westlye, I. Amlien et al., "High consistency of regional cortical thinning in aging across multiple samples," *Cerebral Cortex*, vol. 19, no. 9, pp. 2001–2012, 2009.

[15] J. Xu, S. W. Sun, R. T. Naismith, A. Z. Snyder, A. H. Cross, and S.-K. Song, "Assessing optic nerve pathology with diffusion MRI: from mouse to human," *NMR in Biomedicine*, vol. 21, no. 9, pp. 928–940, 2008.

[16] M. Fiedorowicz, W. Dyda, R. Rejdak, and P. Grieb, "Magnetic resonance in studies of glaucoma," *Medical Science Monitor*, vol. 17, no. 10, pp. RA227–RA232, 2011.

[17] G. Michelson, S. Wärntges, T. Engelhorn, A. El-Rafei, J. Hornegger, and A. Dörfler, "Integrity/demyelination of the optic radiation, morphology of the papilla, and contrast sensitivity in glaucoma patients," *Klinische Monatsblätter für Augenheilkunde*, vol. 229, no. 2, pp. 143–148, 2012.

[18] F. G. Garaci, F. Bolacchi, A. Cerulli et al., "Optic nerve and optic radiation neurodegeneration in patients with glaucoma: in vivo analysis with 3-T diffusion-tensor MR imaging," *Radiology*, vol. 252, no. 2, pp. 496–501, 2009.

[19] C. Nucci, R. Mancino, A. Martucci et al., "3-T Diffusion tensor imaging of the optic nerve in subjects with glaucoma: correlation with GDx-VCC, HRT-III and Stratus optical coherence tomography findings," *British Journal of Ophthalmology*, vol. 96, no. 7, pp. 976–980, 2012.

[20] F. Bolacchi, F. G. Garaci, A. Martucci et al., "Differences between proximal versus distal intraorbital optic nerve diffusion tensor magnetic resonance imaging properties in glaucoma patients," *Investigative Ophthalmology and Visual Science*, vol. 53, no. 7, pp. 4191–4196, 2012.

[21] C. A. M. Wheeler-Kingshott, S. A. Trip, M. R. Symms, G. J. M. Parker, G. J. Barker, and D. H. Miller, "In vivo diffusion tensor imaging of the human optic nerve: pilot study in normal controls," *Magnetic Resonance in Medicine*, vol. 56, no. 2, pp. 446–451, 2006.

[22] D. A. Wolk and J. A. Detre, "Arterial spin labeling MRI: an emerging biomarker for Alzheimer's disease and other neurodegenerative conditions," *Current Opinion in Neurology*, vol. 25, no. 4, pp. 421–428, 2012.

[23] W. J. Lavery, E. R. Muir, J. W. Kiel, and T. Q. Duong, "Magnetic resonance imaging indicates decreased choroidal and retinal blood flow in the DBA/2J mouse model of glaucoma," *Investigative Ophthalmology and Visual Science*, vol. 53, no. 2, pp. 560–564, 2012.

[24] R. O. Duncan, P. A. Sample, C. Bowd, R. N. Weinreb, and L. M. Zangwill, "Arterial spin labeling fMRI measurements of decreased blood flow in primary visual cortex correlates with decreased visual function in human glaucoma," *Vision Research*, vol. 60, pp. 51–60, 2012.

[25] H. Dai, J. N. Morelli, F. Ai et al., "Resting-state functional MRI: functional connectivity analysis of the visual cortex in primary open-angle glaucoma patients," *Human Brain Mapping*, vol. 34, no. 10, pp. 2455–2463, 2013.

[26] P. Frezzotti, A. Giorgio, I. Motolese et al., "Structural and functional brain changes beyond visual system in patients with advanced glaucoma," *PLoS ONE*, vol. 9, no. 8, Article ID e105931, 2014.

[27] R. Mastropasqua, V. Fasanella, L. Agnifili, C. Curcio, M. Ciancaglini, and L. Mastropasqua, "Anterior segment optical coherence tomography imaging of conjunctival filtering blebs after glaucoma surgery," *BioMed Research International*, vol. 2014, Article ID 610623, 11 pages, 2014.

[28] M. Ciancaglini, P. Carpineto, L. Agnifili et al., "Conjunctival characteristics in primary open-angle glaucoma and modifications induced by trabeculectomy with mitomycin C: an in vivo confocal microscopy study," *British Journal of Ophthalmology*, vol. 93, no. 9, pp. 1204–1209, 2009.

Hindawi Publishing Corporation
BioMed Research International
Volume 2015, Article ID 968672, 4 pages
http://dx.doi.org/10.1155/2015/968672

Research Article

Structural and Function Correlation of Cone Packing Utilizing Adaptive Optics and Microperimetry

Dabir Supriya,[1] Mangalesh Shwetha,[1] Kumar Kiran Anupama,[1] Kurian Kummelil Mathew,[2] Tos T. J. M. Berendschot,[3] Jan S. A. G. Schouten,[3] Roopa Bharamshetter,[1] Yadav K. Naresh,[1] Shetty Rohit,[4] and Bharath Hegde[5]

[1]*Department of Retina, Narayana Nethralaya, No. 121/C, 1st R Block, Rajajinagar, Bangalore 560010, India*
[2]*Department of Cataract & Refractive Surgery, Narayana Nethralaya, No. 121/C, 1st R Block, Rajajinagar, Bangalore 560010, India*
[3]*Department of Cornea & Refractive Surgery, Narayana Nethralaya, No. 121/C, 1st R Block, Rajajinagar, Bangalore 560010, India*
[4]*Department of Ophthalmology, Maastricht University, P.O. Box 616, 6200 MD Maastricht, Netherlands*
[5]*Forus Health Pvt. Ltd, No. 2234, 23rd Cross Road, Banashankari Stage II, Banashankari, Bangalore, India*

Correspondence should be addressed to Dabir Supriya; supriad@gmail.com

Received 12 September 2014; Accepted 16 January 2015

Academic Editor: Michele Figus

Aim. To assess the functional aspects of cone mosaic and correlate cone packing with retinal sensitivity utilizing microperimetry in emmetropes at different eccentricities. *Methods*. Twenty-four healthy volunteers underwent microperimetry (MAIA Centervue, Italy) and assessment of photoreceptors using adaptive optics retinal camera, rtx1 (Imagine Eyes, Orsay, France), at 2 and 3 degrees from the foveal centre in 4 quadrants: superior, inferior, temporal, and nasal. Data was analyzed using SPSS version 17 (IBM). Spearman's correlation tests were used to establish correlation between mean cone packing density and retinal sensitivity at different quadrants. *Results*. Thirteen females and 11 males (age range 20–40 years) were included. The cone density was found to be significantly different among all quadrants (temporal = 25786.68/mm^2 ± 4367.07/mm^2, superior = 23009.35/mm^2 ± 5415.81/mm^2, nasal = 22838.09/mm^2 ± 4166.22/mm^2, and inferior = 21097.53/mm^2 ± 4235.84/mm^2). A statistical significance ($P < 0.008$) was found between orthogonal meridians, that is, temporal, nasal (48624.77/mm^2) > superior, inferior (44106.88/mm^2). A drop in retinal sensitivity was observed as the eccentricity increased ($P < 0.05$). It was also found that as cone packing density decreased retinal sensitivity also decreased ($P < 0.05$) in all quadrants. This was observed at both 2 and 3 degrees. *Conclusion*. It is of crucial importance to establish normative variations in cone structure-function correlation. This may help in detection of subtle pathology and its early intervention.

1. Introduction

Adaptive optics (AO) is emerging as an objective tool in assessment of the architecture of the photoreceptor layer of retina. It can be used to quantify the cone mosaic including the density and packing arrangements. Studying the cone mosaic shows different reflectance patterns with wide temporal and spatial variations. Multiple AO systems have described this variation in the cone reflectivity to be secondary to differences in the phase of phototransduction, length of the outer segment, disc shedding, wavelength of the light, and so forth [1–3].

By just studying the cone mosaic, we are unable to assess the functional aspect of a visible cone and correlate whether a visible cone is a functional cone.

Our study aims to assess the functional aspects of the cone mosaic and correlate the cone packing with the retinal sensitivity utilizing microperimetry (MAIA) in emmetropes at different eccentricities.

2. Subjects

Twenty-four healthy volunteers were included in the study after an informed consent was obtained, approved by

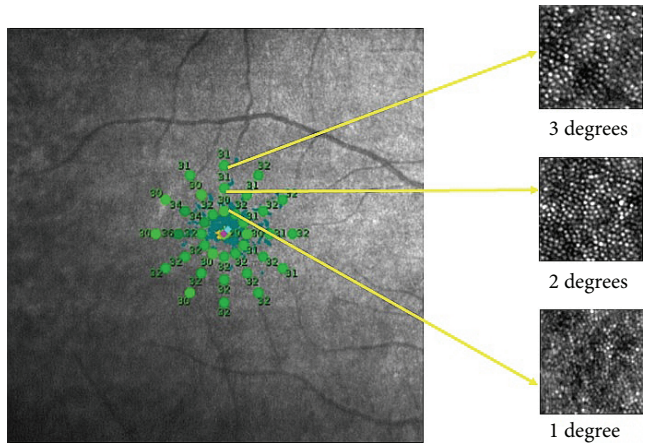

Figure 1: The retinal sensitivity on the MAIA image being correlated to the cone packing density at 1, 2, and 3 degrees from the fovea and 4 quadrants (superior, inferior, temporal, and nasal).

the institutional review board and in adherence to the tenets of Helsinki declaration. Inclusion criteria were emmetropia or best correct visual acuity of 20/20 or better with astigmatism less than 2 diopters (as assessed by the Tonoref RKT-7000 autorefractometer, Nidek). Subjects with ocular or systemic diseases or previous eye surgery were excluded from the study.

3. Methods

All subjects underwent objective refraction, noncontact biometry (IOL master; Carl Zeiss Meditec, Germany) for axial length, and microperimetry (MAIA Centervue-100809). A compact AO retinal camera prototype, the rtx1 (Imagine Eyes, Orsay, France), was used to image the photoreceptor layer. Core components of the apparatus include a Shack-Hartmann wavefront sensor (HASO 32-eye; Imagine Optics, Orsay, France), a deformable mirror (MIRAO 52; Imagine Optics), and a low-noise high-resolution camera (Roper Scientific, Tucson, AZ). AO imaging sessions were conducted after dilating the pupils with 1 drop each of 0.5% tropicamide and 10% phenylephrine hydrochloride. Stable fixation was maintained by having the patient look at the system's inbuilt target moved by the investigator to predetermined coordinates. The patient was instructed to fixate at 0°, 2°, and 3° eccentricity along all the four quadrants, superior, inferior, nasal, and temporal retina. A series of 40 frames, 4° field size, was captured at each of the above retinal locations. After acquisition, a program provided by the manufacturer correlated and averaged the captured image frames to produce a final image [4]. At each site a sampling window square of 100 microns width was chosen avoiding blood vessels. Cone counting software created on MATLAB by Imagine Eyes was used to process the images and calculate the cone density (cones/mm^2) and spacing. The axial length was entered into the automated software to account for differences in magnification.

Macular integrity was tested with MAIA, a nonmydriatic, near infrared, line SLO scanning laser ophthalmoscope with high frequency eye tracker, a third generation automated macular perimeter with normative database and a statistical analysis module. An expert or detailed threshold test takes about 4–7 min for each eye and was performed. The grid selected was 37 point stimuli covering the central 6 degrees with 25 μm stimulus size, that is, Goldmann III. The threshold values at radius of 2 degrees and 3 degrees from the fovea were considered in all the 4 quadrants: superior, inferior, nasal, and temporal. The Goldmann size III target subtends 0.431° of visual angle and represents 0.123 mm ($0.431^{\circ} * 0.286$ mm/$^{\circ}$) on the retina and an area of 0.012 mm^2 [5]. The sampling window that we have used with the AO image processing is 0.1 mm, and hence the correlation has the potential for fine retinotopic precision as seen in Figure 1.

4. Statistical Analysis

The data collected was analyzed using SPSS version 17 (IBM). Spearman's correlation tests were used to establish the correlation between the mean cone packing density and the retinal sensitivity at the different quadrants. To look for possible differences between MAIA threshold values at the different quadrants and eccentricities, a Linear Mixed Models analysis (LMM) was performed with subject ID as grouping factor and cone density, eccentricity, and quadrant and their interaction term as covariates. The LMM procedure expands the general linear model so that the data are permitted to exhibit correlated and nonconstant variability. The LMM analysis, therefore, provides the flexibility of modeling not only the means of the data but their variances and covariances as well. LMM handle data where observations are not independent, as in this study. That is, LMM correctly models correlated errors, whereas procedures in the general linear model family usually do not [6, 7]. P values smaller than 0.05 were considered to be significant.

5. Results

Twenty-four subjects were included in the study. The study group comprised of 13 females and 11 males between the ages

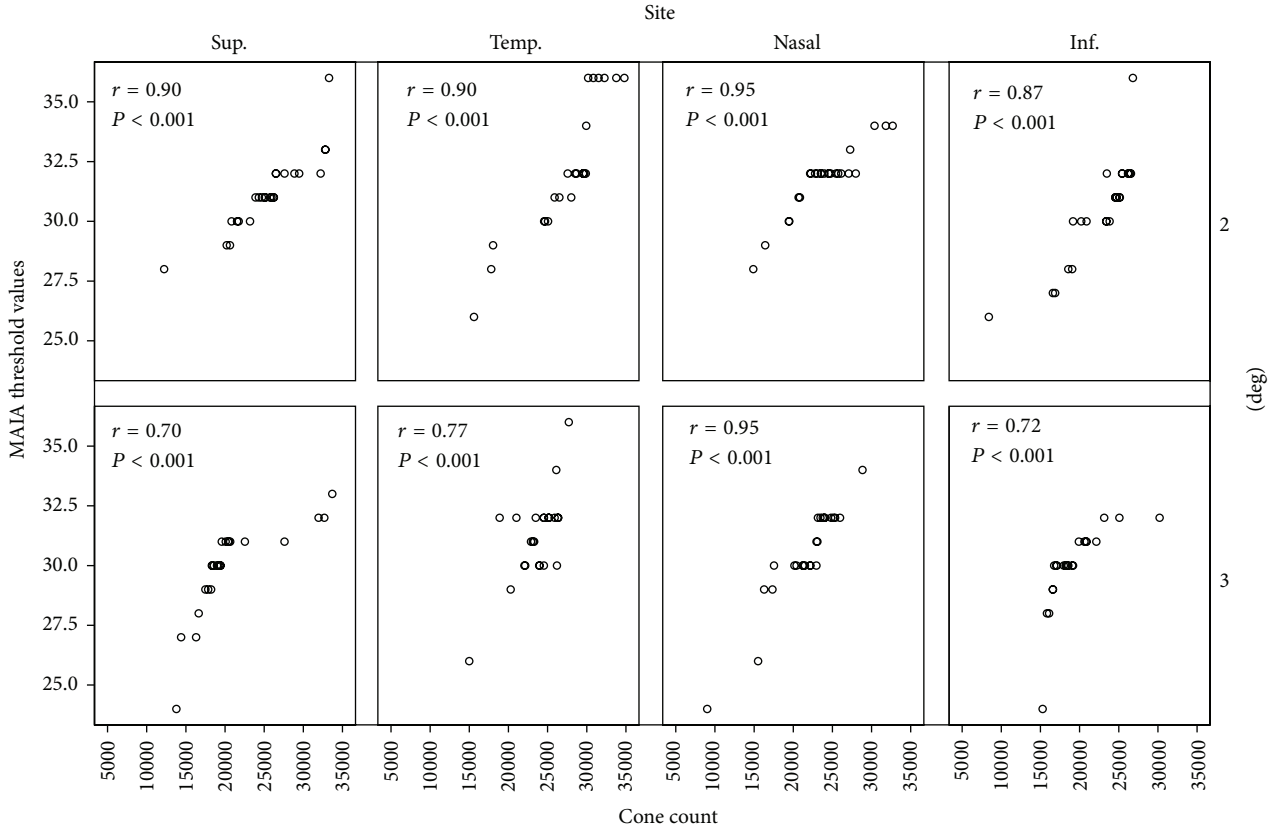

Figure 2: Scatter plot showing correlation between cone density and average threshold at 4 quadrants, both at 2 and 3 degrees.

of 20 and 40 years. Figure 2 shows MAIA threshold values as a function of cone density for the different quadrants. The Pearson correlation coefficient, r, was significant for all sites ($P < 0.001$). The cone density was found to be significantly different among all the four quadrants (temporal: 25786 ± 4367 mm^{-2}, superior: 23009 ± 5415 mm^{-2}, nasal: 22838 ± 4166 mm^{-2}, and inferior: 21097 ± 4235 mm^{-2}). A statistical significance ($P < 0.008$) was found between the orthogonal meridians, that is, temporal, nasal > superior, inferior (temporal + nasal = 48624 mm^{-2} > superior + inferior = 44106 mm^{-2}). Figure 3 shows mean MAIA thresholds at 2 and 3 degrees for the different quadrants. A drop in the retinal sensitivity was observed as the eccentricity increased. LMM analysis revealed that MAIA threshold values differed significantly between the four quadrants (temporal = 32.2 ± 2.7 dB, superior = 31.2 ± 1.6 dB, nasal: 31.8 ± 1.4 dB, and inferior: 30.5 ± 2.1 dB, $P = 0.001$) and also between the two eccentricities (see Figure 3, $P = 0.01$).

6. Discussion

With the advent of adaptive optics leading to compensation of higher order aberrations, the in vivo imaging of the photoreceptor mosaic is now a reality. The challenge now comes in assessing the correlation of the cone mosaic with their functioning. It is interesting to understand whether areas with dense cone packing are associated with higher retinal sensitivities. Establishing the normative database in emmetropes is essential before we understand pathology. This may be useful in establishing the functional correlates of photoreceptor mosaic structure in patients with macular disease who develop central scotomas due to various diseases like age related macular degeneration. They can then be coached to prefer a certain peripheral part of retina to fixate with, depending on the cone density and retinal sensitivity at that area [8, 9]. Even in children after squint surgeries, they may be trained to develop fixation by utilizing the structure-function knowledge of the retinal areas.

There has been a lot of literature on the use of microperimetry alone to find the preferential retinal locus in patients with central macular disease and they have found it to be differing with respect to the task assigned to the patient [8–12]. This however does not happen in normal adults where the preferential retinal locus is fixed. Hence it may be possible to rehabilitate these patients once we understand the areas in which relative structural photoreceptor loss has led to relative functional loss.

The Goldmann size III target has the diameter which subtends 0.431° of visual angle which corresponds to the sampling window of the adaptive optics and hence the correlation has the potential for fine retinotopic precision.

Our study shows that when the mean cone packing density decreased with increasing eccentricity, the corresponding retinal sensitivity also decreased ($P < 0.05$).

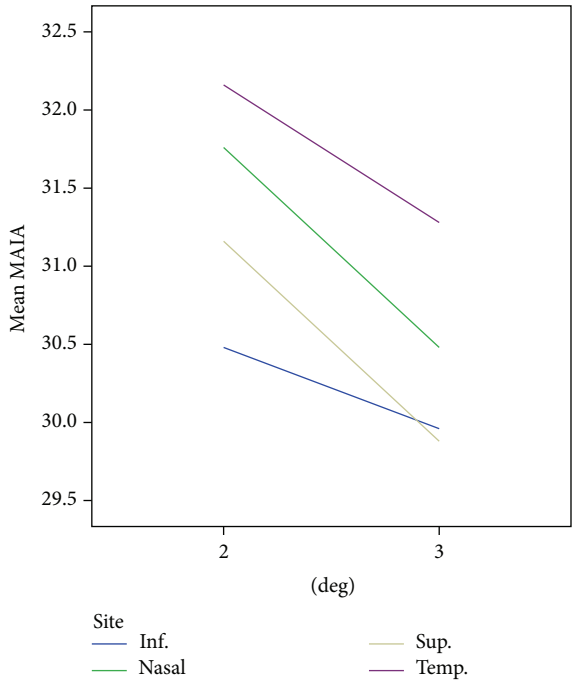

Figure 3: Mean MAIA thresholds at 2 and 3 degrees for the different quadrants.

The limitations of our study are that we have used a flood illuminated AO camera and not an AO-SLO based microperimetry system [13] which would have better localizing. Also multifocal electrophysiology would have been a more objective tool to analyze the macular function but the costs of tests were a limiting factor.

This study may help establish a sensitive outcome measure to evaluate the safety and efficacy of newer treatment modalities like stem cell therapy and gene therapy in the management of genetic retinal disorders.

7. Conclusion

Understanding the correlation between the anatomy of a structure and its function is crucial to plan management of any disease. Knowing the variations in a healthy population helps us analyze pathology better.

Conflict of Interests

The authors declare that there is no conflict of interests regarding the publication of this paper.

Acknowledgments

The authors acknowledge Dr. Shyam Vasudev, Forus Health Pvt. Ltd, Bangalore, India, and Dr. Preetam Samant, PD Hinduja Hospital, Mumbai, India.

References

[1] R. S. Jonnal, J. R. Besecker, J. C. Derby et al., "Imaging outer segment renewal in living human cone photoreceptors," *Optics Express*, vol. 18, no. 5, pp. 5257–5270, 2010.

[2] M. Pircher, R. J. Zawadzki, J. W. Evans, J. S. Werner, and C. K. Hitzenberger, "Simultaneous imaging of human cone mosaic with adaptive optics enhanced scanning laser ophthalmoscopy and high-speed transversal scanning optical coherence tomography," *Optics Letters*, vol. 33, no. 1, pp. 22–24, 2008.

[3] A. Pallikaris, D. R. Williams, and H. Hofer, "The reflectance of single cones in the living human eye," *Investigative Ophthalmology and Visual Science*, vol. 44, no. 10, pp. 4580–4592, 2003.

[4] M. Lombardo, S. Serrao, P. Ducoli, and G. Lombardo, "Influence of sampling window size and orientation on parafoveal cone packing density," *Biomedical Optics Express*, vol. 4, no. 8, pp. 1318–1331, 2013.

[5] D. F. Garway-Heath, J. Caprioli, F. W. Fitzke, and R. A. Hitchings, "Scaling the hill of vision: the physiological relationship between light sensitivity and ganglion cell numbers," *Investigative Ophthalmology and Visual Science*, vol. 41, no. 7, pp. 1774–1782, 2000.

[6] I. Jansen, C. Beunckens, G. Molenberghs, G. Verbeke, and C. Mallinckrodt, "Analyzing incomplete discrete longitudinal clinical trial data," *Statistical Science*, vol. 21, no. 1, pp. 52–69, 2006.

[7] N. M. Laird and J. H. Ware, "Random-effects models for longitudinal data," *Biometrics*, vol. 38, no. 4, pp. 963–974, 1982.

[8] A. Calabrèse, J.-B. Bernard, L. Hoffart et al., "Wet versus dry age-related macular degeneration in patients with central field loss: different effects on maximum reading speed," *Investigative Ophthalmology and Visual Science*, vol. 52, no. 5, pp. 2417–2424, 2011.

[9] U. L. Nilsson, C. Frennesson, and S. E. G. Nilsson, "Patients with AMD and a large absolute central scotoma can be trained successfully to use eccentric viewing, as demonstrated in a scanning laser ophthalmoscope," *Vision Research*, vol. 43, no. 16, pp. 1777–1787, 2003.

[10] N. Shima, S. N. Markowitz, and S. V. Reyes, "Concept of a functional retinal locus in age-related macular degeneration," *Canadian Journal of Ophthalmology*, vol. 45, no. 1, pp. 62–66, 2010.

[11] E. Pacella, F. Pacella, F. Mazzeo et al., "Effectiveness of vision rehabilitation treatment through MP-1 microperimeter in patients with visual loss due to macular disease," *Clinica Terapeutica*, vol. 163, no. 6, pp. e423–e428, 2012.

[12] K. Fujita and M. Yuzawa, "Preferred retinal locus in patients with age-related macular degeneration," *Nippon Ganka Gakkai zasshi*, vol. 107, no. 10, pp. 602–606, 2003.

[13] W. S. Tuten, P. Tiruveedhula, and A. Roorda, "Adaptive optics scanning laser ophthalmoscope-based microperimetry," *Optometry and Vision Science*, vol. 89, no. 5, pp. 563–574, 2012.

Hindawi Publishing Corporation
BioMed Research International
Volume 2015, Article ID 752957, 10 pages
http://dx.doi.org/10.1155/2015/752957

Research Article

Novel Method for Automated Analysis of Retinal Images: Results in Subjects with Hypertensive Retinopathy and CADASIL

Michele Cavallari,[1,2] Claudio Stamile,[3] Renato Umeton,[2] Francesco Calimeri,[3] and Francesco Orzi[2]

[1]*Center for Neurological Imaging, Department of Radiology, Brigham and Women's Hospital, Harvard Medical School, 221 Longwood Avenue, Boston, MA 02115, USA*
[2]*Department of Neurosciences, Mental Health and Sensory Organs (NESMOS), University of Rome "La Sapienza", Sant'Andrea Hospital, Via di Grottarossa 1035, 00189 Rome, Italy*
[3]*Department of Mathematics and Computer Science (DeMaCS), University of Calabria, 87036 Rende, Italy*

Correspondence should be addressed to Michele Cavallari; miches@bwh.harvard.edu
and Francesco Orzi; francesco.orzi@uniroma1.it

Received 11 August 2014; Accepted 16 March 2015

Academic Editor: Paolo Frezzotti

Morphological analysis of the retinal vessels by fundoscopy provides noninvasive means for detecting and staging systemic microvascular damage. However, full exploitation of fundoscopy in clinical settings is limited by paucity of quantitative, objective information obtainable through the observer-driven evaluations currently employed in routine practice. Here, we report on the development of a semiautomated, computer-based method to assess retinal vessel morphology. The method allows simultaneous and operator-independent quantitative assessment of arteriole-to-venule ratio, tortuosity index, and mean fractal dimension. The method was implemented in two conditions known for being associated with retinal vessel changes: hypertensive retinopathy and Cerebral Autosomal Dominant Arteriopathy with Subcortical Infarcts and Leukoencephalopathy (CADASIL). The results showed that our approach is effective in detecting and quantifying the retinal vessel abnormalities. Arteriole-to-venule ratio, tortuosity index, and mean fractal dimension were altered in the subjects with hypertensive retinopathy or CADASIL with respect to age- and gender-matched controls. The interrater reliability was excellent for all the three indices (intraclass correlation coefficient $\geq 85\%$). The method represents simple and highly reproducible means for discriminating pathological conditions characterized by morphological changes of retinal vessels. The advantages of our method include simultaneous and operator-independent assessment of different parameters and improved reliability of the measurements.

1. Introduction

It has been known for long time that retinal changes reflect systemic microvascular damage associated with a number of pathological conditions, such as hypertension or diabetes [1]. Because of anatomical and developmental similarities with the central nervous system [2], the retinal vessels are thought to especially mirror the brain microvasculature. In fact, there is evidence that retinal vessel abnormalities are associated with increased risk of stroke [3], stroke mortality [4], cerebral white matter damage [5], carotid atherosclerosis [6], intracranial large artery disease [7], cerebral amyloid angiopathy [8], or Cerebral Autosomal Dominant Arteriopathy with Subcortical Infarcts and Leukoencephalopathy (CADASIL) [9]. Retinal vessels can be easily inspected by fundoscopy, and all these findings together support the use of fundoscopy as a tool for staging or early diagnosis of cerebral small-vessel diseases. However, full exploitation of fundoscopy in clinical settings is limited because quantitative information can hardly be obtained through the observer-driven evaluations currently employed in routine clinical practice.

The recent development of digital imaging techniques allows for impressive capabilities of storage, transfer, and quantitation of retinal images. In the last decade, several

Table 1: Characteristics of the study subjects.

	Age	Gender (F)	Smoking	Dyslipidemia	Hypertension	Diabetes
Hypertensive retinopathy	63 ± 15	7/16	2/16	3/16	16/16	3/16
Controls	62 ± 14	7/16	5/16	None	None	None
P^* ($n = 16$)	*0.85*	*0.99*	*0.39*	*0.23*	*0.0001*	*0.23*
CADASIL	45 ± 8	7/11	2/11	2/11	1/11	1/11
Controls	44 ± 8	7/11	3/11	1/11	None	None
P^* ($n = 11$)	*0.77*	*0.99*	*0.99*	*0.99*	*0.99*	*0.99*

Age is expressed as mean ± SD. All the other variables are expressed as ratio *n*/total.
Dyslipidemia was defined as total cholesterol ≥200 mg/dL or LDL ≥100 mg/dL or statin treatment. Hypertension was defined as elevated blood pressure (ambulatory systolic blood pressure ≥140 mmHg and/or diastolic blood pressure ≥90 mmHg) or current antihypertensive drug therapy. Diabetes was defined as fasting glucose levels ≥126 mg/dL on two different test occasions or current use of hypoglycemic agents.
* Wilcoxon rank sum test (age) or Chi-squared test (all the other variables).

computer-assisted methods have been developed to automate the analysis of retinal images [10–15]. Morphometric parameters of the retinal vasculature, such as vessel diameter, tortuosity, and mean fractal dimension (mean-D), constitute the main output of these approaches.

Retinal vessel diameter is consistently expressed as arteriole-to-venule ratio (AVR). Probably, the most largely employed method is the one by Hubbard et al. [10], which computes the diameter on the basis of measurements carried out at a single, arbitrarily selected point of the vessel. Similar to more recent approaches [12–15], our method exploits vessel extraction and tracking techniques to compute diameter along an extended retinal vessel segment, rather than at a given point.

Tortuosity of the retinal vessels is also a relevant parameter to assess retinopathy [16]. A number of different methods have been proposed to assess retinal vessel tortuosity (for a review, see [17]). The two most largely employed methods compute tortuosity by using the integral of the vessel curvature [18] or the ratio between arc and cord length of the vessel segment [19]. Our newly developed method has the advantage of taking into account both the area under the curve delineated by the vessel and the directional changes along the vessel path, with improved sensitivity.

Mean-D is the main output of fractal analysis, which constitutes an operator-independent, quantitative means to assess the complexity or density of the retinal vessel branching [20]. Changes in mean-D of the retinal vascular tree are associated with hypertension [21], diabetes [22], and cerebrovascular diseases, such as lacunar stroke [23]. We recently reported clear-cut changes of mean-D values in subjects with CADASIL [24], an inherited disorder affecting the cerebral small vessels and leading to stroke and dementia.

Here, we report on the development of a semiautomated, computer-based method to assess retinal vessel morphology. The method (a) allows simultaneous and operator-independent assessment of the three parameters (AVR, tortuosity, and mean-D), (b) improves reliability of AVR by performing the assessment along extended vessel segments instead of at a single, arbitrarily selected point, (c) increases the sensitivity of tortuosity measurements, as they are carried out by a new approach, and (d) allows fully automated fractal analysis. The method implements two custom plugins (*Cioran* and *BRetina*), which are embedded into the widely used *ImageJ* free software (http://rsb.info.nih.gov/ij/).

In order to test the method, we implemented it in two different clinical conditions, previously shown to present changes in AVR, tortuosity, and mean-D: hypertensive retinopathy [18, 21, 25] and CADASIL [24, 26].

2. Methods

2.1. Subjects. Four groups were considered: subjects with hypertensive retinopathy ($n = 16$), subjects with CADASIL ($n = 11$), and the respective age- and gender-matched controls ($n = 16$ and 11). Subjects with hypertensive retinopathy were consecutive patients referred to our neurology unit because of presumed cerebrovascular disease or to the ophthalmology outpatient unit of our hospital because of visual symptoms. Diagnosis of hypertensive retinopathy was carried out by an independent ophthalmologist, and the severity was scored according to the established, three-grade classification proposed by Wong and Mitchell [27]. Subjects with genetically defined CADASIL had been examined for retinopathy in a previous study [24]. The very same subjects were included in this study for the purpose of quantifying the retinal vessel changes by using the newly developed automated analysis. Control subjects were recruited among the medical or nursing staff, as well as patient relatives. From an original cohort of 54 control subjects, individuals were randomly sorted and then enrolled or rejected on the basis of matching (age ± 3 years and gender) with each of the hypertensive retinopathy or CADASIL subjects. Clinical history, including cerebrovascular risk factors, was collected to account for potential confounders (Table 1).

Retinal photographs from patients with CADASIL were obtained following approval by the local ethics committee. Fundoscopy in patients with hypertensive retinopathy was performed according to good clinical practice routine. Informed consent was obtained from all the participants. Given the noninvasiveness of the procedure, a verbal consent was deemed satisfactory.

2.2. Image Processing and Analysis. Fundoscopy was carried out using a digital fundus camera (Canon CR-DGI equipped with Canon EOS-40D digital camera). After pupil dilation

(topical solution of tropicamide 1%), a 45° retinal photograph of one eye, centered on the region of the optic disc, was acquired. All the images were processed using *Image-J* (http://rsb.info.nih.gov/ij/) and *Frac Lac* (http://rsbweb.nih.gov/ij/plugins/fraclac/), both available as free software. The analysis was completed by means of the two custom plugins that we named *Cioran* and *BRetina*, to be embedded in *Image-J*. *Cioran* and *BRetina* were developed for the purpose and are herewith presented.

Cioran was developed to trace the path of the main retinal vessels and to measure their thickness (AVR) and tortuosity (tortuosity index: TI) along a segment. Once launched, *Cioran* automatically identifies and tracks the visible retinal vessels (Figure 1). Among the highlighted vessels, the operator selects 2 major arterioles and 2 venules and, for each vessel, defines a segment comprised between the edge of the optic nerve and the first vascular bifurcation (Figure 1). Following this initial, arbitrary vessel and segment selection, the software computes all the parameters in an operator-independent way.

The software computes the average width of the 2 arterioles and 2 venules along the entire segments. AVR is expressed as the ratio between the average width of the 2 arterioles and the 2 venules.

On the very same vessel segments, *Cioran* computes also TI. Two parameters define TI: (a) the counts of the directional changes along the vessel path; (b) the area under the curve delineated by the same vessel segment. Both parameters are normalized by the length of the vessel segment. The TI measurements obtained by means of our new implemented software were compared with data obtained using two different methods, which define TI as the area under the curve delineated by the vessel normalized by the length of the vessel segment analyzed [18] or the ratio between arc and cord length of the vessel segment [19]. For statistical analysis, we used the average TI from the 2 arterioles and the 2 venules.

BRetina was developed to automatize the processing of the retinal images required by the *Frac Lac* software to perform the fractal analysis (measurement of mean-D) (Figure 1; *Box*).

Box

(a) Cioran. The workflow of *Cioran* image processing may be summarized in the following 3 steps (Figure 1): (a) vessel extraction, (b) tracking, and (c) measurement. Vessel extraction is based on iterative runs of the *Subtract Background* task [35], followed by further filtering obtained by the *Skeletonize* command, enclosed in *Image-J*. The resulting image constitutes the basis for the vessel tracking step. The operator selects the start and end points of each vessel segment to be analyzed. The A^* "walking" algorithm [36] is then exploited in order to obtain the basic parameters of the vessel geometry. The third step is devoted to the measurement of the diameter of the selected vessel segments. For that purpose the shortest distance between the edges of the vessel is computed for each pixel of the segment length. The average value is then taken for final result. The computation of tortuosity index is based on a combination of Bézier and Spline interpolations [37, 38], so as to obtain a regular analytical function $y = f(x)$, describing the vessel path. The start and end points selected by the operator were set to $y = 0$. TI was computed taking into account (1) the area of the curve delineated by the vessel segment; (2) the number of directional changes along the vessel path, normalized by the total length of the selected vessel segments. The directional changes were defined as points where the first derivative of the analytical function is equal to zero, corresponding to the points where vessel path changes its slope. Confounding conditions that may impair the analysis in subjects with hypertensive retinopathy, such as microaneurysms, exudates, and hemorrhages, were removed by using the *Remove Outliers* filter enclosed in *Image-J* and by subtracting the resulting mask from the retinal image.

(b) BRetina. The *BRetina* algorithm is based on the following 4 fundamental steps, displayed in Figure 1: (a) identification of the optic nerve; (b) selection of the region of interest (ROI); (c) execution of the blood vessel filters; (d) fractal analysis. The first step includes the application of the *Variance* filter to red-free images, which allows the main retinal structures (optic nerve and vessels) to emerge from the background. The resulting image undergoes a quality check based on the *Otsu Thresholding* [39]. The software identifies the optical nerve in the most circular pattern of the image. The radius of the optical nerve is then adopted to select a circular ROI of 3.5x optic disc diameter, concentric with the optic nerve. In order to extract the retinal vessels from the background (as evaluated by *Otsu Thresholding*), the following filters (enclosed in *Image-J*) are then applied: *Subtract Background*, *Binary Conversion*, *Despeckle*, and *Outline*. The last step consists in running the external plugin *Frac Lac*, which performs the fractal analysis of the retinal vascular tree using a box counting algorithm. The whole procedure is automated and works as a single click. Nevertheless, the operator is allowed to interfere with the outcome of the automated processing at each step. For example, if the algorithm of optic nerve identification fails (e.g., due to papilledema), the operator can select and position the region of interest manually and then start over the *BRetina* workflow from that particular step.

The analyses were carried out by a trained physician (MC), blind to demographic and clinical data. A second user (CS) carried out the measurements on the entire data set to assess interrater reliability. Screenshots depicting the main steps of image processing and analysis by *Cioran* and *BRetina* are shown in Figure 1. The plugins' workflow is described in the *Box*.

2.3. Statistical Analysis. Wilcoxon signed rank test was used for analyzing group differences in AVR, TI, and mean-D. Sensitivity, specificity, and positive and negative predictive values of each retinal index, separately and cumulatively for the three indices, were obtained using 2×2 contingency tables. K-means was performed to classify subjects with normal versus abnormal retinal features. Intraclass correlation was used to assess interrater reliability between the two operators. Statistical analyses were performed using Graph Pad (http://www.graphpad.com/) (Wilcoxon, intraclass correlation and contingency tables) and KNIME (http://www.knime.org/) (cluster analysis).

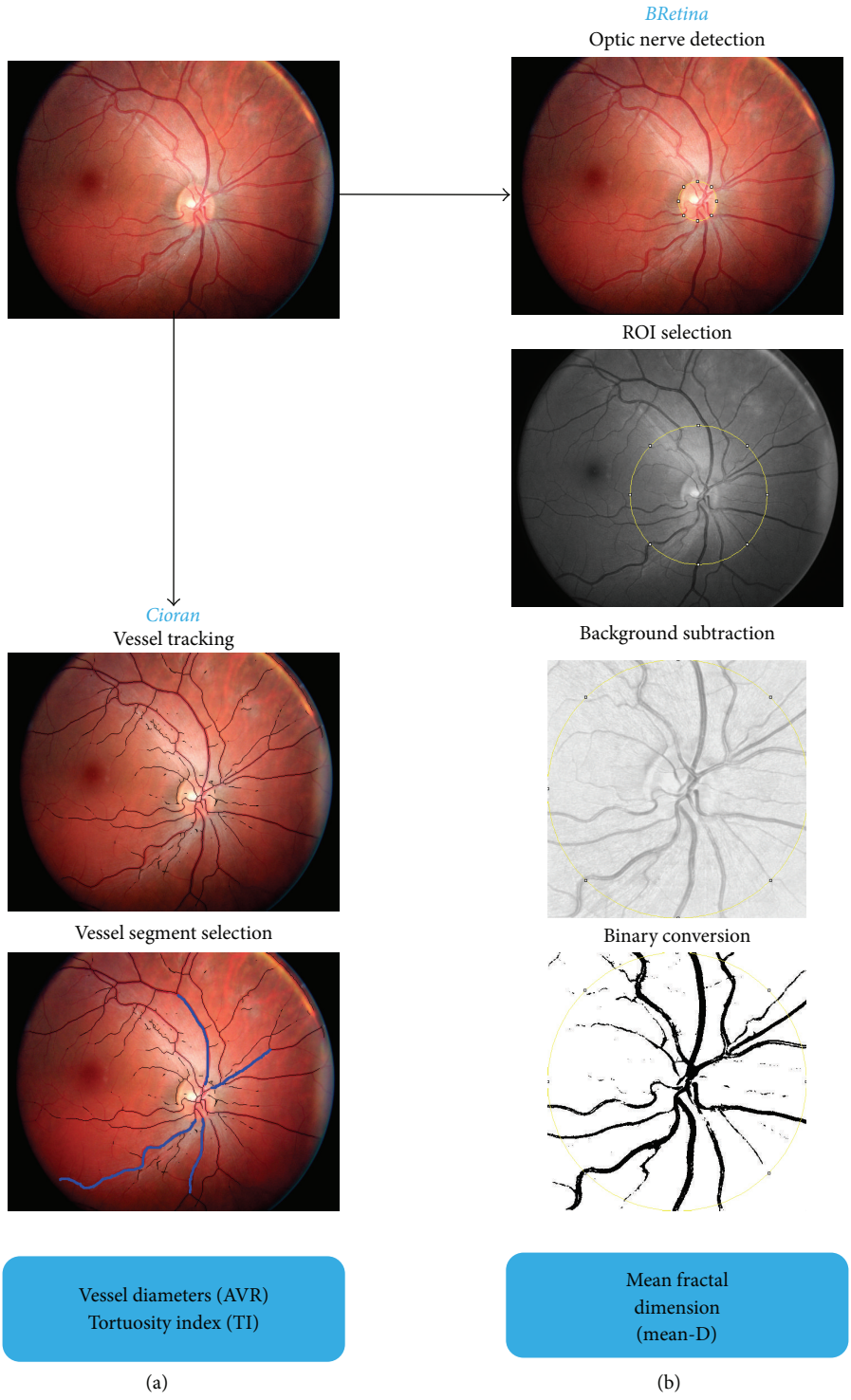

FIGURE 1: Main steps of the image processing. From an individual retinal photograph, vessel tracking and vessel segment selection is carried out by means of the *Cioran* plugin (a). The *BRetina* plugin allows the automated image processing needed to provide the mean-D value of the fractal analysis (the fundamental steps are represented in (b)). Details are in the *Box*.

3. Results

Demographics and cerebrovascular risk factors of the study subjects are reported in Table 1. Among the 16 subjects with hypertensive retinopathy, 11 had no other major disease, 3 had suffered from ischemic stroke, 1 had suffered from transient ischemic attack, and 1 had suffered from subdural hematoma. The retinopathy was graded as follows: moderate in 12/16 cases, mild in 2, and malignant in 2 of the subjects. Of the 11 subjects with CADASIL, 4 were asymptomatic, 3 exhibited

Table 2: Arteriole-to-venule ratio (AVR), mean fractal dimension (mean-D), and tortuosity index (TI) values of the study groups.

	AVR	Mean-D	TI[1]	TI[2]
Hypertensive retinopathy	0.68 ± 0.09	1.41 ± 0.04	72 ± 26	1.52 ± 1.36
Controls	0.77 ± 0.07	1.45 ± 0.04	64 ± 24	1.44 ± 0.74
P^* ($n = 16$)	*0.01*	*0.04*	*0.03*	*0.84*
CADASIL	0.67 ± 0.10	1.40 ± 0.04	67 ± 23	1.29 ± 1.06
Controls	0.78 ± 0.07	1.45 ± 0.04	61 ± 22	1.32 ± 0.94
P^* ($n = 11$)	*0.03*	*0.002*	*0.08*	*0.70*

Values are expressed as mean ± SD.
*Wilcoxon signed rank test.
TI[1]: tortuosity index measured by using the method implemented in *Cioran*.
TI[2]: tortuosity index measured using the method by Cheung et al. [18].

a history of transient ischemic attack or stroke, 3 had chronic migraine, and 1 had seizures.

Analysis of the retinal images showed a marked difference between disease and control groups for all the parameters measured. AVR and mean-D were lower than control in both patients with hypertensive retinopathy and CADASIL ($P < 0.05$). TI values were higher than control in the hypertensive retinopathy ($P < 0.05$) and CADASIL ($P = 0.08$) groups. The results are reported in Table 2 and Figure 2. The following cutoffs, derived from K-means clustering, were applied to define the retinal indices as abnormal: <0.70 for AVR, >72 for TI, and <1.42 for mean-D. Sensitivity, specificity, and positive and negative predictive values of each retinal index separately, and of all the three indices together, are shown in Table 3. Representative fundoscopy images for each group and the main output of the analysis carried out by *Cioran* and *BRetina* are shown in Figure 3.

The interrater reliability showed an intraclass correlation coefficient of 85% for AVR, 89% for TI, and 92% for mean-D.

4. Discussion

We developed two custom-made plugins and embedded them into the free software *Image-J* in order to provide a novel method for quantitative, semiautomated analysis of retinal vessel features in fundoscopy images. We sought to validate the method by implementing it in two conditions known for being associated with retinal vessel changes, hypertensive retinopathy, and CADASIL [21, 24–26].

The results of the study show that the method allows us to reveal the expected retinal vessel abnormalities and to provide a quantitative assessment of the changes. Namely, we found abnormal AVR, TI, and mean-D in the hypertensive retinopathy and CADASIL groups, as compared to the matched control subjects (although in the CADASIL group the TI difference only approached statistical significance).

Our findings are in line with previous studies. Leung et al. [25] showed an inverse linear relationship between retinal vessel diameter and blood pressure in subjects with hypertension, while Ikram et al. [28] found that arteriolar narrowing was predictive of hypertension in a prospective population-based study. It is worth stressing that the AVR measurements carried out in the present study have the confidence of an approach that averages measures gathered along an extended retinal vessel segment. Most of the AVR values reported in the literature represent ratios of diameters measured at a given point. A limited number of studies measured tortuosity of retinal vessels in subjects with hypertension [29, 30]. Most of those studies are of a subjective and qualitative nature, with a few exceptions [18]. Our findings support and reinforce the findings in the literature, as the measurements performed in this study are based on a near operator-independent approach. Furthermore, our approach increases the sensitivity of the TI measurement by taking into account the number of directional changes along the selected vessel path, in addition to the area of the curve delineated by the same vessel segment. Our approach showed significant differences in TI measurements between subjects with hypertensive retinopathy and controls. Such differences were not detectable by implementing, in the very same retinal images, methods based solely on the integral of the vessel curvature [18] or the ratio between arc and cord length of the vessel segment [19] (Table 2; Figure 3). There are also very few studies of fractal analysis of the retinal vessels in subjects with hypertension. The available data obtained in adult subjects [21] or children [31] are consistent with our findings, which show a reduced complexity of the retinal vessel branching.

Reports concerning retinal vessel abnormalities in subjects with CADASIL are scant. Narrowing, sheathing, and nicking of the retinal arterioles were reported in subjects with CADASIL by means of qualitative evaluations of fundoscopy [32] or fluorescein angiography images [33]. Similar to our findings, one quantitative assessment reported reduced AVR in CADASIL [26]. In regard to TI values, to our knowledge, this is the first measurement of tortuosity carried out in CADASIL patients. Previous reports concern evaluations based on subjective scoring. Roine et al. [26] observed "straightening" of retinal arterioles in 6 and "curliness" in 1 over 38 subjects. Cumurciuc et al. [32] reported "tortuous arterioles" in 1 over 18 patients. Our findings suggest an increased tortuosity in the retinal vessel of subjects with CADASIL (Table 2). Data regarding fractal analysis of retinal vessels in CADASIL are limited to our own previous study, in which we reported clear changes of mean-D values in subjects with disease compared to matched controls [24]. The present study confirms the previous results and adds the novelty of an automatized, operator-independent method. It is worth stressing that 4 out of the 11 subjects with CADASIL were

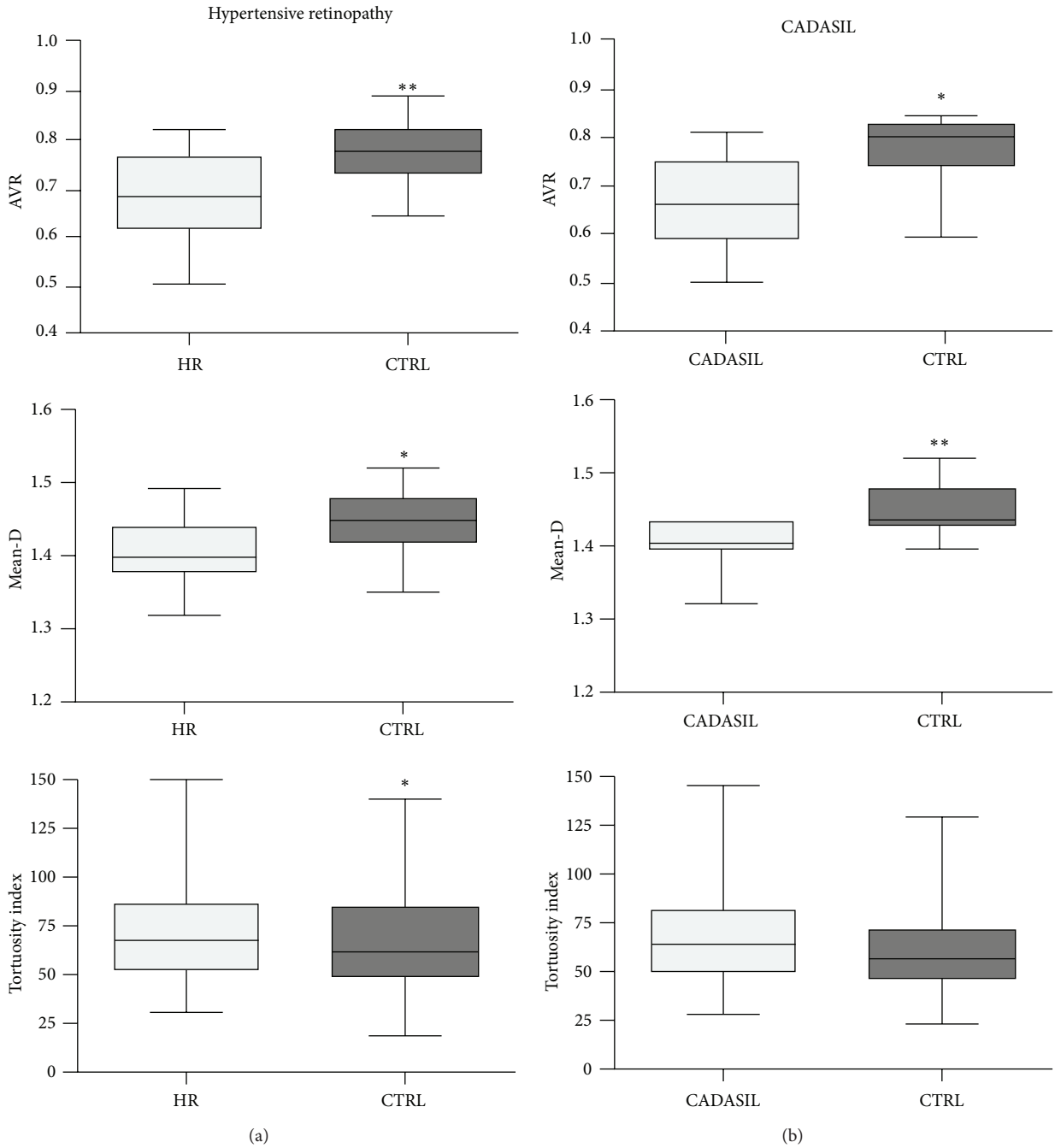

Figure 2: Box plots illustrating group differences in arteriole-to-venule ratio (AVR), mean fractal dimension (mean-D), and tortuosity index (TI) of the retinal vessels. Both AVR and mean-D of the subjects with hypertensive retinopathy (HR) (a) or CADASIL (b) were lower than age- and gender-matched controls. The increment of TI was significant in HR and uncertain in CADASIL group. Statistically significant differences between the groups are indicated as $*$ for P values ≤ 0.05 and as $**$ for P values ≤ 0.01. The boxes include data between 25th and 75th percentiles. Horizontal line in the box represents the median. The whiskers indicate the minimum and maximum values.

asymptomatic. Therefore, the vessel changes appear to reflect early changes.

In an exploratory fashion, we sought to verify whether the retinal indices would cluster the subjects according to the diagnosis (i.e., hypertensive retinopathy or CADASIL versus controls). AVR showed the best profile in terms of sensitivity, specificity, and positive and negative predicting values. Both TI and mean-D, in fact, showed lower predictive power compared to AVR, and the inclusion of these variables in the clustering workflow did not contribute to correctly classifying the subjects (Table 3).

The methodology reported in this study has the advantage of minimizing the analysis time and the strength of being almost operator-independent. The operator's intervention is

Table 3: Sensitivity, specificity, and positive and negative predictive values of the retinal indices to classify subjects with hypertensive retinopathy or CADASIL.

Indices	Sensitivity		Specificity		PPV		NPV	
	HR versus controls	CADASIL versus controls	HR versus controls	CADASIL versus controls	HR versus controls	CADASIL versus controls	HR versus controls	CADASIL versus controls
AVR	68.8 (41.4–88.9)	54.5 (23.5–83.1)	87.5 (61.6–98.1)	90.9 (58.7–98.5)	84.6 (54.5–97.6)	85.7 (42.2–97.6)	73.7 (48.8–90.8)	66.7 (38.4–88.1)
Mean-D	62.5 (35.5–84.7)	99.9 (71.3–99.9)	68.8 (41.4–88.9)	36.4 (11.1–69.1)	66.7 (38.4–88.1)	61.1 (35.8–82.6)	64.7 (38.4–85.7)	99.9 (40.2–99.9)
TI	43.8 (19.8–70.1)	54.6 (23.5–83.1)	75.0 (47.6–92.6)	63.6 (30.1–88.9)	63.6 (30.1–88.9)	60.0 (26.4–87.6)	57.1 (34.0–78.1)	58.3 (27.7–84.7)
AVR + mean-D + TI	68.8 (41.4–88.9)	54.5 (23.5–83.1)	87.5 (61.6–98.1)	90.9 (58.7–98.5)	84.6 (54.5–97.6)	85.7 (42.2–97.6)	73.7 (48.8–90.8)	66.7 (38.4–88.1)

Results are expressed as % (95% CI).

AVR: arteriole-to-venule ratio; HR: hypertensive retinopathy; mean-D: mean fractal dimension; NPV: negative predictive value; PPV: positive predictive value; TI: tortuosity index.

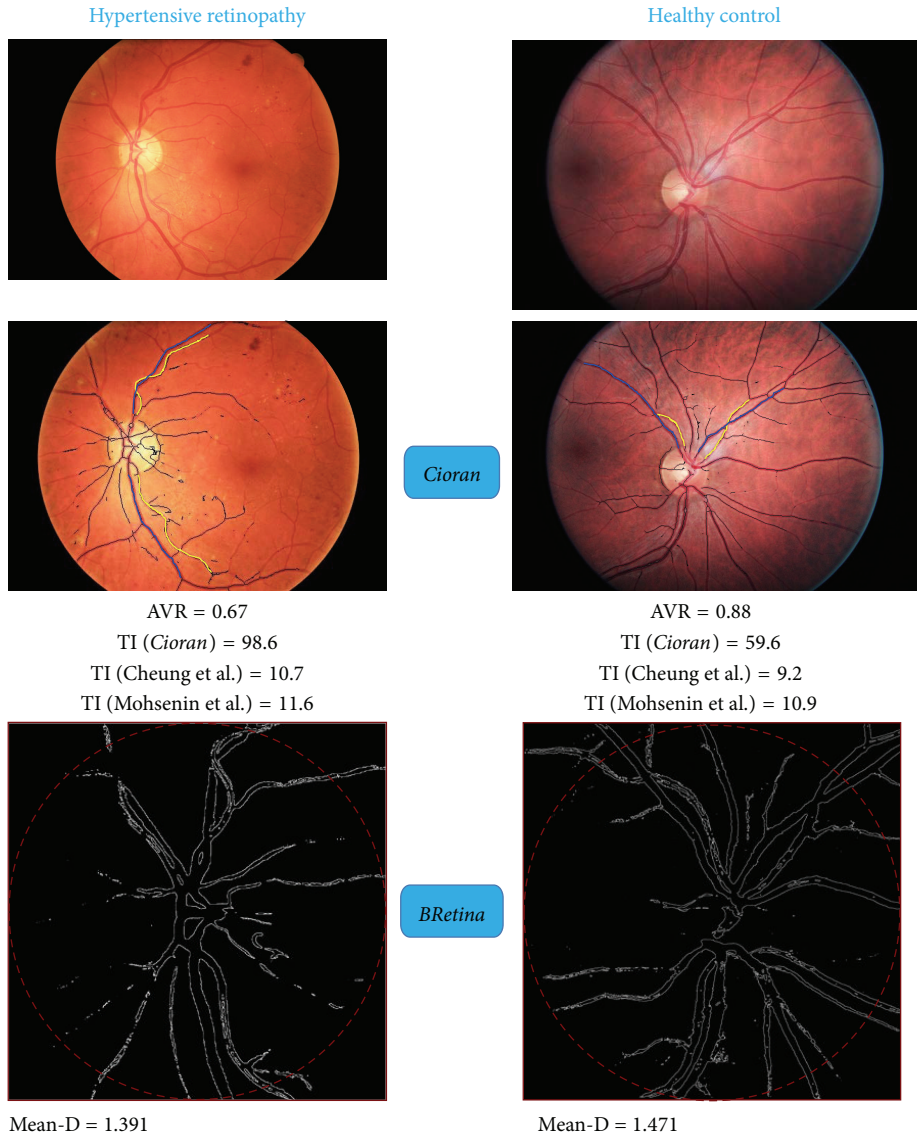

Figure 3: Examples of retinal image analysis of a subject with hypertensive retinopathy and matched healthy control. Arteriole-to-venule ratio (AVR), tortuosity index (TI), and mean fractal dimension (mean-D) carried out by *Cioran* and *BRetina* are reported. Tortuosity index (TI) values obtained using *Cioran* are compared to the values obtained using two different approaches to show that TI as measured using our approach is more sensitive to detect abnormal twisting of the retinal vessels. TI as measured by Cioran showed 40% relative increase in the subject with hypertensive retinopathy compared to the control, while TI as measured using the integral of the vessel curvature [18] or the ratio between arc and cord length of the vessel segment [19] showed 14% and 6% relative increase, respectively.

in fact limited to the application of standardized rules, which guide in the selection of the vessel segments to be analyzed. The limited subjectivity of the entire procedure based on the *Cioran* and *BRetina* plugins is confirmed by the high inter-rater concordance. Therefore, the method described here is a simple and highly reproducible approach for discriminating pathological conditions characterized by changes of retinal vessel parameters.

To our knowledge, there is similar software, reported and validated in clinical setting. The software, known as Singapore I Vessel Assessment (SIVA), allows the measurement of a number of parameters from digital retinal images, including retinal vascular caliber and tortuosity [12]. Studies carried out by employing the SIVA software show changes of the measured parameters in subjects with hypertensive or diabetic retinopathy [18, 34]. Similar to SIVA, our approach allows the computation of AVR along an extended retinal vessel segment, rather than at a given point. Our method also combines simultaneous assessment of retinal vessel diameter and tortuosity with fractal analysis of retinal vascular trees. Furthermore, TI as measured by the *Cioran* software reflects both the integral of the curvature and the number of directional changes of the vessel path. The number of directional changes seems to be the relevant parameter, as the value of the integral itself (area under the curve described by the vessel path) did not give significant results in this study (Figure 3).

The method herein described may improve confidence in fundoscopy as a tool to be exploited in clinical settings or trials.

Disclosure

The publication of this paper is approved by all authors.

Conflict of Interests

The authors declare that they have no conflict of interests regarding the publication of this paper.

Authors' Contribution

Michele Cavallari and Claudio Stamile contributed equally to this work.

References

[1] A. Grosso, N. Cheung, F. Veglio, and T. Y. Wong, "Similarities and differences in early retinal phenotypes in hypertension and diabetes," *Journal of Hypertension*, vol. 29, no. 9, pp. 1667–1675, 2011.

[2] N. Patton, T. Aslam, T. MacGillivray, A. Pattie, I. J. Deary, and B. Dhillon, "Retinal vascular image analysis as a potential screening tool for cerebrovascular disease: a rationale based on homology between cerebral and retinal microvasculatures," *Journal of Anatomy*, vol. 206, no. 4, pp. 319–348, 2005.

[3] T. Y. Wong, R. Klein, D. J. Couper et al., "Retinal microvascular abnormalities and incident stroke: the Atherosclerosis Risk in Communities Study," *The Lancet*, vol. 358, no. 9288, pp. 1134–1140, 2001.

[4] P. Mitchell, J. J. Wang, T. Y. Wong, W. Smith, R. Klein, and S. R. Leeder, "Retinal microvascular signs and risk of stroke and stroke mortality," *Neurology*, vol. 65, no. 7, pp. 1005–1009, 2005.

[5] T. Y. Wong, R. Klein, A. R. Sharrett et al., "Cerebral white matter lesions, retinopathy, and incident clinical stroke," *The Journal of the American Medical Association*, vol. 288, no. 1, pp. 67–74, 2002.

[6] D. Liao, T. Y. Wong, R. Klein, D. Jones, L. Hubbard, and A. R. Sharrett, "Relationship between carotid artery stiffness and retinal arteriolar narrowing in healthy middle-aged persons," *Stroke*, vol. 35, no. 4, pp. 837–842, 2004.

[7] D. A. de Silva, J. J. F. Manzano, F.-P. Woon et al., "Associations of retinal microvascular signs and intracranial large artery disease," *Stroke*, vol. 42, no. 3, pp. 812–814, 2011.

[8] A. Lee, A. Rudkin, M. Agzarian, S. Patel, S. Lake, and C. Chen, "Retinal vascular abnormalities in patients with cerebral amyloid angiopathy," *Cerebrovascular Diseases*, vol. 28, no. 6, pp. 618–622, 2009.

[9] A. Rufa, E. Pretegiani, P. Frezzotti et al., "Retinal nerve fiber layer thinning in CADASIL: an optical coherence tomography and MRI study," *Cerebrovascular Diseases*, vol. 31, no. 1, pp. 77–82, 2011.

[10] L. D. Hubbard, R. J. Brothers, W. N. King et al., "Methods for evaluation of retinal microvascular abnormalities associated with hypertension/sclerosis in the Atherosclerosis Risk in Communities Study," *Ophthalmology*, vol. 106, no. 12, pp. 2269–2280, 1999.

[11] N. Patton, T. M. Aslam, T. MacGillivray et al., "Retinal image analysis: concepts, applications and potential," *Progress in Retinal and Eye Research*, vol. 25, no. 1, pp. 99–127, 2006.

[12] T. Y. Wong, M. D. Knudtson, R. Klein, B. E. K. Klein, S. M. Meuer, and L. D. Hubbard, "Computer-assisted measurement of retinal vessel diameters in the Beaver Dam Eye Study: methodology, correlation between eyes, and effect of refractive errors," *Ophthalmology*, vol. 111, no. 6, pp. 1183–1190, 2004.

[13] A. Perez-Rovira, T. MacGillivray, E. Trucco et al., "VAMPIRE: vessel assessment and measurement platform for images of the REtina," in *Proceedings of the Annual International Conference of the IEEE Engineering in Medicine and Biology Society (EMBS '11)*, vol. 2011, pp. 3391–3394, IEEE, Boston, Mass, USA, September 2011.

[14] Y. Yin, M. Adel, and S. Bourennane, "Automatic segmentation and measurement of vasculature in retinal fundus images using probabilistic formulation," *Computational and Mathematical Methods in Medicine*, vol. 2013, Article ID 260410, 6 pages, 2013.

[15] A. K.-G. Schuster, J. E. Fischer, and U. Vossmerbaeumer, "Semiautomated retinal vessel analysis in nonmydriatic fundus photography," *Acta Ophthalmologica*, vol. 92, no. 1, pp. e42–e49, 2014.

[16] N. M. Keith, H. P. Wagener, and N. W. Barker, "Some different types of essential hypertension: their course and prognosis," *The American Journal of the Medical Sciences*, vol. 268, no. 6, pp. 336–345, 1974.

[17] A. A. Kalitzeos, G. Y. H. Lip, and R. Heitmar, "Retinal vessel tortuosity measures and their applications," *Experimental Eye Research*, vol. 106, pp. 40–46, 2013.

[18] C. Y.-L. Cheung, Y. Zheng, W. Hsu et al., "Retinal vascular tortuosity, blood pressure, and cardiovascular risk factors," *Ophthalmology*, vol. 118, no. 5, pp. 812–818, 2011.

[19] A. Mohsenin, V. Mohsenin, and R. A. Adelman, "Retinal vascular tortuosity in obstructive sleep apnea," *Clinical Ophthalmology*, vol. 7, pp. 787–792, 2013.

[20] B. R. Masters, "Fractal analysis of the vascular tree in the human retina," *Annual Review of Biomedical Engineering*, vol. 6, pp. 427–452, 2004.

[21] G. Liew, J. J. Wang, N. Cheung et al., "The retinal vasculature as a fractal: methodology, reliability, and relationship to blood pressure," *Ophthalmology*, vol. 115, no. 11, pp. 1951.e1–1956.e1, 2008.

[22] N. Cheung, K. C. Donaghue, G. Liew et al., "Quantitative assessment of early diabetic retinopathy using fractal analysis," *Diabetes Care*, vol. 32, no. 1, pp. 106–110, 2009.

[23] N. Cheung, G. Liew, R. I. Lindley et al., "Retinal fractals and acute lacunar stroke," *Annals of Neurology*, vol. 68, no. 1, pp. 107–111, 2010.

[24] M. Cavallari, T. Falco, M. Frontali, S. Romano, F. Bagnato, and F. Orzi, "Fractal analysis reveals reduced complexity of retinal vessels in CADASIL," *PLoS ONE*, vol. 6, no. 4, Article ID e19150, 2011.

[25] H. Leung, J. J. Wang, E. Rochtchina et al., "Relationships between age, blood pressure, and retinal vessel diameters in an older population," *Investigative Ophthalmology & Visual Science*, vol. 44, no. 7, pp. 2900–2904, 2003.

[26] S. Roine, M. Harju, T. T. Kivelä et al., "Ophthalmologic findings in cerebral autosomal dominant arteriopathy with subcortical infarcts and leukoencephalopathy: a cross-sectional study," *Ophthalmology*, vol. 113, no. 8, pp. 1411–1417, 2006.

[27] T. Y. Wong and P. Mitchell, "Hypertensive retinopathy," *The New England Journal of Medicine*, vol. 351, no. 22, pp. 2310–2317, 2004.

[28] M. K. Ikram, J. C. M. Witteman, J. R. Vingerling, M. M. B. Breteler, A. Hofman, and P. T. V. M. de Jong, "Retinal vessel diameters and risk of hypertension: the Rotterdam Study," *Hypertension*, vol. 47, no. 2, pp. 189–194, 2006.

[29] S. R. Daniels, M. J. Lipman, M. J. Burke, and J. M. H. Loggie, "Determinants of retinal vascular abnormalities in children and adolescents with essential hypertension," *Journal of Human Hypertension*, vol. 7, no. 3, pp. 223–228, 1993.

[30] J. S. Wolffsohn, G. A. Napper, S.-M. Ho, A. Jaworski, and T. L. Pollard, "Improving the description of the retinal vasculature and patient history taking for monitoring systemic hypertension," *Ophthalmic and Physiological Optics*, vol. 21, no. 6, pp. 441–449, 2001.

[31] E. D. Kurniawan, N. Cheung, C. Y. Cheung, W. T. Tay, S. M. Saw, and T. Y. Wong, "Elevated blood pressure is associated with rarefaction of the retinal vasculature in children," *Investigative Ophthalmology & Visual Science*, vol. 53, no. 1, pp. 470–474, 2012.

[32] R. Cumurciuc, P. Massin, M. Pâques et al., "Retinal abnormalities in CADASIL: a retrospective study of 18 patients," *Journal of Neurology, Neurosurgery and Psychiatry*, vol. 75, no. 7, pp. 1058–1060, 2004.

[33] C. Haritoglou, G. Rudolph, J. P. Hoops, C. Opherk, A. Kampik, and M. Dichgans, "Retinal vascular abnormalities in CADASIL," *Neurology*, vol. 62, no. 7, pp. 1202–1205, 2004.

[34] F. M. A. Islam, T. T. Nguyen, J. J. Wang et al., "Quantitative retinal vascular calibre changes in diabetes and retinopathy: the Singapore Malay eye study," *Eye*, vol. 23, no. 8, pp. 1719–1724, 2009.

[35] S. R. Sternberg, "Biomedical image processing," *Computer*, vol. 16, no. 1, pp. 22–34, 1983.

[36] P. Hart, N. Nilsson, and B. Raphael, "A formal basis for the heuristic determination of minimum cost paths," *IEEE Transactions on Systems Science and Cybernetics*, vol. 4, no. 2, pp. 100–107, 1968.

[37] P. de Casteljau, *Courbes et Surfaces à Pôles*, Enveloppe, Institut National de la Propriété Industrielle, Paris, France, 1959.

[38] I. J. Schoenberg, "Contributions to the problem of approximation of equidistant data by analytic functions. Part A. On the problem of smoothing or graduation. A First class of analytic approximation formulae," *Quarterly of Applied Mathematics*, vol. 4, pp. 45–99, 1946.

[39] N. Otsu, "A threshold selection method from gray-level histograms," *IEEE Transactions on Systems, Man and Cybernetics*, vol. 9, no. 1, pp. 62–66, 1979.

Hindawi Publishing Corporation
BioMed Research International
Volume 2015, Article ID 571314, 11 pages
http://dx.doi.org/10.1155/2015/571314

Clinical Study

Can Variability of Pattern ERG Signal Help to Detect Retinal Ganglion Cells Dysfunction in Glaucomatous Eyes?

Alberto Mavilio,[1] Francesca Scrimieri,[2] and Donato Errico[2]

[1]*Social Health District, Glaucoma Center, Azienda Sanitaria Locale, Via Fermi, 72015 Fasano, Brindisi, Italy*
[2]*Ophthalmology Unit, Glaucoma Service, Azienda Ospedaliera "Cardinale G. Panico", 73039 Tricase, Lecce, Italy*

Correspondence should be addressed to Alberto Mavilio; a.mavilio@gmail.com

Received 29 August 2014; Revised 30 December 2014; Accepted 1 January 2015

Academic Editor: Antonio Ferreras

Objective. To evaluate variability of steady-state pattern electroretinogram (SS-PERG) signal in normal, suspected, and glaucomatous eyes. *Methods*. Twenty-one subjects with suspected glaucoma due to disc abnormalities (GS), 37 patients with early glaucoma (EG), and 24 normal control (NC) were tested with spectral-domain optical coherence tomography (SD-OCT), standard automated perimetry (SAP), and SS-PERG. Mean deviation (MD), pattern standard deviation (PSD), retinal nerve fiber layer (RNFL), and ganglionar complex cells (GCC) were evaluated. The SS-PERG was recorded five consecutive times and the amplitude and phase of second harmonic were measured. PERG amplitude and coefficient of variation of phase (CVphase) were recorded, and correlation with structural and functional parameters of disease, by means of one-way ANOVA and Pearson's correlation, was analysed. *Results*. PERG amplitude was reduced, as expression of retinal ganglion cells (RGCs) dysfunction, in EG patients and GS subjects compared to NC patients ($P < 0.0001$). CVphase was significantly increased in EG patients and GS subjects, compared to healthy ($P < 0.0001$), and it was also correlated with PSD ($P = 0.0009$), GCC ($P = 0.028$), and RNFL ($P = 0.0078$) only in EG patients. *Conclusions*. Increased intrasession variability of phase in suspected glaucomatous eyes may be a sign of RGCs dysfunction.

1. Introduction

Glaucoma is a progressive optic neuropathy characterized by death of retinal ganglion cells (RGCs), clinically manifested as typical alterations of the optic nerve head (ONH) and retinal nerve fiber layer (RNFL) correlated with visual field defects.

The standard automated perimetry (SAP) is the main tool for the detection of visual field loss. However, the subjective nature of the test and the fact that the examination reveals glaucomatous defects only when 30 to 40% of the fibers have already been lost [1, 2] have increased the interest of research towards alternative diagnostic tools.

The spectral-domain optical coherence tomography (SD-OCT), a good surrogate accepted for the diagnosis of glaucoma, has been shown to objectively measure ONH and RNFL [3–5].

Because most of the retinal ganglion cells are located in the macula, the study of this area, in particular the ganglion cells complex (GCC), has been proposed in the early evaluation of glaucoma variations, in addition to the changes that occur in ONH and RNFL [6–10].

Pattern electroretinogram (PERG) alterations reflect the electrical activity of RGCs [11, 12] and has been widely used to detect the loss of function of RGCs in glaucoma [13, 14]. Cross-sectional studies have shown that PERG is frequently altered in glaucoma suspects (GS) and patients with early glaucoma with respect to normal controls [13–19].

PERG has been shown to be abnormal before both the occurrence of visual field defects, as measured by SAP, and RNFL loss, as assessed by OCT [13].

An optimized model of PERG for glaucoma screening (PERGLA) is a relatively new diagnostic tool and fast and user-friendly for the evaluation RGCs dysfunction [20, 21].

The steady-state PERG is recorded in response to stimulus of high temporal frequency [22]. Better than a transient stimulus (slow), a steady-state stimulus (fast) is able to show a glaucomatous dysfunction since it submits the RGCs to a greater metabolic stress [20]. The steady-state stimulus

determines a sinusoidal response that is analysed by the Fourier transform [23–25]. In this way, the second harmonic, that is, the harmonic that has a frequency twice that of the stimulus, is isolated. Two components of this harmonic, that is, amplitude and phase, show typical alterations in glaucoma. In particular, the amplitude is reduced in patients with glaucoma and ocular high pressure (OHT) compared to healthy subjects [14, 21], while the phase remains constant or at most tends to delay with age [20]. Steady-state PERG has been reported to have high test-retest repeatability [26]. However it is very important to work with a good signal-to-noise ratio (SNR) [27]. In particular the phase variability has been showed to be very limited in the retest within and between trials [16, 26].

The biological variability of a measurement is a physiological characteristic that can bias not only diagnostic imaging [28] but also the different adaptation of the bioelectrical response to an external visual stimulus [29, 30].

Variations of the phase are little affected by opacity of the media and deterioration of optics that may cause a nonspecific reduction of PERG amplitude [31].

If the variability of the phase is the expression of a dysfunction of RGCs that precedes cell death, we hypothesized that the within-trial variability of the PERG signal, individual test-retest of the same eye of early glaucoma patients, is greater than the one physiologically present in healthy individuals. Therefore, we checked if such variability correlates with markers of disease severity such as retinal thickness and visual field indices.

2. Materials and Methods

Participants were recruited from the Glaucoma Center of the Brindisi Social Health District, Mesagne, Italy. The participants were divided into 3 groups: early glaucoma (EG), glaucoma suspects (SG), and normal control (NC).

A total of eighty-two eyes were included. The criteria for classification in the EG group, in accordance with the EGS guidelines (http://www.eugs.org/eng/EGS_guidelines.asp), were as follows: appearance of the optic disc and peripapillary nerve fiber layer suspected for glaucoma damage (increased ratio cup/disc, asymmetry ratio of cup/disc, notch or narrowing of the neuroretinal rim, disc haemorrhage, and thinning of the peripapillary nerve fiber layer) or visual field suspicious for glaucomatous damage in the absence of clinical signs of other optic neuropathies (nasal step, paracentral scotoma, and altitudinal defect) or a constant elevated intraocular pressure.

The severity of glaucoma was evaluated functionally by means of SAP and anatomically by means of RNFL and GCC thickness measurement by SD-OCT.

Thirty-seven patients had early glaucoma (EG), defined as consecutive repeatable abnormal SAP results according to the normative database of the instrument; 21 had suspected glaucoma, defined as optical discs apparently abnormal (presence of thinning of the neuroretinal rim or localized or diffuse RNFL defects indicative of glaucoma as evaluated by Stereo photography of the fundus) without repeatable abnormal SAP results. 24 age-matched healthy subjects, defined as those with IOP <22 mmHg with no history of elevated IOP, optic disc apparently healthy, and normal SAP repeatable results, were included in the control group. The EG patients were under medical topical treatment with beta-blockers, prostaglandin analogues, and alpha adrenergic receptors eye drops. Each participant of the trial underwent a comprehensive ophthalmic evaluation, including review of medical history, best-corrected visual acuity testing, IOP measuring by means of Goldmann applanation tonometry, ultrasound pachymetry (Pachmate GH55), slit lamp biomicroscopy, gonioscopy, and dilated fundus examination with a 78 D lens. All participants had best-corrected visual acuity ≥20/30 (Snellen), spherical refraction within ±5.0 D and cylinder correction within ±2.0 D, transparent ocular media (nuclear color/opalescence, cortical or posterior subcapsular lens opacity <1) according to the Lens Opacity Classification System III, and open angle on gonioscopy. Coexisting retinal disease, diabetes, Parkinson's disease, or nonglaucomatous optic neuropathy, potentially able to determine nonspecific PERG abnormality, were excluded [32–34].

One eye per patient who met the criteria mentioned above was included in the study. When both eyes of the patient were eligible, the one with best-corrected visual acuity was selected. In case of equal visual acuity, right eye, by convention, was selected for evaluation.

This trial followed the tenets of the Declaration of Helsinki for human studies. The study was approved by Ethical Committee of the Brindisi Social Health District. Informed written consent was obtained by all subjects after the nature of the test and possible risks were explained in detail.

2.1. Spectral-Domain Optical Coherence Tomography. Peripapillary RNFL thickness was assessed by Zeiss Cirrus HD-OCT 500 (software version 7.0.1.290, Carl Zeiss Meditec, Dublin, CA). The protocol Optic Disc Cube 200 × 200 was used to perform a circular scan 3.46 mm in diameter, which was automatically targeted around the optic disc to provide the RNFL thickness of the four quadrants and each of the 12 clock-hour positions. The protocol Macular Cube 512 × 128 was used to obtain measurements of retinal ganglion cell macular thickness.

All images were obtained by the same experienced technician with a quality score of at least 7/10. Three consecutive scans of the optic disc and macular region were acquired and analysed for each eye. Measurements of RNFL and GCC were averaged using the data of each of the three scans.

2.2. Standard Automated Perimetry. The visual field was assessed by means of a Humphrey Field Analyzer, model 745i II (Carl Zeiss Meditec, Germany), using the 24-2 test program, SITA standard strategy. Near addition was added to the refractive correction, where needed. If fixation losses were greater than 20% and false-positive or false-negative results were higher than 15%, the test was repeated. At least 2 reliable SAPs were performed to minimize the learning effect [35]. Visual field defects were defined as being typically glaucomatous when a standard deviation of the model (PSD) significantly higher than the 5% level and/or a glaucoma hemifield test outside normal limits was recorded.

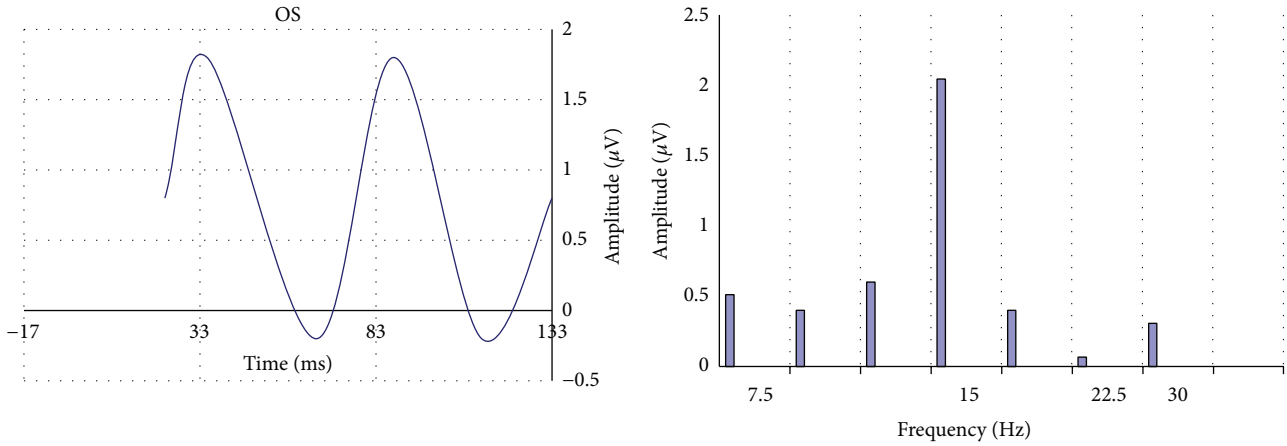

Figure 1: Example of steady-state PERGs of left eyes, presented in time domain (line chart) and frequency domain (bar chart). At a frequency of the stimulus of 7.5 Hz the second harmonic is observed at 15 Hz.

2.3. Pattern Electroretinogram. PERG was recorded by means of an instrument supplied by our laboratory (RETIMAX Advanced version 4.3 CSO, Pisa, Italy), using a method similar to the paradigm PERGLA [20], with some minor changes made by our laboratory.

We used as a stimulus horizontal bars with a spatial frequency of 1.7 cycles/degree, which resulted from previous studies as the most sensitive in detecting RGCs dysfunction in early glaucoma [36, 37], modulated in counterphase at 15 reversals/second and electronically generated on a high-resolution LCD monitor (contrast: 90%; luminance: 80 cd/m^2; field size: 24° [width] × 24° [height]). The subjects had undilated pupils, of size between 3 and 4 mm, with an appropriate correction for the working distance (57 cm). The signals were recorded from a skin electrode 9 mm Ag/AgCl placed on the lower eyelid. A similar electrode, placed on the lid of the not stimulated eye, was used as a reference, as described in other studies [38].

In all cases the impedance was below 5 k. The responses were amplified (gain of 100.000), filtered (bandwidth: 130 Hz), and sampled with a resolution of 12 bits. The analysis time was 133 ms, equal to the time of presentation of the stimulus (Figure 1). An average (100 events), with automatic rejection of artefacts, was obtained. Five consecutive tests were recorded with a short break, so the duration of the examination was no more than 5 minutes per eye (the total duration being no longer than a visual field examination). The data were then exported to a text file. The amplitude (μV) and phase (π rad) of the second harmonic were then analysed with the Fourier transform (Figures 2 and 3) using a special software programmed by one of the authors (Alberto Mavilio).

The repeatability of the amplitude and phase of the second harmonic was calculated as coefficients of variation (CV, the ratio of the measurement standard deviation to the mean), CVamp (coefficient of variation of amplitude), and CVphase (coefficient of variation of phase), respectively, and as the intraclass correlation coefficients (ICC, describing proportion of total variance accounted for by within-subject variation).

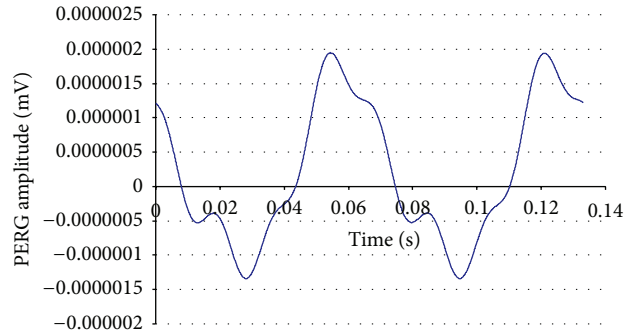

Figure 2: Example of steady-state PERGs recorded in response to a pattern of horizontal gratings (1.7 cy/deg. 90% contrast; 80 cd/m^2 mean luminance; field size: 24° [width] × 24° [height]) alternating at 15 times/s or every 66.6 ms.

The noise level obtained by recording a response to an occluded stimulus was ≤0.097 ± 0 : 04 μV in both normal subjects and patients.

In our laboratory the phase decreases with increasing peak time; that is, a delayed response corresponds to lower phase values.

At a reversal rate of 15 Hz the modulo value of 2 π rad corresponds to 66.6 ms (1/15 ∗ 1000 = 66.6 ms). As described previously [31], to avoid the inherent discontinuity of phase, the recorded value was subtracted from the value of the modulo (2 less than the recorded value). This is needed to prevent negative values of the phase that may affect the calculation of the coefficient of variation.

Statistical analyses were performed using a commercially available software (MedCalc 13.3.1.0). A P value of ≤ 0.05 was considered statistically significant.

3. Results

Demographic, structural, and functional data are shown in Tables 1, 2, and 3.

The differences of the variables between groups were analysed using one-way ANOVA analysis of variance, with

Table 1: Demographic data.

	Patients						
	EG (37)		GS (21)		NC (24)		P value*
	Mean	SD ±	Mean	SD ±	Mean	SD ±	
Age	57.1	11.6	56.1	10.5	53	6.3	$P = 0.46$
Male (%)	40.5		42.4		41.5		$P = 0.078$**
IOP (mmHg)	15.6	1.1	17.9[ac]	1.6	15.1	1.7	$P < 0.001$
CCT (μm)	546.6	26.6	553.1	32.1	558.7	19.1	$P = 0.337$
MD (dB)	−3.010[ab]	1.95	0.004	1.04	−0.02	1.5	$P < 0.001$
PSD (dB)	3.45[ab]	2.04	1.59	0.49	1.47	0.23	$P < 0.001$
RNFL (μm)	81.56[ab]	9.26	90.8	7.5	94.9	10.1	$P < 0.001$
GCC (μm)	76.13[ab]	6.88	82.09	6.53	84.7	4.9	$P < 0.001$
Amplitude (μV)	0.96[ab]	0.33	0.96[a]	0.27	1.2	0.26	$P = 0.028$
Phase (π rad)	−0.06	0.36	−0.01	0.26	0.19	0.38	$P = 0.069$
CV_amp (%)	20.25[ab]	13.52	14.27[a]	7.05	9.42	3.99	$P = 0.004$
CV_phase (%)	8.97[b]	2.52	7.30[a]	2.51	3.4	1.13	$P < 0.001$

*One-way analysis of variance (Bonferroni corrected).
**Chi-square.
[a]Statistically significant difference from normal control (NC).
[b]Statistically significant difference from glaucoma suspects (GS).
[c]Statistically significant difference from early manifest glaucoma patients (EG).

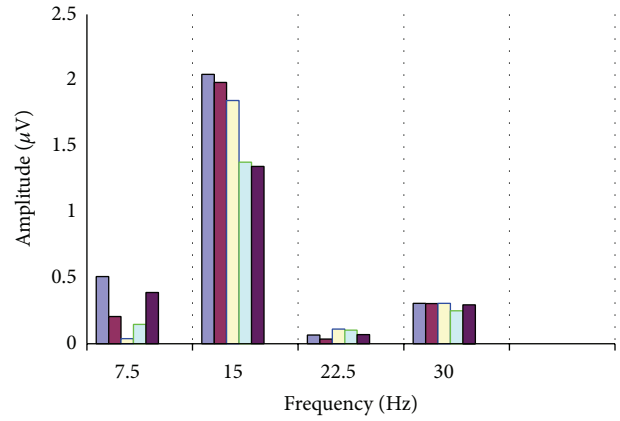

Figure 3: Fourier spectrum of 5 consecutive tests of steady-state PERG in the same subject. The bar chart shows the amplitude expressed in μV of second harmonic of the signal in response to stimulus of 7.5 Hz.

Bonferroni adjustment. Both linear and logarithmic regressions were used for structural measurements; RNFL and GCC were expressed in linear units (micrometers); functional measurements, PSD, and MD were expressed in logarithmic units (decibels). Pearson correlation in PERG amplitude, phase, coefficients of variation, thickness measurements SD-OCT, and visual field indices are shown in Table 4.

Age, which can affect the amplitude of the PERG and retinal thickness, was not a confounding factor; in fact there was no statistically significant difference of age between all groups (see Table 1).

Because the RNFL thickness shows a slight decrease with age, as suggested by previous studies [39, 40], the data were adjusted for age by a factor of 0.2 μm/year (0.18%/year).

The IOP values were significantly higher in the GS group (17.95 ± 1.65 mmHg) than in the EG group (15.67 ± 1.13 mmHg), because the EG patients were in drug treatment.

PERG amplitude was reduced in EG (0.96 ± 0.33 μV) and GS (0.96±0.27 μV) subjects with respect to NC (1.20±0.26 μV, $P < 0.0001$) and was weakly associated with RNFL thickness ($r = 0.444$, $P = 0.0059$).

CVamp correlates negatively with GCC ($r = -0.379$, $P = 0.0206$), while CVphase correlates better with RNFL ($r = 0.427$, $P = 0.0083$) than with CGG ($r = 0.361$, $P = 0.0283$).

Finally, CVphase correlates fairly strongly with PSD ($r = -0.524$, $P < 0.0009$) and weakly with IOP ($r = 0.362$, $P = 0.0277$).

When the data from normal eyes were entered into a multiple linear regression analysis, with CVphase and CVamp as independent variables and PSD as dependent variable, the significance of the coefficient of variation for CVphase term and for CVamp term was not significant.

In a similar analysis of the EG group, the significance of the coefficient for the CVphase term was $P = 0.0010$ and for the CVamp term was $P = 0.9767$. Table 5 shows the intraclass correlation coefficients (ICC).

4. Discussion

Our results are similar to previous studies. Many authors evaluated the PERG procedure which inspired us in this trial, the PERGLA paradigm, with regard to its reliability in the early diagnosis of glaucoma [16, 18, 19, 26, 27, 41–43].

Several studies also verified structure-function relationship using PERGLA paradigm and methods of analysis of the structure as retinal OCT [13, 28, 41, 44, 45].

Other studies reported that the total thickness of the retina is a good surrogate for glaucomatous damage ganglion

Table 2: Clinical characteristics of 37 early glaucoma patients.

EGp	Age	Eye	ph1 (π rad)	ph2 (π rad)	ph3 (π rad)	ph4 (π rad)	ph5 (π rad)	amp1 (μV)	amp2 (μV)	amp3 (μV)	amp4 (μV)	amp5 (μV)	MD (db)	PSD (db)	RNFL (μm)	GCC (μm)	CV_p (%)	CV_a (%)	Phase (π rad)	Ampl (μV)	SD_p	SD_a	CCT (μm)	IOP (mmHg)
#1	49	R	0.09	0.40	0.16	0.33	−0.11	1.57	1.47	1.44	1.43	1.38	−3	2.84	89	83	8.32	4.18	0.17	1.46	0.18	0.06	560	16
#2	49	L	0.27	0.44	0.72	0.60	0.33	1.52	1.24	0.81	0.32	1.37	−2	7	75	70	6.67	41.5	0.47	1.05	0.17	0.44	543	15
#3	69	R	0.24	0.35	0.18	0.19	−0.01	0.73	0.60	0.63	0.75	0.57	−1.02	1.89	82	80	5.42	10.8	0.19	0.66	0.12	0.07	515	14
#4	62	R	0.12	0.42	0.52	0.63	0.63	1.61	1.87	1.70	1.86	1.80	−4	4.29	92	83	7.76	5.52	0.46	1.77	0.19	0.1	537	15
#5	46	L	−0.61	−0.43	−0.80	−0.50	−0.30	1.11	0.81	0.84	0.95	0.79	−0.74	1.25	82	78	11.3	13.5	−0.53	0.9	0.17	0.12	595	17
#6	65	R	−0.44	−0.30	−0.58	−0.42	−0.29	1.34	0.72	1.11	1.06	0.74	−5.9	7.85	74	71	6.53	23.6	−0.41	0.99	0.1	0.23	518	14
#7	60	L	−0.16	0.34	−0.03	0.09	−0.04	1.20	1.04	1.12	0.96	1.01	−2.14	4.36	63	77	8.39	7.93	0.04	1.07	0.17	0.08	540	14
#8	45	R	−0.49	−0.80	−0.55	−0.45	−0.77	0.70	0.60	0.18	0.40	0.91	−6.25	1.76	95	82	10.5	44.9	−0.61	0.56	0.15	0.25	612	17
#9	63	L	0.01	−0.44	0.20	0.32	−0.29	1.03	0.70	0.94	0.88	0.71	−3.54	2.65	100	94	14.6	15.1	−0.04	0.85	0.29	0.13	560	15
#10	35	R	0.22	−0.18	0.12	0.27	0.41	1.85	1.45	1.29	1.46	1.30	−6.11	2.18	71	77	9.06	13.7	0.17	1.47	0.2	0.2	550	16
#11	59	L	−0.26	0.32	0.47	0.06	0.35	1.11	0.67	0.78	0.76	0.79	−2.01	1.22	73	70	11.9	18.4	0.19	0.82	0.26	0.15	530	15
#12	39	L	−0.37	−0.10	−0.19	0.27	0.10	1.21	0.77	1.04	0.79	0.82	−1.5	1.87	83	77	11.5	18.3	−0.06	0.93	0.22	0.17	525	15
#13	57	R	0.13	−0.08	0.14	−0.01	0.20	1.42	1.48	0.94	1.11	1.00	−5.11	7.75	77	67	5.07	18.5	0.08	1.19	0.11	0.22	570	16
#14	54	L	−0.51	−0.31	−0.22	0.01	0.07	1.37	1.17	1.16	1.35	0.97	−3.21	2.79	97	85	11.7	12.4	−0.19	1.2	0.21	0.15	595	17
#15	59	L	0.36	0.76	0.10	0.27	0.36	1.05	0.79	1.10	1.03	1.11	−1.11	2.94	95	84	9.1	11.6	0.37	1.02	0.22	0.12	560	16
#16	75	R	−0.72	−0.08	−0.20	−0.06	−0.10	0.76	0.92	0.75	0.82	0.83	−2.13	3.55	87	88	14.1	7.46	−0.23	0.82	0.25	0.06	525	17
#17	65	R	−0.31	−0.59	−0.29	−0.31	−0.46	0.77	1.03	1.05	0.60	0.87	−3.57	2.61	92	86	7.09	19.4	−0.39	0.87	0.11	0.17	505	16
#18	60	R	0.19	0.32	−0.08	0.19	−0.19	0.56	0.52	0.87	0.56	0.62	−5.65	3.96	85	69	9.07	20	0.09	0.63	0.19	0.12	543	15
#19	81	R	−0.97	−0.63	−0.86	−0.71	−0.92	1.13	0.40	0.79	0.39	1.01	0.35	1.38	83	68	10.8	40.9	−0.82	0.75	0.13	0.3	575	16
#20	45	R	0.22	0.58	0.51	0.66	0.33	1.41	1.52	1.49	0.92	1.07	−1.2	6.3	73	69	6.58	18.9	0.46	1.28	0.16	0.24	555	15
#21	40	L	−0.11	0.11	0.32	0.18	0.55	1.82	1.58	1.06	1.85	1.46	−2.06	2.38	77	74	10	18.6	0.21	1.55	0.22	0.29	523	14
#22	72	L	0.48	0.12	0.50	0.37	0.48	1.18	0.93	1.19	0.98	0.83	−2.89	3.03	78	72	5.88	13.8	0.39	1.02	0.14	0.14	545	14
#23	52	R	−0.57	−0.38	−0.04	−0.21	−0.31	1.45	1.54	1.39	1.13	1.55	−4.5	1.62	90	82	10.3	10.8	−0.3	1.41	0.17	0.15	569	15
#24	76	L	0.12	−0.28	0.03	−0.07	−0.44	0.35	1.59	0.66	0.35	0.35	−6.49	3.76	78	66	10.9	72.7	−0.13	0.66	0.2	0.48	555	15
#25	40	R	−0.20	0.08	−0.06	0.03	0.09	1.02	0.64	0.75	0.71	0.79	−3.22	5.72	69	77	5.55	16.8	−0.01	0.78	0.11	0.13	525	16
#26	49	R	0.04	−0.04	0.07	0.27	−0.41	1.16	1.03	0.99	1.00	1.18	−2.15	1.08	77	67	11.3	7.81	−0.02	1.07	0.22	0.08	495	17
#27	43	L	−0.37	−0.19	0.05	−0.14	−0.21	0.88	1.67	1.28	1.21	0.71	−1.52	2.33	88	74	7.5	29.1	−0.17	1.15	0.14	0.33	536	15
#28	68	L	−0.09	−0.41	−0.04	−0.49	−0.07	1.18	1.38	0.88	1.22	1.04	−0.06	1.48	96	84	10.7	15	−0.22	1.14	0.19	0.17	520	16
#29	49	R	0.75	0.14	0.57	0.58	0.54	0.88	0.85	0.64	1.04	0.57	−4.55	2.24	71	74	7.99	21.2	0.52	0.8	0.2	0.17	578	17
#30	70	R	0.45	0.68	0.22	0.74	0.26	0.61	0.61	0.52	0.51	0.38	−0.45	1.59	78	76	8.64	15.5	0.47	0.53	0.21	0.08	542	17
#31	67	R	−0.43	−0.82	−0.45	−0.45	−0.29	0.40	0.34	0.29	0.40	0.77	−5.94	7.15	80	78	11.6	38.5	−0.49	0.44	0.18	0.17	523	17
#32	42	R	−0.71	−0.91	−0.86	−0.62	−0.72	0.24	0.26	0.54	0.44	0.63	−2.26	3.45	86	69	8.52	36	−0.76	0.42	0.11	0.15	555	18
#33	65	R	−0.41	−0.17	0.04	0.15	−0.05	1.64	1.17	1.02	1.31	1.02	−2.25	3.32	88	73	10.1	18.7	−0.09	1.23	0.19	0.23	567	17
#34	62	L	−0.85	−0.77	−0.82	−0.71	−0.49	0.43	0.29	0.48	0.42	0.24	−1.16	1.69	76	79	10.1	24.7	−0.73	0.37	0.13	0.09	545	17
#35	63	L	−0.26	−0.10	−0.22	0.02	−0.24	1.38	1.32	1.11	1.43	1.24	−2.06	3.92	81	72	5.7	8.65	−0.16	1.3	0.11	0.11	515	15
#36	58	R	−0.04	−0.01	0.16	0.06	−0.03	1.12	1.18	0.81	1.05	0.67	−6.71	7.78	60	76	3.74	19.9	0.03	0.97	0.08	0.19	535	15
#37	61	L	−0.33	−0.29	0.07	−0.20	−0.26	0.67	0.75	0.56	0.48	0.65	−3.25	5.02	70	76	8.09	15.3	−0.2	0.62	0.15	0.1	585	14

PERG phase and amplitude (values of 5 consecutive tests), mean deviation (MD), pattern standard deviation (PSD), retinal nerve fiber layer thickness (RNFL), ganglion cell complex (GCC), coefficient of variation of amplitude (CV_a), coefficient of variation of phase (CV_p), mean phase (phase), mean amplitude (Ampl), standard deviation of amplitude (SD_a), standard deviation of phase (CV_p), central corneal thickness (CCTi), and intraocular pressure (IOP) in 37 early glaucoma patients (EGp).

Table 3: Clinical characteristics of 21 glaucoma suspect patients.

SGp	Age	Eye	ph1 (π rad)	ph2 (π rad)	ph3 (π rad)	ph4 (π rad)	ph5 (π rad)	amp1 (μV)	amp2 (μV)	amp3 (μV)	amp4 (μV)	amp5 (μV)	MD (db)	PSD (db)	RNFL (μm)	GCC (μm)	CV_p (%)	CV_a (%)	Phase (π rad)	Ampl (μV)	SD_p	SD_a	CCT (μm)	IOP (mmHg)
#1	47	R	0.60	0.20	0.25	0.33	0.16	1.35	1.30	1.32	1.49	1.13	1.51	1.36	86	83	6.79	8.75	0.31	1.32	0.16	0.12	535	16
#2	54	R	0.04	−0.30	−0.37	−0.20	−0.08	1.00	1.01	0.88	0.83	0.76	−0.23	1.24	92	90	8.09	10.67	−0.18	0.9	0.15	0.1	570	16
#3	49	L	0.12	−0.24	−0.01	0.17	0.10	1.10	1.08	0.95	0.95	0.92	−0.59	1.78	90	78	7.23	7.69	0.03	1	0.15	0.08	597	18
#4	53	R	−0.20	0.12	0.04	−0.04	−0.08	0.95	0.73	0.87	0.89	0.70	−0.21	1.88	91	86	5.52	11.72	−0.03	1	0.11	0.1	515	18
#5	58	L	0.33	0.24	0.01	0.32	0.21	1.47	1.35	1.09	1.51	1.19	−0.78	1.88	84	79	5.11	12.02	0.22	1.32	0.11	0.16	565	20
#6	57	R	−0.16	0.17	0.27	−0.30	0.10	0.59	0.43	0.48	0.66	0.49	0.62	1.16	84	98	10.5	15.79	0.02	0.53	0.21	0.08	525	18
#7	73	L	−0.06	−0.03	−0.04	−0.08	0.17	1.43	1.05	0.87	1.08	1.23	−0.33	1.63	93	74	4.61	16.73	−0.01	1.13	0.09	0.19	549	16
#8	35	R	0.25	0.71	0.66	0.79	0.74	1.58	1.16	1.29	1.62	1.31	−0.25	1.23	96	78	7.3	12.76	0.63	1.39	0.19	0.18	508	16
#9	63	R	0.04	0.42	0.14	0.07	0.14	0.89	0.82	0.98	0.64	0.89	−0.74	1.87	108	91	6.24	13.44	0.16	1.01	0.13	0.11	578	16
#10	77	R	0.14	0.00	0.15	0.01	0.24	0.97	0.56	0.98	0.67	0.64	0.65	1.24	93	72	4.31	23.01	0.11	0.92	0.09	0.18	562	17
#11	53	L	0.42	0.33	0.11	0.37	0.38	0.94	0.65	0.69	0.54	0.66	0.02	1.33	80	80	4.72	19.1	0.32	0.7	0.11	0.13	601	18
#12	64	L	−0.04	0.00	−0.39	−0.16	−0.11	0.70	0.89	0.34	0.37	0.40	−0.01	1.23	96	88	7.25	40.32	−0.14	0.65	0.13	0.22	555	17
#13	50	L	−0.52	−0.64	−0.13	−0.34	−0.33	1.00	0.58	0.65	0.78	0.89	−0.66	1.33	87	82	10.78	19.59	−0.39	0.94	0.17	0.15	495	22
#14	62	L	−0.02	0.20	−0.03	0.23	0.14	0.53	0.40	0.51	0.59	0.48	0.68	1.1	75	74	5.25	12.25	0.1	0.5	0.11	0.06	575	18
#15	57	R	−0.51	−0.68	−0.66	−0.33	−0.62	1.34	1.54	0.86	1.03	0.65	0.84	1.24	93	86	8.93	29.8	−0.56	1.08	0.13	0.32	535	18
#16	64	L	−0.31	−0.15	−0.05	−0.07	0.20	0.66	0.67	0.73	0.55	0.72	1.43	1.4	87	73	8.52	9.33	−0.07	0.8	0.16	0.06	560	21
#17	59	L	−0.12	−0.02	0.05	−0.16	0.01	1.29	1.56	1.45	1.16	1.60	0.27	1.53	94	83	4.04	11.75	−0.05	1.41	0.08	0.17	525	18
#18	51	L	−0.41	0.00	−0.33	−0.12	−0.40	0.65	0.64	0.66	0.66	0.58	0.88	1.43	93	84	9.36	5.09	−0.25	0.77	0.16	0.03	565	18
#19	32	L	−0.09	0.18	0.12	0.03	0.21	1.40	1.42	1.12	1.17	1.24	−0.37	1.34	89	82	5.29	9.76	0.09	1.27	0.11	0.12	608	18
#20	60	L	−0.30	−0.46	−0.22	−0.52	0.13	0.78	0.70	0.66	0.47	0.85	0.25	2.08	106	85	13.18	18.58	−0.27	0.69	0.23	0.13	512	18
#21	61	R	−0.22	−0.17	0.00	−0.35	−0.54	0.82	0.64	0.63	0.88	0.88	0.99	1.45	90	78	10.38	14.46	−0.26	0.93	0.18	0.11	582	20

PERG phase and amplitude (values of 5 consecutive tests), mean deviation (MD), pattern standard deviation (PSD), retinal nerve fiber layer thickness (RNFL), ganglion cell complex (GCC), coefficient of variation of amplitude (CV_a), coefficient of variation of phase (CV_p), mean phase (phase), mean amplitude (Ampl), standard deviation of amplitude (SD_a), standard deviation of phase (CV_p), central corneal thickness (CCTi), and intraocular pressure (IOP) in 21 glaucoma suspect patients (SGp).

Table 4: Pearson correlation coefficient (CC) and significance level P (SL-P) in 37 early manifest glaucoma patients.

		Age	IOP (mmHg)	CCT (μm)	MD (dB)	PSD (dB)	RNFL (μm)	GCC (μm)	Amplitude (μV)	Phase (π rad)	CV_amp (%)	CV_phase (%)
Age	CC		−0.108	−0.133	0.082	0.038	0.133	0.051	−0.181	−0.128	0.126	0.105
	SL-P		0.523	0.433	0.629	0.823	0.432	0.762	0.284	0.449	0.457	0.536
IOP (mmHg)	CC	−0.108		0.269	0.078	−0.252	0.296	0.177	−0.251	−0.364	0.11	0.362
	SL-P	0.523		0.108	0.646	0.133	0.075	0.294	0.134	0.026	0.516	0.0277
CCT (μm)	CC	−0.133	0.269		−0.131	−0.108	0.181	0.019	0.043	−0.157	0.207	0.178
	SL-P	0.433	0.108		0.441	0.526	0.282	0.908	0.8	0.352	0.218	0.292
MD (dB)	CC	0.082	0.078	−0.131		−0.465	0.117	0.05	0.025	0.011	−0.287	0.153
	SL-P	0.629	0.646	0.441		0.0037	0.491	0.766	0.882	0.949	0.084	0.366
PSD (dB)	CC	0.038	−0.252	−0.108	−0.465		−0.386	−0.279	0.024	0.138	0.152	−0.524
	SL-P	0.823	0.133	0.526	0.0037		0.018	0.0945	0.889	0.414	0.369	0.0009
RNFL (μm)	CC	0.133	0.296	0.181	0.117	−0.386		0.636	0.444	−0.228	−0.05	0.427
	SL-P	0.432	0.075	0.282	0.491	0.0184		<0.0001	0.005	0.175	0.768	0.0083
GCC (μm)	CC	0.051	0.177	0.019	0.05	−0.279	0.636		0.24	−0.054	−0.379	0.361
	SL-P	0.762	0.294	0.908	0.766	0.094	<0.0001		0.152	0.753	0.0206	0.0283
Amplitude (μV)	CC	−0.181	−0.251	0.043	0.025	0.024	0.444	0.24		0.285	−0.32	−0.037
	SL-P	0.284	0.134	0.8	0.882	0.889	0.0059	0.152		0.087	0.0536	0.828
Phase (π rad)	CC	−0.128	−0.364	−0.157	0.011	0.138	−0.228	−0.054	0.285		−0.346	−0.33
	SL-P	0.449	0.0268	0.352	0.949	0.414	0.175	0.753	0.087		0.0358	0.0461
CV_amp (%)	CC	0.126	0.11	0.207	−0.287	0.152	−0.05	−0.379	−0.32	−0.346		0.09
	SL-P	0.457	0.516	0.218	0.084	0.369	0.768	*0.02*	0.053	0.0358		0.597
CV_phase (%)	CC	0.105	0.362	0.178	0.153	−0.524	0.427	0.361	−0.037	−0.33	0.09	
	SL-P	0.536	0.0277	0.292	0.368	0.0009	0.0083	0.028	0.828	0.0461	0.597	

Intraocular pressure (IOP), central corneal thickness (CCT), mean deviation (MD), pattern standard deviation (PSD), retinal nerve fiber layer thickness (RNFL), ganglion cell complex (GCC), PERG amplitude, PERG phase, coefficient of variation PERG amplitude (CV_amp), and coefficient of variation PERG phase (CV_Phase).

Table 5: Intraclass correlation coefficient.

	Patients					
	EG (37)		GS (21)		NC (24)	
	ICC[a]	95% CI	ICC[a]	95% CI	ICC[a]	95% CI
PERG amplitude (μV)	0.9187	0.8684 to 0.9538	0.9466	0.8993 to 0.9756	0.9642	0.9226 to 0.9869
PERG phase (π rad)	0.9459	0.9124 to 0.9692	0.9232	0.8554 to 0.9650	0.9879	0.9739 to 0.9956

[a]The degree of consistency among measurements.
ICC = intraclass correlation coefficient.
IC = confidence interval.

cell layer measured as SD-OCT [46, 47] and that the total macular thickness was significantly associated with glaucoma [7]. Nevertheless, we observed a better association between PSD, which indicates the severity of the disease, and RNFL ($R^2 = 0.1487$, $P = 0.0184$) than GCC ($R^2 = 0.07782$, $P = 0.0945$).

Longitudinal studies have shown that the PERG amplitude is able to detect signs of glaucomatous damage before psychometric and morphological techniques [15, 48, 49].

The PERG amplitude was significantly lower in EG and GS patients (0.96±0.33 μV and 0.96±0.27 μV, resp.) compared to healthy (1.20 ± 0.26 μV). Our data demonstrate that the reduction of PERG amplitude in SG subjects that, unlike EG patients, still do not show abnormal visual field and reduced retinal thickness, is an indicator of RGCs dysfunction. As noted by other authors [13] PERG amplitude is weakly but significantly associated with RNFL thickness reduction in EG patients ($R^2 = 0.1975$, $P = 0.0059$), whereas PERG phase in the current study did not show statistically significant differences between the subjects of the different groups.

It must be said that our trial PERG amplitude was higher than that previously reported by Bowd et al. [18] (0.96 μV compared to 0.83 μV) and similar to that previously reported by in healthy eyes (1.2 μV compared to 1.1 μV [20]). This can be explained by the different degree of severity of glaucoma, worse in Bowd patients (MD −9.0 dB), compared to −3.0 dB found in our EG patients.

Amplitude in the first test tended to be greater than that in successive tests. This finding may be related to the percentage of decrease in the amplitude due to adaptation to the stimulus PERG [30]. For this reason we have focused our attention on CVphase.

It is known that amplitude and phase of the PERG represent two distinct aspects of neural activity [31]. Briefly, the amplitude is related to the number of neurons; the phase delay is a further indicator of viability of activated neurons that may or may not be associated with amplitude reduction and in particular may mean that RGCs active respond more slowly. The last becomes progressively delayed with aging [20] and may be further delayed in early glaucoma [21].

Falsini et al. [44] showed that the loss of RGCs electrophysiological function is relatively greater than expected from the anatomical loss of RGCs axons in early glaucoma and that RNFL thickness reduction, less than expected, could be explained by glial remodelling.

In addition, changes in dendrites typically precede neuronal loss and lead to a reduction in the responsiveness of RGCs in glaucoma [50].

PERG generation includes a mixed population of RGCs [51], which are commonly divided into two major classes: P-cells (approximately 80% of the total) and M-cells (approximately 10%). M-cells are much more sensitive to changes than P-cells [52], and their response is temporally faster than P-cells [53], the first responding promptly to the steady-state PERG stimulus.

Since M-cells are relatively few and sparse, even a partial malfunction can be early detected by doubling perimetry frequency [54]. The increase of CVphase in SG subjects suggests that in early glaucoma there would be a progressive loss of the ability of RGCs to adapt in response to the growing demand for energy associated with the high-contrast PERG stimulus [55].

Porciatti and Ventura reported that PERG phase delays suggest pathophysiological mechanisms such as dendritic dysfunction or delay in axonal transport and may represent an opportunity to detect RGCs dysfunction preceding cell death [30].

In this study we demonstrated a significant but modest relationship between the RGCs function using steady-state PERG and some structural measures such as GCC and RNFL measured by OCT (see Table 4). These results suggest that a population of viable RGCs responds with reduced activity, thus signalling a period of discomfort that precedes cell death.

The primary purpose of this study was to evaluate the variability of the PERG signal because, in our opinion, it is increased more in patients suffering from glaucoma than in healthy subjects. In glaucoma suspects, reduced amplitude and increased variability of the phase of the PERG may indicate the presence of a functional impairment.

In fact, the variability of PERG signal has been evaluated in several studies: Bowd et al. [16] studied medium amplitudes and phases, their noise level, SNR, within-subject variability, CV, and ICC PERGLA recordings for within and between trials.

For amplitude, Bowd et al. observed that the variability of successive measurements was approximately 10% to 12% for healthy eyes and glaucoma patients, respectively. These values were similar within and between trials.

As for the phase, repeat measurement variability observed in this study was very low, about 1% to 2%; furthermore, ICC indicated that the percentage of total variance accounted for by intrasubject variation was similar in within and between trials and for healthy eyes and patient (range: 82% to 92%).

We observed within-trial variability of the amplitude higher than previous study, on the order of 15–20% for glaucoma patients and 10% for controls. The variability of

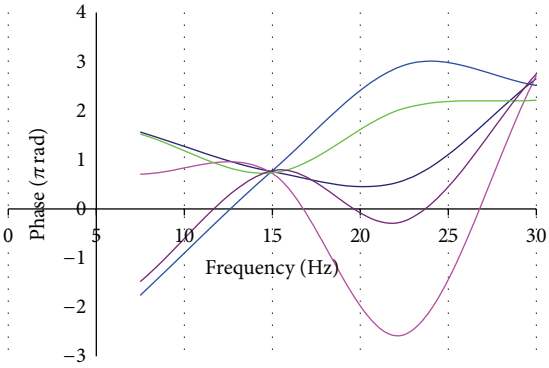

Figure 4: Five consecutive tests of steady-state PERG in the same subject. The line chart shows the trend of the phase in the frequency domain from 7.5 Hz to 30 Hz. The phase always passes from the same point at 15 Hz that corresponds to the second harmonic of the signal in response to stimulus of 7.5 Hz.

the phase was also higher than quoted study, of 8–10% for glaucomatous eyes versus 3-4% for healthy subjects.

In this study the variability of the phase has been observed not as an element of repeatability of the method but as a discriminating feature between healthy and diseased eyes. This approach can help to detect nonspecific reduction in the amplitude of PERG.

In fact, the phase is not delayed when the contrast stimulus is artificially deteriorated by simulating the visual acuity reduction due to the cataract [30]; that is, conditions like cataract reduce the PERG amplitude but do not influence the phase delay. In other words, while the PERG amplitude and its variability may depend on the opacity of the media, the phase delay and its variability, as showed in our work, are not affected by the same conditions and may express RGCs dysfunction.

In our study we did not evaluate phase delay, but its greater variability that may be a sign of RGCs dysfunction.

If you look at the phase in the frequency domain (Figure 4), by repeating the test you will see that it has an almost chaotic behavior but passes always from the same point that corresponds with the frequency of the second harmonic.

CVamp and CVphase were significantly lower in healthy individuals (3.54 ± 1.13%), compared to the groups GS (7.30 ± 2.51%) and EG (8.97 ± 2.52%), respectively (see Table 1).

Our work did not include between-proof recordings, but Fredette et al. [26] observed the test-retest variability of the PERG amplitude, expressed in terms of standard deviation (SD) of the results obtained for each subject of glaucoma during the 5 sessions in 5 different days. They also assessed the intrinsic variability (intratest), which was defined as the standard deviation of 2 consecutive recordings divided by the square root of 2. Fredette et al. argue that the amplitude variability could not be used to discriminate healthy from the glaucomatous eyes because they attributed the greater variability amplitude to the reduced amplitude of the signal in glaucomatous patients. In fact, mean amplitude and variability in their work were correlated significantly ($r^2 = 0.164$, $P = 0.003$), indicating that the variability amplitude was due to the low SNR.

Our trial showed no significant association between amplitude and SD ($r^2 = 0.010$, $P = 0.546$), probably because the amplitude of our signal and probably also our SNR were higher than measurement previously reported by Fredette et al. ($0.09 \pm 0:04\ \mu$V versus $0.08 \pm 0.03\ \mu$V).

In addition, our trial showed no association between PERG amplitude and CVphase ($r^2 = 0.001$, $P = 0.821$), confirming that variability of the phase was not dependent on the magnitude of the signal.

The structure-function relationship between CVphase and RNFL or GCC was significant only in EG group (Table 4).

The intraclass correlation coefficients indicated that the percentage of the total variance represented by the within-trial variation (i.e., the measurement reliability) was very low with regard to both the phase (0.9124 to 0.9692 95% CI) and the amplitude (0.8684 to 0.9538 95% CI), so our procedure appeared reliable.

5. Conclusions

To our knowledge, this is the first approach focusing on the intrasession phase variability. The evaluation of intraindividual and intrasession variability signal has undeniable advantages in that it minimizes interindividual variations.

This research has several limitations. In our study, we limited the variables that could contribute to measurement artifacts including cataracts or other media opacities, poor visual acuity, and pupillary miosis, but the loss of fixation of the patient cannot be quantified with our technology.

The test-retest variability should vary with the dynamic range of each instrument, so each laboratory should determine its own variability on a normative sample of healthy subjects. In our study the variability of the signal does not correlate with age, but our control sample is too small to know whether any normative database should be corrected for age.

In clinical practice it is not easy to identify with certainty the actual visual acuity at a distance of work and the transparency of the dioptric media that can compromise the signal-to-noise ratio.

The values of the impedances should be constantly controlled by the operator, but most of the tools do not have these characteristics.

Standardizing the SNR is not an easy task and the assumptions of this work are governed by the reliability and experience of the laboratory, especially when working with a steady-state stimulus [25].

Further studies are needed, but our hypothesis is that increased phase variability of intrasession PERG may represent an opportunity to detect RGCs dysfunction preceding cell death.

Conflict of Interests

None of the authors has conflict of interests with the submission. No financial support was received for this submission.

Acknowledgment

The authors thank Dario Sisto, MD, who gave them kind suggestions and some important fixes.

References

[1] R. S. Harwerth, L. Carter-Dawson, F. Shen, E. L. Smith III, and M. L. J. Crawford, "Ganglion cell losses underlying visual field defects from experimental glaucoma," *Investigative Ophthalmology and Visual Science*, vol. 40, no. 10, pp. 2242–2250, 1999.

[2] L. A. Kerrigan-Baumrind, H. A. Quigley, M. E. Pease, D. F. Kerrigan, and R. S. Mitchell, "Number of ganglion cells in glaucoma eyes compared with threshold visual field tests in the same persons," *Investigative Ophthalmology and Visual Science*, vol. 41, no. 3, pp. 741–748, 2000.

[3] G. Wollstein, H. Ishikawa, J. Wang, S. A. Beaton, and J. S. Schuman, "Comparison of three optical coherence tomography scanning areas for detection of glaucomatous damage," *The American Journal of Ophthalmology*, vol. 139, no. 1, pp. 39–43, 2005.

[4] G. Wollstein, J. S. Schuman, L. L. Price et al., "Optical coherence tomography (OCT) macular and peripapillary retinal nerve fiber layer measurements and automated visual fields," *The American Journal of Ophthalmology*, vol. 138, no. 2, pp. 218–225, 2004.

[5] J. L. Hougaard, A. Heijl, and B. Bengtsson, "Glaucoma detection by stratus OCT," *Journal of Glaucoma*, vol. 16, no. 3, pp. 302–306, 2007.

[6] O. Tan, V. Chopra, A. T.-H. Lu et al., "Detection of macular ganglion cell loss in glaucoma by Fourier-domain optical coherence tomography," *Ophthalmology*, vol. 116, no. 12, pp. 2305–14.e1-2, 2009.

[7] H. L. Rao, L. M. Zangwill, R. N. Weinreb, P. A. Sample, L. M. Alencar, and F. A. Medeiros, "Comparison of different spectral domain optical coherence tomography scanning areas for glaucoma diagnosis," *Ophthalmology*, vol. 117, no. 9, pp. 1692–1699, 2010.

[8] S. Mori, M. Hangai, A. Sakamoto, and N. Yoshimura, "Spectral-domain optical coherence tomography measurement of macular volume for diagnosing glaucoma," *Journal of Glaucoma*, vol. 19, no. 8, pp. 528–534, 2010.

[9] J. Kotowski, G. Wollstein, L. S. Folio, H. Ishikawa, and J. S. Schuman, "Clinical use of OCT in assessing glaucoma progression," *Ophthalmic Surgery, Lasers & Imaging*, vol. 42, pp. S6–S14, 2011.

[10] C. A. Curcio and K. A. Allen, "Topography of ganglion cells in human retina," *Journal of Comparative Neurology*, vol. 300, no. 1, pp. 5–25, 1990.

[11] L. Maffei and A. Fiorentini, "Electroretinographic responses to alternating gratings before and after section of the optic nerve," *Science*, vol. 211, no. 4485, pp. 953–955, 1981.

[12] E. Zrenner, "The physiological basis of the pattern electroretinogram," in *Progress in Retinal Research*, pp. 427–464, Pergamon Press, Oxford, UK, 1990.

[13] L. M. Ventura, N. Sorokac, R. de Los Santos, W. J. Feuer, and V. Porciatti, "The relationship between retinal ganglion cell function and retinal nerve fiber thickness in early glaucoma," *Investigative Ophthalmology and Visual Science*, vol. 47, no. 9, pp. 3904–3911, 2006.

[14] M. Bach and M. B. Hoffmann, "Update on the pattern electroretinogram in glaucoma," *Optometry and Vision Science*, vol. 85, no. 6, pp. 386–395, 2008.

[15] N. Pfeiffer and M. Bach, "The pattern-electroretinogram in glaucoma and ocular hypertension. A cross-sectional and longitudinal study," *German Journal of Ophthalmology*, vol. 1, no. 1, pp. 35–40, 1992.

[16] C. Bowd, A. Tafreshi, G. Vizzeri, L. M. Zangwill, P. A. Sample, and R. N. Weinreb, "Repeatability of pattern electroretinogram measurements using a new paradigm optimized for glaucoma detection," *Journal of Glaucoma*, vol. 18, no. 6, pp. 437–442, 2009.

[17] C. Bowd, A. Tafreshi, L. M. Zangwill, F. A. Medeiros, P. A. Sample, and R. N. Weinreb, "Pattern electroretinogram association with spectral domain-OCT structural measurements in glaucoma," *Eye*, vol. 25, no. 2, pp. 224–232, 2011.

[18] C. Bowd, G. Vizzeri, A. Tafreshi, L. M. Zangwill, P. A. Sample, and R. N. Weinreb, "Diagnostic accuracy of pattern electroretinogram optimized for glaucoma detection," *Ophthalmology*, vol. 116, no. 3, pp. 437–443, 2009.

[19] A. Tafreshi, L. Racette, R. N. Weinreb et al., "Pattern electroretinogram and psychophysical tests of visual function for discriminating between healthy and glaucoma eyes," *The American Journal of Ophthalmology*, vol. 149, no. 3, pp. 488–495, 2010.

[20] V. Porciatti and L. M. Ventura, "Normative data for a user-friendly paradigm for pattern electroretinogram recording," *Ophthalmology*, vol. 111, no. 1, pp. 161–168, 2004.

[21] L. M. Ventura and V. Porciatti, "Restoration of retinal ganglion cell function in early glaucoma after intraocular pressure reduction: a pilot study," *Ophthalmology*, vol. 112, no. 1, pp. 20–27, 2005.

[22] M. Bach, M. G. Brigell, M. Hawlina et al., "ISCEV standard for clinical pattern electroretinography (PERG): 2012 update," *Documenta Ophthalmologica*, vol. 126, no. 1, pp. 1–7, 2013.

[23] J. W. Cooley and J. W. Tukey, "An algorithm for the machine calculation of complex fourier series," *Mathematics of Computation*, vol. 19, no. 90, pp. 297–301, 1965.

[24] M. A. O'Neill, "Faster than fast Fourier," *Byte*, vol. 4, pp. 293–300, 1988.

[25] M. Bach and T. Meigen, "Do's and don'ts in Fourier analysis of steady-state potentials," *Documenta Ophthalmologica*, vol. 99, no. 1, pp. 69–82, 1999.

[26] M.-J. Fredette, D. R. Anderson, V. Porciatti, and W. Feuer, "Reproducibility of pattern electroretinogram in glaucoma patients with a range of severity of disease with the new glaucoma paradigm," *Ophthalmology*, vol. 115, no. 6, pp. 957–963, 2008.

[27] A. Yang and W. H. Swanson, "A new pattern electroretinogram paradigm evaluated in terms of user friendliness and agreement with perimetry," *Ophthalmology*, vol. 114, no. 4, pp. 671–679, 2007.

[28] M. Araie, "Test–retest variability in structural parameters measured with glaucoma imaging devices," *Japanese Journal of Ophthalmology*, vol. 57, no. 1, pp. 1–24, 2013.

[29] V. Porciatti, N. Sorokac, and W. Buchser, "Habituation of retinal ganglion cell activity in response to steady state pattern visual stimuli in normal subjects," *Investigative Ophthalmology and Visual Science*, vol. 46, no. 4, pp. 1296–1302, 2005.

[30] V. Porciatti and L. M. Ventura, "Adaptive changes of inner retina function in response to sustained pattern stimulation," *Vision Research*, vol. 49, no. 5, pp. 505–513, 2009.

[31] V. Porciatti and L. M. Ventura, "Physiologic significance of steady-state pattern electroretinogram losses in glaucoma: clues from simulation of abnormalities in normal subjects," *Journal of Glaucoma*, vol. 18, no. 7, pp. 535–542, 2009.

[32] B. L. Lam, W. J. Feuer, F. Abukhalil, V. Porciatti, W. W. Hauswirth, and J. Guy, "Leber hereditary optic neuropathy gene therapy clinical trial recruitment: year 1," *Archives of Ophthalmology*, vol. 128, no. 9, pp. 1129–1135, 2010.

[33] L. M. Ventura, I. Golubev, W. J. Feuer, and V. Porciatti, "The PERG in diabetic glaucoma suspects with no evidence of retinopathy," *Journal of Glaucoma*, vol. 19, no. 4, pp. 243–247, 2010.

[34] I. Bodis-Wollner, "Visual electrophysiology in Parkinson's disease: PERG, VEP and visual P300," *Clinical EEG Electroencephalography*, vol. 28, no. 3, pp. 143–147, 1997.

[35] A. Heijl, G. Lindgren, and J. Olsson, "The effect of perimetric experience in normal subjects," *Archives of Ophthalmology*, vol. 107, no. 1, pp. 81–86, 1989.

[36] V. Porciatti, B. Falsini, G. Scalia, A. Fadda, and G. Fontanesi, "The pattern electroretinogram by skin electrodes: effect of spatial frequency and age," *Documenta Ophthalmologica*, vol. 70, no. 1, pp. 117–122, 1988.

[37] L. M. Ventura, V. Porciatti, K. Ishida, W. J. Feuer, and R. K. Parrish II, "Pattern electroretinogram abnormality and glaucoma," *Ophthalmology*, vol. 112, no. 1, pp. 10–19, 2005.

[38] T. Salgarello, A. Colotto, B. Falsini et al., "Correlation of pattern electroretinogram with optic disc cup shape in ocular hypertension," *Investigative Ophthalmology and Visual Science*, vol. 40, no. 9, pp. 1989–1997, 1999.

[39] A. Kanamori, M. Nakamura, M. Tomioka, Y. Kawaka, Y. Yamada, and A. Negi, "Structure-function relationship among three types of spectral-domain optical coherent tomography instruments in measuring parapapillary retinal nerve fibre layer thickness," *Acta Ophthalmologica*, vol. 91, no. 3, pp. e196–e202, 2013.

[40] P. Sony, R. Sihota, H. K. Tewari, P. Venkatesh, and R. Singh, "Quantification of the retinal nerve fibre layer thickness in normal Indian eyes with optical coherence tomography," *Indian Journal of Ophthalmology*, vol. 52, no. 4, pp. 303–309, 2004.

[41] M. Sehi, M. Pinzon-Plazas, W. J. Feuer, and D. S. Greenfield, "Relationship between pattern electroretinogram, standard automated perimetry, and optic nerve structural assessments," *Journal of Glaucoma*, vol. 18, no. 8, pp. 608–617, 2009.

[42] R. Forte, L. Ambrosio, P. Bonavolontá, and G. Ambrosio, "Pattern electroretinogram optimized for glaucoma screening (PERGLA) and retinal nerve fiber thickness in suspected glaucoma and ocular hypertension," *Documenta Ophthalmologica*, vol. 120, no. 2, pp. 187–192, 2010.

[43] G. Vizzeri, A. Tafreshi, R. N. Weinreb, and C. Bowd, "Effect of operator and optical defocus on the variability of pattern electroretinogram optimized for glaucoma detection (PERGLA)," *Journal of Glaucoma*, vol. 19, no. 2, pp. 77–82, 2010.

[44] B. Falsini, D. Marangoni, T. Salgarello et al., "Structure—function relationship in ocular hypertension and glaucoma: interindividual and interocular analysis by OCT and pattern ERG," *Graefe's Archive for Clinical and Experimental Ophthalmology*, vol. 246, no. 8, pp. 1153–1162, 2008.

[45] M. R. Banitt, L. M. Ventura, W. J. Feuer et al., "Progressive loss of retinal ganglion cell function precedes structural loss by several years in glaucoma suspects," *Investigative Ophthalmology and Visual Science*, vol. 54, no. 3, pp. 2346–2352, 2013.

[46] V. Guedes, J. S. Schuman, E. Hertzmark et al., "Optical coherence tomography measurement of macular and nerve fiber layer thickness in normal and glaucomatous human eyes," *Ophthalmology*, vol. 110, no. 1, pp. 177–189, 2003.

[47] T. Ojima, T. Tanabe, M. Hangai, S. Yu, S. Morishita, and N. Yoshimura, "Measurement of retinal nerve fiber layer thickness and macular volume for glaucoma detection using optical coherence tomography," *Japanese Journal of Ophthalmology*, vol. 51, no. 3, pp. 197–203, 2007.

[48] S. F. N. Bode, T. Jehle, and M. Bach, "Pattern electroretinogram in glaucoma suspects: new findings from a longitudinal study," *Investigative Ophthalmology and Visual Science*, vol. 52, no. 7, pp. 4300–4306, 2011.

[49] M. Bach, A. S. Unsoeld, H. Philippin et al., "Pattern ERG as an early glaucoma indicator in ocular hypertension: a long-term, prospective study," *Investigative Ophthalmology & Visual Science*, vol. 47, no. 11, pp. 4881–4887, 2006.

[50] A. J. Weber and C. D. Harman, "Structure-function relations of parasol cells in the normal and glaucomatous primate retina," *Investigative Ophthalmology and Visual Science*, vol. 46, no. 9, pp. 3197–3207, 2005.

[51] E. Kaplan, B. B. Lee, and R. M. Shapley, "New views of primate retinal function," *Progress in Retinal Research*, vol. 9, pp. 273–336, 1990.

[52] E. Kaplan and R. M. Shapley, "The primate retina contains two types of ganglion cells, with high and low contrast sensitivity," *Proceedings of the National Academy of Sciences of the United States of America*, vol. 83, no. 8, pp. 2755–2757, 1986.

[53] E. Kaplan and E. Benardete, "The dynamics of primate retinal ganglion cells," *Progress in Brain Research*, vol. 134, pp. 17–34, 2001.

[54] B. C. Chauhan and C. A. Johnson, "Test-retest variability of frequency-doubling perimetry and conventional perimetry in glaucoma patients and normal subjects," *Investigative Ophthalmology and Visual Science*, vol. 40, no. 3, pp. 648–656, 1999.

[55] V. Porciatti, B. Bosse, P. K. Parekh, O. A. Shif, W. J. Feuer, and L. M. Ventura, "Adaptation of the steady-state PERG in early glaucoma," *Journal of Glaucoma*, vol. 23, no. 8, pp. 494–500, 2014.

Hindawi Publishing Corporation
BioMed Research International
Volume 2015, Article ID 832863, 5 pages
http://dx.doi.org/10.1155/2015/832863

Research Article

Comparison of Macular Thickness in Patients with Keratoconus and Control Subjects Using the Cirrus HD-OCT

R. L. Brautaset,[1] R. Rosén,[1] A. Cerviño,[2] W. L. Miller,[3] J. Bergmanson,[3] and M. Nilsson[1]

[1]*Unit of Optometry, Department of Clinical Neuroscience, Karolinska Institutet, P.O. Box 8056, 10420 Stockholm, Sweden*
[2]*Optics Department, University of Valencia, C/Dr. Moliner 50, 46100 Burjassot, Spain*
[3]*TERTC, University of Houston, College of Optometry, Houston, TX 77204-2020, USA*

Correspondence should be addressed to R. L. Brautaset; rlb@eyelab.se

Received 8 September 2014; Revised 19 December 2014; Accepted 6 February 2015

Academic Editor: Michele Figus

Purpose. The aim of the present study was to compare macular thickness in patients with keratoconus (KC) with macular thickness in healthy subjects. *Subjects and Methods.* Twenty-six patients with KC and 52 control subjects were included. The macular structure was evaluated using a Zeiss Cirrus HD-OCT. The scan pattern used was 512 × 128, which covers an area of approximately 6 × 6 mm of the retina. The cube volume was assessed as well as macular thickness in each of the 9 sectors defined by the software. *Results.* The mean signal strength was significantly lower in the KC group (mean 8.4, range 6–10) compared with the control group (mean 9.7, range 7–10), $P < 0.0001$ (unpaired t-test). There were no significant differences in cube volume (unpaired t-test), cube average thickness, or macular thickness between the KC group and the control subjects in any of the retinal locations (one-way ANOVA). *Conclusion.* Macular structure as measured by OCT in KC subjects should be expected to lie within the range of age and sex matched controls.

1. Introduction

Keratoconus (KC) is a degenerative corneal disease, but the exact pathophysiologic process of keratoconus is still unknown. The abnormalities in keratoconus include the degeneration of epithelial basal cells and breaks accompanied by down growth of epithelium into the anterior limiting lamina, as well as the release of catabolic enzymes and biochemical cytokines that cause thinning of collagen matrix lamella, loss of corneal stroma, and apoptosis [1–3].

The morphological alterations of keratoconic corneas are usually observed at the apex of the cone but the peripheral cornea has also been shown to exhibit disease related changes [4, 5].

Keratoconus has been associated with other systemic and ocular conditions, for example, Ehlers-Danlos syndrome and Leber's congenital amaurosis [6]. Both of these conditions are able to cause retinal degeneration. There are also a few case reports, describing central serous chorioretinopathy (CSC) in patients with KC [7] and choroidal neovascularisation [8]. Even if it is unclear whether these conditions have any common pathological features, data all together suggests that posterior segment disorders might be associated with, or at least can coexist with, keratoconus. Therefore, a thorough retinal examination before corneal transplantation seems relevant to avoid exaggerated expectations on surgery outcome.

It is often difficult to visualize the fundus in patients with keratoconus because of high refractive errors and advanced corneal astigmatism as well as corneal opacities caused by striae and corneal scarring [9]. The limited view makes it sometimes hard for clinicians to reveal maculopathy preoperatively and there are occasions when patients have been diagnosed with maculopathy first after corneal transplantation. Although a clear graft has been implemented, best corrected visual acuity (BCVA) has not been satisfyingly improved in these cases [10].

For evaluation of macular structure *in vivo*, Optical Coherence Tomography (OCT) is nowadays a well-established method [11]. The technique has the potential to reveal macular lesions due to various conditions and it is valuable for visualization of, for example, macular oedema. OCT has been shown to be able to measure retinal thickness

Table 1: Demographic data over study population.

	KC patients	Controls
Number of subjects	26	52
Number of eyes	48	52
Age (mean ± SD)	37.3 ± 12.2	37.6 ± 12.6
Male/female	13/13	25/27
Spherical equivalent (dioptres)	−9.0 (±7.6)	−2.5 (±3.5)
Visual acuity (log MAR)	0.35 (±0.3)	0.02 (±0.1)
Sim's *K* value		
Max. (dioptres)	52.30 ± 6.28	44.14 ± 1.40
Min. (dioptres)	57.29 ± 5.20	43.23 ± 1.42

Age, spherical equivalent, and visual acuity are given as mean values and standard deviations.

despite the reduced optical quality of the cornea in KC subjects [12–14]; however, very little data is available to demonstrate if macular thickness is normal or unaffected by the disease. Therefore, the aim of this study was to compare the macular thickness in patients with KC with macular thickness in healthy subjects.

2. Subjects and Methods

Twenty-six patients, with keratoconus and 52 control subjects, were recruited from the Texas Eye Research and Technology Centre (TERTC), at the University of Houston. To be included, a KC subject must manifest one or more of the following clinical signs: posterior stress lines (Vogt striae), Fleischer ring, external sign (Munson sign) together with a topography positive for KC (central corneal power superior to 48.7 D), and an inferior superior asymmetry above 1.9 [15–17]. Exclusion criteria included the following: any previous ocular surgery, the use of any systemic or ocular medications, and any chronic disorder that can affect the eye. Control subjects needed to fulfill the following criteria: asymptomatic, no ocular pathology, no history of ocular treatment, no medication with known effect on visual acuity, and visual acuity of 0.1 (Log MAR) or better. All participants in the KC group were patients from the clinic, while the control subjects were staff and students from the TERTC clinic as well as friends of the KC patients. For demographic data, see Table 1. For the KC group both eyes were included in the analysis if both eyes were affected by KC and in the control group only the right eye was included.

This study followed the tenants of the Declaration of Helsinki, was in accord with the Health Insurance Portability and Accountability Act of 1996, and was approved by the Committee for the Protection of Human Subjects of the University of Houston. Written informed consent was obtained from all KC patients and control subjects.

2.1. Observational Procedure. All patients and subjects underwent refraction to determine BCVA. They also underwent Orbscan measurements for determination of corneal astigmatism; see Table 1. Biomicroscopy was performed using a Haag Streit (BQ900) biomicroscope and all subjects were graded/classified by the same investigator (RB) and presence of prominent nerve fibres, Fleischer's ring, Vogt's striae, Munson's sign, and anterior/posterior corneal scarring was noted; see Table 2.

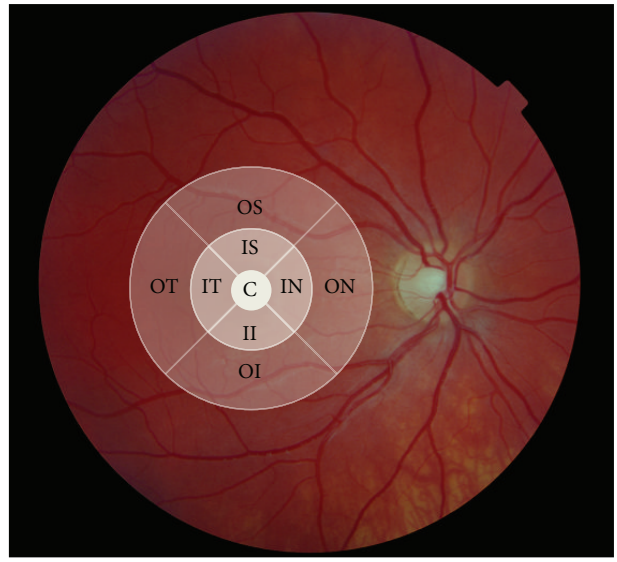

Figure 1: The cube volume and macular thickness was determined according to the 9 sectors originating from the Early Diabetic Retinopathy Study Group (C: centre, IS: inner superior, IN: inner nasal, II: inner inferior, IT: inner temporal, OS: outer superior, ON: outer nasal, OI: outer inferior, and OT: outer temporal).

The severity of keratoconus was graded according to the CLEK system using the greatest corneal curvature based on Orbscan measurements [18]. Twenty-four of the patients' eyes were classified with grade 3, eighteen with grade 2, and six with grade 1.

2.2. Macular Structure Measurements. The macular structure was evaluated using a Zeiss Cirrus HD-OCT. The scan pattern used was 512 × 128, which covers an area of approximately 6 × 6 mm of the retina. The cube volume was assessed as well as macular thickness in each of the 9 sectors defined by the software (originally from the Early Diabetic Retinopathy Study Group); see Figure 1. When needed, several scans were obtained and the scan with the highest quality/signal strength was used for analysis.

3. Results

OCT scans were successfully obtained from all subjects except in one KC patient. Because of high refractive error, outside the limits of the machine (−30 D) the image quality was poor (signal strength 2) and the images were excluded from the analysis. Another patient in the KC group showed abnormal macular measurements with scarring after choroidal lesions in one eye. Although the image quality was very good (see Figure 2) and the measurements could be regarded as reliable, it did not seem appropriate for calculation of reference values and the data was excluded from further analysis.

Table 2: Slit lamp findings.

Prominent nerve fibres	Fleischer's ring	Vogt's striae	Munson's sign	Anterior corneal scarring	posterior corneal scarring
38	15	47	3	9	21

Number of eyes with each clinical finding in the KC group.

Table 3

	Cube vol.	Cube average	Central	IS	II	IT	IN	OS	OI	OT	ON
KC eyes $n = 44$	9.9 ± 0.5	274.8 ± 13.9	254.1 ± 26.6	318.8 ± 17.9	316.8 ± 17.6	308.8 ± 21.1	317.2 ± 19.7	276.2 ± 16.6	270.6 ± 22.2	260.6 ± 18.7	280.7 ± 25.9
Control eyes $n = 80$	10.0 ± 0.5	276.8 ± 13.8	257.8 ± 15.9	32.0 ± 13.7	320.8 ± 14.4	312.2 ± 14.3	322.2 ± 18.0	278.0 ± 11.7	275.3 ± 19.5	264.65 ± 20.92	285.7 ± 22.2
Mean diff.	+0.1	−2.0	−3.70	−5.2	−3.4	−3.4	−5.0	−1.8	−4.7	−4.0	−5.0
P value	0.343	0.466	0.491	0.122	0.352	0.399	0.198	0.485	0.262	0.317	0.320

The values given in this table showed no statistically significant differences between the KC group and the control subjects (diff.: difference, cube vol.: cube volume, IS: inner superior, II: inner inferior, IT: inner temporal, IN: inner nasal, OS: outer superior, OI: outer inferior, OT: outer temporal, and ON: outer nasal).

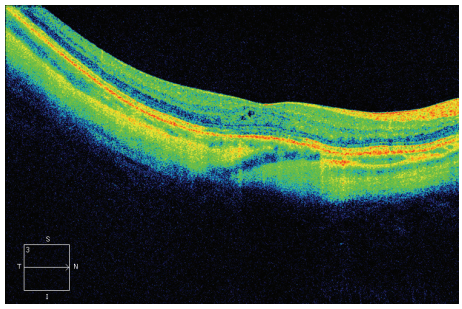

Figure 2: HD 5-line raster scan from one of the keratoconus patient showing signs of scarring after a choroidal lesion.

The mean signal strength was significantly lower in the KC group (mean 8.4 ± 1.4 SD, range 6–10) compared with the control group (mean 9.7 ± 0.49 SD, range 7–10), $P < 0.0001$ (unpaired t-test).

There was a statistical significant correlation between signal strength and astigmatism (Sim's K value) ($P > 0.001$, $r = -0.63$) and between signal strength and visual acuity ($P = 0.01$, $r = -0.37$) in the KC group (Spearman rank correlation).

There were no significant differences (see Table 3) in cube volume (unpaired t-test), cube average thickness, or macular thickness between the KC group and the control subjects in any of the retinal locations (one-way ANOVA).

4. Discussion

Macular thickness measurements were successfully obtained from all KC patients except in one patient who had a high refractive error (> −30 D), outside the correction limits of the OCT machine used in this study (Zeiss Cirrus HD-OCT). On average, no difference in macular thickness could be found when comparing the KC group and controls. This finding is in line with the findings of Moschos et al. [13]. One KC subject had maculopathy which was easily detected and not masked although the patient had high refractive error (−24 D), prominent nerve fibres, Vogt's striae, and Fleisher's ring, indicating severe keratoconus or grade 3 according to the CLEK grading system [18]; see Figure 2. It could be argued if the maculopathy found in one of the KC subjects could be related to keratoconus, but that is outside the scope of this study. To answer such a question large cross-sectional studies are needed including not only OCT measurements. However, it is important information that macular changes seem easy to detect also in patients with poor optics caused by changes seen in KC. In 1996, Moschos and coworkers [19], performed electroretinogram (ERGs) and visual evoked potentials (VERs) in patients with keratoconus. In a handful of patients (5 out of 255) abnormal results were obtained and explained by coexisting diffuse or central tapetoretinal degeneration. The low visual acuity among those patients was, therefore, not only explained by the corneal lesions but also explained by the photoreceptor dysfunction. After successful corneal graft surgery, visual acuity was not increased and the transplantation of cornea in these cases was in vain. Preoperatively OCT examinations might have given useful information in these cases, which has been described in the case report by Meyer et al. [20].

In our subjects the signal strength of the OCT measurements were significantly lower in the KC group compared with the control subjects but all the images were possible to interpret. The signal strength ranged from 6 to 10, values which have been referred to as moderate to excellent [21]. Differences in signal strength have been proven to influence measurements but the differences have not been regarded as of any clinical importance [21]. In a recent study aiming to evaluate the effects of different parameters like signal strength, age, sex, and axial length on macular measurements using OCT, no parameter except age influenced the measurements [22]. Further, the influence of astigmatism on macular thickness measurements was recently evaluated by Hwang et al. [23]. They measured macular thickness in healthy subjects before and after fitting a soft contact lens inducing approximately 3 diopters astigmatism in 90 and 180 degrees, respectively. No changes in macular thickness could be found although retinal nerve fibre layer (RNFL)

thickness measurements were affected and the range in mean difference with and without the lens was 0.75–5.11 μm. Such small differences are, however, only clinically relevant when one, through follow up, is trying to detect degenerative changes and not when trying to detect an abnormal RNFL thickness. Cankaya and coworkers [24] recently described the outcome of RNFL thickness and optic nerve head (ONH) measurements in patients with KC. They found that RNFL thickness measurements were more comparable than ONH parameters when comparing patients with keratoconus and healthy subjects. Altogether, these two studies indicate that it is fully possible to obtain reliable data from measurements of retinal structures also in patients with keratoconus.

Since the values of the parameters analysed by the OCT in this study did not differ between KC subjects and controls, combined with the fact that several of the KC patients had pronounced signs of Keratoconus, abnormal OCT values from examination of patients with KC should be considered with gravity. Furthermore, the results from this study indicate that OCT should be regarded as a valuable instrument for macular evaluation in patients before corneal transplantation and used in order to improve the anticipation of the outcome of a corneal graft implant.

5. Conclusion

Even though the optical quality in aspects of astigmatism will influence the quality of OCT measurements, the current study indicates that macular structure as measured by OCT in KC subjects should be expected to lie within the range of age and sex matched controls.

Conflict of Interests

The authors declare that there is no conflict of interests regarding the publication of this paper.

References

[1] S. E. Wilson, R. R. Mohan, R. Ambrósio Jr., J. Hong, and J. Lee, "The corneal wound healing response: cytokine-mediated interaction of the epithelium, stroma, and inflammatory cells," *Progress in Retinal and Eye Research*, vol. 20, no. 5, pp. 625–637, 2001.

[2] M. C. Kenney and D. J. Brown, "The cascade hypothesis of keratoconus," *Contact Lens and Anterior Eye*, vol. 26, no. 3, pp. 139–146, 2003.

[3] J. G. Hollingsworth, R. E. Bonshek, and N. Efron, "Correlation of the appearance of the keratoconic cornea *in vivo* by confocal microscopy and *in vitro* by light microscopy," *Cornea*, vol. 24, no. 4, pp. 397–405, 2005.

[4] J. R. Horne, J. D. Goosey, and J. P. G. Bergmanson, "Pathological and morphometrical alteration in the keratoconic cornea," ARVO E-Abstract1863, 2007.

[5] R. L. Brautaset, M. Nilsson, W. L. Miller, N. E. Leach, J. H. Tukler, and J. P. G. Bergmanson, "Central and peripheral corneal thinning in keratoconus," *Cornea*, vol. 32, no. 3, pp. 257–261, 2013.

[6] M. Romero-Jiménez, J. Santodomingo-Rubido, and J. S. Wolffsohn, "Keratoconus: a review," *Contact Lens and Anterior Eye*, vol. 33, no. 4, pp. 157–166, 2010.

[7] C. M. Eandi, L. V. Del Priore, E. Bertelli, M. D. Ober, and L. A. Yannuzzi, "Central serous chorioretinopathy in patients with keratoconus," *Retina*, vol. 28, no. 1, pp. 94–96, 2008.

[8] J. Y. Oh and H. G. Yu, "Keratoconus associated with choroidal neovascularization: a case report," *Journal of Medical Case Reports*, vol. 4, article 58, 2010.

[9] H. Wagner, J. T. Barr, and K. Zadnik, "Collaborative Longitudinal Evaluation of Keratoconus (CLEK) Study: methods and findings to date," *Contact Lens and Anterior Eye*, vol. 30, no. 4, pp. 223–232, 2007.

[10] R. Fogla and G. K. Iyer, "Keratoconus associated with cone-rod dystrophy: a case report," *Cornea*, vol. 21, no. 3, pp. 331–332, 2002.

[11] W. Geitzenauer, C. K. Hitzenberger, and U. M. Schmidt-Erfurth, "Retinal optical coherence tomography: past, present and future perspectives," *British Journal of Ophthalmology*, vol. 95, no. 2, pp. 171–177, 2011.

[12] B. T. Acar, O. Muftuoglu, and S. Acar, "Comparison of macular thickness measured by optical coherence tomography after deep anterior lamellar keratoplasty and penetrating keratoplasty," *The American Journal of Ophthalmology*, vol. 152, no. 5, pp. 756–761, 2011.

[13] M. M. Moschos, I. P. Chatziralli, C. Koutsandrea, G. Siasou, and D. Droutsas, "Assessment of the macula in keratoconus: an optical coherence tomography and multifocal electroretinography study," *Ophthalmologica*, vol. 229, no. 4, pp. 203–207, 2013.

[14] A. Koytak, A. Kubaloglu, E. S. Sari, M. Atakan, S. Culfa, and Y. Ozerturk, "Changes in central macular thickness after uncomplicated corneal transplantation for keratoconus: penetrating keratoplasty versus deep anterior lamellar keratoplasty," *Cornea*, vol. 30, no. 12, pp. 1318–1321, 2011.

[15] N. Maeda, S. D. Klyce, and M. K. Smolek, "Comparison of methods for detecting keratoconus using videokeratography," *Archives of Ophthalmology*, vol. 113, no. 7, pp. 870–874, 1995.

[16] Y. S. Rabinowitz and P. J. McDonnell, "Computer-assisted corneal topography in keratoconus," *Refractive and Corneal Surgery*, vol. 5, no. 6, pp. 400–408, 1989.

[17] M. B. Souza, F. W. Medeiros, D. B. Souza, R. Garcia, and M. R. Alves, "Evaluation of machine learning classifiers in keratoconus detection from orbscan II examinations," *Clinics*, vol. 65, no. 12, pp. 1223–1228, 2010.

[18] K. Zadnik, J. T. Barr, M. O. Gordon, T. B. Edrington, and CLEK Study Group, "Biomicroscopic signs and disease severity in keratoconus," *Cornea*, vol. 15, no. 2, pp. 139–146, 1996.

[19] M. Moschos, D. Droutsas, E. Panagakis, G. Tsioulias, and M. Tsalouki, "Keratoconus and tapetoretinal degeneration," *Cornea*, vol. 15, no. 5, pp. 473–476, 1996.

[20] C. H. Meyer, E. B. Rodrigues, S. Mennel, and J. C. Schmidt, "Optical coherence tomography in a case of Bietti's crystalline dystrophy," *Acta Ophthalmologica Scandinavica*, vol. 82, no. 5, pp. 609–612, 2004.

[21] C. Samarawickrama, A. Pai, S. C. Huynh, G. Burlutsky, T. Y. Wong, and P. Mitchell, "Influence of OCT signal strength on macular, optic nerve head, and retinal nerve fiber layer parameters," *Investigative Ophthalmology and Visual Science*, vol. 51, no. 9, pp. 4471–4475, 2010.

[22] H. L. Rao, A. U. Kumar, J. G. Babu, A. Kumar, S. Senthil, and C. S. Garudadri, "Predictors of normal optic nerve head,

retinal nerve fiber layer, and macular parameters measured by spectral domain optical coherence tomography," *Investigative Ophthalmology and Visual Science*, vol. 52, no. 2, pp. 1103–1110, 2011.

[23] Y. H. Hwang, S. M. Lee, Y. Y. Kim, J. Y. Lee, and C. Yoo, "Astigmatism and optical coherence tomography measurements," *Graefe's Archive for Clinical and Experimental Ophthalmology*, vol. 250, no. 2, pp. 247–254, 2012.

[24] A. B. Cankaya, E. Beyazyildiz, D. Ileri, and P. Yilmazbas, "Optic disc and retinal nerve fiber layer parameters of eyes with keratoconus," *Ophthalmic Surgery Lasers and Imaging*, vol. 43, no. 5, pp. 401–407, 2012.

Hindawi Publishing Corporation
BioMed Research International
Volume 2014, Article ID 128517, 10 pages
http://dx.doi.org/10.1155/2014/128517

Clinical Study

Comparative Diagnostic Accuracy of Ganglion Cell-Inner Plexiform and Retinal Nerve Fiber Layer Thickness Measures by Cirrus and Spectralis Optical Coherence Tomography in Relapsing-Remitting Multiple Sclerosis

Julio J. González-López,[1,2,3] Gema Rebolleda,[1,2] Marina Leal,[1] Noelia Oblanca,[1] Francisco J. Muñoz-Negrete,[1,2] Lucienne Costa-Frossard,[4] and José C. Álvarez-Cermeño[4]

[1] *Department of Ophthalmology, Ramón y Cajal University Hospital, Carretera de Colmenar Km 9, 1, 28034 Madrid, Spain*
[2] *Department of Surgery, Alcalá de Henares University, Madrid, Spain*
[3] *Medical Retina Department, Moorfields Eye Hospital, London, UK*
[4] *Department of Neurology, Ramón y Cajal University Hospital, Madrid, Spain*

Correspondence should be addressed to Gema Rebolleda; grebolleda@telefonica.net

Received 29 July 2014; Revised 23 August 2014; Accepted 26 August 2014; Published 18 September 2014

Academic Editor: Antonio Ferreras

Objective. To estimate sensitivity and specificity of several optical coherence tomography (OCT) measurements for detecting retinal thickness changes in patients with relapsing-remitting multiple sclerosis (RRMS), such as macular ganglion cell-inner plexiform layer (GCIPL) thickness measured with Cirrus (OCT) and peripapillary retinal nerve fiber layer (pRNFL) thickness measured with Cirrus and Spectralis OCT. *Methods*. Seventy patients (140 eyes) with RRMS and seventy matched healthy subjects underwent pRNFL and GCIPL thickness analysis using Cirrus OCT and pRNFL using Spectralis OCT. A prospective, cross-sectional evaluation of sensitivities and specificities was performed using latent class analysis due to the absence of a gold standard. *Results*. GCIPL measures had higher sensitivity and specificity than temporal pRNFL measures obtained with both OCT devices. Average GCIPL thickness was significantly more sensitive than temporal pRNFL by Cirrus (96.34% versus 58.41%) and minimum GCIPL thickness was significantly more sensitive than temporal pRNFL by Spectralis (96.41% versus 69.69%). Generalised estimating equation analysis revealed that age ($P = 0.030$), optic neuritis antecedent ($P = 0.001$), and disease duration ($P = 0.002$) were significantly associated with abnormal results in average GCIPL thickness. *Conclusion*. Average and minimum GCIPL measurements had significantly better sensitivity to detect retinal thickness changes in RRMS than temporal pRNFL thickness measured by Cirrus and Spectralis OCT, respectively.

1. Introduction

Relapsing-remitting multiple sclerosis (RRMS) is a chronic, immune-mediated demyelinating disease of the central nervous system that frequently involves the visual pathways, usually in the form of optic neuritis (ON) [1]. Postmortem analysis revealed optic nerve lesions in 94–99% of RRMS patients, even in the absence of a clinical history of ON [2].

Optical coherence tomography (OCT) is a noninvasive and reproducible tool for evaluating the retinal and optic disc anatomy of patients with this clinical disorder. It uses low-coherence interferometry to obtain detailed images of the retinal architecture. Modern high-speed spectral-domain (SD) OCT devices can obtain high resolution images of the retina. Computerised algorithms can be used on these images in order to automatically identify and obtain thickness measurements of discrete retinal layers, including the retinal nerve fiber layer (RNFL) and the macular ganglion cell-inner plexiform layers (GCIPL) [3].

In patients with RRMS, the main focus has been the evaluation of the peripapillary retinal nerve fiber layer (pRNFL). The RNFL contains the unmyelinated axons originating from

the ganglion cell neurons. In a previous report, we found that Spectralis showed a significantly higher thinning for temporal quadrant than Cirrus in eyes of RRMS patients, suggesting that N-site axonal analysis could define axonal damage in relapsing-remitting multiple sclerosis patients earlier than conventional pRNFL analysis [4].

Optic nerve demyelination, due to clinical or subclinical ON, can result in retrograde degeneration of the optic nerve axons, leading to RNFL and GCIPL thinning [5, 6]. In fact, several studies have reported statistically significant thinning of the pRNFL and GCIPL in patients with RRMS with and without optic neuritis compared to healthy control subjects [7–10].

Moreover, macular GCIPL thickness has been found to have better structure-function correlations than pRNFL thickness with both visual function and disability in RRMS patients [11]. At least in part, this observation may be due to the superior reproducibility of GCIPL over pRNFL thickness measurements [11].

Thus, we hypothesize that GCIPL measurements can be more sensitive to and specific of retinal involvement in patients with RRMS than those with pRNFL measurements.

The main purpose of this study was to estimate the sensitivity and specificity of macular GCIPL thickness measured with the Cirrus OCT ganglion cell analysis (GCA) algorithm (Carl Zeiss Meditec AG, Jena, Germany) and pRNFL thickness analysis with Cirrus and Spectralis (Heidelberg Engineering GmbH, Heidelberg, Germany) OCTs in detecting retinal thickness changes in eyes from patients with a clinical diagnosis of RRMS versus age-matched normal subjects using latent class analysis.

Ancillary objectives were to quantify color-code abnormalities in GCIPL and pRNFL measures by Cirrus and Spectralis OCTs in eyes from patients with RRMS and healthy control subjects, to quantify the correlations of GCIPL and pRNFL measurements with the visual function and disability in MS patients, and to study the effect of optic neuritis antecedent on the obtained measurements.

2. Methods

2.1. Subjects. An observational, prospectively recruited, cross-sectional study was performed. The study was approved by the Research Ethics Committee in the Ramón y Cajal University Hospital. All research complied with the tenets of the declaration of Helsinki, and all subjects participating in the study gave their written informed consent. Confidentiality of participating subjects was protected throughout the study.

We included 70 patients with a diagnosis of RRMS and 70 healthy control subjects. Patients were enrolled consecutively from the Neuroophthalmology Department from January 2012 to September 2012. Healthy controls without a history of neurological and ophthalmological disease were recruited among the hospital staff.

Diagnosis of RRMS was based on McDonald criteria by the treating neurologist [12]. None of the included patients had a diagnosis of secondary progressive multiple sclerosis.

All participants underwent a complete neuroophthalmic evaluation that included pupillary, anterior segment, and funduscopic examinations; assessment of logMAR best corrected visual acuity (BCVA), and they were scanned after pupillary dilation with Cirrus (Carl Zeiss Meditec AG, Jena, Germany) and Spectralis (Heidelberg Engineering GmbH, Heidelberg, Germany) OCTs on the same day in random order. Both eyes of each subject were included. Exclusion criteria were intraocular pressure of 21 mm Hg or higher, an optic disc suspicious for glaucoma under dilated funduscopy, a refractive error greater than 5.0 diopters (D) of spherical equivalent or 3.0 D of astigmatism in either eye, media opacity, a recent history of optic neuritis 6 months prior to the day of imaging, systemic conditions that could affect the visual system, a history of ocular trauma, or concomitant ocular diseases, including glaucoma.

Related medical records were carefully reviewed, including the duration of the disease, the Expanded Disability Status Scale (EDSS) scored by a neurologist (LC), and the presence of prior episodes of optic neuritis (ON) as reported by the treating neurologist and the patient.

The visual field (VF) was tested only in the eyes of patients with RRMS, using a Humphrey Field Analyzer (Carl Zeiss Meditec AG, Jena, Germany) and the SITA Standard protocol (program 24-2). VF test was considered reliable when fixation losses were less than 20% and false-positive and false-negative errors were less than 15%.

2.2. Optical Coherence Tomography Measurements. A single, well-trained optometrist (NO) performed all OCT examinations in random order to prevent any fatigue bias. All poor-quality scans were rejected, defined as those with signal strength of ≤6 by Cirrus. For Spectralis OCT only those images with a signal-to-noise score higher than 25 dB were analyzed. Scans with misalignment, segmentation failure, decentration of the measurement circle, and poor illumination or those out of focus were excluded from the analysis. Thus, manual correction of plotting errors of automated segmentation was not performed in this study.

Methodology for pRNFL imaging in Cirrus and Spectralis has been reported previously [3]. Briefly, cross-sectional imaging of the peripapillary area was performed using Cirrus OCT. pRNFL thickness was determined using the optic disc cube protocol (software version 5.1.1.6) that generates a cube of data through a 6 mm square grid. A 3.46 mm in diameter calculation circle was automatically positioned around the optic disc. Cirrus OCT provides average pRNFL thickness and maps with 4 quadrants (superior, inferior, nasal, and temporal) and 12 clock hours, including classification from an internal normative database.

Spectralis OCT (software version 5.2.0.3) simultaneously captures infrared fundus and SD-OCT images at 40,000 A-scans per second. A real-time eye-tracking system measures eye movements and provides feedback to the scanning mechanism to stabilize the retinal position of the B-scan. The instrument uses 1024 A-scan points from a 3.45 mm circle centered on the optic disc. The examiner is required to manually place the scan around the optic disc. Peripapillary RNFL measurements were obtained using the N-site

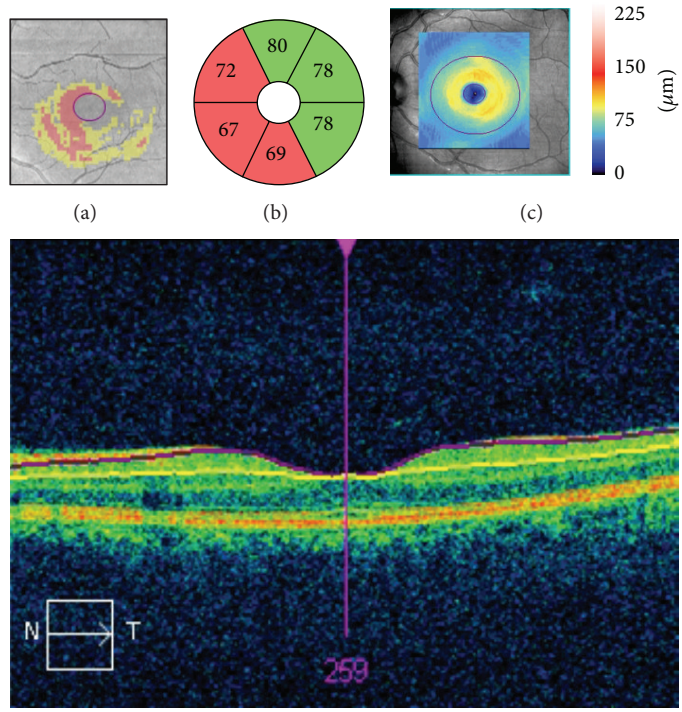

Figure 1: Ganglion cell-inner plexiform layer (GCIPL) analysis of the left eye of a patient with relapsing-remitting multiple sclerosis without optic neuritis antecedent in a 6 × 6 × 2 mm macular cube using a Cirrus optical coherence tomography. (a) Deviation map of the GCIPL thickness (red: below percentile 1; yellow: below percentile 5). (b) Sector distribution. (c) GCIPL thickness map, with overlying ellipses showing the dimensions of the analyzed annulus. The outer ellipse has a vertical diameter of 4 mm and the inner ellipse of 1 mm. (d) Horizontal B-scan centered in the fovea, showing the automated segmentation of the GCIPL.

axonal protocol, which differs from the standard pRNFL scan because it starts and terminates in the nasal side of optic nerve. Scans were obtained using the high resolution (HR) mode and using automatic real-time (ART) for averaging 9 B-scan frames in order to improve image quality. The pRNFL Spectralis protocol generates a map showing the average thickness, maps with 4 quadrants (superior, inferior, nasal, and temporal), and maps with 6 sector thicknesses (superonasal, nasal, inferonasal, inferotemporal, temporal, and superotemporal).

The pRNFL thicknesses in the normal range are represented by green backgrounds. Those that are abnormal at the 5% and at the 1% level are represented by yellow and red backgrounds, respectively. The hypernormal (95th to 100th percentiles) pRNFL thicknesses are presented by a white color in Cirrus and by a blue/purple color in Spectralis.

Cross-sectional imaging of the macular area was performed using Cirrus OCT macular cube (512 × 128). This acquisition protocol generates a cube through a 6 mm square grid of 128 B-scans of 512 A-scans each. A built-in GCIPL analysis algorithm detects and measures the thickness of the macular GCIPL within a 6 × 6 × 2 mm elliptical annulus area centered on the fovea. The annulus has an inner vertical diameter of 1 mm, which was chosen to exclude the portions of the fovea where the layers are very thin and difficult to detect accurately, and an outer vertical diameter of 4 mm, which was chosen according to where the GCL again becomes thin and difficult to detect. The GCA algorithm identifies the outer boundaries of the RNFL and IPL. The difference between the RNFL and the IPL outer boundary segmentations yields the combined thickness of the RGC layer and IPL. Cirrus OCT provides quantitative assessment of the ganglion cell and inner plexiform layers (GCIPL) in 6 circular sectors centered in the fovea (superonasal, superior, inferonasal, inferotemporal, inferior, and superotemporal). It also gives information on the mean and minimum GCIPL thickness for each eye and compares these figures with a normative database (Figure 1). The GCIPL thicknesses in the normal range are represented by green backgrounds. Those that are abnormal at the 5% and at the 1% level are represented by yellow and red backgrounds, respectively. The hypernormal (95th to 100th percentiles) pRNFL thicknesses are presented by a white color.

2.3. Statistical Analysis. Data were analyzed using Stata/SE 12.0 for Unix and IBM SPSS Version 20 for Unix. A P value of less than 0.05 was considered statistically significant.

Quantitative variables were summarized as mean ± standard deviation. Qualitative variables were summarized as absolute value (percentage). Generalized estimating equation models accounting for sex, age, and within-patient intereye correlations were used to examine correlations and associations between variables.

When evaluating new medical diagnostic tests, data may be obtained from one or more tests, but none of these can be considered a gold standard, that is, a diagnostic test with 100% sensitivity and specificity [13]. Latent class analysis (LCA) is based on the concept that observed results of different imperfect tests for the same disease are influenced by a latent common variable, the true disease status, which cannot be directly measured. In a group of patients with unknown disease status, for whom results from several diagnostic tests are available, LCA will model the probability of each combination of test results on the latent class and will provide an estimate of sensitivity and specificity for each of the diagnostic tests evaluated [14, 15]. LCA has been used extensively for the estimation of sensitivity and specificity of diagnostic tests in the absence of a valid gold standard, mainly in microbiology [16, 17] and psychology [18], but also in ophthalmology [19].

In this study, we implemented the basic latent class model, using the assumption of conditional independence given the latent class. In basic LCA, there are no associations between the observed variables within each category of the latent variable. The latent variable is the true status on the disease, and the hypothesis is that there are two latent classes (presence or absence of retinal thickness changes). As more than one pRNFL measure could not be fitted into the same model due to the conditional independence assumption, two LCA models were built. Four variables were included in each LCA; average and minimum macular GCIPL thicknesses by Cirrus OCT and BCVA were present in both models; temporal pRNFL thicknesses by Cirrus OCT or by Spectralis OCT were present in one model each. LCA requires tests with binary outcomes to create the model. For simplification of the analysis, white, blue, purple, and green sectors have been labeled as "normal," and yellow and red ones as "abnormal." For BCVA, values better than or equal to 0.3 LogMAR were labeled as normal and those worse than 0.3 as "abnormal." BCVA was included in the model in order to provide a functional outcome that could help better define the latent class "retinal thickness change." Temporal pRNFL was selected as it was the quadrant with a higher frequency of pRNFL thinning and abnormal results in previous studies [4, 20–23].

LCA was performed using TAGS software implemented in R version 2.2 (R Development Core Team and R Foundation for Statistical Computing, 2005). The fit of LCA model for the assumption of conditional independence was performed through the goodness-of-fit test followed by the evaluation of residual correlations between tests.

3. Results

Seventy RRMS patients and seventy age- and gender-matched healthy controls were enrolled in the study. All participants were of Caucasian descent. Table 1 summarizes the demographic and clinical characteristics of the participants.

Overall, average pRNFL and temporal quadrant pRNFL thickness by both Cirrus and Spectralis OCTs were significantly lower in both ON and non-ON RRMS eyes compared to healthy eyes ($P < 0.001$). Similarly, average, minimum, and each of the 6 sectors GCIPL thicknesses yielded by Cirrus were significantly lower in RRMS compared to healthy eyes in both ON and non-ON eyes ($P < 0.001$).

All these measurements were significantly lower in eyes with a prior history of ON compared to non-ON eyes ($P < 0.001$).

Table 2 shows the percentage of abnormal color-coded measurements (defined as red or yellow color codes) obtained by GCIPL and pRNFL analysis in healthy and RRMS patients. Abnormal results were significantly more common in ON and non-ON RRMS eyes versus healthy eyes and in eyes with ON antecedent versus those without this antecedent in RRMS patients.

Overall, the highest abnormal percentage was observed in minimum (47.8%) followed by average (46.4%) GCIPL analysis. The sector in GCIPL test showing the highest abnormality rate was the superonasal (47.1%) followed by superotemporal sector (45.7%). The abnormality rates were significantly higher in eyes with a prior ON compared to non-ON eyes (Figure 2).

Using Cirrus OCT, average GCIPL was altered more frequently than average pRNFL in eyes of patients with RRMS (46% versus 33%, resp.; $P < 0.001$).

In a subgroup analysis comparing abnormal results between GCIPL and pRNFL by ON antecedent, average and minimum GCIPL measurements yielded the highest abnormal results for both ON and non-ON eyes (Table 2).

Table 3 shows the estimated sensitivity and specificity to detect retinal thickness changes by OCT with the two LCA models. The test for evaluating the fit of the model with conditional independence (goodness-of-fit test) proved to be adjusted (P value = 0.938 for model A and 0.836 for model B). The residual correlations between tests were randomly distributed around 0.

Both GCIPL measurements appeared to be more sensitive and specific than temporal pRNFL thickness measured by Cirrus or Spectralis OCT (Table 3). Estimated sensitivities using Cirrus were 96.34%, 98.43%, and 58.41% for average, minimum GCIPL, and temporal pRNFL, respectively. Using Spectralis, estimated sensitivity for temporal pRNFL was lower (69.69%) than for Cirrus GCIPL measurements (average: 97.15% and minimum: 96.41%).

Importantly, average GCIPL thickness was significantly more sensitive than temporal pRNFL by Cirrus ($P < 0.05$), and minimum GCIPL was significantly more sensitive than temporal pRNFL by Spectralis for the detection of retinal thickness changes in RRMS ($P < 0.05$). The model appeared to be robust, as sensitivities and specificities for both GCIPL measurements and BCVA were similar in both models.

Abnormal results in average GCIPL thickness in RRMS patients were independently associated to age in years (OR = 0.942, $P = 0.030$), years since the diagnosis of RRMS (OR = 1.185, $P = 0.002$), and ON antecedent (OR = 4.123, $P = 0.001$), after correcting by sex and intereye correlation using binary logistic generalized estimating equations ($N = 140$).

Generalised estimating equations accounting for sex, age, and within-patient intereye correlation were used to measure standardised correlations between pRNFL and GCIPL

Table 1: Clinical and demographic characteristics of healthy subjects and relapsing-remitting multiple sclerosis (RRMS) patients regarding optic neuritis (ON) antecedent. Differences were tested using generalized estimating equations accounting for sex, age, and within-patient intereye correlation.

	Healthy subjects $N = 70$	RRMS $N = 70$	ON eyes $N = 36$	Non-ON eyes $N = 104$	P (healthy versus RRMS)	P (healthy versus ON eyes)	P (healthy versus non-ON eyes)	P (ON versus non-ON eyes)
	Mean ± SD							
Age (years)	37 ± 10	40 ± 10	42 ± 9	40 ± 11	0.077	0.008	0.077	0.302
Female (%)	40 (57%)	44 (63%)	14 (78%)	30 (58%)	0.387	0.627	0.363	0.552
LogMAR BCVA	0.00 ± 0.02	0.04 ± 0.18	0.10 ± 0.26	0.02 ± 0.14	0.006	0.023	0.115	0.083
EDSS score	N/A	2.42 ± 1.72	2.43 ± 1.61	2.41 ± 1.76	N/A	N/A	N/A	0.873
Years since diagnosis	N/A	6.82 ± 6.95	7.31 ± 6.25	6.66 ± 7.19	N/A	N/A	N/A	0.754
MD (in dB)	N/A	−2.7 ± 3.8	−3.8 ± 5.2	−2.4 ± 3.1	N/A	N/A	N/A	<0.001
Average pRNFL (Sp; in μm)	99.3 ± 8.7	87.8 ± 13.8	79.6 ± 13.6	90.7 ± 12.7	<0.001	<0.001	<0.001	<0.001
Temporal pRNFL (Sp; in μm)	71.4 ± 10.6	58.8 ± 16.0	50.2 ± 16.2	61.9 ± 14.8	<0.001	<0.001	<0.001	<0.001
PMB pRNFL (Sp; in μm)	54.9 ± 7.6	44.4 ± 11.4	38.8 ± 11.8	46.4 ± 10.7	<0.001	<0.001	<0.001	<0.001
Average pRNFL (Ci; in μm)	93.9 ± 8.5	84.9 ± 12.5	78.9 ± 13.0	87.0 ± 11.7	<0.001	<0.001	<0.001	<0.001
Temporal pRNFL (Ci; in μm)	64.7 ± 9.5	54.2 ± 13.8	47.4 ± 14.0	56.6 ± 13.0	<0.001	<0.001	<0.001	<0.001
Average GCIPL (Ci; in μm)	83.8 ± 5.9	72.2 ± 11.3	66.4 ± 10.9	74.3 ± 10.7	<0.001	<0.001	<0.001	<0.001
Minimum GCIPL (Ci; in μm)	81.9 ± 6.1	68.1 ± 12.9	61.4 ± 13.2	70.4 ± 12.0	<0.001	<0.001	<0.001	<0.001
Superior GCIPL (Ci; in μm)	80.5 ± 6.2	73.0 ± 11.7	66.7 ± 11.4	75.2 ± 11.1	<0.001	<0.001	<0.001	<0.001
Superonasal GCIPL (Ci; in μm)	85.5 ± 6.3	73.0 ± 11.7	65.8 ± 10.8	75.5 ± 11.0	<0.001	<0.001	<0.001	<0.001
Inferonasal GCIPL (Ci; in μm)	84.0 ± 6.3	72.0 ± 12.2	64.5 ± 11.8	74.6 ± 11.2	<0.001	<0.001	<0.001	<0.001
Inferior GCIPL (Ci; in μm)	82.7 ± 6.2	71.6 ± 12.0	65.6 ± 12.5	73.7 ± 11.1	<0.001	<0.001	<0.001	<0.001
Inferotemporal GCIPL (Ci; in μm)	83.8 ± 6.1	73.3 ± 11.0	68.6 ± 12.3	74.9 ± 10.1	<0.001	<0.001	<0.001	<0.001
Superotemporal GCIPL (Ci; in μm)	82.4 ± 6.5	72.3 ± 10.9	67.0 ± 11.0	74.2 ± 10.4	<0.001	<0.001	<0.001	<0.001

SD: standard deviation; BCVA: best corrected visual acuity; EDSS: Expanded Disability Status Scale; MD: 24-2 SITA Standard Visual Field Mean Deviation; pRNFL: peripapillary retinal nerve fiber layer; Sp: Spectralis OCT; PMB: papillomacular bundle; Ci: Cirrus OCT; GCIPL: ganglion cell and inner plexiform layers.

Table 2: Number of eyes (and percentage) with abnormal results (yellow or red color-coded) in healthy and relapsing-remitting multiple sclerosis (RRMS) patients and according to optic neuritis (ON) antecedent. Statistical significance of associations was tested using generalized estimating equations accounting for sex, age, and within-patient intereye correlation.

Abnormal result	Healthy $N = 140$	RRMS $N = 140$	ON eyes $N = 36$	Non-ON eyes $N = 104$	P (healthy versus RRMS)	P (healthy versus ON eyes)	P (healthy versus non-ON eyes)	P (ON versus non-ON eyes)
Average pRNFL (Sp)	5 (3.6)	49 (35.0)	20 (55.6)	29 (27.9)	<0.001	<0.001	<0.001	<0.001
Temporal pRNFL (Sp)	5 (3.6)	65 (46.4)	22 (61.1)	43 (41.3)	<0.001	<0.001	<0.001	<0.001
PMB pRNFL (Sp)	4 (2.9)	43 (30.7)	17 (47.22)	26 (25.0)	<0.001	<0.001	<0.001	0.012
Average pRNFL (Ci)	9 (6.4)	46 (32.9)	19 (52.8)	27 (26.0)	<0.001	<0.001	0.001	0.001
Temporal pRNFL (Ci)	2 (1.4)	49 (35.0)	24 (66.7)	25 (24.0)	<0.001	<0.001	<0.001	<0.001
Average GCIPL (Ci)	8 (5.7)	65 (46.4)	25 (69.4)	40 (38.5)	<0.001	<0.001	<0.001	<0.001
Minimum GCIPL (Ci)	7 (5.0)	67 (47.9)	28 (77.8)	39 (37.5)	<0.001	<0.001	<0.001	<0.001
Superior GCIPL (Ci)	8 (5.7)	63 (45.0)	26 (72.2)	37 (35.6)	<0.001	<0.001	<0.001	<0.001
Superonasal GCIPL (Ci)	4 (2.9)	66 (47.1)	26 (72.2)	40 (38.5)	<0.001	<0.001	<0.001	<0.001
Inferonasal GCIPL (Ci)	4 (2.9)	58 (41.4)	27 (75.0)	31 (29.8)	<0.001	<0.001	<0.001	<0.001
Inferior GCIPL (Ci)	2 (1.4)	50 (35.7)	23 (63.9)	27 (26.0)	<0.001	<0.001	<0.001	<0.001
Inferotemporal GCIPL (Ci)	6 (4.3)	55 (39.3)	22 (61.1)	33 (31.7)	<0.001	<0.001	<0.001	0.002
Superotemporal GCIPL (Ci)	12 (8.9)	64 (45.7)	25 (69.4)	39 (37.5)	<0.001	<0.001	<0.001	<0.001

pRNFL: peripapillary retinal nerve fiber layer; Sp: Spectralis OCT; PMB: papillomacular bundle; Ci: Cirrus OCT; GCIPL: ganglion cell and inner plexiform layers.

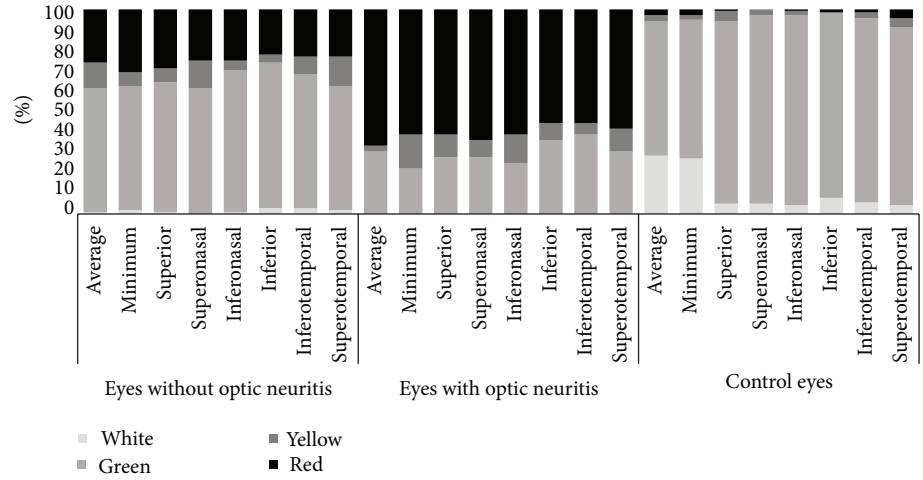

Figure 2: Comparison of the color scale frequency for each sector using ganglion cell-inner plexiform layer analysis with Cirrus optical coherence tomography among eyes with and without optic neuritis in relapsing-remitting multiple sclerosis patients and from healthy control subjects. Black represents eyes classified as red (below percentile 1); dark gray represents eyes labeled as yellow (below percentile 5); light gray represents green (between percentiles 5 and 95), and white represents white (above percentile 95).

thicknesses and disease duration, EDSS, and visual function parameters (Table 4).

Average pRNFL thickness measured with Cirrus ($\beta = -0.233$; $P = 0.031$) and Spectralis ($\beta = -0.228$; $P = 0.025$) OCTs, temporal ($\beta = -0.261$; $P = 0.017$) and papillomacular bundle ($\beta = -0.275$; $P = 0.006$) pRNFL thickness measured with Spectralis OCT, average GCIPL thickness ($\beta = -0.262$; $P = 0.026$), and minimum GCIPL thickness ($\beta = -0.299$; $P = 0.008$) correlated inversely with disease duration.

A strong, positive correlation was observed between average GCIPL thickness and pRNFL thickness using Cirrus ($\beta = 0.692$; $P < 0.001$) and Spectralis ($\beta = 0.642$; $P < 0.001$) OCTs.

After adjusting by age, sex, and within-patient intereye correlation, Cirrus GCIPL average and minimum measures showed a weak but significant correlation with EDSS only in eyes with ON antecedent (Table 4).

4. Discussion

Loss of RNFL is a well-documented structural marker of axonal degeneration in the eyes of patients with multiple sclerosis with and without a history of ON [8, 24–26]. Historically, OCT studies in multiple sclerosis have focused mostly on the RNFL, but retinal ganglion cell neuronal loss may also be implicated in the pathogenesis of visual dysfunction in MS [10].

To the best of our knowledge, apart from direct comparisons between pRNFL and GCIPL measurements in RRMS and healthy eyes [7–10], there is no information about the sensitivity and specificity of the different measurements to detect retinal thickness changes in RRMS patients.

Although strong positive correlation was found between GCIPL and pRNFL thickness values, average and minimum GCIPL measures showed higher sensitivity and specificity than temporal pRNFL measures. Remarkably, average GCIPL showed a significantly better sensitivity than temporal pRNFL by Cirrus, and minimum GCIPL showed a significantly better sensitivity than temporal pRNFL by Spectralis for the detection of retinal thickness changes in RRMS.

In agreement with previous studies [21], we found that eyes from patients with RRMS had significant thinning in average and temporal quadrant pRNFL values by Cirrus and Spectralis OCT, and, in each of six sectors, average and minimum GCIPL results obtained by Cirrus, when compared to healthy eyes (Table 1). This was true for eyes with and without ON antecedent. Nevertheless, eyes with ON history showed greater pRNFL and GCIPL thinning than eyes without ON antecedent [10] (Table 1).

In a previous study [4] analyzing the color-code classification of pRNFL in RRMS patients, we identified the temporal quadrant to be the most abnormally color-coded by both Cirrus and Spectralis. Additionally, temporal pRNFL quadrants were abnormally color-coded more frequently in ON eyes than in non-ON eyes by both devices, Cirrus and Spectralis.

The abnormality rate in temporal pRNFL color code in eyes with previous history of ON was 66.7% by Cirrus and 61.1% by Spectralis. The current study agrees with previous reports that eyes from patients with RRMS exhibit a significant thinning of the pRNFL and GCIPL compared with the healthy eyes [7, 10, 11] and that pRNFL thinning in RRMS patients typically occurs in the temporal sector [4, 20–23, 27–29].

As expected, the sector showing the highest abnormality rate in GCIPL test was the superonasal (47.1%).

Unsurprisingly, GCIPL thinning showed an association with disease duration and ON antecedent in eyes of patients with RRMS. GCIPL minimum represents the lowest GCIPL thickness over a single meridian crossing the annulus, which is expected to be sensitive to focal damage [30]. This measurement had previously been found to have the highest correlation with visual field pattern standard deviation in patients

Table 3: Estimated sensitivity and specificity of different optic coherence tomography measures for retinal thickness changes detection in eyes of patients with relapsing-remitting multiple sclerosis ($N = 140$) and from healthy control subjects ($N = 140$) using latent class analysis. Model A: temporal pRNFL thickness as measured by Cirrus OCT; estimated prevalence of retinal thickness changes in the sample was 23.42%; 95% confidence interval (95CI) 18.50 to 29.17%. Model B: temporal pRNFL thickness as measured by Spectralis OCT; estimated prevalence of retinal thickness changes in the sample was 24.25%; 95% confidence interval (95CI) 19.26 to 30.04%.

	Sensitivity		Specificity	
	Estimate	95CI	Estimate	95CI
Model A				
Cirrus average GCIPL	96.34%	76.11 to 99.54%	97.05%	92.77 to 98.83%
Cirrus minimum GCIPL	98.43%	64.61 to 99.95%	95.81%	91.00 to 98.10%
Cirrus temporal pRNFL	58.41%	45.82 to 70.00%	93.91%	89.56 to 96.52%
Best corrected visual acuity	6.14%	2.32 to 15.30%	98.59%	95.72 to 99.54%
Model B				
Cirrus average GCIPL	97.15%	76.94 to 99.71%	97.61%	93.16 to 99.19%
Cirrus minimum GCIPL	96.41%	81.48 to 99.39%	95.43%	90.80 to 97.78%
Spectralis temporal pRNFL	69.69%	57.14 to 79.86%	92.70%	88.01 to 95.65%
Best corrected visual acuity	6.08%	2.30 to 15.15%	98.55%	95.58 to 99.53%

GCIPL: ganglion cell-inner plexiform layers; pRNFL: peripapillary retinal nerve fiber layer.

Table 4: Standardized correlation coefficients between OCT measurements and neurologic and visual function parameters in eyes of patients with relapsing-remitting multiple sclerosis, calculated using generalized estimating equations accounting for sex, age, and within-patient intereye correlation ($n = 140$).

	BCVA	MD	EDSS	Disease duration
Cirrus average pRNFL	0.286*	0.418*	−0.014	−0.233‡
Cirrus temporal pRNFL	−0.013	0.062	0.001	−0.141
Spectralis average pRNFL	0.314*	0.360*	0.033	−0.228‡
Spectralis temporal pRNFL	0.122‡	0.268†	−0.101	−0.261‡
Spectralis PMB pRNFL	0.125‡	0.209‡	−0.066	−0.275†
GCIPL average	0.226*	0.513*	−0.178	−0.262‡
GCIPL minimum	0.204†	0.412*	−0.161	−0.299†
Non-ON eyes ($N = 104$)				
Cirrus average pRNFL	−0.019	0.098	0.033	−0.253‡
Cirrus temporal pRNFL	−0.270‡	−0.030	−0.046	−0.146
Spectralis average pRNFL	0.210*	0.145	0.109	−0.274‡
Spectralis temporal pRNFL	−0.025	0.093	−0.092	−0.284†
Spectralis PMB pRNFL	0.002	0.083	−0.040	−0.332†
GCIPL average	−0.062	0.109	−0.113	−0.297‡
GCIPL minimum	0.029	0.138	−0.092	−0.314†
ON eyes ($N = 36$)				
Cirrus average pRNFL	0.188	0.161	−0.173	0.012
Cirrus temporal pRNFL	−0.043	0.001	0.105	−0.013
Spectralis average pRNFL	0.175	0.149	−0.151	0.109
Spectralis temporal pRNFL	0.112	0.030	−0.195	0.065
Spectralis PMB pRNFL	0.059	−0.022	−0.120	0.097
GCIPL average	0.145	0.133	−0.429†	−0.079
GCIPL minimum	0.144	0.120	−0.421‡	−0.227

*$P < 0.001$; †$P < 0.01$; ‡$P < 0.05$.

OCT: optic coherence tomography; BCVA: best corrected visual acuity; MD: Goldman 24-2 SITA standard visual field mean deviation; EDSS: Expanded Disability Status Scale; pRNFL: peripapillary retinal nerve fiber layer; PMB: papillomacular bundle; GCIPL: ganglion cell and inner plexiform layers; ON: optic neuritis.

with chronic open angle glaucoma [31]. In our study, Cirrus GCIPL minimum measures showed a significant correlation with BCVA, mean deviation, and EDSS. Importantly, only GCIPL measures showed significant correlation with EDSS in ON eyes (Table 4).

A superior structure-function correlation between GCIPL thickness and clinical measures compared to pRNFL has been reported recently, suggesting that GCIPL analysis might be a better approach than pRNFL to examine MS neurodegeneration [11].

Previous studies have shown that GCIPL thickness can be altered in patients with RRMS [10, 32–34] and that these alterations correlated with visual function [10, 11] and central nervous system findings using magnetic resonance imaging [28]. Some of these studies have suggested that GCIPL thickness can be a more reliable measure for the detection of retinal anomalies in RRMS than pRNFL thickness [10]. Interestingly, our study demonstrates that a decrease in GCIPL thickness is more sensitive to retinal involvement in RRMS than an alteration in the temporal pRNFL.

This study has a number of limitations warranting discussion. Firstly, exact sensitivity and specificity cannot be obtained without a gold standard test. The values obtained through LCA can be useful when comparing different tests; however, the sensitivities and specificities provided are estimates. Studies with bigger sample size and including information on other diagnostic tests, such as electrodiagnostic testing and magnetic resonance imaging, could help to improve this estimation. Secondly, both eyes were included in this study. However, most MS studies published to date have included both eyes because they can be individually evaluated and do not necessarily follow the same disease course [1, 4]. Additionally, generalized estimating equations were used in order to account for sex, age, and within-patient intereye correlation. With these methods, information from both eyes can be used for the study, without the risk of increasing the risk of bias due to intereye correlation or increase in sample size [35].

The retinal segmentation algorithm used by Cirrus OCT combines GCL and IPL, since the boundaries between these two layers cannot be visually discriminated on this device. Although Spectralis OCT has developed a specific software that provides automated differentiation and quantification of the individual retinal layers, it was not available when the data was collected. Additionally, this software does not provide comparison to a normative database, so binary outcomes necessary for LCA would not be available.

Finally, we have included only patients with relapsing-remitting multiple sclerosis; therefore, our results cannot be extrapolated to other types of multiple sclerosis or to patients with more advanced disease (mean EDSS was 2.42).

5. Conclusions

In conclusion, OCT GCIPL analysis is more sensitive than temporal pRNFL analysis to detect retinal thickness changes in RRMS eyes. GCIPL measures correlate better than pRNFL measures with visual function parameters such as BCVA, visual field mean deviation, or EDSS. As such, GCIPL thickness measured by retinal segmentation of OCT scans may be an ideal marker for monitoring neurodegeneration in RRMS patients.

Conflict of Interests

The authors have no proprietary or commercial interest in any materials discussed in this paper. All authors have completed and submitted the ICMJE form for disclosure of potential conflict of interests and none were reported.

Authors' Contribution

Conception and design was done by Julio J. González-López, Gema Rebolleda, Francisco J. Muñoz-Negrete, Marina Leal, Noelia Oblanca, Lucienne Costa-Frossard, and José C. Álvarez-Cermeño; analysis and interpretation was done by Julio J. González-López and Gema Rebolleda; writing the paper was done by Julio J. González-López, Gema Rebolleda, and Francisco J. Muñoz-Negrete; critical revision of the paper was done by Marina Leal, Noelia Oblanca, Lucienne Costa-Frossard, and José C. Álvarez-Cermeño. Final approval of the paper was done by Julio J. González-López, Gema Rebolleda, Francisco J. Muñoz-Negrete, Marina Leal, Noelia Oblanca, Lucienne Costa-Frossard, and José C. Álvarez-Cermeño; data collection was done by Julio J. González-López, Marina Leal, and Noelia Oblanca; provision of materials, patients, or resources was done by Gema Rebolleda, Francisco J. Muñoz-Negrete, Lucienne Costa-Frossard, and José C. Álvarez-Cermeño; statistical expertise was provided by Julio J. González-López; obtaining funding was done by Gema Rebolleda and Francisco J. Muñoz-Negrete; and literature search was done by Julio J. González-López and Gema Rebolleda.

Acknowledgments

Julio J. González-López is a Ph.D. candidate at the Surgery Department, Universidad de Alcalá School of Medicine, Madrid, Spain. This study has been granted by the "Fondo de Investigaciones Sanitarias," from the Spanish Ministry of Health and Consumer Affairs.

References

[1] E. Ojeda, D. Díaz-Cortes, D. Rosales, C. Duarte-Rey, J.-M. Anaya, and A. Rojas-Villarraga, "Prevalence and clinical features of multiple sclerosis in Latin America," *Clinical Neurology and Neurosurgery*, vol. 115, no. 4, pp. 381–387, 2013.

[2] F. Ikuta and H. M. Zimmerman, "Distribution of plaques in seventy autopsy cases of multiple sclerosis in the United States," *Neurology*, vol. 26, part 2, no. 6, pp. 26–28, 1976.

[3] R. H. Kardon, "Role of the macular optical coherence tomography scan in neuro-ophthalmology," *Journal of Neuro-Ophthalmology*, vol. 31, no. 4, pp. 353–361, 2011.

[4] G. Rebolleda, J. J. González-López, F. J. Muñoz-Negrete, N. Oblanca, L. Costa-Frossard, and J. C. Álvarez-Cermeño, "Color-code agreement among stratus, cirrus, and spectralis optical coherence tomography in relapsing-remitting multiple sclerosis

with and without prior optic neuritis," *The American Journal of Ophthalmology*, vol. 155, no. 5, pp. 890–897, 2013.

[5] A. J. Green, S. McQuaid, S. L. Hauser, I. V. Allen, and R. Lyness, "Ocular pathology in multiple sclerosis: retinal atrophy and inflammation irrespective of disease duration," *Brain*, vol. 133, part 6, pp. 1591–1601, 2010.

[6] K. S. Shindler, E. Ventura, M. Dutt, and A. Rostami, "Inflammatory demyelination induces axonal injury and retinal ganglion cell apoptosis in experimental optic neuritis," *Experimental Eye Research*, vol. 87, no. 3, pp. 208–213, 2008.

[7] P. Albrecht, M. Ringelstein, A. K. Müller et al., "Degeneration of retinal layers in multiple sclerosis subtypes quantified by optical coherence tomography," *Multiple Sclerosis*, vol. 18, no. 10, pp. 1422–1429, 2012.

[8] S. B. Syc, S. Saidha, S. D. Newsome et al., "Optical coherence tomography segmentation reveals ganglion cell layer pathology after optic neuritis," *Brain*, vol. 135, part 2, pp. 521–533, 2012.

[9] L. S. Talman, E. R. Bisker, D. J. Sackel et al., "Longitudinal study of vision and retinal nerve fiber layer thickness in multiple sclerosis," *Annals of Neurology*, vol. 67, no. 6, pp. 749–760, 2010.

[10] S. D. Walter, H. Ishikawa, K. M. Galetta et al., "Ganglion cell loss in relation to visual disability in multiple sclerosis," *Ophthalmology*, vol. 119, no. 6, pp. 1250–1257, 2012.

[11] S. Saidha, S. B. Syc, M. K. Durbin et al., "Visual dysfunction in multiple sclerosis correlates better with optical coherence tomography derived estimates of macular ganglion cell layer thickness than peripapillary retinal nerve fiber layer thickness," *Multiple Sclerosis*, vol. 17, no. 12, pp. 1449–1463, 2011.

[12] C. H. Polman, S. C. Reingold, G. Edan et al., "Diagnostic criteria for multiple sclerosis: 2005 revisions to the 'McDonald Criteria'," *Annals of Neurology*, vol. 58, no. 6, pp. 840–846, 2005.

[13] M. Sadatsafavi, N. Shahidi, F. Marra et al., "A statistical method was used for the meta-analysis of tests for latent TB in the absence of a gold standard, combining random-effect and latent-class methods to estimate test accuracy," *Journal of Clinical Epidemiology*, vol. 63, no. 3, pp. 257–269, 2010.

[14] S. L. Hui and S. D. Walter, "Estimating the error rates of diagnostic tests," *Biometrics*, vol. 36, no. 1, pp. 167–171, 1980.

[15] D. Rindskopf and W. Rindskopf, "The value of latent class analysis in medical diagnosis," *Statistics in Medicine*, vol. 5, no. 1, pp. 21–27, 1986.

[16] E. Girardi, C. Angeletti, V. Puro et al., "Estimating diagnostic accuracy of tests for latent tuberculosis infection without a gold standard among healthcare workers," *Euro Surveillance*, vol. 14, no. 43, 2009.

[17] T. S. Machado de Assis, A. Rabello, and G. L. Werneck, "Latent class analysis of diagnostic tests for visceral leishmaniasis in Brazil," *Tropical Medicine and International Health*, vol. 17, no. 10, pp. 1202–1207, 2012.

[18] M. Shevlin, S. Murphy, and J. Murphy, "Adolescent loneliness and psychiatric morbidity in the general population: Identifying "at risk" groups using latent class analysis," *Nordic Journal of Psychiatry*, 2014.

[19] M. Ang, W. L. Wong, X. Li, and S.-P. Chee, "Interferon γ release assay for the diagnosis of uveitis associated with tuberculosis: a Bayesian evaluation in the absence of a gold standard," *The British Journal of Ophthalmology*, vol. 97, no. 8, pp. 1062–1067, 2013.

[20] C. Fjeldstad, M. Bemben, and G. Pardo, "Reduced retinal nerve fiber layer and macular thickness in patients with multiple sclerosis with no history of optic neuritis identified by the use of spectral domain high-definition optical coherence tomography," *Journal of Clinical Neuroscience*, vol. 18, no. 11, pp. 1469–1472, 2011.

[21] E. Garcia-Martin, V. Pueyo, I. Pinilla, J.-R. Ara, J. Martin, and J. Fernandez, "Fourier-domain OCT in multiple sclerosis patients: reproducibility and ability to detect retinal nerve fiber layer atrophy," *Investigative Ophthalmology and Visual Science*, vol. 52, no. 7, pp. 4124–4131, 2011.

[22] S. Noval, I. Contreras, S. Munoz, C. Oreja-Guevara, B. Manzano, and G. Rebolleda, "Optical coherence tomography in multiple sclerosis and neuromyelitis optica: an update," *Multiple Sclerosis International*, vol. 2011, Article ID 472790, 11 pages, 2011.

[23] G. Rebolleda, A. García-García, H. R. Won Kim, and F. J. Mũoz-Negrete, "Comparison of retinal nerve fiber layer measured by time domain and spectral domain optical coherence tomography in optic neuritis," *Eye*, vol. 25, no. 2, pp. 233–238, 2011.

[24] K. M. Galetta, P. A. Calabresi, E. M. Frohman, and L. J. Balcer, "Optical coherence tomography (OCT): imaging the visual pathway as a model for neurodegeneration," *Neurotherapeutics*, vol. 8, no. 1, pp. 117–132, 2011.

[25] A. Petzold, J. F. de Boer, S. Schippling et al., "Optical coherence tomography in multiple sclerosis: a systematic review and meta-analysis," *The Lancet Neurology*, vol. 9, no. 9, pp. 921–932, 2010.

[26] S. Saidha, S. B. Syc, M. A. Ibrahim et al., "Primary retinal pathology in multiple sclerosis as detected by optical coherence tomography," *Brain*, vol. 134, part 2, pp. 518–533, 2011.

[27] J. B. Fisher, D. A. Jacobs, C. E. Markowitz et al., "Relation of visual function to retinal nerve fiber layer thickness in multiple sclerosis," *Ophthalmology*, vol. 113, no. 2, pp. 324–332, 2006.

[28] E. García-Martín, V. Pueyo, J. Martin et al., "Progressive changes in the retinal nerve fiber layer in patients with multiple sclerosis," *European Journal of Ophthalmology*, vol. 20, no. 1, pp. 167–173, 2010.

[29] V. Pueyo, J. R. Ara, C. Almarcegui et al., "Sub-clinical atrophy of the retinal nerve fibre layer in multiple sclerosis," *Acta Ophthalmologica*, vol. 88, no. 7, pp. 748–752, 2010.

[30] J.-C. Mwanza, M. K. Durbin, D. L. Budenz et al., "Profile and predictors of normal ganglion cell-inner plexiform layer thickness measured with frequency-domain optical coherence tomography," *Investigative Ophthalmology & Visual Science*, vol. 52, no. 11, pp. 7872–7879, 2011.

[31] H. El Chehab, M. Delbarre, J. Fenolland et al., "Structure function relationship: specific index of ganglion cell complex assessment of 2 spectral domain OCT and standard automated perimetry," *Acta Ophthalmologica Scandinavica*, vol. 91, supplement s252, 2013.

[32] D. B. Fernandes, A. S. Raza, R. G. Nogueira et al., "Evaluation of inner retinal layers in patients with multiple sclerosis or neuromyelitis optica using optical coherence tomography," *Ophthalmology*, vol. 120, no. 2, pp. 387–394, 2013.

[33] J. N. Ratchford, S. Saidha, E. S. Sotirchos et al., "Active MS is associated with accelerated retinal ganglion cell/inner plexiform layer thinning," *Neurology*, vol. 80, no. 1, pp. 47–54, 2013.

[34] S. Saidha, E. S. Sotirchos, J. Oh et al., "Relationships between retinal axonal and neuronal measures and global central nervous system pathology in multiple sclerosis," *Archives of Neurology*, vol. 70, no. 1, pp. 34–43, 2013.

[35] I. E. Murdoch, S. S. Morris, and S. N. Cousens, "People and eyes: statistical approaches in ophthalmology," *British Journal of Ophthalmology*, vol. 82, no. 8, pp. 971–973, 1998.

Hindawi Publishing Corporation
BioMed Research International
Volume 2014, Article ID 741538, 6 pages
http://dx.doi.org/10.1155/2014/741538

Clinical Study

Hyperautofluorescence in Outer Retinal Layers Thinning

Marina Bertolotto,[1] Luigi Borgia,[1] and Michele Iester[2]

[1] *Is.PreOftalmica, Via Antiochia 29r, 16129 Genoa, Italy*
[2] *Anatomical-Clinical Laboratory for Functional Diagnosis and Treatment of Glaucoma and Neuroophthalmology, Eye Clinic, DINOGMI, University of Genoa, Viale Benedetto XV 5, 16132 Genoa, Italy*

Correspondence should be addressed to Michele Iester; iester@unige.it

Received 21 April 2014; Accepted 18 July 2014; Published 9 September 2014

Academic Editor: Michele Figus

Purpose. To evaluate if paracentral hyperautofluorescence (HAF) retinal regions, which can be occasionally found and analyzed by optical coherence tomography (OCT), were related to retinal layer changes and to detect which layer was involved. *Methods*. This is a cross-sectional and retrospective study. 648 OCT files were revised. OCTs that showed a paracentral HAF area by using the fundus autofluorescence imaging in Heidelberg Spectralis (Heidelberg Engineering, Germany) were selected. Then retinal layer morphology was analyzed observing OCT scans and a retinal thickness was measured. *Results*. 31 patients were selected: 20 patients had chronic serous epitheliopathy (CSE), 8 patients had resolved central serous chorioretinopathy (CSC), and 3 patients wet age related macular degeneration (ARMD). The HAF zones corresponded to areas of thickness reduction of the external hyporeflective band. In all these areas the retinal pigment epithelium was not atrophic and the neuroepithelium was more or less dystrophic. In particular the retinal thickness was 264 um, 232 um, and 243 um in wet ARMD, CSE, and CSC, respectively; the reduction was significant ($P < 0.01$) compared to the same area of the other eye. *Discussion*. The presence of HAF imaging might be mostly due to a "window effect" rather than an accumulation of lipofuscin.

1. Introduction

The predominant fluorophores arising from the fundus have been shown to be located within the retinal pigment epithelium (RPE) lipofuscin (LF) [1], which derives primarily from phagocytosed photoreceptor outer segments. These fluorophores most likely accumulate in RPE cells because the structures of the fluorophores are unusual and not amenable to degradation, rather than because the lysosomal enzymes are defective in these cells [2]. Progressive LF buildup is mainly caused by incomplete degradation of photoreceptor outer segment disks with subsequent incomplete release of degraded material. Over the course of a lifetime, each RPE cell phagocytoses more than 3,000,000,000 outer segments [3–5].

Fundus autofluorescence (AF) imaging is a method that allows topographic mapping of LF distribution in the retinal pigment epithelium cell monolayer as well as of other fluorophores that may occur with disease in the outer retina and the subneurosensory. At the posterior pole autofluorescence is dependent on either outer segment metabolism with an increase of LF concentration [6] or a window effect for the decrease or lack of pigment along plexiform layer which covers the physiological AF [7].

The aim of this study was to evaluate if paracentral hyperautofluorescence (HAF) retinal regions, which can occasionally be found by a user and analyzed by optical coherence tomography (OCT), were related to retinal layer changes and to detect which layer was involved.

2. Patient and Methods

This is a retrospective, cross-sectional study. This study followed the principles of the Declaration of Helsinki.

Patients were imaged using the Heidelberg Spectralis HRA + OCT (Heidelberg Engineering, Heidelberg, Germany) in Spectral Domain SD-OCT mode, using a scan field of 30 degrees horizontally and 15 degrees vertically and 19 to 25 OCT horizontal sections (one section at least every

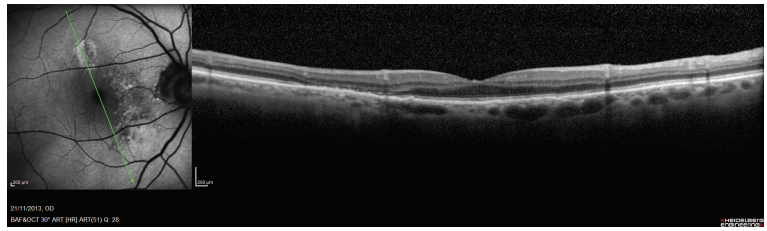

(a) Chronic serous epitheliopathy

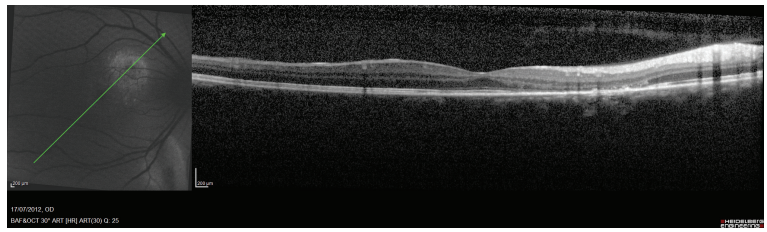

(b) Resolved central serous chorioretinopathy

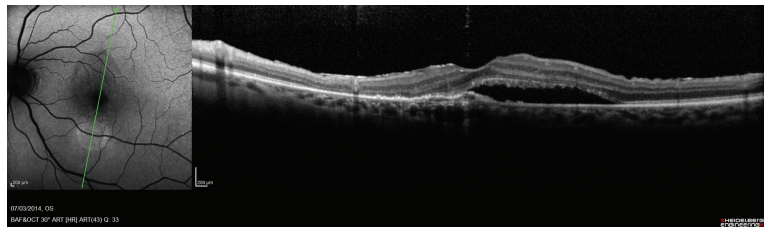

(c) Wet ARMD

Figure 1: (a) Chronic serous epitheliopathy, (b) resolved central serous chorioretinopathy, and (c) wet ARMD.

Table 1: Descriptive analysis of the included patients.

Disease	Age	Retinal thickness
Wet ARMD ($n = 3$)	73.3 (10)	264.7 (54.24)
CSE ($n = 20$)	64.3 (10.5)	232.3 (48.09)
CSC ($n = 8$)	44.3 (6.9)	243.13 (39.68)

n: number of eyes, mean (standard deviation), ARMD: age related macular degeneration, CSE: chronic serous epitheliopathy, CSC: resolved central serous chorioretinopathy.

240 μm). The Heidelberg Spectralis HRA + OCT (Heidelberg Engineering, Heidelberg, Germany; Software version 1.6.1.0) can be used in any one of six imaging modes, that is, SD-OCT, fluorescein angiography, indocyanine green angiography, autofluorescence, red-free, and infrared imaging. This paper details use of the instrument in SD-OCT mode only. The Heidelberg Spectralis utilizes a broadband light source centered at 870 nm (i.e., no visible light "beacon") to simultaneously measure multiple wavelengths, a prerequisite of SD-OCT imaging. Simultaneous confocal scanning laser ophthalmoscopy is used to generate high-resolution images of the retinal surface, thereby providing precise location information of each A-scan within a cross-sectional SD-OCT image. SD-OCT scanning generates 40,000 A-scans/second with an axial resolution of 3.5 microns/pixel digital (7 microns optical) and a transverse resolution of 14 microns [8]. Alignment software continuously tracks any eye movement during image acquisition and then adjusts the position of the A-scan on the retinal surface to ensure accurate registration of cross-sectional OCT images. Using eye tracking and registration technology, multiple images are obtained from a precise location to then be averaged and filtered to remove random noise from the final image. The same eye tracking/registration technology is used to ensure that the instrument automatically rescans images that are influenced by blink artifacts. Similarly, follow-up images are derived from the same area of retina, thereby eliminating subjective placement of the scan by the operator. The SD-OCTs can also scan the fundus with a low-power optically pumped semiconductor laser ($\lambda > 488$ nm) to elicit autofluorescence, which is detected through a barrier filter ($\lambda > 500$ nm) and captured at rate of 16 frames per second over a $30^\circ \times 30^\circ$ or a $55^\circ \times 55^\circ$ field (768×768 pixels). To enhance the signal-to-noise ratio, 30 to 100 single-line OCT frames were averaged during simultaneous fundus AF and SD-OCT imaging. In each eye, several OCT line scans through separate regions with increased AF were obtained to examine the retinal architecture [9].

2.1. Patient's Inclusion/Exclusion Criteria. All the patients were referred to LB for an OCT analysis, and only the OCTs with AF images done from January 2011 to June 2012 were

Table 2: Comparison of the HFA area with the corresponding area in the healthy eye.

Disease	Involved area (IA)	Corresponding area in the opposite eye (CIA)	Difference (CIA − IA)	P value
Wet ARMD	264.7 (54.24)	312.3 (47.12)	47.67 (8.74)	$P < 0.01$
CSE	232.3 (48.09)	306.65 (38.96)	71.85 (28.88)	$P < 0.001$
CSC	243.13 (39.68)	307 (47.02)	63.88 (27.67)	$P < 0.001$

Mean (standard deviation), IA: the area involved by the pathology, CIA: the corresponding IA in the contralateral eye, ARMD: age related macular degeneration, CSE: chronic serous epitheliopathy, CSC: resolved central serous chorioretinopathy.

Table 3: Qualitative changes of retinal layers.

Morphological change of	Dystrophic neuroepithelium	Retinal thickness reduction	Hyperautofluorescence
Wet ARMD ($n = 3$)	3++	3	3
CSE ($n = 20$)	8+ 12++	20	13
CSC ($n = 8$)	1+ 7−	8	3

ARMD: age related macular degeneration, CSE: chronic serous epitheliopathy, CSC: resolved central serous chorioretinopathy, n = number of eyes. Dystrophic neuroepithelium was assessed from less "−" to more "+" or "++."

revised. To find patients with a paracentral hyperautofluorescence (HAF) retinal region by OCT, all the AF images were revised. Patients with unilateral disease were considered in the study.

Then all the OCT scans were subjectively analyzed by the three users just observing the Spectralis screen to value if the retinal layers were modified and to distinguish which retinal layers were involved [10, 11].

For HAF areas, the following features of the outer retina were analyzed: the morphological alteration of the EPR, the outer nuclear layer (ONL), and the outer plexiform layer (OPL).

2.2. Statistical Analysis. Student's t-test was used to compare the thickness of the HFA areas with the corresponding area of the opposite healthy eye. A P value >0.05 was considered statistically significant.

3. Results

Six hundred and 48 patients' files were revised and 31 eyes of 31 patients had a paracentral HAF region. Twenty patients had chronic serous epitheliopathy, eight patients had resolved central serous chorioretinopathy, and three patients had wet ARMD (Table 1) (Figure 1).

All HAF regions showed a retinal thickness reduction, which when compared to the corresponding area of the other eye showed a significant change (Table 2, Figure 2). In all these areas the RPE was not atrophic (Figure 3). The HAF intensity was related to the thickness reduction or atrophy of the outer hyporeflectiveband, corresponding to the ONL and to a part of the OPL or Henle Fiber Layer. When this band was thin, the neuroepithelium was more or less dystrophic (Figure 4). In 19 patients (61.29%) the external hyperreflective band was found irregular (Figure 3) (Table 3).

4. Discussion

Beyond normal aging processes, LF accumulation is thought to represent a common downstream pathogenetic mechanism in various blinding hereditary and complex retinal diseases, including age related macular degeneration and inherited retinal dystrophies, and Stargardt disease [12–17].

Fundus AF imaging is a clinical tool that allows evaluation of the interaction between photoreceptor cells and RPE in macular disease. The predominant fluorophores arising from the fundus have been shown to be located within the RPE LP [1]. LP is a pigment that exhibits a characteristic AF when excited in ultraviolet or blue light [18].

A decreased AF may indicate photoreceptor death and RPE atrophy or increased RPE melanin content or absorption from extracellular material or cells or fluid which is anterior to RPE. On the other hand, an increased AF might suggest a compromised RPE function related to an ongoing metabolic demand [18–21].

In a normal fundus, the distribution of AF is diffuse with decreased intensity at the optic nerve head, under the retinal blood vessels which appear dark, and at the macula [1, 18]. Macular AF is attenuated by the luteal pigment, and the concentration of this pigment in the fovea is most dense along the outer plexiform layer [22].

Abnormal accumulation of LF produces abnormally increased HAF. Retinal-choroidal diseases, which caused an increased shedding of photoreceptor outer segments, disrupted RPE phagocytic function, or an ability of the RPE to recycle metabolites, produced hyperfluorescence because of LF accumulation as seen in age related macular degeneration and inherited retinal diseases [23].

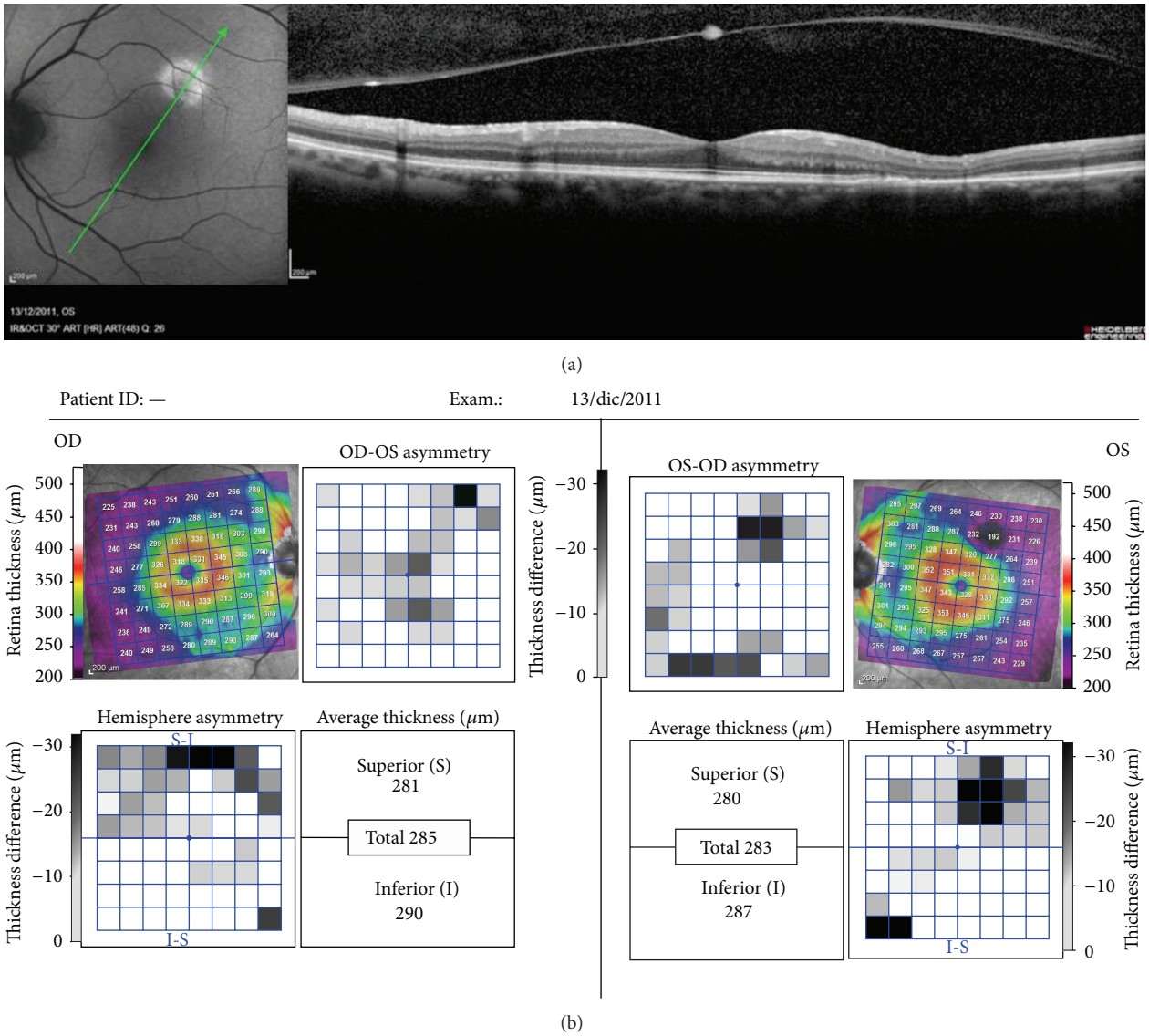

Figure 2: All HAF regions showed a retinal thickness reduction, which when compared to the corresponding area of the other eye showed a significant change.

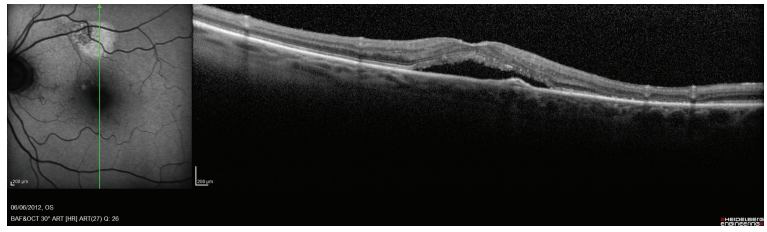

Figure 3: In all the HAF areas the RPE was not atrophic.

In 1984 Snodderly et al. showed in primate retinas that most of the pigment in fovea is along the outer plexiform layer, interposed between the foveal photoreceptors and the stimulating light [22]. In our study we found that HAF correlates with thickness reduction in the retinal outer layers and in particular with the thickness reduction or atrophy of the external hyporeflective OCT band which is the ONL and a part of the OPL or Henle fiber layer.

These data suggested the possibility that the presence of HAF could be due to a "window effect" for the OPL thinning rather than an accumulation of LP. Clinically, after a localized serous retinal detachment due to different pathologies, it

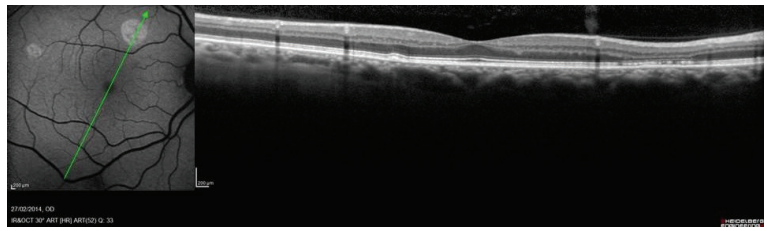

(a)

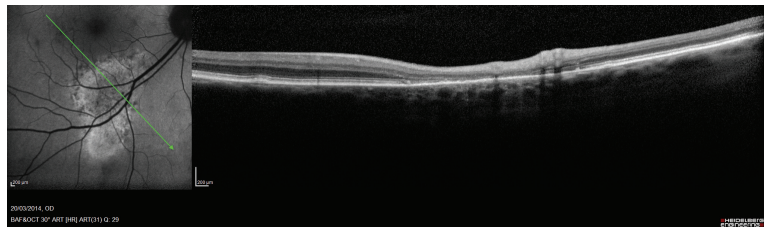

(b)

Figure 4: When the outer hyporeflective band was thin, the neuroepithelium was more or less dystrophic.

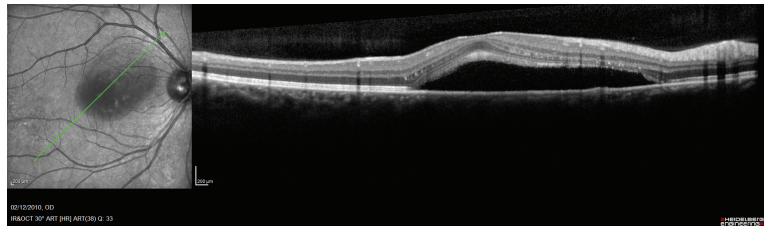

(a)

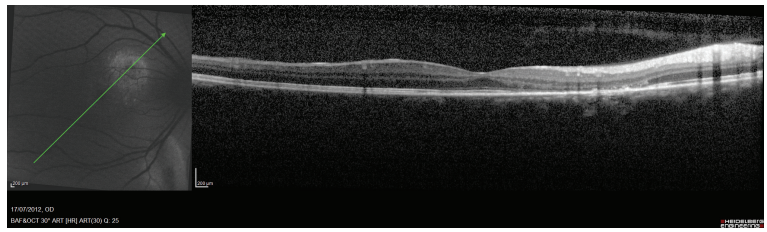

(b)

Figure 5: (a) Chronic serous epitheliopathy (CSE) and (b) resolution of the CSE; a retinal thinning with an atrophy of the outer retinal layers (ONL and OPL) can be seen.

is possible to find hyperautofluorescence areas in that area together with a retinal thinning with an atrophy of the outer retinal layers (ONL and OPL) (Figure 5).

In conclusion our observation suggests that the presence of HAF could be considered the easiest sign to detect retinal thinning and in particular a reduction of ONL and OPL.

Disclosure

M. Bertolotto, L. Borgia, and M. Iester are the authorship of this study based on the ICMJE guidelines.

Conflict of Interests

None of the authors has proprietary interests in the development and marketing of any products mentioned in the paper.

References

[1] F. C. Delori, C. K. Dorey, G. Staurenghi, O. Arend, D. G. Goger, and J. J. Weiter, "In vivo fluorescence of the ocular fundus exhibits retinal pigment epithelium lipofuscin characteristics," *Investigative Ophthalmology and Visual Science*, vol. 36, no. 3, pp. 718–729, 1995.

[2] A. M. Cuervo and J. F. Dice, "When lysosomes get old," *Experimental Gerontology*, vol. 35, no. 2, pp. 119–131, 2000.

[3] G. L. Wing, G. C. Blanchard, and J. J. Weiter, "The topography and age relationship of lipofuscin concentration in the retinal pigment epithelium," *Investigative Ophthalmology and Visual Science*, vol. 17, no. 7, pp. 601–607, 1978.

[4] L. Feeney-Burns, E. R. Berman, and H. Rothmann, "Lipofuscin of human retinal pigment epithelium," *American Journal of Ophthalmology*, vol. 90, no. 6, pp. 783–791, 1980.

[5] J. J. Weiter, F. C. Delori, G. L. Wing, and K. A. Fitch, "Retinal pigment epithelial lipofuscin and melanin and choroidal melanin in human eyes," *Investigative Ophthalmology and Visual Science*, vol. 27, no. 2, pp. 145–152, 1986.

[6] S. Schmitz-Valckenberg, F. G. Holz, A. C. Bird, and R. F. Spaide, "Fundus autofluorescence imaging: review and perspectives," *Retina*, vol. 28, no. 3, pp. 385–409, 2008.

[7] F. Bottoni, L. Carmassi, M. Cigada, S. Moschini, and F. Bergamini, "Diagnosis of macular pseudoholes and lamellar macular holes: is optical coherence tomography the "gold standard"?" *The British Journal of Ophthalmology*, vol. 92, no. 5, pp. 635–639, 2008.

[8] Heidelberg Enginneering, "Spectralis hardware operating instructions," Technical Specifications, 2007:22–25.

[9] F. K. Chen, P. J. Patel, P. J. Coffey, A. Tufail, and L. da Cruz, "Increased fundus autofluorescence associated with outer segment shortening in macular translocation model of neovascular age-related macular degeneration," *Investigative Ophthalmology and Visual Science*, vol. 51, no. 8, pp. 4207–4212, 2010.

[10] V. Tanner, D. S. Chauhan, T. L. Jackson, and T. H. Williamson, "Optical coherence tomography of the vitreoretinal interface in macular hole formation," *British Journal of Ophthalmology*, vol. 85, no. 9, pp. 1092–1097, 2001.

[11] B. Haouchine, P. Massin, R. Tadayoni, A. Erginay, and A. Gaudric, "Diagnosis of macular pseudoholes and lamellar macular holes by optical coherence tomography," *The American Journal of Ophthalmology*, vol. 138, no. 5, pp. 732–739, 2004.

[12] R. C. Eagle Jr., A. C. Lucier, V. B. Bernardino Jr., and M. Yanoff, "Retinal pigment epithelial abnormalities in fundus flavimaculatus: a light and electron microscopic study," *Ophthalmology*, vol. 87, no. 12, pp. 1189–1200, 1980.

[13] S. A. Miller, "Fluorescence in Best's vitelliform dystrophy, lipofuscin, and fundus flavimaculatus," *British Journal of Ophthalmology*, vol. 62, no. 4, pp. 256–260, 1978.

[14] S. O'Gorman, W. A. Flaherty, G. A. Fishman, and E. L. Berson, "Histopathologic findings in Best's vitelliform macular dystrophy," *Archives of Ophthalmology*, vol. 106, no. 9, pp. 1261–1268, 1988.

[15] C. K. Dorey, G. Wu, D. Ebenstein, A. Garsd, and J. J. Weiter, "Cell loss in the aging retina. Relationship to lipofuscin accumulation and macular degeneration," *Investigative Ophthalmology and Visual Science*, vol. 30, no. 8, pp. 1691–1699, 1989.

[16] R. L. Steinmetz, A. Garner, J. I. Maguire, and A. C. Bird, "Histopathology of incipient fundus flavimaculatus," *Ophthalmology*, vol. 98, no. 6, pp. 953–956, 1991.

[17] M. L. Katz, "Potential role of retinal pigment epithelial lipofuscin accumulation in age-related macular degeneration," *Archives of Gerontology and Geriatrics*, vol. 34, no. 3, pp. 359–370, 2002.

[18] F. Delori, C. Keilhauer, J. R. Sparrow, and G. Staurenghi, "Origin of fundus autofluorescence," in *Atlas of Fundus Autofluorescence Imaging*, F. G. Holz, S. Schmitz-Valckenberg, R. F. Spaide, and A. C. Bird, Eds., chapter 2, pp. 17–29, Springer, Berlin, Germany, 2007.

[19] C. J. Kennedy, P. E. Rakoczy, and I. J. Constable, "Lipofuscin of the retinal pigment epithelium: a review," *Eye*, vol. 9, no. 6, pp. 763–771, 1995.

[20] L. H. Lima, J. P. Greenberg, V. C. Greenstein et al., "Hyperautofluorescent ring in autoimmune retinopathy," *Retina*, vol. 32, no. 7, pp. 1385–1394, 2012.

[21] A. Von Ruckmann, F. W. Fitzke, and A. C. Bird, "Distribution of fundus autofluorescence with a scanning laser ophthalmoscope," *British Journal of Ophthalmology*, vol. 79, no. 5, pp. 407–412, 1995.

[22] D. M. Snodderly, J. D. Auran, and F. C. Delori, "The macular pigment. II. Spatial distribution in primate retinas," *Investigative Ophthalmology and Visual Science*, vol. 25, no. 6, pp. 674–685, 1984.

[23] F. G. Holz, S. Schmitz-Valckenberg, R. F. Spaide, and A. C. Bird, *Atlas of Fundus Autofluorescence Imaging*, chapter 8, Springer, Heidelberg, Germany, 2007.